

DISS. ETH No. 27017

**Mass Spectrometric quantification
of DNA adducts:
from damage formation to toxicological impacts**

A thesis submitted to attain the degree of

DOCTOR OF SCIENCES of ETH Zurich

(Dr. sc. ETH Zurich)

presented by

Susanne Marlene Geisen

Diploma in Food Chemistry, Karlsruhe Institute of Technology, Germany

born on 22.06.1989

Citizen of

Germany

accepted on the recommendation of

Prof. Dr. Shana J. Sturla

Prof. Dr. Bernd Wollscheid

Assistant Prof. Dr. Maureen McKeague

PD Dr. Beat Bornhauser

2020

Für meine Familie

Acknowledgements

I would like to thank, first and foremost, my advisor *Prof. Dr. Shana Sturla* for giving me the opportunity to grow and learn in her lab. Your trust and belief in me allowed me to become an independent researcher. Thank you for always being open for discussions and for understanding every situation. It has been a great experience to work with you. Thank you also for the amazing time we could spend at group events – those moments contribute tremendously to a great team atmosphere.

I thank my committee members for the guidance, critical inputs and constructive discussion: *Prof. Dr. Bernd Wollscheid* your analytical knowledge and your innovative thinking have been essential to this thesis. *PD Dr. Beat Bornhauser* for opening his lab to me and allowing me to learn so much more about chemotherapy. Your patience and understanding in working with us is highly appreciated. *Assistant Prof. Dr. Maureen McKeague*, your enthusiasm for science is inspiring. You always knew how to motivate me and always had the right suggestions for overcoming my problems. Thank you!

Thank you also to my collaborators, that I had the pleasure to work with, discuss science and exchange samples and material: *Prof. Dr. Bernd Kaina*, *Prof. Dr. Jörg Fahrner*, *Prof. Dr. Pablo Steinberg*, *Dr. Michael Empl*, *Dr. Tina Kostka*, *Prof. Dr. Richard Lock*, *Dr. Cara Toscan* and *Dr. Nadia Barrozi*.

A special thank you goes to the Functional Genomic Center Zürich, namely *Dr. Serena di Palma*, *Dr. Bernd Roschitzki*, *Dr. Peter Gehrige* and *Dr. Endre Latzko* and *Laura Kunz*.

A big thank you to the members of the Sturla lab. Each single one of you is contributing to a truly amazing atmosphere and I enjoyed the fun times we could share in and outside the lab. Thank you *Ally Zhai* (for volunteering to proof-read this thesis, for taking care of “my” HPLC, for being my cake buddy, for constant chocolate supply and overall for being that great empathic and intelligent person – you will do great in your PhD), *Cécile Mingard* (you were there from the beginning, always having an open ear and I am so happy to have done this together with you), *Dr. Claudia Aloisi* (we all benefit from your scientific input next to all the retreat organizations and your warm personality), *Dr. Hailey Gahlon* and *Dr. Katherine Hurley* (for your guidance and always finding the time to discuss science with me), *Daniela Kalbermatter* (thank you for always being on top of things and knowing what to do in every situation), *Nathalie Ziegler* (for all the time you helped me with the MS and HPLC, your personality is important to the Sturla group), *Prisca Iseli* (for all the amazing work you are doing), *Jeanne Cresson* (merci for initiating the pasta-club), *Fabrice Müller* (D19 doesn't want to hear it, but we had the better office atmosphere), *Emma Sandell* (for sharing frustration and time during fraction collection), *Nikolai Püllen* (we share a love for vegan cakes), *Yang Jiang* (you are dealing very well with all the girls), *Dr. Gabriele Fontana* (for bringing some Italian flair to the group), *Katharina Blatter* (for cake supply and nice conversations in the corridor), *Dr. Sabrina Huber* (for MS support and of course Yannis), *Sabine Dietrich* (for all the nice chats and well-organized ordering). And former members, especially *Dr. Alessia Stornetta* for introducing me to her project, mass spec analysis and the Sturla lab. Your guidance and feedback was highly appreciated. Thank you *Dr. Jingjing Sun* (you are missed) and *Dr. Junzhou Wu* (for fixing every instrument and all the fun), *Dr. Stefano Malvezzi* and *Dr. Florence Berger* (both of you gave me a wonderful start in the Sturla group), *Dr. Michael Rätz*, *Aida Huber*, *Mirjam Schneider*, *Dr. Marianna Stamou*, *Vanessa Mazotti*, *Dr. Nicole Antczak* and *Dr. Jianbo Zhang*.

Also thank you to *Teresa Demuth* and *Cristina Lupo* for always understanding my situation and turning frustration into fun. I am looking forward to your defenses and more fun outside of LFO.

A special thanks goes to the master students, Hiwi's, and vocational trainee I mentored during these years and that contributed to the work presented in this thesis. *Sara Danielli*, *Nora Escher*, it was a pleasure working with you and I am excited to follow your scientific path. I am sure your PhD's will be strong. *Jonne van Dijk*, I had a great time working with and I wish you all the best for your future. Thank you also *Valeria Guidolin* for the great time we spent together in the lab. I am looking forward to see the final outcome of the research we initiated together.

Thanks to my friends who were always there from the early beginning. *Melissa Frick*, *Katharina Siebers*, *Melanie Stein*, *Julia Korzonek* our friendship is really something special and I hope we will be part of each other's life for a long long time. A big thank you also to *Christiane Ernst* and *Bianca Gmeiner* for their support along studies and beyond. I had a great time learning with and from you and I value you a lot as my friends. Thank you *Dr. Dorothee Dollenmayer*, not only for marrying into my family but also for all the fun times we had. You could give me advice in every situation and I am very happy to have you in my life. Special thanks also to *AnCeDoLuMaRe(Su)* for a great friendship. I have lovely memories with each single one of you and I am looking forward to hear more from you over zoom and in person. Thank you also *Thomas Ketterer* for the support throughout the years. Last but not least, to my lovely former roommates *Dr. Christian Stockinger*, *Lucas Bednorsch* and *Dr. Cécile Karrer*. You always made me feel like home.

An enormous Merci to *Mahmoud* and *Rokhi*. You welcomed me in your family and supported me throughout these years in an unbelievable manner. I never saw such great, openhearted, supportive persons and I can never thank you enough for all the great things you did for me. You contributed to my success more than you can imagine.

Arman, you were always there for me, understanding every situation. Your support and trust is the key to my success. I am extremely grateful that I can count on somebody like you. Life is only beautiful with you.

Lastly, and most of all, I would like to thank my *family* and my wonderful *parents*. Your support, patience, and motivation made me face the challenges along the way. Thank you for allowing me to pursue my interests and the trust you put in me. To my *grandparents* for their endless love and support. *Stefan* and *Valentina*, I am happy that I can count on such wonderful people. *Katharina* and *Philipp*, I am very proud to have such wonderful siblings. From day one, you were caring about me, supported me, pushed me and always had my back. Thank you to all of you for showing me every day what is important in life. This thesis is dedicated to you.

Table of Contents

Abstract	1
Zusammenfassung	4
Abbreviations	8
Chapter 1: Introduction	15
1.1 DNA damage in carcinogenesis	15
1.1.1 DNA as storage of genetic information	15
1.1.2 Sources and types of DNA damage	16
1.1.3 Consequences of DNA adducts	17
1.1.4 <i>O</i> ⁶ -alkylguanine adducts from N-nitroso compounds	19
1.1.5 Repair of <i>O</i> ⁶ -alkylguanine DNA adducts	20
1.1.6 DNA adducts as biomarkers	21
1.2 DNA adduct detection	22
1.2.1 Immunological Methods	22
1.2.2 Radiolabeling	23
1.2.3 Mass Spectrometry	24
1.3 Overview of thesis work	25
1.4 References	27
Chapter 2: Chemical mechanism of <i>O</i> ⁶ -carboxymethyldeoxy-guanosine formation from azaserine and abundance in cells	31
2.1 Abstract	33
2.2 Introduction	33
2.3 Experimental Procedure	36
2.4 Results	41
2.5 Discussion	49
2.6 Conclusion	51
2.7 References	52

Chapter 3: A combination of direct reversion and excision repair in cells reduces the mutagenic effects of DNA carboxymethylation	64
3.1 Abstract	66
3.2 Introduction	66
3.3 Results	68
3.4 Discussion and Future studies	79
3.5 Material and Methods	80
3.6 References	84
Chapter 4. The role of <i>O</i> ⁶ -methylguanine-DNA methyltransferase in the repair of the mutagenic DNA lesion <i>O</i> ⁶ -carboxymethyl-guanine in human colon epithelial cells	90
4.1 Abstract	92
4.2 Introduction	93
4.3 Material and methods	94
4.4 Results	96
4.5 Discussion	103
4.6 References	105
Chapter 5: Immunological and mass spectrometry-based approaches to determine thresholds of the mutagenic DNA adduct <i>O</i> ⁶ -methylguanine in vivo	108
Chapter 6: Summary and Outlook	127
6.1 References	131
Appendix I: Can foods or herbs alter the bioavailability of chemotherapy drugs?	134
Appendix II: Clinical evidence for pharmacokinetics-based herb-drug interactions with chemotherapy drugs	139
Appendix III: Clofarabine sensitises paediatric ETP-ALL to PR-104	161
Curriculum vitae	
<u>Error! Bookmark not defined.</u>	

Abstract

The structural integrity of nucleobases in DNA dramatically impacts cell viability, and chemical alteration via DNA adduct formation endangers genomic integrity. Exogenous and endogenous alkylating agents react with nucleophilic positions of DNA nucleobases to form DNA adducts. Alkylation of the O^6 -position of guanine results in altered capacity of the nucleobase for hydrogen bonding, and thereby disturbs DNA replication and genomic stability. Several cellular repair mechanisms exist to prevent genotoxic effects, but if left unrepaired, DNA adduct formation is considered a molecular initiating event in cancer development. N-nitroso compounds (NOCs) are known (carboxy)methylating agents inducing O^6 -carboxymethyldeoxyguanosine (O^6 -CMdG) and O^6 -methyldeoxyguanosine (O^6 -MedG). Both exogenous sources and endogenous formation contribute to human exposure to NOCs, associated with colorectal cancer. The work described in here addresses O^6 -guanine adduct formation by NOCs and linking the biological impact of carboxymethylated and methylated O^6 -guanine with the persistence of specific forms of DNA damage.

In *Chapter 1*, current knowledge of NOC-induced DNA adduct formation and its association with colon cancer is summarized. The focus is hereby O^6 -CMdG and O^6 -MedG occurrence and biological consequences. Further, a general introduction into DNA damage formation and cellular DNA damage response is provided. Finally, detection methods for DNA adducts in biological samples are discussed.

In *Chapter 2*, the use of L-azaserine as a model compound to study NOC exposure is highlighted. The chemical mechanism of L-azaserine-induced O^6 -CMdG formation was evaluated. Results indicated that hydrolysis of L-azaserine to L-serine is promoted by acid, and under physiological pH-conditions, L-azaserine is stable. Evidence for the formation of an O^6 -Ser-CMdG intermediate in azaserine-induced O^6 -CMdG formation was demonstrated for the first time. Further, a nano-liquid chromatography high resolution tandem mass spectrometry (nanoLC-hrMS2) method was developed to assess the persistence of O^6 -CMdG and O^6 -MedG in cells upon exposure to L-azaserine. Dose- and time-dependent formation of adducts were established, further characterizing L-azaserine induced O^6 -CMdG and O^6 -MedG formation. Results are anticipated to not only help future study design using L-azaserine to study NOC exposure but also shed light on NOC-induced DNA adduct formation in a biological matrix.

In *Chapter 3*, the impact of the two repair mechanisms, nucleotide excision repair (NER) and O^6 -methylguanine DNA methyltransferase (MGMT), on O^6 -CMdG-induced mutagenicity was assessed. Exposure of cells to L-azaserine resulted in decreased cell viability, increased mutagenicity and persistence of O^6 -CMdG adduct levels in MGMT-inhibited cells, thereby suggesting MGMT to be involved in mitigating biological consequences upon exposure to carboxymethylating agents. Further, sensitivity towards L-azaserine exposure was also demonstrated in NER-deficient cells. However, preliminary results assessing activity of NER on O^6 -CMdG were contradictory. Persistence of O^6 -CMdG adduct levels was more pronounced in MGMT-inhibited and NER-deficient cells compared to cells lacking activity in only one repair pathway, thereby suggesting that the interplay between NER and MGMT is

important for efficient cellular O^6 -CMdG damage response. Future studies investigating the contribution of NER and MGMT to O^6 -CMdG repair are suggested.

In *Chapter 4*, the involvement of the repair enzyme MGMT in O^6 -CMdG removal is demonstrated. Upon exposure to L-azaserine, cell viability, genotoxicity, and O^6 -MedG and O^6 -CMdG adduct levels were assessed in MGMT-deficient and MGMT-inhibited HCEC cells and compared to Wild type (WT) and MGMT-proficient cells, respectively. As quantified by nanoLC-hrMS², O^6 -MedG and O^6 -CMdG adduct levels persisted in MGMT-deficient and MGMT-inhibited HCEC cells. Further, MGMT-deficient cells revealed decreased cell viability and increased genotoxicity after exposure to L-azaserine compared to WT. Thus, the data support the hypothesis that highly active MGMT in colon epithelial cells confers protection against colorectal carcinogenesis initiated by exposure to methylating and carboxymethylating agents such as NOCs that are present in the diet.

In *Chapter 5*, dose-response relationships were established for O^6 -MeG adduct levels in various biological systems after exposure to increasing concentrations of methylating agents. Different analytical approaches were compared with regard to their sensitivity and specificity for the quantification of O^6 -MedG. A highly sensitive LC-MS/MS approach revealed improved sensitivity and specificity in O^6 -MeG quantification compared to the antibody-based methods immuno-slot blot and immunofluorescence microscopy, thereby allowing for better distinction at low adduct levels. Applying the LC-MS/MS approach, O^6 -MeG adducts could be detected in peripheral blood mononuclear cells exposed to clinically relevant doses of the methylating anticancer drug temozolomide (TMZ). Further, a genotoxic threshold for O^6 -MeG adduct levels was established by applying the LC-MS/MS approach to colonic and hepatic genomic DNA extracted from mice challenged with increasing concentrations of a methylating agent. Interestingly, MGMT-deficient mice revealed a linear dose response, supporting the current mechanistic understanding of the impact of cellular repair status on DNA adduct levels and the onset of carcinogenesis. The data further highlights the usage of LC-MS in DNA adduct quantification for biomonitoring approaches to assess therapeutic efficacy of alkylating agents but also to assess exposure to methylating agents.

In *Chapter 6*, the key findings of the thesis work are summarized and critically evaluated. Future studies are described to further improve the current understanding of NOC-induced DNA adduct formation and biological consequences. Results from these studies are anticipated to address an important gap in genotoxic risk assessment of NOC exposure.

The work presented in *Appendix I-III* is additional findings concerning factors that impact chemotherapy drug function. *Appendix I* summarizes available clinical data of well-studied examples of foods and herbal supplements that lower bioavailability of chemotherapy drugs, thereby suggesting that concomitant use should be avoided. Also, pre-clinical evidence for the anti-cancer activity of an herbal supplement is presented and critically discussed. *Appendix II* provides a broader perspective on clinical herb-drug interactions. Pharmacologically active compounds in foods and herbal supplements are presented and their impact on drug-metabolizing enzymes or transporters discussed with regard to altered drug-bioavailability. Results from clinical studies, combining the use of a single chemotherapy agent with a single herbal supplement and include pharmacokinetic monitoring, are presented. While pre-clinical

data suggest beneficial effects, clinical studies mostly reveal that concomitant use of herbal supplements with chemotherapy drugs results in lowered drug-bioavailability, thereby most likely reducing efficacy. To address the complexity of herb-drug interactions, it was suggested to monitor metabolic biomarkers in clinical studies and to screen for genetic polymorphisms of drug-metabolizing enzyme. Further, databases summarizing herb-drug interactions are anticipated to become a useful tool to guide decision making in clinical practice.

In *Appendix III*, the underlying mechanism for drug synergy in resistant cases of early T-cell precursor acute lymphoblastic leukemia (ETP-ALL) patient derived xenografts (PDXs) is elucidated. *In vivo* and *in vitro* results confirm synergistic effect of the alkylating agent and clinical pro-drug PR-104A with the antimetabolite clofarabine. The working hypothesis is that clofarabine inhibits the repair of PR-104A-derived interstrand crosslinks (ICLs) and the increased persistence of ICLs results in improved PR-104A activity. Assessing PR-104A derived DNA adducts in PDXs by mass spectrometry suggested candidate structures that persist under sensitive conditions, but the experimental variance associated with addressing individual adducts was high, thereby not allowing for a significant conclusion. Therefore, ICLs were assessed by the alkaline comet assay. Combinatorial treatment resulted in increased DNA damage and delayed ICL repair kinetics in resistant PDXs, further highlighting the potential of clofarabine to preserve PR-104A-induced DNA ICLs as basis for drug synergy. Future studies elucidating the mechanism for clofarabine-mediated suppression of ICL repair are suggested.

Zusammenfassung

Die Zellviabilität wird massgeblich von der strukturellen Integrität der Nukleobasen der DNA beeinflusst und jede chemische Modifizierung der DNA zu einem sogenannten DNA-Addukt stellt eine Gefahr für die genomische Stabilität dar. Exogene und endogene alkylierende Substanzen reagieren mit nukleophilen Positionen der DNA Nukleobasen und bilden DNA-Addukte. Die Alkylierung der O^6 -Position von Guanin verändert das Vermögen dieser Nukleobase, Wasserstoffbrücken auszubilden, und beeinträchtigt damit die DNA-Replikation und die genomische Stabilität. Es existieren verschiedene zelluläre Reparaturmechanismen, um genotoxischen Effekten vorzubeugen. Auf molekularer Ebene gelten nicht reparierte DNA-Addukte als initiiierendes Ereignis in der Krebsentstehung. N-Nitroso-Verbindungen sind bekannt als (carboxy)methylierende Verbindungen und induzieren O^6 -Carboxymethyldeoxyguanosin (O^6 -CMdG) und O^6 -Methyldeoxyguanosin (O^6 -MedG). Darmkrebs steht in Verbindung mit der Exposition von Menschen mit N-Nitroso-Verbindungen, welche sowohl exogenen als auch endogenen Ursprungs sein können. Die vorliegende Arbeit befasst sich mit der Bildung von O^6 -CMdG durch N-Nitroso-Verbindungen und verbindet die biologischen Konsequenzen von carboxymethyliertem und methyliertem O^6 -Guanin mit der Persistenz von bestimmten Formen von DNA-Schäden.

In *Kapitel 1* wird das gegenwärtige Wissen über die DNA-Adduktbildung durch N-Nitroso-Verbindungen und deren Assoziierung mit Darmkrebs zusammengefasst. Der Fokus liegt hierbei auf dem Vorkommen von O^6 -CMdG und O^6 -MedG und deren biologischen Konsequenzen. Des Weiteren wird in diesem Kapitel eine allgemeine Einführung in die DNA-Schadensbildung und die zelluläre DNA-Schadensantwort aufgeführt. Zum Schluss werden noch Detektionsmethoden für DNA-Addukte in biologischen Proben erläutert.

In *Kapitel 2* wird die Eignung von L-Azaserin als Musterverbindung, um die Exposition von N-Nitroso-Verbindungen zu studieren, hervorgehoben. Hierfür wurde der chemische Mechanismus der L-Azaserin-induzierten O^6 -CMdG-Bildung untersucht. Die Ergebnisse lassen darauf schliessen, dass die Hydrolyse von L-Azaserin zu L-Serin säurekatalysiert ist und dass L-Azaserin unter physiologischen pH-Bedingungen stabil ist. Es wurde zum ersten Mal ein O^6 -Ser-CMdG Intermediat in der von Azaserin induzierten O^6 -CMdG Bildung nachgewiesen. Ausserdem wurde eine Methode, die auf der Kopplung der Nano-Flüssigkeitschromatographie mit der hochauflösenden Tandem-Massenspektrometrie (nanoLC-hrMS²) basiert, entwickelt, um die Persistenz von O^6 -CMdG und O^6 -MedG nach der Exponierung von Zellen mit Azaserin bestimmen zu können. Es wurde eine konzentrations- und zeitabhängige Bildung von Addukten bestimmt, welche die durch L-Azaserin induzierte Bildung von O^6 -CMdG und O^6 -MedG näher charakterisieren. Es wird angenommen, dass die Ergebnisse die zukünftige Planung von Studien hinsichtlich der Exponierung mit N-Nitroso-Verbindungen erleichtern und die Bildung von DNA-Addukten durch N-Nitroso-Verbindungen in der biologischen Matrix erklären.

In *Kapitel 3* wird der Einfluss zweier Reparaturmechanismen, namentlich Nukleotid-exzision Reparatur (NER) und O^6 -Methylguanin-DNA-Methyltransferase (MGMT), auf die von O^6 -CMdG induzierte Mutagenität bestimmt. Die Exponierung von Zellen, welche in ihrer MGMT-Aktivität inhibiert waren, mit L-Azaserin resultierte in einer verminderten

Zellviabilität, einer gesteigerten Mutagenität und anhaltenden O^6 -CMdG-Adduktleveln. Diese Ergebnisse legen nahe, dass MGMT darin involviert ist, biologische Konsequenzen, welche sich aus einer Exponierung von carboxymethylierenden Substanzen ergeben, abzumildern. NER-defiziente Zellen waren ebenfalls sensitiv gegenüber einer Exponierung mit carboxymethylierenden Substanzen. Jedoch waren vorläufige Ergebnisse zur NER-Aktivität an O^6 -CMdG widersprüchlich. Verglichen mit Zellen, welche lediglich in einem Reparaturmechanismus defizient waren, war die Persistenz von O^6 -CMdG-Adduktleveln in MGMT-inhibierten und NER-defizienten Zellen stärker ausgeprägt. Diese Ergebnisse deuten an, dass das Zusammenspiel von NER und MGMT für eine effiziente O^6 -CMdG Schadensantwort wichtig ist. Es werden zukünftige Studien diskutiert, die den Beitrag von NER und MGMT zur O^6 -CMdG-Reparatur untersuchen.

In *Kapitel 4* wird aufgezeigt, dass MGMT an der Beseitigung von O^6 -CMdG involviert ist. Nach Exponierung mit L-Azaserin, wurden die Zellviabilität, die Genotoxizität und die Adduktlevel an O^6 -MeG und O^6 -CMdG in MGMT-defizienten und MGMT-inhibierten Darmepithelzellen bestimmt und mit den entsprechenden Daten in Wildtypzellen mit MGMT-Aktivität verglichen. Wie mit der nanoLC-hrMS² bestimmt wurde, sind die O^6 -MeG- und die O^6 -CMdG-Adduktlevel in MGMT-defizienten und MGMT-inhibierten Zellen persistent. Des Weiteren wiesen MGMT-defiziente Zellen im Vergleich zu Wildtypzellen eine verminderte Zellviabilität und eine gesteigerte Genotoxizität nach der Exponierung mit L-Azaserin auf. Demnach unterstützen die Ergebnisse die Hypothese, dass eine hochaktive MGMT in Darmepithelzellen diesen Schutz gegenüber Darmkrebsentstehung verleiht, welche von methylierenden und carboxymethylierenden Substanzen, darunter N-Nitroso-Verbindungen, welche auch in der Ernährung präsent sind, initiiert wird.

In *Kapitel 5* wurden Dosis-Wirkungs-Beziehungen für O^6 -MeG-Adduktlevel in verschiedenen biologischen Systemen nach deren Exponierung mit einer ansteigenden Konzentration von methylierenden Verbindungen nachgewiesen. Verschiedene analytische Methoden wurden hierbei hinsichtlich ihrer Sensitivität und Spezifität für die Quantifizierung von O^6 -MeG verglichen. Im Vergleich mit den Antikörper-basierten Methoden Immuno-Slot Blot und Immunofluoreszenz-Mikroskopie zeigte ein hoch sensitiver LC-MS/MS-Ansatz verbesserte Sensitivität und Spezifität für die Quantifizierung von O^6 -MeG auf und ermöglichte damit eine bessere Unterscheidung von niedrigen Adduktleveln. Mit der Verwendung dieses LC-MS/MS-Ansatzes konnten O^6 -MeG-Addukte in peripheren mononukleären Zellen, welche mit klinisch relevanten Dosen des methylierenden Antikrebsmittels Temozolomide (TMZ) exponiert wurden, nachgewiesen werden. Die LC-MS/MS-Methode wurde auch für die Analyse von Darm- und Leber-DNA von Mäusen angewendet, nachdem diese mit verschiedenen Konzentrationen einer methylierenden Substanz behandelt wurden, wobei ein genotoxischer Schwellenwert für O^6 -MeG-Adduktlevel etabliert wurde. Interessanter Weise wiesen Mäuse, welche defizient in MGMT waren, eine lineare Dosis-Wirkungs-Beziehung auf, was das derzeitige Verständnis vom Einfluss des zellulären Reparaturstatus auf DNA-Adduktlevel und auf den Beginn der Krebsentstehung befürwortet. Die Daten unterstreichen auch den Einsatz von LC-MS in der DNA-Adduktquantifizierung in Biomonitoring-Ansätzen zur Bestimmung der therapeutischen

Wirksamkeit von alkylierenden Verbindungen und zur Bestimmung der Exponierung mit methylierenden Verbindungen.

In *Kapitel 6* werden die wesentlichen Ergebnisse dieser Arbeit zusammengefasst und kritisch evaluiert. Es werden zukünftige Studien beschrieben, welche das derzeitige Verständnis der DNA-Adduktbildung durch N-Nitroso-Verbindungen, aber auch die biologischen Konsequenzen dieser Addukte weiter verbessern können. Es wird angenommen, dass die Ergebnisse dieser Studien einen wichtigen Beitrag zur genotoxischen Risikobewertung der Exponierung mit N-Nitroso-Verbindungen leisten.

Die Arbeiten in *Appendix I-III* befassen sich mit zusätzlichen Ergebnissen bezüglich einiger Faktoren, welche die Wirkung von Chemotherapeutika beeinflussen. In *Appendix I* werden verfügbare klinische Daten zu gut erforschten Beispielen an Lebensmitteln und pflanzlichen Nahrungsergänzungsmitteln, welche die Bioverfügbarkeit von Chemotherapeutika vermindern, zusammengefasst. Die Daten legen nahe, dass die gleichzeitige Einnahme vermieden werden sollte. Zusätzlich werden präklinische Hinweise auf eine Antikrebsaktivität eines pflanzlichen Nahrungsergänzungsmittels dargelegt und kritisch diskutiert. In *Appendix II* werden klinische Daten zur Wechselwirkung zwischen pflanzlichen Nahrungsergänzungsmitteln und Chemotherapeutika umfassender zusammengefasst. Pharmakologisch aktive Bestandteile in Lebensmitteln und pflanzlichen Nahrungsergänzungsmitteln werden aufgezeigt und deren Einfluss auf Enzyme, welche für die Metabolisierung und die Aufnahme von Medikamenten verantwortlich sind, diskutiert um darauf aufbauend die veränderte Bioverfügbarkeit der Chemotherapeutika zu erklären. Ergebnisse von klinischen Studien werden präsentiert, welche die Einnahme eines Chemotherapeutikums mit der Einnahme eines einzigen pflanzlichen Nahrungsergänzungsmittel kombinieren und pharmakokinetische Parameter überwachen. Während präklinische Daten förderliche Effekte durch die gleichzeitige Einnahme von pflanzlichen Nahrungsergänzungsmitteln vermuten lassen, zeigen klinische Studien größtenteils eine verminderte Bioverfügbarkeit von Chemotherapeutika auf, welche vermutlich wiederum deren Wirksamkeit beeinträchtigt. Um die Komplexität dieser Wechselwirkung präziser zu verstehen, wurde vorgeschlagen, metabolische Biomarker in klinischen Studien zu überwachen und genetische Polymorphismen in metabolisierenden Enzymen zu erfassen. Des Weiteren wird davon ausgegangen, dass Datenbanken, welche relevante Wechselwirkungen zwischen pflanzlichen Nahrungsergänzungsmitteln und Chemotherapeutika erfassen, wesentlich zur Entscheidungsfindung in der klinischen Praxis beitragen werden.

In *Appendix III* wird der Mechanismus untersucht, welcher die synergistische Wirkung zweier Chemotherapeutika in resistenten Fällen der akuten lymphoblastischen Leukämie in Patienten-abgeleiteten Xenografts (PDX) bestimmt. *In vivo* und *in vitro* Ergebnisse bestätigen einen synergistischen Effekt zwischen dem alkylierenden Agenz PR-104A und dem Antimetaboliten Clofarabin. Es wird davon ausgegangen, dass Clofarabin die Reparatur von DNA-Interstrand-Crosslinks (ICLs), welche von PR-104A induziert werden, inhibiert und somit über persistente ICL-Level die Aktivität von PR-104A verbessert. Die Untersuchung von PR-104A-induzierten DNA-Addukten in PDX ergab potentielle Kandidaten, welche unter sensitiven Bedingungen persistent sind, jedoch war die experimentelle Varianz zu groß und

erlaubte keine signifikanten Schlüsse. Deshalb wurden ICLs mit dem alkalischen Comet Assay erfasst. Die Kombination der zwei Chemotherapeutika in resistenten PDXs führte zu erhöhten DNA-Schäden und verzögerte ICL-Reparaturkinetiken. Die Ergebnisse unterstreichen das Vermögen von Clofarabin, die Reparatur von PR-104A-induzierten ICLs zu verhindern, und können somit die ermittelte synergistische Wirkung erklären. Es werden weitere Studien vorgeschlagen, welche die Unterdrückung der ICL-Reparatur durch Clofarabin untersuchen.

Abbreviations

A	Adenine
AAF	Acetylaminofluorene
ABL	Abelson murine leukemia
ACN	Acetonitrile
ADP	Adenosine 5` - diphosphate
AGC	Automatic gain control
AIC	5-aminoimidazole-4-carboxamide
AKR	Aldo-keto reductase
ALL	Acute lymphoblastic leukemia
AML	Acute myeloid leukemia
AOM	Azoxymethane
APNG	N-(N-acetyl)-l-prolyl-)N-nitrosoglycine
AUC	Area under the curve
B-ALL	B-cell acute lymphoblastic leukemia
BER	Base excision repair
BSA	Bovine serum albumin
C	Cytosine
CBD	Cannabidiol
CI	Confidence interval
CID	Collision-induced dissociation
CL	Clearance
CRC	Colorectal cancer
ctDNA	Calf thymus deoxyribonucleic acid
dsDNA	Double stranded deoxyribonucleic acid

ssDNA	Single stranded deoxyribonucleic acid
CYP450	Cytochrome P450 enzymes
DAD	Diode array detector
DDA	Data dependent acquisition
DDR	DNA damage response
DIA	Data independent acquisition
dG	Deoxyguanosine
DMSO	Dimethylsulfoxide
DNA	Deoxyribonucleic acid
dR	Deoxyribose
DSB	Double strand break
DTIC	Dacarbazine
EC	Effective concentration
EDTA	Ethylenediaminetetraacetic acid
ELISA	Enzyme-linked immunosorbent assay
EMA	European Medicines Agency
EMS	Ethyl methansulfonate
EMSA	Electrophoretic Mobility Shift Assay
ENU	Ethyl nitrosurea
ESI	Electrospray ionization
ETP-ALL	Early T-cell precursor ALL
eV	Electron volt
FA	Formic acid
FCS	Fetal calf serum
FDA	US Food and Drug Administration

FFPE	Formalin-fixed, paraffin-embedded
FWHM	Full width of half maximum
G	Guanine
GAPDH	Glyceraldehyde 3-phosphate dehydrogenase
GC	Gas chromatography
gg NER	Global-genome nucleotide excision repair
Gy	Gray
HCD	High-energy collisional dissociation
HCEC	Human colon epithelial cells
HCl	Hydrochloric acid
HPLC	High performance liquid chromatography
HPRT	Hypoxanthine-guanine phosphoribosyltransferase
HR	Homologous recombination
hrMS	High resolution mass spectrometry
IARC	International Agency for Research on Cancer
IC	Inhibitory concentration
ICLs	Interstrand crosslinks
IF	Immunofluorescence
IR	Ionizing radiation
ISB	Immuno-slot blot
IS	Internal standard
iv	Intravenous
KDA	Potassium diazoacetate
<i>KRAS</i>	Kirsten rat sarcoma viral oncogene homologue
LA	α -lipoic acid

LC-MS	Liquid chromatography-mass spectrometry
LC-MS/MS	Tandem LC-MS
LOD	Limit of detection
NOGEL	No observed genotoxic effect level
LOQ	Limit of quantification
MAM	Methylazoxymethanol
MeOH	Methanol
MGMT	<i>O</i> ⁶ -methylguanine DNA methyltransferase
MHz	Mega Hertz
MMR	Mismatch repair
MMS	Methyl methanesulfonate
MNNG	1-Methyl-3-nitro-1-nitrosoguanidine
MNU	methylnitrosurea
MTIC	Methyl-(triazen-1-yl)imidazole-4-carboxamide
NADPH	Nicotinamide adenine dinucleotide phosphate
NaOMe	Sodium methoxide
NCI	National cancer institute
NDMA	N-nitrosodimethylamine
NER	Nucleotide excision repair
NHEJ	Non-homologous end-joining
NH ₄ OAc	Ammonium acetate
NH ₄ OH	Ammonium hydroxide
NMR	Nuclear magnetic resonance
NNU	4-(methyl-nitrosamino)-1-3-pyridyl-1-butanone
NOC	N-nitroso compound

NOGC	N-nitrosoglycocholic acid
nd	Not detectable
nq	Not quantifiable
ns	Not significant
OATPs	Organic anion transporting polypeptides
8-oxoG	8-Oxoguanine
<i>O</i> ⁶ -AGT	<i>O</i> ⁶ -Alkylguanine DNA methyltransferase
<i>O</i> ⁶ -alkylGs	<i>O</i> ⁶ -Alkylguanines
<i>O</i> ⁶ -BG	<i>O</i> ⁶ -Benzylguanine
<i>O</i> ⁶ -CMdG	<i>O</i> ⁶ -Carboxymethyldeoxyguanosine
<i>O</i> ⁶ -CMG	<i>O</i> ⁶ -Carboxymethylguanine
<i>O</i> ⁶ -MedG	<i>O</i> ⁶ -Methyldeoxyguanosine
<i>O</i> ⁶ -MeG	<i>O</i> ⁶ -Methylguanine
OT	Orbitrap
PAH	Polycyclic aromatic hydrocarbon
PARP	Poly-ADP-ribose-polymerase
PBMCs	Peripheral blood mononuclear cells
PBS	Phosphate buffered saline
PCR	Polymerase chain reaction
PDL	Population doubling time
PDX	Patient-derived xenograft
PE	Plating efficiency
P-gp	P-glycoprotein
PRM	Parallel reaction monitoring
Rec	Recovery

RLU	Relative luminescence units
RNA	Ribonucleic acid
ROS	Reactive oxygen species
RP	Reversed phase
RSD	Relative standard deviation
RT	Retention time
RT-qPCR	Reverse transcription quantitative polymerase chain reaction
SD	Standard deviation
SEM	Standard error of the mean
shRNA	Small hairpin ribonucleic acid
S/N	Signal to noise
SN-38	7-ethyl-10-hydroxycamptothecin
SNP	Single nucleotide polymorphism
SPE	Solid phase extraction
SRM	Selected reaction monitoring
SSB	Single strand break
SJW	St. John's wort
6-TG	6-Thioguanine
T	Thymine
T-ALL	T-cell acute lymphoblastic leukemia
TBS	Tris-buffered saline
tc-NER	Transcription-coupled nucleotide excision repair
TEAA	Triethylammonium acetate
THC	Delta-9-tetrahydrocannabinol
TLS	Translesion DNA synthesis

Abbreviations

TMZ	Temozolomide
UDP	Uridine diphosphate
UGT	UDP-glucuronosyl-transferase
UPLC	Ultra-high pressure liquid chromatography
UV	Ultraviolet
V	Volt
WT	Wild type
XIC	Extracted Ion Chromatogram

Chapter 1: Introduction

1.1 DNA damage in carcinogenesis

1.1.1 DNA as storage of genetic information

Deoxyribonucleic acid (DNA) is essential to living organisms as it represents the storage of genetic information that is copied and passed to the next generation during reproduction. While first isolated in 1869,¹ the importance of DNA as the carrier of genetic information was only revealed 75 years later.² A milestone in DNA research was the discovery of its double helical structure in 1953,³ which was followed by elucidating the mechanisms of replication and translation of the genetic sequence into proteins.⁴ The DNA molecule consists of the four nucleobases that are covalently bound to deoxyribose to form nucleosides (Figure 1). The nucleosides are then covalently linked to a polynucleotide chain via the phosphate groups on the 3'OH and 5'OH of the deoxyribose. Two complementary polynucleotide chains are paired anti-parallel, meaning the 5'OH end of one strand is paired with the 3'OH end of its complementary strand, to form the DNA double helix. The helix is connected via hydrogen bonding of the four nucleobases, comprised of the two purine bases adenine and guanine, and the two pyrimidine bases thymine and cytosine. Each purine base pairs only with its complementary pyrimidine base on the other strand, meaning adenine pairs with thymine via two hydrogen bonds and guanine pairs with cytosine via three hydrogen bonds (Figure 1). The specific base pairing is crucial for the double helical structure of DNA and enables carrying and copying of the genetic information.⁴⁻⁵ The genetic information is stored in the order, or sequence, of the nucleobases along each strand. During transcription, this information is translated into ribonucleic acids (RNA), and subsequent into proteins. Hereby, a sequence of three bases encodes for a specific amino acid.⁶⁻⁷ Further, the genetic information is passed-on to progeny cells via replication, a process during which DNA is duplicated and divided into daughter cells. Essential for the transfer of genetic information is that the DNA double helix is copied correctly. DNA polymerases are responsible for the correct insertion of nucleobases into the new strand during replication.⁸ While DNA polymerases generally exhibit high fidelity in undamaged DNA, increased misincorporation rates are seen in damaged DNA contributing to replication errors.⁹ An insertion of a wrong base can have crucial consequences and lead to cancer and inflammation or cell death. In this chapter, sources and types of DNA damage will be presented and the subsequent consequences discussed.

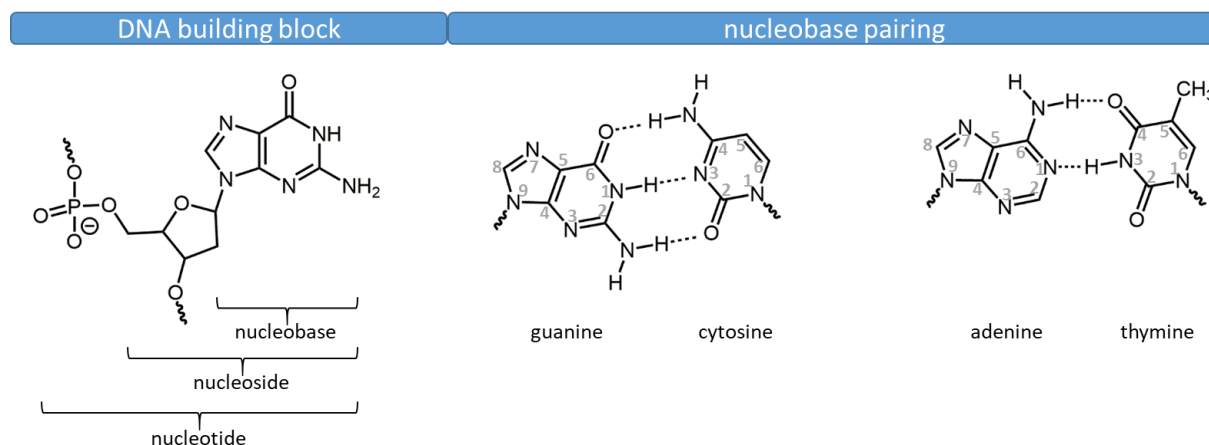


Figure 1. DNA building block and nucleobase pairing. Nucleotides are covalently linked via phosphate groups to a polynucleotide chain. Two complementary polynucleotide chains are paired anti-parallel via specific hydrogen bondings of the four nucleobases.

1.1.2 Sources and types of DNA damage

DNA is a reactive molecule and highly susceptible to chemical modifications induced by endogenous and exogenous sources.⁹⁻¹⁰ Endogenous DNA damage can arise from replication errors, spontaneous base deamination and abasic sites.¹¹ In addition, under oxidative stress, endogenously formed reactive oxygen species (ROS) can cause approximately 100 different oxidative base lesions and 2-deoxyribose modifications.^{9, 11} Further, ROS can attack the DNA backbone and oxidize lipid molecules that subsequently react with DNA. Besides oxygen, other small reactive molecules can cause endogenous DNA damage, e.g. S-adenosylmethionine (SAM), a co-substrate in enzymatic methyl transfer. As a methyl donor, it is involved in regulating gene expression via methylation but it can also methylate DNA non-enzymatically.¹¹ Endogenous single strand breaks (SSBs) resulting from oxidative damage (e.g. 2300 ROS-induced SSBs per cell per hour and 20,000 oxidative base damage per cell per day) and base hydrolysis (e.g. 10,000 depurinations per day per cell) occur at high frequency.^{9, 12, 11} During replication, SSBs can be converted to double strand breaks (DSBs) which occur less frequently but represent a serious threat to genomic stability

Exogenous sources of DNA damage are ultraviolet (UV) radiation, ionizing radiation (IR) and reactive chemicals that covalently bind to a chemical moiety to form DNA-adducts.⁹ Such alkylating agents are polycyclic aromatic hydrocarbons (PAH) and heterocyclic aromatic amines (HAA), N-nitroso compounds (NOCs) and mycotoxins that can be found in cigarette smoke, fuel and polluted air and food. Furthermore, some anticancer drugs rely on exogenous DNA adduct formation to fight cancer.¹³ Some of those chemicals require metabolic activation via enzymes, e.g. in the liver or from bacterial sources¹⁴⁻¹⁵, while others can directly attack DNA. This behavior can be reflected in the adduct type and the location where it occurs in the organism. Other forms of exogenous induced DNA damage include base dimerization, alkylated and oxidated lesions, SSBs and DSBs. UV light, mainly occurring from sunlight, primarily damages the DNA by causing pyrimidine dimers, which are covalent linkages between two adjacent pyrimidines.⁹ IR derived from environmental sources or medical devices can damage the DNA directly by inducing SSBs and in case of neighboring multiple damages sites, DSBs. In addition, IR can damage the DNA indirectly via

intracellular generated ROS. While ROS damages DNA via free radicals or reactive intermediates from lipid peroxidation, DNA adducts are mainly formed via alkylation of nucleophilic sites of the DNA bases by electrophilic alkylating agents.¹⁰ Therefore, oxidative and alkylated DNA damage occur at different sites of the DNA nucleoside.¹⁴ ROS damages DNA mainly carbons in the DNA bases or the 2-deoxyribose moiety. Purine bases (guanine, adenine) are oxidized at C^4 , C^5 and C^8 and pyrimidine (cytosine, thymine) bases mostly at C^5 and C^6 (Figure 1). DNA adducts induced by reactive electrophiles, arising from ROS-oxidized polyunsaturated fatty acids or alkylating agents, can be formed on different ring and exocyclic nitrogen and oxygen atoms. The most nucleophilic and therefore reactive positions are the N^3 and the N^7 of adenine and guanine, respectively. Next to nucleophilicity, steric factors also influence DNA adduct formation, e.g. the N^7 of guanine is exposed in the major groove of the DNA double helix and therefore is more accessible compared to positions in the minor groove, resulting in higher levels of N^7 -alkylated guanine.¹⁴ Some chemicals can react with two nucleophilic sites to form endocyclic adducts or in case of anticancer drugs, inter- and intrastrand crosslinks.¹⁶ The chemical stability between DNA adducts differ, e.g. linkage on the N^7 position creates a labile glycosidic linkage and results in the loss of the adducted base and formation of an apurinic site.¹⁴ Unrepaired DNA damage can interfere with DNA transcription and replication and result in inhibition of cell division, cell death and genomic instability.¹⁷⁻¹⁸

1.1.3 Consequences of DNA adducts

Unrepaired lesions can be a serious threat to genomic stability during replication.^{9, 19-20} Most of the DNA adducts induced by alkylating agents, including genotoxic anticancer agents, PAHs and HAAs, are direct steric hindrances to DNA polymerases and affect their progression. The stalling of the polymerase initiates DNA damage response (DDR) including cell cycle arrest and DNA repair. The main DNA repair pathways are non-homologous end joining (NHEJ) and homologous recombination (HR) for DSBs; base excision repair (BER) for simple base modifications; nucleotide excision repair (NER) for bulky adducts and interstrand-crosslinks (ICLs); and NHEJ, NER and HR for single strand breaks (SSBs).¹⁹ If the repair capacity of the cell is exceeded, most DNA base damage arising from oxidation and alkylation can trigger cell death.²⁰ However, prolonged polymerase stalling during replication can result in a collapse of the replication fork and subsequent to DSBs and genomic instability. As a damage tolerance mechanism, bypass of pre-toxic lesions by specific polymerases in translesion synthesis (TLS) prevents replication fork collapse. Polymerases involved in TLS exhibit lower fidelity, thereby resulting in higher misincorporation and mutagenicity rates. Some DNA adducts are already tolerated by normal replicative DNA polymerases but with a higher risk of misincorporation, e.g. for the oxidative damage 8-oxoguanine, DNA polymerases tend to favor the incorporation of adenine instead of cytosine.⁸ Insertion of the wrong base can still be repaired via mismatch repair (MMR). If not repaired, the misincorporation gets fixed during the next replication step in a mutation with loss of the genetic information.²⁰⁻²¹ In fact, a single-base substitution might be enough to disrupt the 3-nucleobase-code for an amino acid with subsequent loss of activity of the encoding protein.⁶⁻⁷ The accumulation of mutations in specific genes that control cell cycle progression are linked with excessive cell proliferation and subsequent can initiate carcinogenesis.²² Proto-oncogenes code for proteins that stimulate cell division but when mutated, can drive abnormal

cell proliferation. Tumor suppressor genes prevent inappropriate growth and an inactivating mutation can induce excessive cell proliferation.²³

The proto-oncogene *Kirsten RAS* (*KRAS*) encodes for a membrane protein involved in the regulation of multiple signal transduction pathways and thereby promoting cell cycle progression.²⁴ Activating point mutations in the proto-oncogene *KRAS* are found in many types of cancer, which include pancreatic cancer (> 80 % of cases), colon cancer (50 % of cases), lung cancer (10-30% of cases) and breast cancer (5-12.5 % of cases). The most two common mutations found in *KRAS* are GC to TA transversion and GC to AT transition mutations and they match the two most common mutations found in colorectal cancer.²⁵⁻²⁶ A carboxymethylating agent, inducing *O*⁶-carboxymethylguanine (*O*⁶-CMG, Figure 2) and *O*⁶-methylguanine (*O*⁶-MeG, Figure 2) was found to induce a similar mutation pattern to that found in colorectal cancer patients, with almost similar levels of GC to AT transition and GC to TA transversion mutations in the *p53* gene.²⁵ *In vitro* studies with DNA TLS polymerases and oligonucleotides containing *O*⁶-CMG confirmed that bypass of adduct by TLS results in misincorporation of an adenine or thymine.²⁷ Further, GC to AT transition mutations are well known to be induced by *O*⁶-substituted guanine adducts.²⁸ After alkylation, the *O*⁶-oxygen of guanine cannot longer be involved in hydrogen bonding, thereby explaining mutagenicity.²⁹ The mutation frequency is hereby decreasing with increasing alky length, probably as larger alky groups are able to block replication fork more efficiently thereby inducing DDR.³⁰ *O*⁶-MeG is a poor substrate for excision repair and can be readily bypassed.³⁰ It is believed that methylation at the *O*⁶-position of guanine confers the greatest mutagenic and carcinogenic potential.³¹ DNA polymerases tend to insert cytosine and thymine with similar efficiency opposite *O*⁶-MeG, resulting in GC to AT transition mutations.^{28, 32} While alkylation of the *N*⁷-position of guanine occurs more frequently (up to 70%), it seems to not be biologically relevant as no correlation between the extent of formation, mutagenicity and tumor frequency could be established.^{29, 33} Alkylation at the *O*⁶-position of guanine is minor, but based on the mutagenicity data presented, *O*⁶-CMG and *O*⁶-MeG seem to be highly biological relevant and therefore alkylating agents that can induce both of them, such as NOCs, represent a threat to genetic stability.³⁴⁻³⁷

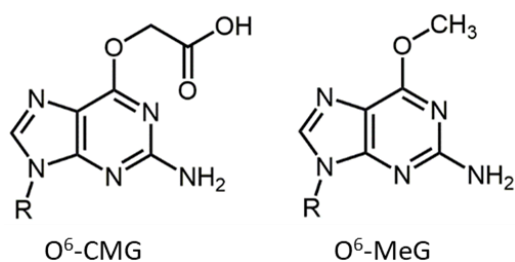


Figure 2. Chemical structure of *O*⁶-carboxymethylguanine (*O*⁶-CMG) and *O*⁶-methylguanine (*O*⁶-MeG).

1.1.4 *O*⁶-alkylguanine adducts from N-nitroso compounds

NOCs can be found in tobacco smoke, pharmaceuticals, cosmetics³⁸ and in dietary sources, with especially high concentrations in cured meat, smoked meat and fish, cheese and beer.³⁹ Next to exogenous sources, NOCs can be formed *in vivo* from nitrate and nitrite via acid catalyzed or bacterial nitrosation and via nitric oxide formation during inflammation⁴⁰. Endogenous formation accounts for approximately 75% of the total NOCs exposure.³⁸ NOCs consist of a nitroso group (-N=O) being bound to a nitrogen atom and are comprised by nitrosamines (R₁NNOR₂) and nitrosamides (R₁CONNOR₂). They are generally formed by the reaction of nitrites with secondary amines and N-alkylamides (Figure 3).⁴⁰ The first step of nitrosation involves the acidification of nitrite to form nitrous acid (HNO₂) and the following spontaneous decomposition to the nitrosating agents (as donor of NO⁺) N₂O₃ and N₂O₄ leads to the nitrosation of amines (Figure 3).⁴¹⁻⁴² Nitrosamides are preferably formed via the protonated nitrous acid.⁴⁰ The acidification needed for activation indicates that this reaction most likely takes place in the stomach. Sources of gastric nitrite are ingested nitrite from nitrite-preserved food (~20%) but the majority arises from the reduction of ingested or endogenous nitrate (~80%). The main dietary source of nitrate are vegetables and cured meat, and the main endogenous source is the L-arginine-NO pathways where NO is produced in excess by NO synthases as signaling molecule during inflammatory reactions and infections.^{40, 42} Ingested nitrate can be reduced by bacterial denitrification, a process that reduces nitrate to ammonium via nitrite.⁴² Bacterial denitrification via NO can also contribute to nitrite formation in an achlorhydric stomach.⁴⁰ Ascorbic acid and cysteine can inhibit bacterial nitrosation at neutral pH and might also inhibit NOCs formation from vegetables.⁴²⁻⁴³ Nitrosamines require metabolic activation by Cytochrome P450 enzymes (CYP450), mainly CYP2E1, to become alkylating agents. The mechanism is not fully understood but it is proposed that enzymatically formed alpha-hydroxynitrosamine spontaneously decomposes to yield alkylating agents via monoalkyl nitrosamine and alkyldiazonium ion (Figure 3).³⁴ Nitrosamides do not rely on enzymatic activation but can decompose spontaneously to similar alkylating species via chemical reactions.⁴² The alkyl moiety on the instable alkyldiazonium ion determines the alkyl length on the DNA adduct formed (Figure 3). NOCs form about 11 different methylated DNA base adducts (Figure 3), among 75 % are *N*³-methyladenine and *N*⁷-methylguanine, 6-10 % are *O*⁶-methylguanine and to a lower extent *O*⁴-methylthymine. Nitrosated glycine and bile acid derivatives result in carboxymethylated and methylated DNA bases.^{35 36-37, 43} Up to now, carboxymethylated guanine (*N*⁷, *O*⁶), adenine (*N*³, *N*⁶), cytosine (*N*⁴), thymine (*O*⁴ and *N*³) have been identified after NOC exposure, but only *O*⁶-CMdG, *O*⁶-CMdT and *N*³-CMdT were found to be mutagenic.⁴³⁻⁴⁴ Compared to other alkylating agents, NOCs produce a higher proportion of *O*⁶-alkylated damage correlating with the carcinogenic activity.^{33 34}

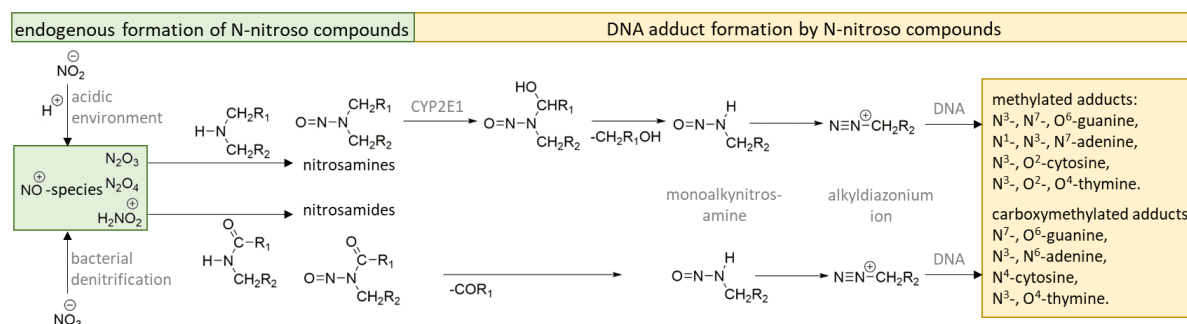


Figure 3. Endogenous formation of N-nitroso compounds and subsequent induction of DNA adducts. Nitrite and nitrate can be reduced to nitrosating agents that form nitrosamine and nitrosamides with secondary amines and N-alkylamides, respectively. While nitrosamines require metabolic activation by CYP enzymes, nitrosamides decompose spontaneously to form the reactive alkyldiazonium ion that alkylates DNA nucleobases.

The relevance of NOC compounds and formation of O^6 -CMdG and O^6 -MedG is indicated from several molecular epidemiology studies. Endogenous NOC-formation via nitrosation of amino acids catalyzed by heme iron in red meat seems to substantially increase the risk for colorectal cancer development.⁴⁵ Indeed, O^6 -CMG adducts could be detected in human blood samples after high red meat consumption,³⁷ in individual *in vitro* gastrointestinal digestion samples of different meat types⁴⁶ and in colonic exfoliated cells from human feces, with levels being elevated after high red meat diet compared to a vegetarian one.⁴⁷ Also, O^6 -CMG and O^6 -MeG adducts have been found in blood and tissue samples from colorectal cancer patients further highlighting the potential of NOC-induced adduct formation as an initiating step in colorectal cancer development.⁴⁸⁻⁵⁰ However, many molecular factors, such as related to the DDR, that influence the biological burden of these adducts or modulate individual cancer risk to etiological exposures remain unclear.

1.1.5 Repair of O^6 -alkylguanine DNA adducts

The protein O^6 -alkylguanine-DNA alkyltransferase (O^6 -AGT) is encoded by the gene *O^6*-methylguanine-DNA methyltransferase (*MGMT*). Often termed MGMT, it is a unique DNA repair enzyme for the direct reversal of O^6 -alkylated guanine adducts, highlighting the evolutionary importance for their repair. O^6 -AGT removes alkylating damage from guanine by transferring the alkyl group to a cysteine residue, most likely via attack of the thiolate anion on the alkyl group. It is thought that adjacent amino acids of O^6 -AGT are important for stabilizing the thiolate anion (histidine, lysine) and the DNA double helix (arginine) while the O^6 -alkylated guanine is flipped out into the binding pocket.⁵¹⁻⁵² The alkylated protein is inactive and is ubiquitinated and degraded, highlighting the importance of intrinsic basal O^6 -AGT levels in response to O^6 -alkylguanine damage. While in bacteria, O^6 -AGT protein expression is found to be dramatically increased after exposure to alkylating agents, the data on human O^6 -AGT protein expression is less clear, with levels most likely being dependent on tissue and individuals.⁵² Further, some human tumor cells do not show significant O^6 -AGT activity. O^6 -AGT preferably acts on O^6 -methylguanine in double stranded DNA, but larger alkyl groups like ethyl, n-butyl and isopropyl can also be removed.⁵³ The reaction rate decreases hereby with increasing alkyl length,⁵⁴ though, larger groups are better substrates for BER,^{53, 55} and also NER was found to be involved in repair of O^6 -alkylguanine-adducts.^{30, 56}

One exception is *O*⁶-Benzylguanine (*O*⁶-BG) that seems to be a good substrate for *O*⁶-AGT too and is often used as inhibitor of *O*⁶-AGT in cellular repair studies, but up to now this adduct was not detected *in vivo*. In the case of unrepaired *O*⁶-MeG, thymine misincorporation might take place during replication.^{28, 32} The mispair is recognized by MMR but as MMR itself is not able to repair the damaged guanine this can result in futile cycles of MMR with DSBs, cell death and genotoxicity as consequences.^{54, 57} Taken together, in concert with functional MMR, BER, and NER, MGMT has overlapping roles in protecting the genome from mutagenic and carcinogenic DNA lesions. While it is known that *O*⁶-AGT repairs *O*⁶-MeG, its activity on *O*⁶-CMG is not clear. In oligodeoxyribonucleotides containing *O*⁶-CMG, transfer of the carboxylgroup to cysteine in the active center of *O*⁶-AGT could be demonstrated by mass spectrometry (MS).⁵⁸ Data from ctDNA reacted with a nitroso compound revealed no transfer of the radiolabeled caboxymethylated group to *O*⁶-AGT, indicating that *O*⁶-AGT does not act on *O*⁶-CMG.⁵⁹ Further, cytotoxicity studies in repair deficient cells exposed to a carboxymethylating agent, suggest NER to be involved in *O*⁶-CMG repair rather than *O*⁶-AGT.⁶⁰

1.1.6 DNA adducts as biomarkers

In anticancer therapy, alkylating agents inducing a high DNA damage level are used to trigger apoptosis in rapidly dividing cells. It is thought that the high damage level will initiate DDR and result in apoptosis. Treatment resistance is linked with DNA damage repair, thereby reducing the DNA damage level. Indeed, in pre-clinical studies a positive correlation between drug-induced DNA adduct levels and response in cell lines, but also patient-derived xenografts and blood samples could be established for anticancer drugs targeting the DNA structure.⁶¹ Further research linking drug-derived DNA adducts with drug-response in clinical settings is needed to establish biomarker-based personalized therapy strategies in anticancer therapy. Overall, these data highlights the importance of DNA adducts formation on biological consequences. While in anticancer therapy cell death is wanted, formation of DNA adducts is also thought to be the initial step in cancer development. When DNA adducts are not repaired correctly alterations in the DNA sequence might occur during replication. Mutations that alter the expression or function of cell cycle regulating proteins can initiate lead to massive progression of cancer. Therefore, DNA adducts have the potential to be used as biomarkers to study exposure to genotoxic chemicals. But personal carcinogenic risk assessment on the basis of DNA adducts is difficult due to the various DNA adducts formed by one chemical, the multi-stage process of carcinogenesis and inter-individual variations in level of damage formation and removal. Further, the discussion on a genotoxic threshold for DNA adducts is still ongoing.¹⁷

Despite these difficulties, there are two specific examples of chemicals, where exposure, induced-DNA adducts and mutation spectra can explain the development of cancer: aflatoxin B1, a fungal toxicant known to induce liver cancer⁶² and aristolochic acid, used in traditional Chinese medicinal herb therapy and known to induce kidney cancer.^{14-15, 63} Both examples provide a fundamental mechanistic understanding of cancer development via chemical-induced DNA damage. However, the relationship between other exogenous DNA damaging chemicals and cancer development has not been elucidated despite the multitude of epidemiological evidence suggesting the chemical's involvement. One example is NOCs in

colorectal cancer. While red meat consumption is known to increase the risk for developing colorectal cancer,⁶⁴ the underlying mechanism is not yet defined but NOC-induced DNA adducts formation is widely discussed.^{40, 43, 45, 47, 65} The research of this thesis will help to understand formation and biological consequences of NOC-induced DNA adducts.

1.2 DNA adduct detection

The quantification and characterization of DNA adducts is of high importance to provide mechanistic information on the toxicological mode of action and for the risk assessment of human exposure to genotoxic chemicals.^{15, 66} Next to DNA adduct measurements in biomonitoring studies on exposure to environmental and dietary chemicals, the quantification of DNA adducts is also a valuable tool to assess the efficacy of anti-cancer agents in chemotherapy when DNA binding is the underlying mechanism of action.⁶¹ The ability to biomonitor many DNA adducts enables strategies for minimizing the risk of cancer and for patient stratification in personalized anti-cancer therapy.^{50, 61, 67} A major analytical challenge is that DNA adducts occur at a level of 0.1-1 adduct/ 10^8 unmodified nucleotides, therefore highly sensitive methodologies are needed. As human are exposed to numerous environmental and dietary genotoxins, specificity of the methodology is warranted. Further, in addition to exogenous sources, the same DNA adduct can be formed endogenously, and levels of exogenously vs endogenously formed DNA adducts do vary between individuals and type of DNA adduct.^{11, 15, 68} Distinguishing between exogenously and endogenously formed DNA adducts and thereby determining their impact on human health remains challenging. Generally, the total measurement of DNA adducts is considered an adequate indicator of genotoxicity, even when only some of these adducts are mutagenic.⁶⁶ The most common methods in DNA adduct analysis make use of antibody-based detection, radiolabeling or detection by m/z in a mass spectrometer (MS), often coupled with separation by liquid chromatography (LC).

1.2.1 Immunological Methods

Immunological methods for DNA adduct analysis rely on antibodies to detect and semi-quantify DNA adducts in fixed tissue samples (immunohistochemistry) and in extracted DNA using immunoassays, e.g the competitive enzyme-linked immunosorbent assay (ELISA) or the immuno slot blot technique.^{66, 68} The sensitivity is depending of the affinity of the antibody to the DNA adduct and is usually around 1 adduct/ 10^8 nucleotides.⁶⁹ This overall sensitivity in immunological methods is achieved by the amplification of the signal in the last detection step via biotinylated secondary antibodies in combination with a colorimetric, fluorescent or chemiluminescent detection. DNA adducts induced by aflatoxins, PAHs, UV light and oxidative stress as well as cisplatin and carboplatin could be detected in human samples by immunological methods.⁶⁹ While the throughput and costs for the assays are favourable, the development of the antibodies is time and cost intensive. Two types of antigens are used to generate animal-derived antibodies: carcinogen-modified DNA or synthesized DNA adduct attached to a larger protein.^{14, 66} Often antibodies exhibit cross-reactivity, therefore reducing the selectivity of the assays. Another limitation of the assays is the high amount of DNA needed (~200 μ g). Nonetheless, antibody based strategies are of

significant current interest as a basis of localization of DNA damage to regions in the genome on the basis of coupled sequencing methods.⁷⁰⁻⁷¹

1.2.2 Radiolabeling

Radiolabeling as a strategy for DNA adduct analysis is usually done by administering a ¹⁴C-radiolabeled compound to experimental animals or *in vitro* incubation of a ¹⁴C radiolabeled compound with purified DNA and, if needed, a metabolic activation system.¹⁸ DNA is extracted and labeled adducts are detected by liquid scintillation counting to quantify the total amount of radioactivity which is then compared to untreated control DNA.⁶⁸ Higher sensitivity is achieved by further processing the DNA prior to radioactivity measurement via enzymatic digestion and chromatographic separation. Critical for the detection of DNA adducts via radiolabeling is that the labeled part of the compound remains during metabolic activation and adduct formation. As the DNA structure does not need to be known ahead, radiolabeling has a great power in elucidating whether a compound forms DNA adducts.^{18, 66} The approach reveals high sensitivity as DNA adduct levels as low as 1 adduct/10⁹ nucleosides have been detected. Limitations are lack of specificity, as the chemical structure is not elucidated, and poor resolving capacity for distinguishing between different adducts. Also, selectivity is limited due to false positive results from background signals and insufficient DNA clean-up.⁶⁸ Furthermore, the synthesis of radiolabeled compounds is labor intensive, costly, and goes along with handling and disposal of radiohazards.

An alternative detection method for radiolabeled DNA adducts is accelerator mass spectrometry (AMS).⁶⁶ Here, DNA is converted to graphite and the ¹⁴C/¹³C isotope ratio measured via a specific set-up of two mass spectrometers equipped with a linking accelerator and a detector that identifies isotopes by their characteristic pattern of energy loss. High sensitivity with a detection limit of less than 1-10 adducts/10¹² nucleotides can be achieved by using a relatively small sample size (1-1000 µg DNA) and low chemical and radioisotope doses.¹⁸ These features enable studies to be performed safely in humans, using relevant (drug) doses, while generating little radioactive waste.⁶⁶ DNA adducts induced by the [¹⁴C] labeled anticancer drug tamoxifen could be detected in human colon samples.⁷² AMS does not provide any structural information and can provide false positive results in genomic DNA, arising from metabolic DNA incorporation in case of degrading compounds, or contamination by RNA and protein adducts.⁶⁸

Another methodology that employs radiolabeling is ³²P Postlabelling. Postlabeling refers to the radiolabeling of the adduct after its formation and therefore the methodology is applicable to human biomonitoring.¹⁴ DNA adducts following exposure to tobacco, the anticancer drug mitomycin C, the mycotoxin ochratoxin A, PAHs could be detected via ³²P postlabeling.⁶⁹ The methodology relies on the labeling of the 5'-position of adducts by polynucleotide kinase-mediated transfer of ³²P-orthophosphate from [γ -³²P] ATP and is usually comprised of four steps.^{66, 73} First, the DNA is extracted and enzymatically digested to nucleoside 3'-monophosphates. In the second step, the DNA adduct is enriched by solid phase extraction (SPE), immunoaffinity chromatography, high-pressure liquid chromatography (HPLC) or further enzymatic digestion. Then the ³²P-postlabeling of the DNA adduct occurs resulting in 5'-³²P-3'-bisphosphate adducts that are resolved by multidimensional thin layer

chromatography (TLC), HPLC or polyacrylamide gel electrophoresis (PAGE) and adduct levels are determined through quantification of radioactive decay by autoradiography or electronic imaging. The ^{32}P -postlabeling assay is a valuable tool in screening biological samples for DNA adducts. Only minimal DNA amount is required (1-10 μg), while achieving high sensitivity.⁶⁸ Limits of detection of up to 1 adduct/ 10^{10} nucleotides was reported, but sensitivity also depends on the selectivity of the enrichment method for the specific adduct and is usually better for aromatic adducts. Selectivity is further limited as the assay can provide false-negative results due to loss of adducts but also false-positive adducts due to postlabeling of endogenously formed adducts. In summary, radiolabeling is a good strategy to assess the covalent binding of a compound to DNA but further studies to characterize type of DNA adduct may be necessary.

1.2.3 Mass Spectrometry

Currently, the most effective technique for characterizing and quantifying DNA adducts in human samples is liquid chromatography- electrospray ionization coupled with high resolution or triple quadrupole tandem mass spectrometry (LC-ESI-hrMSⁿ, LC-ESI-QqQ-MS/MS).^{14-15, 17, 67 74} Mass spectrometer (MS) provides the highest level of structural identification, detecting DNA adducts on the basis of their molecular parent mass and, in case of tandem MS, fragment masses. When coupled with a chromatographic system to separate adducts and undamaged nucleosides, e.g. gas chromatography (GC) and liquid chromatography (LC), it offers ultimate chemical specificity.^{66, 68} Routinely, adducts are measured in the base or 2-deoxynucleoside form, but 2-deoxynucleotides and oligonucleotides can also be measured. Preparation of samples for LC-MS analysis involved DNA extraction followed by enzymatic digestion and sample enrichment via SPE, HPLC or immunoaffinity prior to analysis. Currently the principle method is LC coupled with electrospray ionization followed by mass analysis. For quantification the use of an internal labeled standard is needed, that is added to the sample prior preparation and accounts for samples losses and matrix effects. Synthesis of a labelled adduct can be cost and time intensive.

By measuring only targeted masses, a detection limit of 1 adduct/ 10^8 nucleotides can be achieved while using 1-100 μg DNA. Screening for unknown DNA adducts is limited due to insufficient sensitivity for detecting DNA adducts in human samples. Nanoflow chromatography coupled with ESI can improve the sensitivity due to improved ionization and diminution of ion suppression compared to normal flow.^{14, 17} Further, the application of the high resolution mass analyzer orbitrap has shown to improve sensitivity and selectivity compared to ion trap and triple quadrupole. Limit of detection of 1 adduct/ 10^{11} nucleotides was achieved, sufficient to detect the Benzoapyren-induced N^2 -dG adduct in human lung cancer samples.⁷⁵ Therefore, it is anticipated that high resolution LC-MSⁿ analyzers will be mostly contributing to assess global DNA damage in the field of DNA adductomics.¹⁵ Current approaches allow for the characterization of also unknown DNA adducts based on using common features of DNA adducts, e.g. neutral loss of deoxyribose upon collision induced fragmentation (CID). Data-dependent data acquisition (DDA) of top N ions or via targeted inclusion list or data-independent acquisition (DIA) with post-acquisition evaluation of DNA adduct features have been applied.¹⁴ Summarizing, LC-ESI-tandem mass spectrometry is a

powerful tool for detecting unknown and known DNA adducts and the field of DNA adductomics will further benefit from improved technology.^{15, 67, 76}

1.3 Overview of thesis work

The aim of the work presented in this thesis was to characterize formation and biological consequences of DNA adducts, mainly focusing on O^6 -CMdG and O^6 -MedG in the context of NOC exposure as a risk factor in colorectal cancer development. Elucidating chemical mechanism of NOC-induced O^6 -CMdG formation will help to identify strategies preventing from its formation. Knowledge of cellular responses to DNA damage is crucial for evaluating chemical hazards and enables biomarker-based risk stratification. It was possible to address formation and consequences of DNA adducts in biological samples by application of highly sensitive and specific mass spectrometry-based approaches.

In *Chapter 1*, a general introduction into DNA damage formation and cellular DNA damage response is provided. Of particular focus are the two pro-mutagenic DNA adducts O^6 -carboxymethyldeoxyguanosine (O^6 -CMdG) and O^6 -methyldeoxyguanosine (O^6 -MedG). Current knowledge on induction, repair and biological consequences is summarized, highlighting the correlation to NOC exposure and colon cancer risk. Further, methods for DNA adduct detection in biological samples are discussed, demonstrating the high potential of LC-MS/MS based strategies to characterize and quantify DNA adducts.

In *Chapter 2*, the chemical mechanism of O^6 -CMdG formation by azaserine, as a model compound for NOCs, was elucidated and the intermediate O^6 -Ser-CMdG was characterized for the first time. Further, acidic-promoted hydrolysis of azaserine to L-serine could be demonstrated as a second possible pathway for azaserine-induced O^6 -CMdG formation. A high-resolution tandem mass spectrometry (hrMS²) approach for the concomitant quantification of O^6 -CMdG and O^6 -MedG was developed to characterize adduct formation by azaserine in human colon epithelial cells (HCEC), as a model for human healthy colon tissue. Dose-dependent adduct formation was detected after short time exposure to azaserine, and time-dependent analysis revealed maximal adduct levels after 48 h followed by a steady state up to 120 h. Knowledge of L-azaserine-induced adduct formation has important implications regarding O^6 -CMdG formation and subsequent biological consequences.

In *Chapter 3*, the contribution of cellular repair pathways, namely NER and MGMT, to O^6 -CMdG persistence in cells and their contribution to the rise of DNA mutations was tested. Results demonstrated that the chemical inhibition of MGMT sensitises cells to the carboxymethylating agent azaserine by reducing cell viability and increasing the rate of DNA mutations. Measuring the level of O^6 -CMdG via hrMS² in azaserine-treated cells with varying MGMT capacity demonstrated that levels persisted in MGMT-inhibited cells, supporting the hypothesis that the increased mutagenicity might be due to lack of repair of O^6 -CMdG. Further, when MGMT was inhibited in NER deficient and respective WT cells, higher CMG levels were found compared to WT. However, additional studies on NER activation by O^6 -CMdG failed to confirm its direct function in repair, suggesting a need for future studies to clarify a potentially more complex cross-talk between these pathways.

In *Chapter 4*, the activity of MGMT on O^6 -CMdG was further explored in the specific context of human colorectal cells. Therefore, cytotoxicity, genotoxicity and O^6 -CMdG and O^6 -MedG adduct levels were assessed in HCEC cells with reduced MGMT activity after exposure to the carboxymethylating agent azaserine. Cells lacking MGMT were more susceptible to azaserine toxicity and DNA damage. Thus, O^6 -MedG and O^6 -CMdG persistence in cells lacking MGMT activity could be demonstrated, though fold increase in adduct levels compared to MGMT-proficient cells was higher for O^6 -MedG. The results suggest that MGMT indeed contributes to O^6 -CMdG repair in human colon cells, but less effectively than for O^6 -MedG.

In *Chapter 5*, currently available techniques to detect and quantify O^6 -MeG adducts in cells and murine tissues were compared after exposure to methylating agents, with a focus on their sensitivity and specificity. Immunofluorescence (IF) microscopy allowed for time- and dose-dependent detection of O^6 -MeG in cells and the immuno-slot-blot (ISB) assay for dose-dependent O^6 -MeG formation in genomic DNA isolated from cells and tissues. While both methods are semi-quantitative, an ultra-high pressure liquid chromatography-MS/MS (UHPLC-MS/MS) method allowed for absolute quantification of O^6 -MeG adduct levels in human cells and murine tissue samples (liver and colon). UPLC-MS/MS measurements and hockey-stick dose response modeling revealed a non-linear formation of hepatic and colonic O^6 -MeG adducts in WT, whereas linear O^6 -MeG formation without a threshold was observed in MGMT-deficient mice. Collectively, the UPLC-MS/MS analysis is highly sensitive and specific for O^6 -MeG, thereby allowing for the first time for the determination of a genotoxic threshold upon exposure to O^6 -methylating agents caused by the repair enzyme MGMT.

The work presented in *Appendix I-III* is additional findings concerning factors that impact chemotherapy drug function. In *Appendix I and II*, a basis for clinical evidence of food and herb-drug interactions are reviewed. Finally, in *Appendix III*, drug-induced DNA adducts were for the first time assessed in patient-derived xenografts to provide a mechanistic understanding for *in vivo* drug synergy for anticancer drugs in resistant cases.

1.4 References

1. Dahm, R., Friedrich Miescher and the discovery of DNA. *Developmental Biology* **2005**, 278 (2), 274-288.
2. Avery, O. T.; Macleod, C. M.; McCarty, M., Studies on the chemical nature of the substances inducing transformation of pneumococcal types: Induction of transformation by a desoxyribonucleic acid fraction isolated from pneumococcus type III. *J Exp Med* **1944**, 79 (2), 137-158.
3. Watson, J. D.; Crick, F. H. C., Molecular Structure of Nucleic Acids: A Structure for Deoxyribose Nucleic Acid. *Nature* **1953**, 171 (4356), 737-738.
4. Travers, A.; Muskhelishvili, G., DNA structure and function. *The FEBS Journal* **2015**, 282 (12), 2279-2295.
5. Alberts B, J. A., Lewis J, et al, *Molecular Biology of the Cell*. Garland Science: New York, 2002; Vol. 4th edition.
6. Brenner, S.; Benzer, S.; Barnett, L., Distribution of Proflavin-Induced Mutations in the Genetic Fine Structure. *Nature* **1958**, 182 (4641), 983-985.
7. Yanofsky, C., Establishing the Triplet Nature of the Genetic Code. *Cell* **2007**, 128 (5), 815-818.
8. Ganai, Rais A.; Johansson, E., DNA Replication—A Matter of Fidelity. *Molecular Cell* **2016**, 62 (5), 745-755.
9. Chatterjee, N.; Walker, G. C., Mechanisms of DNA damage, repair, and mutagenesis. *Environmental and molecular mutagenesis* **2017**, 58 (5), 235-263.
10. Gates, K. S., An overview of chemical processes that damage cellular DNA: spontaneous hydrolysis, alkylation, and reactions with radicals. *Chemical research in toxicology* **2009**, 22 (11), 1747-1760.
11. De Bont, R.; van Larebeke, N., Endogenous DNA damage in humans: a review of quantitative data. *Mutagenesis* **2004**, 19 (3), 169-185.
12. Tubbs, A.; Nussenzweig, A., Endogenous DNA Damage as a Source of Genomic Instability in Cancer. *Cell* **2017**, 168 (4), 644-656.
13. Metzler, M., DNA adducts of medicinal drugs: some selected examples. *Journal of Cancer Research and Clinical Oncology* **1986**, 112 (3), 210-215.
14. Hwa Yun, B.; Guo, J.; Bellamri, M.; Turesky, R. J., DNA adducts: Formation, biological effects, and new biospecimens for mass spectrometric measurements in humans. *Mass Spectrometry Reviews* **2020**, 39 (1-2), 55-82.
15. Balbo, S.; Turesky, R. J.; Villalta, P. W., DNA Adductomics. *Chemical Research in Toxicology* **2014**, 27 (3), 356-366.
16. Fu, D.; Calvo, J. A.; Samson, L. D., Balancing repair and tolerance of DNA damage caused by alkylating agents. *Nat Rev Cancer* **2012**, 12, 104.
17. Singh, R.; Farmer, P. B., Liquid chromatography-electrospray ionization-mass spectrometry: the future of DNA adduct detection. *Carcinogenesis* **2005**, 27 (2), 178-196.
18. Himmelstein, M. W.; Boogaard, P. J.; Cadet, J.; Farmer, P. B.; Kim, J. H.; Martin, E. A.; Persaud, R.; Shuker, D. E. G., Creating context for the use of DNA adduct data in cancer risk assessment: II. Overview of methods of identification and quantitation of DNA damage. *Critical Reviews in Toxicology* **2009**, 39 (8), 679-694.
19. Hoeijmakers, J. H., DNA damage, aging, and cancer. *N Engl J Med* **2009**, 361 (15), 1475-85.
20. Roos, W. P.; Thomas, A. D.; Kaina, B., DNA damage and the balance between survival and death in cancer biology. *Nat Rev Cancer* **2016**, 16 (1), 20-33.
21. Eoff, R. L.; Choi, J.-Y.; Guengerich, F. P., Mechanistic Studies with DNA Polymerases Reveal Complex Outcomes following Bypass of DNA Damage. *Journal of Nucleic Acids* **2010**, 2010, 830473.
22. Pitot, H. C., The molecular biology of carcinogenesis. *Cancer* **1993**, 72 (3 Suppl), 962-70.
23. Weinberg, R. A., How cancer arises. *Scientific American* **1996**, 275 (3), 62-70.
24. Jančík, S.; Drábek, J.; Radzioch, D.; Hajdúch, M., Clinical Relevance of KRAS in Human Cancers. *Journal of Biomedicine and Biotechnology* **2010**, 2010, 150960.
25. Gottschalg, E.; Scott, G. B.; Burns, P. A.; Shuker, D. E., Potassium diazoacetate-induced p53 mutations in vitro in relation to formation of O6-carboxymethyl- and O6-methyl-2'-deoxyguanosine DNA adducts: relevance for gastrointestinal cancer. *Carcinogenesis* **2007**, 28 (2), 356-62.
26. Andreyev, H. J.; Norman, A. R.; Cunningham, D.; Oates, J.; Dix, B. R.; Iacopetta, B. J.; Young, J.; Walsh, T.; Ward, R.; Hawkins, N.; Beranek, M.; Jandik, P.; Benamouzig, R.; Jullian, E.; Laurent-Puig, P.; Olschwang, S.; Muller, O.; Hoffmann, I.; Rabes, H. M.; Zietz, C.; Troungos, C.; Valavanis, C.; Yuen, S. T.; Ho, J. W.; Croke, C. T.; O'Donoghue, D. P.; Giaretti, W.; Rapallo, A.; Russo, A.; Bazan, V.; Tanaka, M.; Omura, K.; Azuma, T.; Ohkusa, T.; Fujimori, T.; Ono, Y.; Pauly, M.; Faber, C.; Glaesener, R.; de Goeij, A. F.; Arends, J. W.; Andersen, S. N.; Lövig, T.; Breivik, J.; Gaudernack, G.; Clausen, O. P.; De Angelis, P. D.; Meling, G. I.; Rognum, T. O.; Smith, R.; Goh, H. S.; Font, A.; Rosell, R.; Sun, X. F.; Zhang, H.; Benhattar, J.; Losi, L.; Lee, J. Q.; Wang, S. T.; Clarke, P. A.; Bell, S.; Quirke, P.; Bubb, V. J.; Piris, J.; Cruickshank, N. R.; Morton, D.; Fox, J.

C.; Al-Mulla, F.; Lees, N.; Hall, C. N.; Snary, D.; Wilkinson, K.; Dillon, D.; Costa, J.; Pricolo, V. E.; Finkelstein, S. D.; Thebo, J. S.; Senagore, A. J.; Halter, S. A.; Wadler, S.; Malik, S.; Krtolica, K.; Urošević, N.; Kirsten ras mutations in patients with colorectal cancer: the 'RASCAL II' study. *British journal of cancer* **2001**, *85* (5), 692-696.

27. Rätz, M. H.; Dexter, H. R.; Millington, C. L.; van Loon, B.; Williams, D. M.; Sturla, S. J., Bypass of Mutagenic O(6)-Carboxymethylguanine DNA Adducts by Human Y- and B-Family Polymerases. *Chem Res Toxicol* **2016**, *29* (9), 1493-503.

28. Pauly, G. T.; Moschel, R. C., Mutagenesis by O6-Methyl-, O6-Ethyl-, and O6-Benzylguanine and O4-Methylthymine in Human Cells: Effects of O6-Alkylguanine-DNA Alkyltransferase and Mismatch Repair. *Chemical Research in Toxicology* **2001**, *14* (7), 894-900.

29. Loveless, A., Possible Relevance of O-6 Alkylation of Deoxyguanosine to the Mutagenicity and Carcinogenicity of Nitrosamines and Nitrosamides. *Nature* **1969**, *223* (5202), 206-207.

30. Du, H.; Wang, P.; Li, L.; Wang, Y., Repair and translesion synthesis of O6-alkylguanine DNA lesions in human cells. *Journal of Biological Chemistry* **2019**, *294* (29), 11144-11153.

31. Warren, J. J.; Forsberg, L. J.; Beese, L. S., The structural basis for the mutagenicity of O⁶-methylguanine lesions. *Proceedings of the National Academy of Sciences* **2006**, *103* (52), 19701-19706.

32. Loechler, E. L.; Green, C. L.; Essigmann, J. M., In vivo mutagenesis by O6-methylguanine built into a unique site in a viral genome. *Proceedings of the National Academy of Sciences* **1984**, *81* (20), 6271-6275.

33. Montesano, R.; Pegg, A. E.; Margison, G. P., Alkylation of DNA and carcinogenicity of N-nitroso compounds. *Journal of toxicology and environmental health* **1980**, *6* (5-6), 1001-8.

34. Guttenplan, J. B., Effects of pH and Structure on the Mutagenic Activity of N-Nitroso Compounds. In *Genotoxicology of N-Nitroso Compounds*, Rao, T. K.; Lijinsky, W.; Epler, J. L., Eds. Springer US: Boston, MA, 1984; pp 59-90.

35. Harrison, K. L.; Jukes, R.; Cooper, D. P.; Shuker, D. E. G., Detection of Concomitant Formation of O6-Carboxymethyl- and O6-Methyl-2'-deoxyguanosine in DNA Exposed to Nitrosated Glycine Derivatives Using a Combined Immunoaffinity/HPLC Method. *Chemical Research in Toxicology* **1999**, *12* (1), 106-111.

36. Shuker, D. E. G.; Margison, G. P., Nitrosated Glycine Derivatives as a Potential Source of O⁶-Methylguanine in DNA. *Cancer research* **1997**, *57* (3), 366-369.

37. Cupid, B. C.; Zeng, Z.; Singh, R.; Shuker, D. E. G., Detection of O6-Carboxymethyl-2'-deoxyguanosine in DNA Following Reaction of Nitric Oxide with Glycine and in Human Blood DNA Using a Quantitative Immunoslot Blot Assay. *Chemical Research in Toxicology* **2004**, *17* (3), 294-300.

38. Tricker, A. R., N-nitroso compounds and man: sources of exposure, endogenous formation and occurrence in body fluids. *Eur J Cancer Prev* **1997**, *6* (3), 226-268.

39. Stuff, J. E.; Goh, E. T.; Barrera, S. L.; Bondy, M. L.; Forman, M. R., Construction of an N-nitroso database for assessing dietary intake. *Journal of Food Composition and Analysis* **2009**, *22*, S42-S47.

40. Mirvish, S. S., Role of N-nitroso compounds (NOC) and N-nitrosation in etiology of gastric, esophageal, nasopharyngeal and bladder cancer and contribution to cancer of known exposures to NOC. *Cancer letters* **1995**, *93* (1), 17-48.

41. Mirvish, S. S., Formation of N-nitroso compounds: Chemistry, kinetics, and in vivo occurrence. *Toxicology and Applied Pharmacology* **1975**, *31* (3), 325-351.

42. Lundberg, J. O.; Weitzberg, E.; Cole, J. A.; Benjamin, N., Nitrate, bacteria and human health. *Nature Reviews Microbiology* **2004**, *2* (7), 593-602.

43. Wang, J.; Wang, Y., Carboxymethylation of DNA Induced by N-Nitroso Compounds and Its Biological Implications. *Advances in Molecular Toxicology* **2011**, *5*, 219-243.

44. Wu, J.; Wang, P.; Li, L.; Williams, N. L.; Ji, D.; Zahurancik, W. J.; You, C.; Wang, J.; Suo, Z.; Wang, Y., Replication studies of carboxymethylated DNA lesions in human cells. *Nucleic Acids Research* **2017**, *45* (12), 7276-7284.

45. Cross, A. J.; Ferrucci, L. M.; Risch, A.; Graubard, B. I.; Ward, M. H.; Park, Y.; Hollenbeck, A. R.; Schatzkin, A.; Sinha, R., A Large Prospective Study of Meat Consumption and Colorectal Cancer Risk: An Investigation of Potential Mechanisms Underlying this Association. *Cancer research* **2010**, *70* (6), 2406-2414.

46. Bussche, J. V.; Hemeryck, L. Y.; Van Hecke, T.; Kuhnle, G. G. C.; Pasmans, F.; Moore, S. A.; Van de Wiele, T.; De Smet, S.; Vanhaecke, L., O6-carboxymethylguanine DNA adduct formation and lipid peroxidation upon in vitro gastrointestinal digestion of haem-rich meat. *Molecular Nutrition & Food Research* **2014**, *58* (9), 1883-1896.

47. Lewin, M. H.; Bailey, N.; Bandaletova, T.; Bowman, R.; Cross, A. J.; Pollock, J.; Shuker, D. E. G.; Bingham, S. A., Red Meat Enhances the Colonic Formation of the DNA Adduct O⁶-Carboxymethyl Guanine: Implications for Colorectal Cancer Risk. *Cancer research* **2006**, *66* (3), 1859-1865.

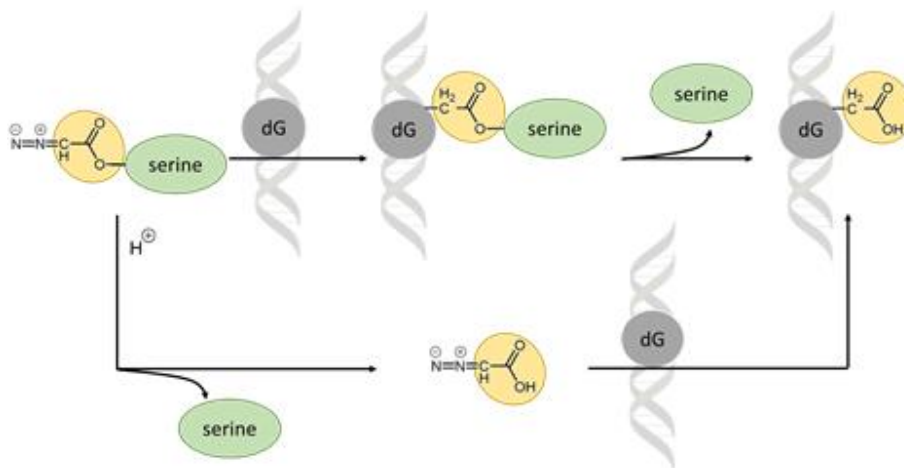
48. Hall, C. N.; Badawi, A. F.; O'Connor, P. J.; Saffhill, R., The detection of alkylation damage in the DNA of human gastrointestinal tissues. *Br J Cancer* **1991**, *64* (1), 59-63.

49. O6-methylguanine in blood leucocyte DNA: an association with the geographic prevalence of gastric cancer and with low levels of serum pepsinogen A, a marker of severe chronic atrophic gastritis. The EUROGAST Study Group. *Carcinogenesis* **1994**, *15* (9), 1815-20.

50. Hemeryck, L. Y.; Decloedt, A. I.; Vanden Bussche, J.; Geboes, K. P.; Vanhaecke, L., High resolution mass spectrometry based profiling of diet-related deoxyribonucleic acid adducts. *Analytica Chimica Acta* **2015**, *892*, 123-131.
51. Duguid, E. M.; Rice, P. A.; He, C., The structure of the human AGT protein bound to DNA and its implications for damage detection. *Journal of molecular biology* **2005**, *350* (4), 657-66.
52. Pegg, A. E., Repair of O(6)-alkylguanine by alkyltransferases. *Mutat Res* **2000**, *462* (2-3), 83-100.
53. Pegg, A. E.; Byers, T. L., Repair of DNA containing O6-alkylguanine. *FASEB journal : official publication of the Federation of American Societies for Experimental Biology* **1992**, *6* (6), 2302-10.
54. Kaina, B.; Christmann, M.; Naumann, S.; Roos, W. P., MGMT: Key node in the battle against genotoxicity, carcinogenicity and apoptosis induced by alkylating agents. *DNA repair* **2007**, *6* (8), 1079-1099.
55. Wirtz, S.; Nagel, G.; Eshkind, L.; Neurath, M. F.; Samson, L. D.; Kaina, B., Both base excision repair and O6-methylguanine-DNA methyltransferase protect against methylation-induced colon carcinogenesis. *Carcinogenesis* **2010**, *31* (12), 2111-2117.
56. Bronstein, S. M.; Skopek, T. R.; Swenberg, J. A., Efficient repair of O6-ethylguanine, but not O4-ethylthymine or O2-ethylthymine, is dependent upon O6-alkylguanine-DNA alkyltransferase and nucleotide excision repair activities in human cells. *Cancer research* **1992**, *52* (7), 2008-11.
57. Mojas, N.; Lopes, M.; Jiricny, J., Mismatch repair-dependent processing of methylation damage gives rise to persistent single-stranded gaps in newly replicated DNA. *Genes Dev* **2007**, *21* (24), 3342-55.
58. Senthong, P.; Millington, C. L.; Wilkinson, O. J.; Marriott, A. S.; Watson, A. J.; Reamtong, O.; Evers, C. E.; Williams, D. M.; Margison, G. P.; Povey, A. C., The nitrosated bile acid DNA lesion O6-carboxymethylguanine is a substrate for the human DNA repair protein O6-methylguanine-DNA methyltransferase. *Nucleic Acids Research* **2013**, *41* (5), 3047-55.
59. Shuker, D. E. G.; Margison, G. P., Nitrosated Glycine Derivatives as a Potential Source of O⁶-Methylguanine in DNA. *Cancer research* **1997**, *57* (3), 366.
60. O'Driscoll, M.; Macpherson, P.; Xu, Y.-Z.; Karran, P., The cytotoxicity of DNA carboxymethylation and methylation by the model carboxymethylating agent azaserine in human cells. *Carcinogenesis* **1999**, *20* (9), 1855-1862.
61. Stornetta, A.; Zimmermann, M.; Cimino, G. D.; Henderson, P. T.; Sturla, S. J., DNA Adducts from Anticancer Drugs as Candidate Predictive Markers for Precision Medicine. *Chem Res Toxicol* **2017**, *30* (1), 388-409.
62. Smela, M. E.; Currier, S. S.; Bailey, E. A.; Essigmann, J. M., The chemistry and biology of aflatoxin B(1): from mutational spectrometry to carcinogenesis. *Carcinogenesis* **2001**, *22* (4), 535-45.
63. Grollman, A. P.; Shibutani, S.; Moriya, M.; Miller, F.; Wu, L.; Moll, U.; Suzuki, N.; Fernandes, A.; Rosenquist, T.; Medverec, Z.; Jakovina, K.; Brdar, B.; Slade, N.; Turesky, R. J.; Goodenough, A. K.; Rieger, R.; Vukelić, M.; Jelaković, B., Aristolochic acid and the etiology of endemic (Balkan) nephropathy. *Proc Natl Acad Sci U S A* **2007**, *104* (29), 12129-34.
64. Bouvard, V.; Loomis, D.; Guyton, K. Z.; Grosse, Y.; Ghissassi, F. E.; Benbrahim-Tallaa, L.; Guha, N.; Mattock, H.; Straif, K., Carcinogenicity of consumption of red and processed meat. *The Lancet Oncology* **2015**, *16* (16), 1599-1600.
65. Thomson CA, L. K., Newton TR, et al, Nutrition and diet in the development of gastrointestinal cancer. *Curr Oncol Rep* **2003**, *5*, 192-202.
66. Brown, K., Methods for the Detection of DNA Adducts. In *Genetic Toxicology: Principles and Methods*, Parry, J. M.; Parry, E. M., Eds. Springer New York: New York, NY, 2012; pp 207-230.
67. Chang, Y.-J.; Cooke, M. S.; Hu, C.-W.; Chao, M.-R., Novel approach to integrated DNA adductomics for the assessment of in vitro and in vivo environmental exposures. *Archives of Toxicology* **2018**, *92* (8), 2665-2680.
68. Phillips, D. H.; Farmer, P. B.; Beland, F. A.; Nath, R. G.; Poirier, M. C.; Reddy, M. V.; Turteltaub, K. W., Methods of DNA adduct determination and their application to testing compounds for genotoxicity. *Environmental and molecular mutagenesis* **2000**, *35* (3), 222-233.
69. Poirier, M. C.; Weston, A., Human DNA adduct measurements: state of the art. *Environmental Health Perspectives* **1996**, *104* (suppl 5), 883-893.
70. Hu, J.; Lieb, J. D.; Sancar, A.; Adar, S., Cisplatin DNA damage and repair maps of the human genome at single-nucleotide resolution. *Proc Natl Acad Sci U S A* **2016**, *113* (41), 11507-11512.
71. Hu, J.; Adar, S.; Selby, C. P.; Lieb, J. D.; Sancar, A., Genome-wide analysis of human global and transcription-coupled excision repair of UV damage at single-nucleotide resolution. *Genes Dev* **2015**, *29* (9), 948-60.
72. Brown, K.; Tompkins, E. M.; Boocock, D. J.; Martin, E. A.; Farmer, P. B.; Turteltaub, K. W.; Ubick, E.; Hemingway, D.; Horner-Glister, E.; White, I. N. H., Tamoxifen Forms DNA Adducts in Human Colon after Administration of a Single [¹⁴C]-Labeled Therapeutic Dose. *Cancer research* **2007**, *67* (14), 6995-7002.
73. Randerath, K.; Randerath, E., 32P-Postlabeling Methods for DNA Adduct Detection: Overview and Critical Evaluation. *Drug Metabolism Reviews* **1994**, *26* (1-2), 67-85.

74. Liu, S.; Wang, Y., Mass spectrometry for the assessment of the occurrence and biological consequences of DNA adducts. *Chemical Society reviews* **2015**, *44* (21), 7829-7854.
75. Villalta, P. W.; Hochalter, J. B.; Hecht, S. S., Ultrasensitive High-Resolution Mass Spectrometric Analysis of a DNA Adduct of the Carcinogen Benzo[a]pyrene in Human Lung. *Anal Chem* **2017**, *89* (23), 12735-12742.
76. Balbo, S.; Hecht, S. S.; Upadhyaya, P.; Villalta, P. W., Application of a High-Resolution Mass-Spectrometry-Based DNA Adductomics Approach for Identification of DNA Adducts in Complex Mixtures. *Analytical Chemistry* **2014**, *86* (3), 1744-1752.

Chapter 2: Chemical mechanism of O⁶-carboxymethyldeoxyguanosine formation from azaserine and abundance in cells



Manuscript in preparation

Geisen S.M., Escher N., Aloisi C.M.N., Sturla S.J.

Geisen S.M. designed the study, established and performed the mass spectrometry analysis and L-azaserine-stability studies, evaluated and interpreted the data and wrote the manuscript. Escher N. performed cell culture work and evaluated the data. Aloisi C.M.N. performed cell culture work and interpreted the data. Sturla S.J. conceived the research, interpreted data, and wrote the manuscript.

**Chemical mechanism of O^6 -carboxymethyldeoxyguanosine
formation from L-azaserine and abundance in cells**

Susanne M. Geisen[†], Nora Escher[†], Claudia M.N. Aloisi[†], Shana J. Sturla^{†}*

[†]Department of Health Science and Technology, ETH Zurich, 8092 Zurich, Switzerland

*Corresponding author: Shana J. Sturla, Email: sturlas@ethz.ch

2.1 Abstract

N-nitroso compounds (NOCs) are genotoxic carcinogens that form pro-mutagenic O⁶-alkylguanine DNA adducts. In particular, the O⁶-alkylguanine adducts O⁶-carboxymethyldeoxyguanosine (O⁶-CMdG) and O⁶-methyldeoxyguanosine (O⁶-MedG) have been detected at elevated levels in blood and tissue samples from colorectal cancer patients and from healthy volunteers after consuming red meat. The diazo compound L-azaserine is an active decomposition product of corresponding NOCs and induces O⁶-CMdG and O⁶-MedG in cells. Despite the use of L-azaserine as a chemical probe in cellular studies concerning DNA damage since 1977, there remain gaps in knowledge concerning the chemical basis of DNA adduct formation by L-azaserine. To characterize O⁶-CMdG formation by L-azaserine, we carried out a combination of cell-free and cell-based stability and reactivity studies supported by liquid chromatography tandem mass spectrometry for the simultaneous quantification of O⁶-CMdG and O⁶-MedG. We found that L-azaserine is hydrolytically stable under physiological and alkaline conditions but undergoes acid-catalyzed hydrolysis. We gained, for the first time, evidence that L-azaserine therefore can react directly with deoxyguanosine to form an O⁶-Ser-CMdG intermediate, and that this intermediate spontaneously decomposes to form O⁶-CMdG. Finally, we characterized the formation of O⁶-CMdG and O⁶-MedG in a human cell line exposed to L-azaserine, and found maximal O⁶-CMdG adduct levels after 48 h. The findings of this work elucidate the chemical basis of how azaserine gives rise to DNA damage and support its use as a chemical probe for NOC exposure in carcinogenesis research, particularly concerning the identification of pathways and factors that promote adduct formation.

2.2 Introduction

The structural integrity of nucleobases in DNA is essential for the correct functioning of cellular processes. The reaction of DNA with electrophilic exogenous and endogenous chemicals can result in chemical adduction products, namely DNA adducts, that can trigger processes of mutagenesis and carcinogenesis. The DNA adducts O⁶-carboxymethyldeoxyguanosine (O⁶-CMdG) and O⁶-methyldeoxyguanosine (O⁶-MedG) are pro-mutagenic lesions of current interest in the context of colon carcinogenesis associated with meat consumption.¹⁻⁵ Both adducts were found to be elevated in blood and tissue samples from colorectal cancer patients.⁶⁻⁹ Further, O⁶-CMdG was detected in colonic exfoliated cells from human feces,¹⁰ and in human blood samples from individuals on high red meat diets.¹¹ The association with meat, particularly red, was confirmed in other studies where O⁶-CMdG was detected at a higher levels in tissues from volunteers with a high red meat diet compared to a vegetarian one¹² and in studies where digestion of red and white meat was modelled in vitro.¹³⁻¹⁵ The formation of O⁶-CMdG and O⁶-MedG was also observed after exposure of DNA to *N*-nitroso compounds (NOCs),^{11, 16-17} which are present in red and cured meat¹⁸ or can be derived from nitrogenous dietary precursors via nitrite-mediated nitrosation of secondary amines that occurs largely endogenously.¹⁹ If unrepaired, the high miscoding potential of O⁶-MedG to pair with thymine results in GC → AT transition mutations upon replication.⁴⁻⁵ For O⁶-CMdG, the misincorporation of thymine, and to a smaller extent of adenine, could be demonstrated,²⁰⁻²¹ therefore providing a mechanistic basis for the GC → AT

transition and GC → TA transversion mutations found in the *p53* gene after treatment with a carboxymethylating agent and replication in yeast.²² Interestingly, these are also the two most common mutations found in colorectal cancer.²²⁻²³

Carboxymethylating agents, such as compounds derived from *N*-carboxymethyl-NOCs and other chemical probes,²⁴ promote the formation of *O*⁶-CMdG and to less extent *O*⁶-MedG.^{17, 11, 25} For example, L-azaserine and potassium diazoacetate (KDA; Figure 1) are commonly used to generate *O*⁶-CMdG and *O*⁶-MedG.^{8, 10, 17, 26-27} In previous studies, KDA induced higher absolute levels of *O*⁶-CMdG and *O*⁶-MedG than L-azaserine, but the carboxymethyl:methyl ratio is lower for KDA.¹⁶⁻¹⁷ The average level of *O*⁶-CMdG and *O*⁶-MedG adducts after exposure to KDA was similar in cells and naked DNA, suggesting that no enzymatic activation is required for KDA. However, the high activity of KDA limits its usage as model carboxymethylating agent and no reproducible results were obtained in cells.¹⁰ Moreover, it is difficult to determine KDA concentration, due to its high instability and fast conversion during characterization. Hence, a nominal concentration is normally assumed based on quantitative production from alkaline hydrolysis of ethyldiazoacetate,^{10, 28} but a true yield to our knowledge has never been determined. Based on technical limitations in the use of KDA, L-azaserine seems to be a preferred chemical for inducing *O*⁶-CMdG and *O*⁶-MedG, and exposure of cells to L-azaserine resulted in reproducible adduct levels.²⁷

L-azaserine was discovered in 1954 as the active component of a crude filtrate from a culture of *Streptomyces* bacteria with antibiotic activity and potent anti-tumour activity in rodents.²⁹ It was positive in the Ames test and induced adenocarcinoma in rats³⁰ via the formation of DNA damage.³¹ The formation of *O*⁶-CMdG by azaserine was demonstrated by reaction with ctDNA and exposure in cells.^{16, 27, 16-17, 26-27} Despite the clear and long-standing understanding that azaserine gives rise to *O*⁶-CMdG, details concerning the mechanism of this reaction remain limited.

It has been hypothesized that L-azaserine gives rise to carboxymethyl adducts by conversion to diazoacetate, which can carboxymethylate DNA. Two potential mechanisms for the conversion of azaserine in diazoacetate have been suggested: enzymatic β-elimination of L-azaserine to diazoacetate and pyruvate, or spontaneous hydrolysis to yield diazoacetate and L-serine (Figure 2 B-C). Evidence for enzymatic β-elimination of L-azaserine was established using enzymatic extracts from mouse liver and a stoichiometric relationship could be demonstrated for L-azaserine disappearance and glycolic acid, ammonia and pyruvate formation with the last two being the hydrolysis products of the β-elimination intermediate 2-aminoacrylate.³² The responsible enzyme was presumed to be in the class of dehydrogenases.³³ Decomposition of azaserine to pyruvate and ammonia was also demonstrated in bicarbonate buffer, but only in the presence of pyridoxal ion as an enzymatic co-factor. A pyridoxal ion-catalyzed β-elimination of L-azaserine via a Schiff base was suggested, resulting in diazoacetate and aminoacrylate that subsequent hydrolyses to pyruvate and ammonia.³⁴ However, the observation that *O*⁶-CMdG and *O*⁶-MedG form from azaserine and ctDNA in the absence of enzymes suggested an additional, non-enzymatic mechanism of L-azaserine breakdown that could yield DNA adducts. This mechanism has been proposed to involve spontaneous hydrolysis to yield serine and diazoacetate (Figure 2 B).¹⁷

The objective of this study was to elucidate the chemical mechanism of O^6 -CMdG formation by L-azaserine and establish a chemical basis for its use to address the corresponding DNA damage in cells. Thus, we evaluated the stability of L-azaserine under varying pH conditions. We characterized in detail the basis of O^6 -CMdG formation from the direct reaction of L-azaserine with guanosine. Finally, we quantified the formation of O^6 -CMdG and O^6 -MedG by L-azaserine in human colon epithelial cells (HCEC) on the basis of dose and time by establishing a mass spectrometry approach for the simultaneous and sensitive quantification of O^6 -CMdG and O^6 -MedG. The findings suggest a new direct reaction mechanism between L-azaserine and dG that gives rise to a O^6 -Ser-CMdG intermediate, which undergoes rapid spontaneous hydrolysis to form O^6 -CMdG. Further, the characterization of adduct formation in cells as a function of L-azaserine dose and time of exposure supports the use of L-azaserine as a chemical probe in future studies addressing biological consequences of O^6 -CMdG.

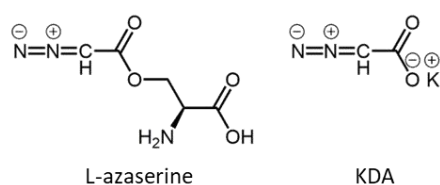


Figure 1. Chemical structure of L-azaserine and KDA.

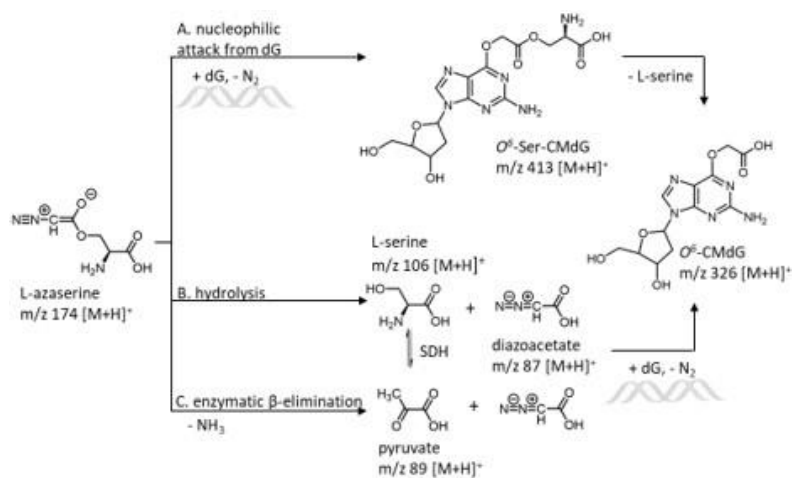


Figure 2. Proposed mechanisms for L-azaserine-induced O^6 -CMdG formation. **A.** nucleophilic attack of dG on L-azaserine result in an O^6 -Ser-CMdG intermediate followed by hydrolysis of L-serine to yield O^6 -CMdG. **B.** L-azaserine decomposes spontaneously to L-serine and diazoacetate which subsequently carboxymethylates dG on O^6 . **C.** Enzymatic β -elimination of L-azaserine results in pyruvate and diazoacetate that subsequent forms O^6 -CMdG.

2.3 Experimental Procedure

Materials. HCEC-1CT cell lines were kindly provided by Prof J.W. Shay (University of Texas, USA),³⁵ and all media and buffers for cell culture were purchased from Invitrogen (Carlsbad, California). KDA was synthesized via alkaline hydrolysis of ethyldiazoacetate as previously described and neutral solutions for further usage obtained by neutralizing with 0.1 M HCl.^{10, 17, 22} L-azaserine was purchased from abcam (Cambridge, UK) and purity confirmed by ¹H NMR. Ethyldiazoacetate was obtained from Pfaltz & Bauer Inc (Waterbury, Connecticut), deoxygunaosine (dG) from fluorochem (Hadfield, UK), and labeled ¹⁵N₅-dG from Cambridge Isotope Laboratories Inc, (Tewksbury, Massachusetts) and were used without further purification. *N*²-MedG standard was purchased from Carbosynth (Compton, UK). If not stated otherwise, all chemicals were purchased from Sigma Aldrich (Buchs, Switzerland) and used without further purification. MilliQ water was received from Millipore SynergyUV device (MilliporeSigma, Merck-Group, Burlington, Massachusetts). Mobile phases for liquid chromatography (LC) were obtained from Sigma-Aldrich (Buchs, Switzerland) and mobile phases for liquid chromatography coupled with mass spectrometry (LC-MS) were purchased from Biosolve Chimie (Dieuze, France).

NMR analysis was performed on a Bruker Biospin 400 MHz NMR instrument (Bruker, Billerica, Massachusetts), and chemical shifts are reported in parts per million (ppm, δ) relative to the chemical shift of the respective solvent. NMR solvents were purchased from Sigma Aldrich (Buchs, Switzerland). NMR files were evaluated by Mnova vs 11 (Mestrelab Research, Santiago de Compostela, Spain).

Data were analysed and plotted using GraphPad Prism, Version 8 (GraphPad Software Inc., San Diego, California). Applied statistical tests are specified for each data set in the figure caption.

Preparation of standards for mass spectrometry. *O*⁶-CMdG was prepared by the copper carbene-based method described by Geigle et al.³⁶ In short, 2.5 mg (9.35 μ mol) dG was allowed to react with 10.7 mg (93.5 μ mol) ethyldiazoacetate in the presence of 300 μ g (1.87 μ mol) CuSO₄. *O*⁶-CMdG was obtained by alkaline hydrolysis followed by purification by reversed phase high pressure liquid chromatography (HPLC) on a LunaC18 column, 4.6 x 250 mm, particle size 5 μ m (Phenomenex, Torrance, California) by using 0.1 % HOAc, mobile phase A, and acetonitrile (ACN), mobile phase B. Chromatographic separation was achieved by starting with an isocratic hold at 100 % 0.1 % HOAc for 10 min, followed by a gradient to 16% ACN in 45 min. Injection volume was 20 μ l. The product (RT 41.3 min, λ = 280, 250 nm) was obtained in 40 % yield as a white powder and stored at -20°C until further analysis. HRMS (ESI) calculated for C₁₂H₁₅N₅O₆: [M+H]⁺ *m/z* 326.1101, found 326.1095, MS² calculated for C₇H₇N₅O₃: [M+H-Gua]⁺ *m/z* 210.0628, found 210.0617. ¹H NMR (Figure S2) matched published data.¹⁶ ¹⁵N₅-*O*⁶-CMdG was prepared by the same protocol using 2.5 mg (9.35 μ mol) dG ¹⁵N₅-dG as starting material yielding 1 mg (40 % yield) of a white powder of ¹⁵N₅-*O*⁶-CMdG. HRMS (ESI) calculated for C₁₂H₁₅¹⁵N₅O₆: [M+H]⁺ *m/z* 331.0952, found 331.0944, MS² calculated for C₇H₇¹⁵N₅O₃: [M+H-Gua]⁺ *m/z* 215.0479, found 215.0469 [M+H-Gua]⁺.

O⁶-MedG was synthesized by the method reported by Reza et al.³⁷ In short, 0.57 g (2 mmol) dG was allowed to react in 10 mL pyridine with 4.3 g (79.6 mmol) sodium methoxide in 300 mL MeOH. The product was purified by reverse phase HPLC on a LunaC18 column 10 × 250 mm, particle size 5 μm (Phenomenex, Torrance, California) with a 15 min hold at 5 % acetonitrile (ACN) in MilliQ H₂O followed by gradient to 35 % ACN MilliQ H₂O in 10 min at a flow rate of 2 mL/min. Injection volume was 200 μl. Product (RT 20.7 min, λ=260 nm) was obtained in a 60 % yield as a light yellow powder. HRMS (ESI) was calculated for C₁₁H₁₅N₅O₄: [M+H]⁺ *m/z* 282.1202, found 282.1197, MS² as calculated for C₆H₇N₅O: [M+H-Gua]⁺ *m/z* 166.0729, found 166.0715. ¹H NMR (Figure S3) matched the published data.³⁷ D₃-O⁶-MedG was synthesized accordingly with 0.19 g (0.67 mmol) dG and 1.51 g (26.5 mmol) D₃-sodium methoxide in 100 mL MeOD (both Armar chemicals, Switzerland). Product was purified by reversed phase liquid chromatography as described for unlabeled O⁶-MedG and obtained as a light-yellow powder in 60% yield. HRMS (ESI) was calculated for C₁₁H₁₂D₃N₅O₄: [M+H]⁺ *m/z* 285.1391, found 285.1383, MS² was calculated for C₆H₅D₃N₅O: [M+H-Gua]⁺ *m/z* 169.0918, found 169.0904. We did not observe any D/H exchange by analyzing a 100 nM D₃-O⁶-MedG standard solution by nanoLC-ESI-HRMS² and following the intensity in the extracted ion chromatograms (XICs) for D₃-O⁶-MedG (*m/z* 285.1383 [M+H]⁺) and O⁶-MedG (*m/z* 282.1197 [M+H]⁺, not detectable (nd)) over time of the analysis.

Cell culture of HCEC cells and L-azaserine exposure. Cells were maintained as monolayers in 10-cm dishes in a humidified, 5% CO₂ atmosphere at 37 °C. Media consisted of 80% DMEM and 20% M199 Earle's salt medium, supplemented with 2% Hyclone fetal bovine serum (Hyclone Laboratories Inc, San Angelo, Texas), 25 ng/L epidermal growth factor, 1 μg/L hydrocortisone, 10 μg/L insulin, 2 μg/L transferrin, 50 μg/L gentamycin, 0.9 ng/L sodium selenite. Cells were regularly confirmed to be mycoplasma free using the MycoAlert Kit (Lonza, Basel, Switzerland).³⁸ L-azaserine stock solutions were prepared in MilliQ water. O⁶-Benzylguanine (O⁶-BG) stock solutions were prepared in dimethylsulfoxide (DMSO) and final concentration of DMSO was 0.1%. To assess cell viability, cells were seeded in 96-well plates at a density of 1 × 10⁴ and exposed to increasing L-azaserine concentrations (0, 1, 10, 50, 250, 750, 1000, 2500 μM) for 120 h. Cells were exposed to TritonX (Sigma Aldrich, Buchs, Switzerland) as positive control for cytotoxicity. Cell survival was measured using CellTiterGlo assay (Promega, Madison, Wisconsin) following the manufacturer's instructions.³⁹ Luminescence values of technical triplicates were averaged and the value for number of viable cells after exposure was normalized to that of negative control cells (assigned as 100% viability, Figure S7).

For DNA adduct analysis, cells were seeded in 10-cm dishes at a density of 2 × 10⁶. Cells were exposed to 0, 125, 250, 500 and 1000 μM L-azaserine for 4 h to evaluate dose-response relationship and with 500 μM L-azaserine for 0.5, 4, 10, 24, 48, 72, 96 and 120 h to determine the time-dependent O⁶-CMdG and O⁶-MedG formation. After chemical exposure, cells were harvested by removing medium, washing with phosphate-buffered saline (PBS) and incubating with trypsin for 6 min at 37 °C. Cells were collected in 10 mL PBS, centrifuged and PBS removed while the cell pellet was stored at -20 °C for subsequent DNA extraction. Cell viability, dose response and time course studies were each performed three independent times.

DNA isolation and sample preparation for adduct analysis by mass spectrometry.

DNA was isolated from cell pellets using the QIAamp® DNA Mini Kit (©QIAGEN, Switzerland). In short, cell pellets were re-suspended in 200 µl PBS and 200 µl Lysis Buffer, 20 µl Proteinase K and 10 µl RNase A was added and cells were incubated for 20 min at 56 °C, 1400 rpm on a ThermoShaker. Afterwards, 20 µl of EtOH was added and the homogenous solution was applied to a spin column and centrifugation was performed for 1 min at 6000 g. The flow through was discarded and the column washed with 500 µl Buffer AW1 (1 min, 6000 g) followed by 500 µl Buffer AW2 (3 min, 16900 g). For DNA-elution, DNA was incubated twice with 100 µl pre-heated (70 °C) MilliQ for 5 min on the column at room temperature, followed by centrifugation for 1 min at 6000 g. DNA was quantified by Quantus™ Fluorometer (Promega, Switzerland) and samples were concentrated in a Thermo Scientific™ Savant™ Universal SpeedVac™ Vakuumsystem (Fisher Scientific, Hampton, New Hampshire) and stored at -20 °C until further analysis.

Extracted DNA was further processed by enzymatic digestion using 2.5 U/µg DNA benzonase, 3 mU/µg DNA phosphodiesterase I and 2 U/µg DNA alkaline phosphatase. A master mix was prepared containing enzymes in tris-Buffer, 10 mM, with 2 mM MgCl₂ adjusted to pH 7.7 with 0.1 M HCl and 100 fmol D₃-O⁶-MedG and 200 fmol ¹⁵N₅-O⁶-CMdG per sample were added. Internal standards were added to account for losses during sample preparation and ionization. 50 µl of master mix were added per sample and DNA was digested for 6 h at 37 °C, 250 rpm on a ThermoShaker. CtDNA (20 µg) and a blank sample containing only master mix was used as control for DNA digestion and background signal. Enzymes were removed by molecular weight filtration with a cutoff of 30 kDa (VWR, Radnor, Pennsylvania) and an aliquot (60 µl) was removed for dG-quantification by high performance liquid chromatography. Samples were concentrated to dryness in a Thermo Scientific™ Savant™ Universal SpeedVac™ Vacuum system (Fisher Scientific, Hampton, New Hampshire) and either stored at -20 °C or directly re-suspended in 200 µl MSwater + 0.1% FA and further processed by solid phase extraction on a C18 cartridge, Sep-Pak Vac 1cc (50 mg) (Waters, Milford, Massachusetts) using MS grade CH₃OH, CH₃OH+FA and H₂O. Cartridges were washed with 2 x 1 mL CH₃OH and 1 mL CH₃OH + 0.1% FA followed by 2 x 1 mL H₂O + 0.1% FA. The samples were loaded on the cartridge, washed with 2 x 1 mL H₂O + 0.1% FA and 1 mL 3% CH₃OH, and eluted with 2 x 500 µL of 80 % CH₃OH in H₂O. The eluted fractions were dried under vacuum and dissolved in 10 µL H₂O for subsequent MS analysis.

dG quantification by liquid chromatography. Quantitation of dG was carried out on an Agilent 1100 Series HPLC (Agilent Technologies, Santa Clara, California) with a UV detector set at $\lambda=254$ nm. A C18 Kinetex, 2.1 x 150 mm, particle size 2.6 µm column was used, (Phenomenex, Torrance, California). The solvent gradient was linear, 3% ACN in MilliQ H₂O to 15 % ACN in MilliQ H₂O over the course of 6 min with a flow rate of 0.2 mL/min. The injection volume was 20 µL. The retention time for nucleosides was the following: dC 3.5 min, dG 8.4 min, dT 9.2 min, dA 10.6 min. A calibration curve for dG was prepared by triplicate quantification of standards of increasing concentration (0.1, 1, 10, 25, 50 and 100 µM dG). The amount of dG was then used to calculate the total number of nucleotides based on the assumption that the GC content is 40.9% in human DNA.⁴⁰

Nano liquid chromatography high resolution mass spectrometry method for simultaneous quantification of O⁶-CMdG and O⁶-MedG. Simultaneous quantification of O⁶-CMdG and O⁶-MedG was achieved on an Orbitrap Fusion™ Lumos™ (Thermo Scientific, Waltham, Massachusetts) equipped with a nano electrospray ionization source and a nanoAcquity UPLC M-class system (Waters, Milford, Massachusetts). Liquid chromatography was performed with an Acquity UPLC M-Class Symmetry C18 Trap column (100 Å, 5 µm, 180 µm x 20 mm, 2D) and an Acquity UPLC M-Class HSS T3 column (100 Å, 1.8 µm, 75 µm x 250 mm) at a column temperature of 40 °C. The sample loop volume was 5 µl, with an injection volume of 2 µl. Mobile phase A and B consist of mass spectrometry grade H₂O with 0.1% FA and mass spectrometry grade ACN with 0.1% formic acid, respectively (Biosolve, Chimie, Dieuze, France). The chromatographic method included trapping for 0.5 min at 99.5% A at a flow rate of 15 µl/min. The solvent gradient was 1 min 3% B, followed by a linear gradient from 3% to 45% B over 19 min, at a flow rate of 0.3 µl/min. Nano electrospray ionization was used in positive mode. The spray voltage was 2.2 kV and the temperature of the heated capillary was set to 270 °C. Mass spectrometry-based detection was performed on an Orbitrap Fusion™ Lumos™ (Thermo Scientific, Waltham, Massachusetts) in PRM HCD OT mode with the following settings: The RF lens was set to 35%. Resolution of the orbitrap was set to 120 K in MS¹ mode with a scan range from 160-400 *m/z* and 1 microscan. AGC target was set to 4*10⁵ with a maximum injection time of 100 ms. Targeted inclusion list was comprised of O⁶-CMdG with *m/z* 326.1096 [M+H]⁺, heavy ¹⁵N₅-O⁶-CMdG with *m/z* 331.0946 [M+H]⁺, O⁶-MedG with *m/z* 282.1995 [M+H]⁺, and heavy D₃-O⁶-MedG with *m/z* 285.1384 [M+H]⁺. The mass tolerance was set to ± 25 ppm. Isolation for MS² was performed in the quadrupole with an isolation window of 1.6 *m/z* and the first mass set to 140 *m/z*. HCD was used for fragmentation with a collision energy of 25%. Fragments were detected in the orbitrap with a resolution of 60 K. The AGC target was set to 5*10⁴ with a maximum injection time of 118 ms. Instrument sensitivity was checked before each analysis and after every 10th samples by comparing intensity and retention time of a 1 nM calibration standard for O⁶-CMdG and O⁶-MedG as well as a standard iRT peptide solution containing 11 peptides (*m/z* range from 487.2511-776.9920). For quantification, neutral loss of deoxyribose was targeted in extracted ion chromatograms (XICs) using O⁶-CMG *m/z* 210.0622 [M+H-Gua]⁺, heavy ¹⁵N₅-O⁶-CMG *m/z* 215.0472 [M+H-Gua]⁺, O⁶-MeG *m/z* 166.0722 [M+H-Gua]⁺, and heavy D₃-O⁶-MeG *m/z* 169.0911 [M+H-Gua]⁺ with a mass tolerance of ± 10 ppm. XICs in MS¹ were used for verification. Calibration standards containing 0.5, 1, 5, 10, 25, 50 and 100 nM of O⁶-CMdG and O⁶-MedG standards undergoing sample preparation served for quantification. The number of lesions were divided by the amount of 10⁷ nucleotides to express final DNA lesion levels.

pH stability of L-azaserine. L-azaserine (25 mM) was dissolved in 500 µl of diverse 0.1 M buffer solutions at pH ranging from pH 2 to 11: pH 2 glycine-HCl buffer, pH 7.2 sodium phosphate buffer, pH 8.5 carbonate buffer, and pH 10.5 tris-buffer. To follow the acid-catalyzed decomposition of L-azaserine, solutions of L-azaserine (25 mM) in 0.1 M buffer solutions (980 µl) in the pH range 2 to 5.8 were prepared: pH 2, 2.4 and 3.4 with glycine-HCl, and pH 5.8 with sodium phosphate. Solutions were analyzed by reversed phase HPLC on an Agilent 1200 (Agilent Technologies, Santa Clara, California) equipped with a diode array detector that was set to monitor λ=254 nm (L-azaserine) and 210 nm (serine,

pyruvate). The starting concentration of L-azaserine was chosen to allow for detection of 0.5% and quantification of 2% hydrolysis to L-serine (LOQ 0.5 mM L-serine). Chromatographic separation was achieved on a LunaC18 column, 4.6 x 250 mm, particle size 5 μm (Phenomenex, Torrance, California) by using MilliQ H₂O, mobile phase A, and ACN, mobile phase B, starting with an isocratic hold at 100% A for 5 min, followed by a 10 min linear gradient to 40%, 10 min wash at 80% ACN and 10 min re-equilibration at 100% at a flow rate of 1 mL/min. Each sample (pH 2-11) was analyzed every 3 h for a total of 120 h. The analytical method was shortened for samples at pH 2-5.8 to the following: isocratic hold at 100% A was set for 6.0 min, followed by 3 min wash with 80% ACN and 5 min re-equilibration at 100% at a flow rate of 1 mL/min. Samples at pH 2 and pH 2.4 were analyzed every 15 min for 8 h and samples at pH 3.4 and 5.8 were analyzed every hour for 90 h or 120 h, respectively. L-serine eluted at retention time 2.6 min, pyruvate at 2.9 min and L-azaserine at 3.8 min. Injection volume was 10 μl . A calibration curve for L-azaserine and L-serine from 0.5, 1, 6, 12, 25 and 50 mM was prepared and analyzed before and after analysis. Data from hydrolysis of L-azaserine was modeled as a pseudo first order reactions (Fig. 3B eq. 1-2) and corresponding half-life ($t_{1/2}$) was calculated with the following equations: $\frac{\ln[A_0]}{\ln[A]} = kt$, $t_{1/2} = \frac{\ln 2}{k_{\text{obs}}}$ (Fig. 3B eq. 3) where $[A_0]$ =starting concentration of L-azaserine (mM), $[A]$ =concentration of L-azaserine at t (mM), k_{obs} =slope (1/h), $t_{1/2}$ = half-life (h). The ratio $\frac{K_{\text{hydrolysis}}}{K_s}$ was calculated via the equation $K_{\text{obs}} = \frac{K_{\text{hydrolysis}}}{K_s} [\text{H}_2\text{O}][\text{H}^+]$ (Fig. 3B eq. 4).

Reaction of dG with L-azaserine. 5 μM dG in 500 μl MilliQ or tris-buffer (10 mM) containing 2 mM MgCl₂, at pH 7, 8, 9, and 10.6 was combined with 5 mM L-azaserine or KDA as control respectively and the reaction mixture was stirred for 0.5, 1, 2, 3 and 24 h at 37 °C, 250 rpm. After the indicated time, 200 fmol of ¹⁵N₅-O⁶-CMdG and 100 fmol of D₃-O⁶-MedG were added to the reaction mixture as internal standards, and samples were concentrated to dryness and isolated by SPE as described in here for quantification of O⁶-CMdG and O⁶-MedG. All samples were analyzed by nanoLC-ESI- HRMS² as described above with the following changes: Trapping time was set to 0.1 min. Resolution was set to 60 K for the orbitrap mass analyzer in MS¹ with a mass range from 68-444 m/z and 1 microscan. AGC target was set to 4×10^5 with a maximum injection time of 100 ms. Target inclusion list was expanded to include potential O⁶-Ser-CMdG intermediate and fragmentation products with O⁶-Ser-CMdG m/z 413.1421 [M+H]⁺, O⁶-Ser-CMG m/z 297.0947 [M+H]⁺ from ion source fragmentation, L-azaserine m/z 174.0515 [M+H]⁺, serine m/z 106.0504 [M+H]⁺, dG m/z 268.1046 [M+H]⁺. The mass tolerance was set to ± 50 ppm. Isolation for MS² was performed in the quadrupole with an isolation window of 1.6 m/z and the first mass set to 50 m/z . HCD was used for fragmentation with a collision energy of 25%. Fragments were detected in the orbitrap with a resolution of 50 K. The AGC target was set to 5×10^4 with a maximum injection time of 86 ms. Fragmentation of a O⁶-Ser-CMdG was targeted in MS² XICs with neutral loss of dR, O⁶-Ser-CMG m/z 297.0947 [M+H-dR]⁺, and serine fragment,⁴¹⁻⁴³ with m/z 251.0893 [M+H-(dR+H₂O+CO)]⁺. Mass tolerance for all XICs was ± 10 ppm.

Preparation of O⁶-Ser-CMdG. 4 mM dG was dissolved in 1200 μl 0.1 M sodium phosphate buffer at pH 7.2. 25 mM L-azaserine was added and the mixture allowed to react at

22 °C for 120 h while being continuously analyzed by reversed phase HPLC on an Agilent 1200 (Agilent Technologies, Santa Clara, California) equipped with a diode array detector that was set to monitor $\lambda=254$ (L-azaserine, dG, G, O⁶-CMdG, O⁶-Ser-CMdG), 210 (L-Serine) and 280 (O⁶-CMdG, O⁶-Ser-CMdG) nm. Chromatographic separation was achieved on a LunaC18 column, 4.6 x 250 mm, particle size 5 μ m (Phenomenex, Torrance, California) by using milliQ, mobile phase A, and ACN, mobile phase B, starting with an isocratic hold at 100% A for 5 min, followed by a gradient to 45 % ACN in 45 min at a flow rate of 1 mL/min. Injection volume was 10 μ l. All eluting peaks were identified by m/z on a Velos Linear Ion Trap (Thermo Scientific, Waltham, Massachusetts) and in case of L-azaserine, dG, guanine and L-serine with co-elution of respective standards and corresponding DAD spectrum. Initial chromatogram (t =5 min) revealed two peaks, that could be identified as L-azaserine (RT 3.9 min, m/z 174) and dG (RT 16.8 min, m/z 268). Other main peaks (Area > 100 mAU) detected were identified as L-serine (RT 2.8 min, m/z 106), and guanine (RT 11.4 min, m/z 152). A peak at retention time 7.9 min revealed m/z of 297 matching the calculated mass for Ser-G, while the peak of interest eluted at retention time of 18.2 min with m/z of 413 as calculated for O⁶-Ser-CMdG (Figure S4 A). The peak eluting at 18.7 min was collected over 200 runs and concentrated to dryness. HRMS was calculated for C₁₅H₂₀N₆O₈: [M+H]⁺ m/z 413.1421, found 413.1411 (Figure S4 B), and MS² was calculated for C₁₀H₁₂N₆O₅: [M+H-Gua]⁺ m/z 297.0947, found 297.0938. Characterization by ¹H NMR in deuterium oxide confirmed presence of O⁶-Ser-CMdG (Figure S4 C). ¹H NMR (400 MHz, Deuterium Oxide) δ 8.14 (s, 1H, Ar-H), 6.38 (t, J = 8.2 Hz, 1H, 1'-H), 5.07 (s, 1H, NH₂-CH), 4.83 – 4.81 (m, 2H, O-CH₂-COO), 4.67 – 4.62 (m, 1H, 4'-H), 4.18 – 4.13 (m, 1H, 3'-H), 3.93 – 3.84 (m, 2H, O-CH₂-CNH₂), 3.83 – 3.74 (m, 2H, 5'-H), 2.84 (dt, J = 14.7, 7.4 Hz, 1H, 2'-H), 2.57 – 2.46 (m, 1H, 2'-H).

Hydrolysis of O⁶-Ser-CMdG. O⁶-Ser-CMdG was dissolved in 0.1 M phosphate buffer at pH 7.2 and the solution was analyzed by reversed phase HPLC analysis every h for a total of 30 h to address the stability of the isolated O⁶-Ser-CMdG intermediate and explore the potential subsequent hydrolysis to O⁶-CMdG. Mobile phase A was 0.1 % HOAc (pH 4) to prevent pH effects affecting O⁶-CMdG. Chromatographic separation was achieved starting with a isocratic hold for 10 min at 100 % 0.1 % HOAc, followed by a gradient to 16% ACN in 45 min. Diode array detector was set to monitor $\lambda= 280$ nm (O⁶-CMdG, O⁶-Ser-CMdG) and is the specific maximum absorption wavelength for O⁶-CMdG. The two peaks visible were collected and identified by their m/z on a Velos Linear Ion Trap (Thermo Scientific, Waltham, Massachusetts). The peak of interest eluted at retention time of 42.5 min (Figure S5 A) and was collected and concentrated for further characterization. ¹H NMR in deuterium oxide matches with the O⁶-CMdG standard (Figure S5 C). HRMS (ESI) calculated for C₁₂H₁₅N₅O₆: [M+H]⁺ 326.1101, found 326.1094.

2.4 Results

Stability of L-azaserine at varying pH. The hydrolysis of L-azaserine to yield L-serine and diazoacetate has been previously suggested as a basis for the formation of O⁶-CMdG (Figure 2 B).¹⁷ However, this mechanism raises concern about the wide use of L-azaserine in cell-based studies and whether the compound is stable under the experimental conditions of in

in vitro toxicological assays. Therefore, we sought to characterize the hydrolytic stability of L-azaserine. Assessing the stability of azaserine at varying pHs, ranging from pH 2 to 11, by measuring by HPLC the level of L-azaserine and of its hydrolysis product L-serine over the course of five days, we observed that the compound was stable and no decomposition products were observed between pH 5.8 and 10.5. On the other hand, at pH 2, L-azaserine was completely hydrolyzed to L-Serine after 2 h (Figure S1). The acid-catalyzed hydrolysis was modeled as a pseudo first order reaction (Figure 3B, eq. 1) and the half-life ($t_{1/2}$) was calculated to be 0.4 h at pH 2, 0.7 h at pH 2.4 and 4.7 h at pH 3.4.

The mechanism of hydrolysis is proposed to involve protonation of the carbon bound to both the diazo and carbonyl groups, thus promoting hydrolysis of the ester and release of L-serine (Figure 3A). On the basis of the pH-dependence of the protonation/hydrolysis rates and having derived the values of k_{obs} for each pH (Table 1), we could estimate the ratio $K_{\text{hydrolysis}} / K_{\text{a}}$ to be $0.90 \times 10^{-4} \text{ M}^{-1} \text{ s}^{-1}$ (Figure 3B, eq. 5). While the pK_{a} of the protonated azaserine (Figure 3A) could not be extracted, it could be estimated on the basis of similar diazo compounds, such as diazomethane, which has a pK_{a} of 10.⁴⁴ Approximating a similar pK_{a} for azaserine would suggest $K_{\text{hydrolysis}}$ for H^+ -azaserine to be $9 \times 10^5 \text{ M}^{-1} \text{ s}^{-1}$ (Figure 3A). These data emphasize the relative hydrolytic stability of L-azaserine under physiological conditions and suggest against it being the initial step in the reaction of L-azaserine with DNA to give rise to O^6 -CMdG.

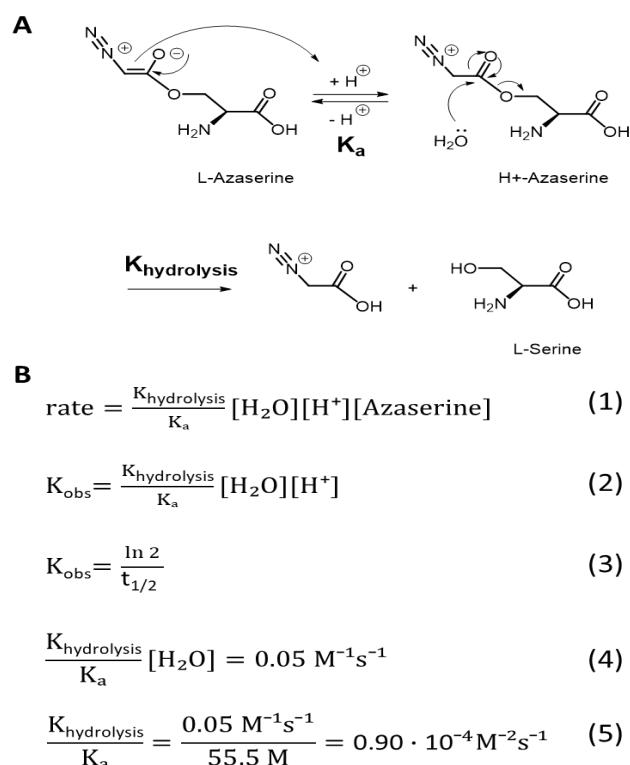


Figure 3. Acid-promoted hydrolysis of L-azaserine. (A) Proposed mechanism of acid-catalyzed hydrolysis of L-azaserine to L-serine, which is governed by equations (1) and (2). (B) Kinetic equation to derive the ratio of $\frac{K_{\text{hydrolysis}}}{K_{\text{a}}}$ is obtained (5).

Table 1. Half-life ($t_{1/2}$) and k_{obs} values at varying pHs.

pH	[H ⁺]	$t_{1/2}^{\text{a}}$ (s)	$k_{\text{obs}}^{\text{b}}$ (s ⁻¹)
2	0.01	1440	0.000481
2.4	0.003981	2520	0.000275
3.4	0.000398	16920	$4.1 \cdot 10^{-5}$
5.8	$1.58 \cdot 10^{-6}$	nd	nd
7.2	$6.31 \cdot 10^{-8}$	nd	nd
8.5	$3.16 \cdot 10^{-9}$	nd	nd
10.5	$1.58 \cdot 10^{-11}$	nd	nd

^a $t_{1/2}$ values are derived via the eq. 3 (Fig. 3B); ^b k_{obs} values were derived via HPLC measurements (Fig. S1); nd = not determined.

Evidence for *O*⁶-Ser-CMdG as the intermediate in the formation of *O*⁶-CMdG by L-azaserine. Having established that L-azaserine does not undergo hydrolysis under physiologically relevant conditions, we considered whether under those conditions L-azaserine may directly react with dG. We hypothesized that an *O*⁶-Ser-CMdG intermediate with m/z 413 could be formed to then hydrolyze and yield *O*⁶-CMdG (Figure 2, A). To gain support for this mechanism, we first explored whether *O*⁶-Ser-CMdG could be formed by reacting dG for 0.5-24 h with an excess of L-azaserine in tris-buffer at pH in the range of 7 to 11. The reaction mixtures were analyzed for the presence of *O*⁶-Ser-CMdG, *O*⁶-CMdG and *O*⁶-MedG by nanoLC-ESI-HRMS² in PRM mode. We monitored mass transitions accounting for neutral loss of deoxyribose followed by possible fragmentation of serine (Table 2).⁴¹⁻⁴³ XICs of all reaction mixtures revealed the appearance of two peaks with the mass corresponding to *O*⁶-Ser-CMdG at a retention time of 17.9 and 18.1 min (Figure 4, A). Their mass-fragments were the same, consistent with being two positional isomers of Ser-CMdG. Further, two peaks were detected with m/z corresponding to carboxymethylated dG with retention times close to the potential Ser-CMdG isomers and one of them co-eluted with the standard ¹⁵N₅-*O*⁶-CMdG (18.35 min), thereby assigned as *O*⁶-CMdG. Similarly, two peaks were detected with m/z corresponding to MedGs; one peak co-eluted with an *N*²-MedG standard (18.01 min), while the second peak co-eluted with the standard for *O*⁶-MedG (18.75 min). In these experiments, Ser-CMdG and *O*⁶-CMdG formation appeared to be independent from time and pH. As a control, we performed the same reaction with KDA, and no peaks were detected corresponding to Ser-CMdG or fragments, but the same two peaks for each carboxymethylation and methylation of dG as for the L-azaserine treated samples were observed (Figure 4, B). None of the targeted m/z values were detected in control samples with any of the single reagents. These results suggest that L-azaserine reacts directly with dG, forming adducts that retain the serine moiety at the *O*⁶- and *N*²-positions.

Table 2. Targeted m/z with proposed structures for O^6 -Ser-CMdG and transitions.

Compound ^a	m/z MS ⁿ	Structure ^b	RT (min)	KDA	L- azaserine	Control	LC RT 18.7
O^6 -Ser-CMdG	413.1421 MS ¹		18.14	nd	413.1415	nd	413.1419
O^6 -Ser-CMG	297.0947 MS ²		18.14	nd	297.0941	nd	297.0937
O^6 -Ser-CMG – (H ₂ O+CO)	251.0893 MS ²		18.15	nd	251.0883	nd	251.0884
O^6 -CMdG	326.1096 MS ¹		18.37	326.1096	326.1094	nd	326.1099
¹⁵ N ₅ - O^6 - CMdG	331.0952 MS ¹		18.37	331.0944	331.0944	331.0944	331.0944
O^6 -MedG	282.1195 MS ¹		18.84	282.1196	282.1187	nd	282.1195
D ₃ - O^6 - MedG	285.1391 MS ¹		18.84	285.1383	285.1383	285.1383	285.1383
N^2 -Ser-CMdG	413.1421 MS ¹		17.91	nd	413.1418	nd	nd
N^2 -Ser-CMG	297.0947 MS ²		17.91	nd	297.0948	nd	nd
N^2 -Ser-CMG – (H ₂ O+CO)	251.0893 MS ²		17.89	nd	251.0882	nd	nd
N^2 -CMdG	326.1096 MS ¹		18.03	326.1095	326.1095	nd	nd
N^2 -MedG	282.1195 MS ¹		18.00	282.1195	282.1197	nd	nd

^a O^6 -coordination is confirmed by isotopically labeled O^6 -CMdG and O^6 -MedG standards. N^2 -coordination is confirmed by N^2 -MedG standard. ^bStructures and m/z of O^6 -CMdG and O^6 -MedG as hydrolysis products are included. Detected structures are indicated for KDA, L-azaserine and control samples from reaction mixture with dG and for the isolated compound by reverse phase liquid chromatography (LC RT 18.7min). nd=not detectable.

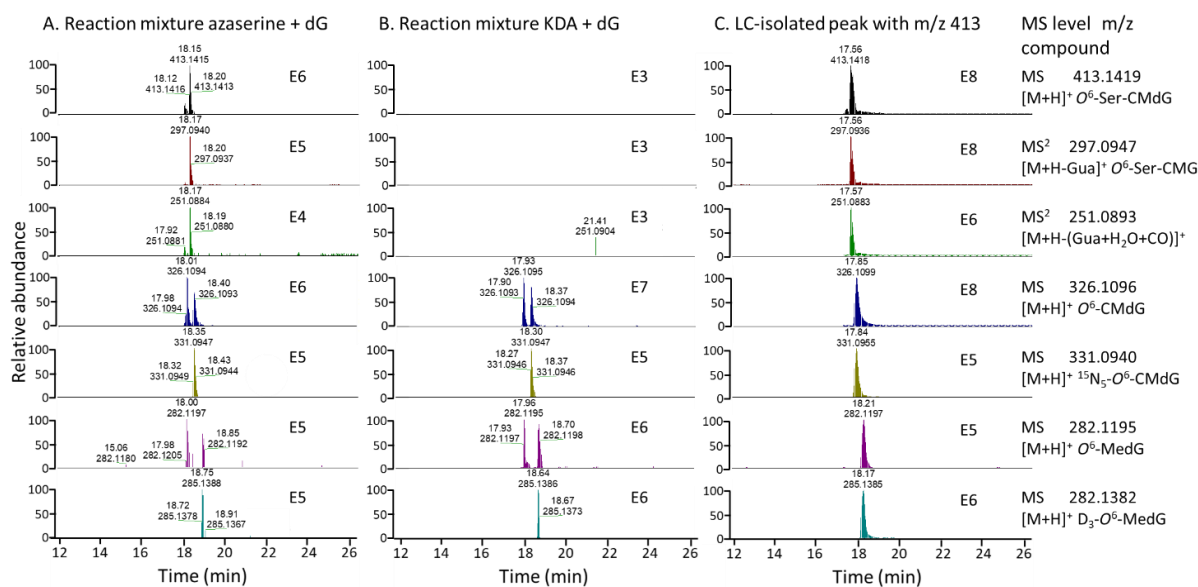


Figure 4. Representative chromatograms for the reaction of dG with L-azaserine or KDA analyzed by nanoLC-ESI-HRMS². A. and B. 5 μ M dG was reacted with 5 mM L-azaserine (A) or KDA (B) as control in 0.1 M tris-buffer, followed by SPE and nanoLC-ESI-HRMS². C. 4 mM dG was reacted with 25 mM L-azaserine in 0.1 M sodium phosphate buffer and peak with *m/z* 413 isolated by LC, concentrated and analyzed by nanoLC-ESI-HRMS². XICs represent parent mass for *O*⁶-Ser-CMdG and two fragmentations, followed by *O*⁶-CMdG, ¹⁵N₅-*O*⁶-CMdG as internal standard, *O*⁶-MedG and D₃-*O*⁶-MedG as internal standard. The sample represented in C was analyzed on a new column, explaining the shift in absolute retention time while Δ between *O*⁶-Ser-CMdG and *O*⁶-CMdG was equal.

Characterization of *O*⁶-Ser-CMdG. Having gained preliminary mass spectrometric evidence for the formation of the *O*⁶-Ser-CMdG intermediate in the reaction of dG with L-azaserine, we further characterized this novel structure and confirmed its conversion to *O*⁶-CMdG. Thus, Ser-CMdG observed from the reaction of dG with L-azaserine was observed by HPLC analysis after 0.5 h, and was present, though at lower intensity, up to 120 h (18.7 min, *m/z* of 413, Figure S4, A). The compound was isolated by HPLC and the ¹H NMR spectrum was consistent with Ser-CMdG due to the presence of three characteristic peaks at 5.07 (s, 1H, NH₂-CH), 4.83-4.81 (m, 2H, O-CH₂-COO) and 3.93-3.84 ppm (m, 2H, O-CH₂), accounting for five additional Hs in addition to those present in dG (Figure S4, C). The HRMS of the isolated peak revealed *m/z* 413.1411 (RT 17.56 min), corresponding to Ser-CMdG (Figure 4 C). Despite isolation of the Ser-CMdG peak on HPLC, *O*⁶-CMdG and *O*⁶-MedG were always detected in the sample as analyzed by nanoLC-ESI-HRMS² (Figure 4 C), but no *N*²-adducts. Thereby, we concluded that Ser-CMdG at RT 17.56 is *O*⁶-Ser-CMdG.

***O*⁶-Ser-CMdG decomposes to *O*⁶-CMdG.** Having established the formation of *O*⁶-Ser-CMdG as a product of reaction between dG and the carboxymethylating agent L-azaserine, we wanted to test whether the *O*⁶-Ser-CMdG adduct can hydrolyze and yield *O*⁶-CMdG. Therefore, we followed the stability of isolated *O*⁶-Ser-CMdG at pH 7.2 over 30 h by HPLC with UV detection at $\lambda=280$ nm. *O*⁶-CMdG was detected already in the first injection after dissolving *O*⁶-Ser-CMdG, and the corresponding peak (retention time 43 min) increased in intensity by 78 % over the 30 h analyzed, while *O*⁶-Ser-CMdG (retention time 23 min) decreased to 17 % of the initial area (Figure S5, A). *O*⁶-CMdG was characterized by HRMS

and ^1H NMR (Figure S5 B, C) and nanoLC-ESI-HRMS² revealed one peak for carboxymethylated dG co-eluting with the internal standard for O^6 -CMdG (Figure 5), and no peak for methylated dG could be detected. We concluded that O^6 -Ser-CMdG represents an intermediate in L-azaserine-induced O^6 -CMdG formation, thereby explaining adduct formation by L-azaserine under physiological conditions.

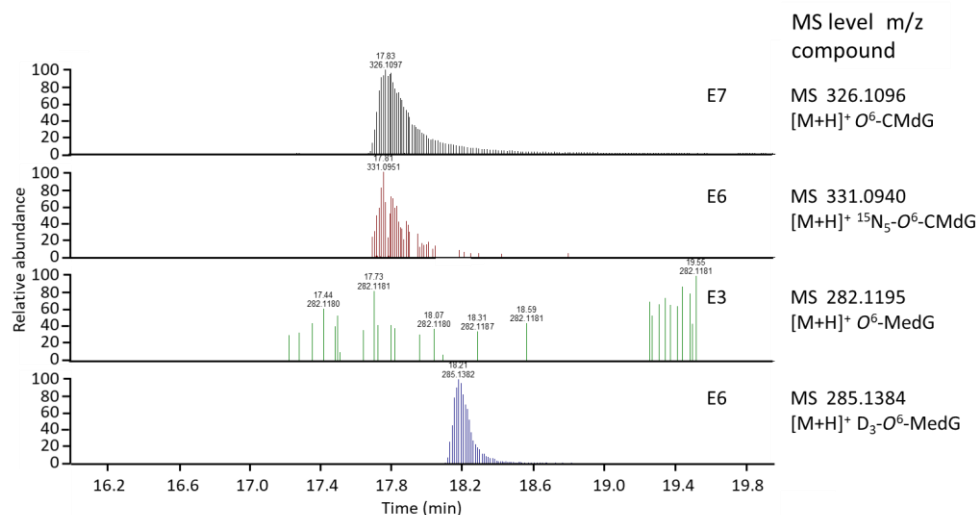


Figure 5. NanoLC-ESI-HRMS² chromatogram for the decomposition product of O^6 -Ser-CMdG. Decomposition product was isolated by reversed phase liquid chromatography and identified as O^6 -CMdG by nanoLC-ESI-HRMS². No methylated dG could be detected.

Quantification of O^6 -CMdG and O^6 -MedG in biological samples by nanoLC-ESI-HRMS². Having established that under neutral conditions direct alkylation of dG by L-azaserine occurs to form O^6 -Ser-CMdG that spontaneously hydrolyzes to yield O^6 -CMdG, we were interested in characterizing the time and dose profile of O^6 -CMdG adduct formation in cells upon exposure to L-azaserine. Therefore, we established a nanoLC-ESI-HRMS² method for the concomitant quantification of O^6 -CMdG and O^6 -MedG based on the stable isotope dilution method that accounts for losses during sample preparation and ionization, and allows for accurate quantification of the analyte (or unlabeled standard) based on the ratio of its signal area to that of labeled internal standard (Figure S2 and S3). Parallel reaction monitoring (PRM) was applied for the mass transitions corresponding to a neutral loss of deoxyribose (dR) from the protonated analytes: O^6 -CMdG (precursor m/z 326.1095 $[\text{M}+\text{H}]^+$, MS² m/z 210.0617 $[\text{M}+\text{H}-\text{dR}]^+$) and O^6 -MedG (precursor m/z 282.1197 $[\text{M}+\text{H}]^+$, MS² m/z 166.0715 $[\text{M}+\text{H}-\text{dR}]^+$), and from the isotopically labeled internal standards $^{15}\text{N}_5$ - O^6 -CMdG (precursor m/z 331.0944 $[\text{M}+\text{H}]^+$, MS² m/z 215.0469 $[\text{M}+\text{H}-\text{dR}]^+$) and D_3 - O^6 -MedG (precursor m/z 285.1383 $[\text{M}+\text{H}]^+$, m/z 169.0904 $[\text{M}+\text{H}-\text{dR}]^+$). Specificity was guaranteed by processing a blank sample for each analysis and selectivity by co-elution with internal standards, accurate parent and fragment mass. Pure standards were used to determine the limit of detection (LOD) and limit of quantification (LOQ) defined as the amount of analyte generating a signal-to-noise ratio (S/N) of 3 or 10 in the XICs. LOD (S/N > 3) was 5 pM (10 amol) and 1 pM (2 amol) for O^6 -CMdG and O^6 -MedG, respectively, and LOQ (S/N > 10) was 0.01 nM (20 amol) for both adducts. We further assessed LOQ in matrix, intra- and interday accuracy (expressed as % recovery) and precision (expressed as the relative standard

deviation, RSD %) using quality control samples consisting of calf thymus DNA (ctDNA, 15 µg) or HCEC genomic DNA (15 µg) spiked with increasing amounts of *O*⁶-CMdG and *O*⁶-MedG (0.01, 0.05, 0.1, 1.0, 10, 50 100 and 200 nM). LOQ in matrix was determined to be 0.05 nM (100 amol) for *O*⁶-CMdG and *O*⁶-MedG. Acceptable precision and accuracy was achieved for the measurement of *O*⁶-CMdG and *O*⁶-MedG in ctDNA and HCEC genomic DNA as matrix (Table 3) with a relative standard deviation (RSD) ranking from 1.7-25.6 % (*O*⁶-CMdG) or 0.8-23.5 % (*O*⁶-MedG) and recovering 83.7-113.4 % (*O*⁶-CMdG) or 92.1-122.6 % (*O*⁶-MedG) of the actual adduct level.

Table 3. Interday and intraday precision and accuracy for the nanoLC-ESI-HRMS² method (S/N > 10).

[nM]	Inter/intraday	<i>O</i> ⁶ -CMdG				<i>O</i> ⁶ -MedG			
		ctDNA		HCEC		ctDNA		HCEC	
		RSD% ^a	Rec% ^b	RSD%	Rec%	RSD%	Rec%	RSD%	Rec%
0.05	interday	8.9	83.7	6.7	97.8	4.9	118.1	23.5	110.4
0.1	interday	2.6	106.8	12.0	113.4	12.9	104.6	12.6	120.9
1.0	interday	25.6	101.5	1.8	103.5	9.8	122.6	0.8	92.1
50	interday	1.7	99.3	4.9	99.9	3.3	99.4	1.0	98.7
	intraday	2.9	96.4	7.7	98.1	0.9	100.9	2.0	101.1

0.05, 0.1, 1.0 and 50 nM *O*⁶-CMdG and *O*⁶-MedG were spiked in ctDNA (15 µg) and isolated DNA (15 µg) from unexposed HCEC cells followed by sample preparation and analysis as described. ^aRSD=relative standard deviation; ^bRec=recovery (accuracy)

Formation of *O*⁶-CMdG and *O*⁶-MedG by L-azaserine in HCEC cells. The establishment of a robust nanoLC-ESI-HRMS² approach for simultaneously quantifying *O*⁶-CMdG and *O*⁶-MedG enabled the measurement of L-azaserine-induced adducts in cells in a dose- and time-dependent manner. Immortalized but normal diploid human colonic epithelial HCEC cells were employed as a model for adduct formation in healthy colon tissue.³⁵ HCEC cells express epithelial and stem cell markers and do not show mutations in genes known to be involved in colon cancer progression (*APC*, *KRAS*, *TP53*).⁴⁵ HCEC cells were exposed to L-azaserine for 4 h, resulting in the formation of *O*⁶-CMdG and *O*⁶-MedG. The level of both adducts increased linearly with L-azaserine concentration (0-1000 µM) and in a dose-dependent manner, with maximum adduct levels of 32.8 ± 7.8 *O*⁶-CMdG and 4.3 ± 0.9 *O*⁶-MedG lesions/10⁷ nucleotides (Figure 6). Formation of *O*⁶-CMdG was minor compared to *O*⁶-

MedG, as reported previously.^{17, 27} We also detected O^6 -CMdG in unexposed control samples but at levels below LOQ, while O^6 -MedG 0.7 ± 1.3 lesions/ 10^7 nucleotides could be quantified in unexposed control samples. Endogenous O^6 -CMdG was previously reported in human colorectal cells (HCT-166) and in XPA-deficient human fibroblast cells, and O^6 -MedG is very well known to be formed endogenously.^{27, 46} We were not able to detect the O^6 -Ser-CMdG intermediate in cells, either because levels were below LOD, suggesting that the intermediate is rapidly hydrolyzed to O^6 -CMdG, or because it is not formed in cells.

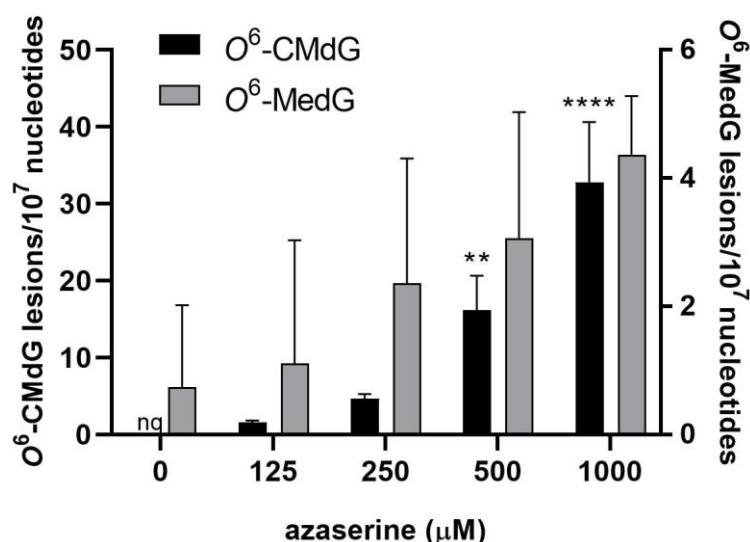


Figure 6. Dose-dependent formation of O^6 -CMdG and O^6 -MedG in HCEC cells. Cells were exposed for 4 h with 0, 125, 250, 500, or 1000 μ M L-azaserine, and extracted DNA was analyzed for O^6 -CMdG and O^6 -MedG by nanoLC-ESI-HRMS². Adduct levels are expressed as lesions/ 10^7 nucleotides (mean \pm SD, n=3). P-values were calculated with one-way ANOVA and Tukey's multiple comparison's test. Significance is shown in comparison to control, * $p < 0.05$, *** $p < 0.001$.

Having established the dose-dependent formation of O^6 -CMdG and O^6 -MedG after 4 h exposure to L-azaserine, we were interested in how levels of DNA adducts correlate with exposure time and specifically after what time of exposure maximal adduct levels were formed. Therefore, we exposed HCEC cells to 500 μ M L-azaserine (EC40 after 120 h, Figure S7) for various times (0.5, 4, 10, 24, 48, 72, 96, 120 h). After 0.5 h, adduct levels were below the LOQ for O^6 -CMdG and O^6 -MedG. O^6 -CMdG levels increased during the first 48 h to a maximum adduct level of 116 ± 21 O^6 -CMdG lesions/ 10^7 nucleotides (Figure 7) and plateaued after, displaying no changes in adduct level for the remaining three days. Also, O^6 -MedG level was maximum after 48 h of exposure; however, we could not establish a time-dependent relationship due to the overall low level of O^6 -MedG adducts formed in HCEC exposed to 500 μ M L-azaserine.

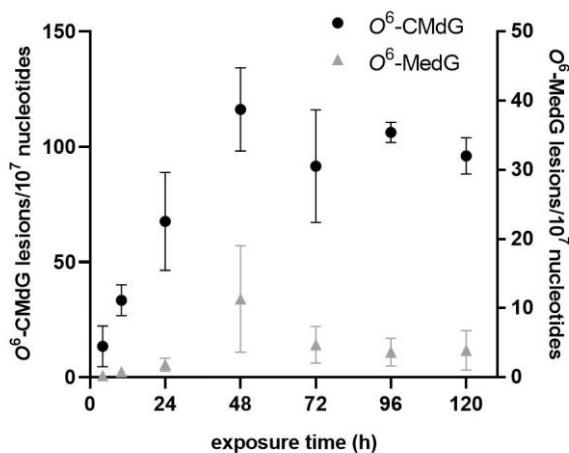


Figure 7. Time-dependent formation of *O*⁶-CMdG and *O*⁶-MedG in HCEC cells. Cells were exposed to 500 μ M L-azaserine and DNA was extracted after 0.5, 4, 10, 24, 48, 72, 96 and 120 h and further analyzed for *O*⁶-CMdG and *O*⁶-MedG levels by nanoLC-ESI-HRMS². Adduct levels are expressed as lesions/10⁷ nucleotides (mean \pm SD, n=3). Statistical analysis was performed using one-way ANOVA and Tukey's multiple comparison's test. (* $p < 0.05$)

2.5 Discussion

NOCs are well known carcinogens linked to diet and lifestyle. The formation of the pro-mutagenic DNA adducts *O*⁶-CMdG and *O*⁶-MedG by NOCs is well established,^{8, 10, 16-17, 27} however, the understanding of the chemical mechanism of NOC-induced *O*⁶-CMdG formation and factors that influence their biological consequences is limited. It has been hypothesized that the release of diazoacetate from NOCs and analogs is responsible for the carboxymethylation and methylation of DNA. However, if the reactive intermediate is the same for various NOCs, such as N-(N-acetyl-L-prolyl)-N-nitrosoglycine (APNG) and N-Nitrosoglycocholic acid (NOGC), and for the reactive intermediates L-azaserine and KDA, it remains unclear why they all result in different ratios of *O*⁶-CMdG to *O*⁶-MedG.^{17, 47} Further, the carboxymethylating decomposition products of N-nitroso bile acid conjugates have not been recovered quantitatively.⁴⁸ The lack of characterization of the metabolism of NOCs and of reactive intermediates raises the question of what are the mechanisms of carboxymethylation and methylation of DNA by NOCs, including the possibility of several pathways and intermediates.

Hydrolysis of L-azaserine to L-serine and diazoacetate has been suggested earlier by Harrison et al.¹⁷ and decomposition to diazoacetate as intermediate in *O*⁶-CMdG formation has been demonstrated for N-nitroso-glycine under physiological conditions.¹¹ However, in this study, we demonstrated that the carboxymethylating agent L-azaserine undergoes hydrolysis to L-serine only under acidic conditions, and that under physiologically relevant conditions, L-azaserine is stable. The half-life of L-azaserine increased from 0.4 h at pH 2 to 4.7 h at pH 3.4 (Figure 3 and S1) as stability increased with increasing pH. The observations of acid-promoted decompositions of L-azaserine are consistent with previous report of loss of antibiotic activity and N₂ formation at pH 2 for L-azaserine.⁴⁹ Indeed, α -diazo compounds are acid-labile, resulting in formation of reactive alkenium ions and loss of N₂.⁵⁰ Acid-promoted

decomposition was also demonstrated for diazopeptides and N-nitrosopeptides while under physiological conditions they are stable.⁵¹⁻⁵² Finally, under neutral conditions, diazoacetate was demonstrated to be an intermediate of N-nitroso-glycine-induced *O*⁶-CMdG and *O*⁶-MedG formation, potentially via formation of carboxymethyldiazonium ion and diazomethane, whereas the decomposition of NOCs with more stabilized α -diazocarboxy-groups,⁵³ e.g diazopeptides, has to our knowledge not been characterized under physiological conditions.¹¹

Based on the lack of evidence for the decomposition of L-azaserine at neutral pHs, we tested whether a direct reaction of dG with L-azaserine occurs under physiological conditions, thereby explaining *O*⁶-CMdG formation (Figure 2, A). After short (0.5 h) and long (24 h) reaction time of dG with L-azaserine, we detected *O*⁶-CMdG and *O*⁶-MedG, as well as *N*²-CMdG and *N*²-MedG. Next to carboxymethylated and methylated dG adducts in the reaction mixture of dG and L-azaserine, we could also identify *O*⁶-Ser-CMdG and, at a lower level, *N*²-Ser-CMdG, and their presence was further confirmed by targeted transitions (Figure 4). Both *O*⁶-Ser-CMdG and *N*²-Ser-CMdG were absent in the reaction mixture with KDA, the diazoacetate salt that was used as negative control. *O*⁶-Ser-CMdG as an intermediate was further confirmed by monitoring the conversion of isolated *O*⁶-Ser-CMdG to *O*⁶-CMdG over time under neutral conditions (Figure S5). The formation of Ser-CMdG from L-azaserine has been previously mentioned as a possibility, but it was never investigated.^{17, 54} Diazo compounds with stabilizing electron withdrawing groups are a useful tool in the modification and detection of biomolecules,⁵³ as demonstrated by the use of ethyldiazoacetate in carboxylation of dG.³⁶ Next to the *O*⁶- position, *N*⁷, *N*³, *N*² and *N*¹ represent nucleophilic sites in dG susceptible to modification by electrophilic reagents.⁵⁵ *N*⁷-CMG and *N*⁷-MeG have been detected after in vitro NOCs exposure, however, these readily depurinate.^{25, 54} Further, two methylated-dG adducts with modification other than at the *O*⁶-position were detected previously after exposure of ctDNA to KDA and one carboxymethylated-dG adduct other than *O*⁶ was present in colon tumor biopsy samples analyzed by a HRMS² approach for establishing a diet-related DNA adduct database.⁸

Finally, we characterized the formation and persistence of adducts in cells, as a function of L-azaserine dose and time of exposure. Therefore, we first developed and validated a nanoLC-ESI-HRMS² method for simultaneously quantifying *O*⁶-CMdG and *O*⁶-MedG in biological samples based on a PRM approach. To our knowledge, this is the first HRMS approach for the absolute quantification of *O*⁶-MedG and *O*⁶-CMdG in biological samples using stable isotope-labeled internal standards for accurate quantification of both adducts. A few methods involving triple quadrupole or ion traps as mass analyzer exist for the detection and quantification of *O*⁶-CM(d)G in biological samples,⁵⁶ also in combination with *O*⁶-Me(d)G.^{10, 27} A HRMS methodology targeting *O*⁶-MeG and *O*⁶-CMG and other targeted and untargeted DNA adducts was successfully applied to colon biopsy samples to establish a diet-related DNA adducts database and to compare the DNA adduct profile from white vs red meat in gastrointestinal digestion samples.^{8, 15} *O*⁶-MedG was further one of the targeted adducts in a reported adductomic approach for nitrosamine-induced DNA adducts.⁵⁷ Validation of our nanoLC-ESI-HRMS² approach revealed LOQs in matrix were in the low amol range and comparable to LOQs previously reported for pure standards on nanoLC-ESI-

MS³,²⁷ and improved compared to a HRMS method targeting four adducts biological matrix.⁸ Applying our methodology to HCEC cell exposed to L-azaserine, we found a linear response between L-azaserine-dose and O⁶-CMdG and O⁶-MedG adduct levels in HCEC cells (Figure 6). Both adducts were present in unexposed control samples, though not quantifiable for O⁶-CMdG and below one O⁶-MedG adduct/10⁷ nucleotides. We measured maximal O⁶-CMdG adduct levels in cells after 48 h of exposure, followed by a steady level up to 120 h (Figure 7). The O⁶-MedG profile showed a similar trend, but the adduct levels were too low for statistical analysis. The low O⁶-MedG levels observed are consistent with the more potent O⁶-CMdG formation by L-azaserine.¹⁶⁻¹⁷ Additionally, low levels of O⁶-MedG measured in cells might be due to efficient repair of O⁶-MedG by O⁶-methylguanine DNA methyl transferase (MGMT).⁵⁸ In a previous study, a maximum N⁷-MeG adduct level was achieved also after 48 h exposure to NDMA, however, in a process requiring metabolic activation by CYP enzymes.⁵⁹ Adduct levels were on the same order of magnitude as previously reported for colorectal cancer cells exposed to L-azaserine,²⁷ which was more potent in inducing O⁶-CMdG.²⁷ Endogenous O⁶-CMdG and O⁶-MedG formation has been reported previously and is likely due to the endogenous formation of s-adenosylmethionine and NOCs,^{27, 60-62} which account for 45-75% of the total human NOC exposure.^{19, 63} Although we collected convincing evidence for the intermediacy of O⁶-Ser-CMdG under biologically relevant conditions, we could find no clear evidence for its presence in azaserine-exposed cell samples. In addition to a chemical mechanism, in a biological system enzymes might also be involved in L-azaserine decomposition followed by formation of O⁶-CMdG and O⁶-MedG (Figure 2 C).³²⁻³³

2.6 Conclusion

In this study, we characterized the chemical basis of L-azaserine-induced O⁶-CMdG formation. We identified two mechanisms, occurring under acidic and physiological conditions respectively, by which L-azaserine converts into reactive intermediates and induces O⁶-CMdG. Our findings have implications for endogenously formed NOCs that do not breakdown to diazoacetate under physiological conditions but can form DNA adducts via nucleophilic attack. We established a highly sensitive nanoLC-ESI-HRMS² methodology and measured a linear-dose response relationship for O⁶-CMdG lesions in cells after exposure to L-azaserine. The knowledge of L-azaserine-induced DNA adduct formation has important implications to understand O⁶-CMdG formation and accumulation in cells, and to study its biological consequences. Overall, this work provides fundamental chemical insight concerning the basis of how azaserine gives rise to DNA damage and supports its use as a chemical probe in NOC-induced carcinogenesis research, particularly concerning the identification of factors that mitigate adverse effects of O⁶-CMdG.

Acknowledgements

The authors wish to thank the staff of the Functional Genomics Center Zurich (FGCZ) for providing nanoLC-ESI-HRMS² instrumentation and technical support, namely Dr. Bernd Roschitzki, Dr. Peter Gehrig, Dr. Serena di Palma, Dr. Endre Laczko and Laura Kunz. We also thank Dr. Hailey Gahlon for scientific advice and Jonne van Dijk for her support during the sample preparation.

2.7 References

1. Bouvard, V.; Loomis, D.; Guyton, K. Z.; Grosse, Y.; Ghissassi, F. E.; Benbrahim-Tallaa, L.; Guha, N.; Mattock, H.; Straif, K., Carcinogenicity of consumption of red and processed meat. *The Lancet Oncology* **2015**, *16* (16), 1599-1600.
2. Cross, A. J.; Pollock, J. R. A.; Bingham, S. A., Haem, not Protein or Inorganic Iron, Is Responsible for Endogenous Intestinal N-Nitrosation Arising from Red Meat. *Cancer research* **2003**, *63* (10), 2358-2360.
3. Turesky, R. J., Mechanistic Evidence for Red Meat and Processed Meat Intake and Cancer Risk: A Follow-up on the International Agency for Research on Cancer Evaluation of 2015. *Chimia* **2018**, *72* (10), 718-724.
4. Loechler, E. L.; Green, C. L.; Essigmann, J. M., In vivo mutagenesis by O6-methylguanine built into a unique site in a viral genome. *Proceedings of the National Academy of Sciences* **1984**, *81* (20), 6271-6275.
5. Pauly, G. T.; Moschel, R. C., Mutagenesis by O6-Methyl-, O6-Ethyl-, and O6-Benzylguanine and O4-Methylthymine in Human Cells: Effects of O6-Alkylguanine-DNA Alkyltransferase and Mismatch Repair. *Chemical Research in Toxicology* **2001**, *14* (7), 894-900.
6. Hall, C. N.; Badawi, A. F.; O'Connor, P. J.; Saffhill, R., The detection of alkylation damage in the DNA of human gastrointestinal tissues. *Br J Cancer* **1991**, *64* (1), 59-63.
7. Group, T. E. S., O6-methylguanine in blood leucocyte DNA: an association with the geographic prevalence of gastric cancer and with low levels of serum pepsinogen A, a marker of severe chronic atrophic gastritis. *Carcinogenesis* **1994**, *15* (9), 1815-20.
8. Hemeryck, L. Y.; Declodt, A. I.; Vanden Bussche, J.; Geboes, K. P.; Vanhaecke, L., High resolution mass spectrometry based profiling of diet-related deoxyribonucleic acid adducts. *Analytica Chimica Acta* **2015**, *892*, 123-131.
9. Povey, A. C.; Hall, C. N.; Badawi, A. F.; Cooper, D. P.; O'Connor, P. J., Elevated levels of the pro-carcinogenic adduct, O(6)-methylguanine, in normal DNA from the cancer prone regions of the large bowel. *Gut* **2000**, *47* (3), 362-365.
10. Vanden Bussche, J.; Moore, S. A.; Pasmans, F.; Kuhnle, G. G. C.; Vanhaecke, L., An approach based on ultra-high pressure liquid chromatography–tandem mass spectrometry to quantify O6-methyl and O6-carboxymethylguanine DNA adducts in intestinal cell lines. *Journal of Chromatography A* **2012**, *1257*, 25-33.
11. Cupid, B. C.; Zeng, Z.; Singh, R.; Shuker, D. E. G., Detection of O6-Carboxymethyl-2'-deoxyguanosine in DNA Following Reaction of Nitric Oxide with Glycine and in Human Blood DNA Using a Quantitative Immunoslot Blot Assay. *Chemical Research in Toxicology* **2004**, *17* (3), 294-300.
12. Lewin, M. H.; Bailey, N.; Bandaletova, T.; Bowman, R.; Cross, A. J.; Pollock, J.; Shuker, D. E. G.; Bingham, S. A., Red Meat Enhances the Colonic Formation of the DNA Adduct O⁶-Carboxymethyl Guanine: Implications for Colorectal Cancer Risk. *Cancer research* **2006**, *66* (3), 1859-1865.
13. Bussche, J. V.; Hemeryck, L. Y.; Van Hecke, T.; Kuhnle, G. G. C.; Pasmans, F.; Moore, S. A.; Van de Wiele, T.; De Smet, S.; Vanhaecke, L., O6-carboxymethylguanine DNA adduct formation and lipid peroxidation upon in vitro gastrointestinal digestion of haem-rich meat. *Molecular Nutrition & Food Research* **2014**, *58* (9), 1883-1896.
14. Hemeryck, L. Y.; Rombouts, C.; Hecke, T. V.; Van Meulebroek, L.; Bussche, J. V.; De Smet, S.; Vanhaecke, L., In vitro DNA adduct profiling to mechanistically link red meat consumption to colon cancer promotion. *Toxicol Res (Camb)* **2016**, *5* (5), 1346-1358.
15. Hemeryck, L. Y.; Rombouts, C.; De Paepe, E.; Vanhaecke, L., DNA adduct profiling of in vitro colonic meat digests to map red vs. white meat genotoxicity. *Food and chemical toxicology : an international journal published for the British Industrial Biological Research Association* **2018**, *115*, 73-87.
16. Harrison, K. L.; Fairhurst, N.; Challis, B. C.; Shuker, D. E. G., Synthesis, Characterization, and Immunochemical Detection of O6-(Carboxymethyl)-2'-deoxyguanosine: A DNA Adduct Formed by Nitrosated Glycine Derivatives. *Chemical Research in Toxicology* **1997**, *10* (6), 652-659.
17. Harrison, K. L.; Jukes, R.; Cooper, D. P.; Shuker, D. E. G., Detection of Concomitant Formation of O6-Carboxymethyl- and O6-Methyl-2'-deoxyguanosine in DNA Exposed to Nitrosated Glycine Derivatives Using a Combined Immunoaffinity/HPLC Method. *Chemical Research in Toxicology* **1999**, *12* (1), 106-111.

18. Stuff, J. E.; Goh, E. T.; Barrera, S. L.; Bondy, M. L.; Forman, M. R., Construction of an N-nitroso database for assessing dietary intake. *Journal of Food Composition and Analysis* **2009**, *22*, S42-S47.
19. Mirvish, S. S., Role of N-nitroso compounds (NOC) and N-nitrosation in etiology of gastric, esophageal, nasopharyngeal and bladder cancer and contribution to cancer of known exposures to NOC. *Cancer letters* **1995**, *93* (1), 17-48.
20. Wu, J.; Wang, P.; Li, L.; Williams, N. L.; Ji, D.; Zahurancik, W. J.; You, C.; Wang, J.; Suo, Z.; Wang, Y., Replication studies of carboxymethylated DNA lesions in human cells. *Nucleic Acids Research* **2017**, *45* (12), 7276-7284.
21. Ráz, M. H.; Dexter, H. R.; Millington, C. L.; van Loon, B.; Williams, D. M.; Sturla, S. J., Bypass of Mutagenic O(6)-Carboxymethylguanine DNA Adducts by Human Y- and B-Family Polymerases. *Chem Res Toxicol* **2016**, *29* (9), 1493-503.
22. Gottschalg, E.; Scott, G. B.; Burns, P. A.; Shuker, D. E., Potassium diazoacetate-induced p53 mutations in vitro in relation to formation of O6-carboxymethyl- and O6-methyl-2'-deoxyguanosine DNA adducts: relevance for gastrointestinal cancer. *Carcinogenesis* **2007**, *28* (2), 356-62.
23. Andreyev, H. J.; Norman, A. R.; Cunningham, D.; Oates, J.; Dix, B. R.; Iacopetta, B. J.; Young, J.; Walsh, T.; Ward, R.; Hawkins, N.; Beranek, M.; Jandik, P.; Benamouzig, R.; Jullian, E.; Laurent-Puig, P.; Olschwang, S.; Muller, O.; Hoffmann, I.; Rabes, H. M.; Zietz, C.; Troungos, C.; Valavanis, C.; Yuen, S. T.; Ho, J. W.; Croke, C. T.; O'Donoghue, D. P.; Giaretti, W.; Rapallo, A.; Russo, A.; Bazan, V.; Tanaka, M.; Omura, K.; Azuma, T.; Ohkusa, T.; Fujimori, T.; Ono, Y.; Pauly, M.; Faber, C.; Glaesener, R.; de Goeij, A. F.; Arends, J. W.; Andersen, S. N.; Lövig, T.; Breivik, J.; Gaudernack, G.; Clausen, O. P.; De Angelis, P. D.; Meling, G. I.; Rognum, T. O.; Smith, R.; Goh, H. S.; Font, A.; Rosell, R.; Sun, X. F.; Zhang, H.; Benhattar, J.; Losi, L.; Lee, J. Q.; Wang, S. T.; Clarke, P. A.; Bell, S.; Quirke, P.; Bubb, V. J.; Piris, J.; Cruickshank, N. R.; Morton, D.; Fox, J. C.; Al-Mulla, F.; Lees, N.; Hall, C. N.; Snary, D.; Wilkinson, K.; Dillon, D.; Costa, J.; Pricolo, V. E.; Finkelstein, S. D.; Thebo, J. S.; Senagore, A. J.; Halter, S. A.; Wadler, S.; Malik, S.; Krtolica, K.; Urošević, N., Kirsten ras mutations in patients with colorectal cancer: the 'RASCAL II' study. *British journal of cancer* **2001**, *85* (5), 692-696.
24. Wang, J.; Wang, Y., Carboxymethylation of DNA Induced by N-Nitroso Compounds and Its Biological Implications. *Advances in Molecular Toxicology* **2011**, *5*, 219-243.
25. Shuker, D. E. G.; Margison, G. P., Nitrosated Glycine Derivatives as a Potential Source of O⁶-Methylguanine in DNA. *Cancer research* **1997**, *57* (3), 366-369.
26. O'Driscoll, M.; Macpherson, P.; Xu, Y.-Z.; Karran, P., The cytotoxicity of DNA carboxymethylation and methylation by the model carboxymethylating agent azaserine in human cells. *Carcinogenesis* **1999**, *20* (9), 1855-1862.
27. Yu, Y.; Wang, J.; Wang, P.; Wang, Y., Quantification of Azaserine-Induced Carboxymethylated and Methylated DNA Lesions in Cells by Nanoflow Liquid Chromatography-Nanoelectrospray Ionization Tandem Mass Spectrometry Coupled with the Stable Isotope-Dilution Method. *Analytical Chemistry* **2016**, *88* (16), 8036-8042.
28. Wang, J.; Wang, Y., Chemical synthesis of oligodeoxyribonucleotides containing N3- and O4-carboxymethylthymidine and their formation in DNA. *Nucleic Acids Research* **2009**, *37* (2), 336-45.
29. Stock, C. C.; Reilly, H. C.; Buckley, S. M.; Clarke, D. A.; Rhodas, C. P., Azaserine, A New Tumour-Inhibitory Substance: Studies with Crocker Mouse Sarcoma 180. *Nature* **1954**, *173* (4393), 71-72.
30. Longnecker, D. S.; Curphey, T. J., Adenocarcinoma of the Pancreas in Azaserine-treated Rats. *Cancer research* **1975**, *35* (8), 2249-2257.
31. Lilja, H. S.; Hyde, E.; Longnecker, D. S.; Yager, J. D., DNA Damage and Repair in Rat Tissues following Administration of Azaserine. *Cancer research* **1977**, *37* (11), 3925-3931.
32. Rosenkrantz, H.; Sprague, R.; Schaeppi, U.; Pittillo, R. T.; Cooney, D. A.; Davis, R. D., The stoichiometric fate of azaserine metabolized in vitro by tissues from azaserine-treated dogs and mice. *Toxicology and Applied Pharmacology* **1972**, *22* (4), 607-620.
33. Jacques, J. A.; Sherman, J. H., Enzymatic Degradation of Azaserine. *Cancer research* **1962**, *22* (1 Part 1), 56.
34. Longenecker, J. B.; Snell, E. E., Pyridoxal and metal ion catalysis of alpha, beta elimination reactions of serine-3-phosphate and related compounds. *The Journal of biological chemistry* **1957**, *225* (1), 409-18.

35. Zhang, L.; Kim, S.; Jia, G.; Buhmeida, A.; Dallol, A.; Wright, W. E.; Fornace, A. J.; Al-Qahtani, M.; Shay, J. W., Exome Sequencing of Normal and Isogenic Transformed Human Colonic Epithelial Cells (HCECs) Reveals Novel Genes Potentially Involved in the Early Stages of Colorectal Tumorigenesis. *BMC genomics* **2015**, *16 Suppl 1* (Suppl 1), S8.
36. Geigle, S. N.; Wyss, L. A.; Sturla, S. J.; Gillingham, D. G., Copper carbenes alkylate guanine chemoselectively through a substrate directed reaction. *Chemical Science* **2017**, *8* (1), 499-506.
37. Reza, F.; Bhaswati, G.; Pei-Pei, K.; Gaffney, B. L.; Jones, R. A., Synthesis of 6-substituted 2'-deoxyguanosine derivatives using trifluoroacetic anhydride in pyridine. *Tetrahedron Letters* **1990**, *31* (3), 319-321.
38. https://bioscience.lonza.com/lonza_bs/CH/en/download/product/asset/27672. Lonza online protocol.
39. <https://ch.promega.com/-/media/files/resources/protocols/technical-bulletins/0/celltiter-glo-luminescent-cell-viability-assay-protocol.pdf>. Promega online protocol.
40. Piovesan, A.; Pelleri, M. C.; Antonaros, F.; Strippoli, P.; Caracausi, M.; Vitale, L., On the length, weight and GC content of the human genome. *BMC Research Notes* **2019**, *12* (1), 106.
41. Zhang, P.; Chan, W.; Ang, I. L.; Wei, R.; Lam, M. M. T.; Lei, K. M. K.; Poon, T. C. W., Revisiting Fragmentation Reactions of Protonated α -Amino Acids by High-Resolution Electrospray Ionization Tandem Mass Spectrometry with Collision-Induced Dissociation. *Scientific Reports* **2019**, *9* (1), 6453.
42. Rogalewicz, F.; Hoppilliard, Y.; Ohanessian, G., Fragmentation mechanisms of α -amino acids protonated under electrospray ionization: a collisional activation and ab initio theoretical study11Dedicated to Bob Squires for his many seminal contributions to mass spectrometry and ion chemistry. *International Journal of Mass Spectrometry* **2000**, *195-196*, 565-590.
43. Piraud, M.; Vianey-Saban, C.; Petritis, K.; Elfakir, C.; Steghens, J.-P.; Morla, A.; Bouchu, D., ESI-MS/MS analysis of underivatized amino acids: a new tool for the diagnosis of inherited disorders of amino acid metabolism. Fragmentation study of 79 molecules of biological interest in positive and negative ionisation mode. *Rapid Communications in Mass Spectrometry* **2003**, *17* (12), 1297-1311.
44. McGarrity, J. F.; Smyth, T., Hydrolysis of diazomethane-kinetics and mechanism. *Journal of the American Chemical Society* **1980**, *102* (24), 7303-7308.
45. Roig, A. I.; Eskioçak, U.; Hight, S. K.; Kim, S. B.; Delgado, O.; Souza, R. F.; Spechler, S. J.; Wright, W. E.; Shay, J. W., Immortalized Epithelial Cells Derived From Human Colon Biopsies Express Stem Cell Markers and Differentiate In Vitro. *Gastroenterology* **2010**, *138* (3), 1012-1021.e5.
46. Nakamura, J.; Mutlu, E.; Sharma, V.; Collins, L.; Bodnar, W.; Yu, R.; Lai, Y.; Moeller, B.; Lu, K.; Swenberg, J., The endogenous exposome. *DNA repair* **2014**, *19*, 3-13.
47. Shuker, D. E. G.; Margison, G. P., Nitrosated Glycine Derivatives as a Potential Source of O⁶-Methylguanine in DNA. *Cancer research* **1997**, *57* (3), 366.
48. Shuker, D. E. G.; Tannenbaum, S. R.; Wishnok, J. S., N-Nitroso bile acid conjugates. 1. Synthesis, chemical reactivity and mutagenic activity. *The Journal of Organic Chemistry* **1981**, *46* (10), 2092-2096.
49. Bartz, Q. R.; Elder, C. C.; Frohardt, R. P.; Fusari, S. A.; Haskell, T. H.; Johannessen, D. W.; Ryder, A., Isolation and characterization of azaserine. *Nature* **1954**, *173* (4393), 72-3.
50. Reglitz, M., *Diazo Compounds: Properties and Synthesis*. Elsevier: 2012.
51. Challis, B. C., Chemistry and biology of nitrosated peptides. *Cancer surveys* **1989**, *8* (2), 363-84.
52. Challis, B. C.; Hopkins, A. R.; Milligan, J. R.; Mitchell, R. C.; Massey, R. C., Nitrosation of peptides. *IARC scientific publications* **1984**, (57), 61-70.
53. Mix, K. A.; Aronoff, M. R.; Raines, R. T., Diazo Compounds: Versatile Tools for Chemical Biology. *ACS Chem Biol* **2016**, *11* (12), 3233-3244.
54. Zurlo, J.; Curphey, T. J.; Hiley, R.; Longnecker, D. S., Identification of 7-Carboxymethylguanine in DNA from Pancreatic Acinar Cells Exposed to Azaserine. *Cancer research* **1982**, *42* (4), 1286-1288.
55. Liu, S.; Wang, Y., Mass spectrometry for the assessment of the occurrence and biological consequences of DNA adducts. *Chemical Society reviews* **2015**, *44* (21), 7829-7854.
56. Da Pieve, C.; Sahgal, N.; Moore, S. A.; Velasco-Garcia, M. N., Development of a liquid chromatography/tandem mass spectrometry method to investigate the presence of biomarkers of DNA damage in

urine related to red meat consumption and risk of colorectal cancer. *Rapid communications in mass spectrometry* : *RCM* **2013**, 27 (21), 2493-503.

57. Balbo, S.; Hecht, S. S.; Upadhyaya, P.; Villalta, P. W., Application of a High-Resolution Mass-Spectrometry-Based DNA Adductomics Approach for Identification of DNA Adducts in Complex Mixtures. *Analytical Chemistry* **2014**, 86 (3), 1744-1752.

58. Pegg, A. E., Repair of O(6)-alkylguanine by alkyltransferases. *Mutat Res* **2000**, 462 (2-3), 83-100.

59. Lin, H.-l.; Hollenberg, P. F., N-Nitrosodimethylamine-Mediated Formation of Oxidized and Methylated DNA Bases in a Cytochrome P450 2E1 Expressing Cell Line. *Chemical Research in Toxicology* **2001**, 14 (5), 562-566.

60. Sharma, V.; Collins, L. B.; Clement, J. M.; Zhang, Z.; Nakamura, J.; Swenberg, J. A., Molecular Dosimetry of Endogenous and Exogenous O6-Methyl-dG and N7-Methyl-G Adducts Following Low Dose [D3]-Methylnitrosourea Exposures in Cultured Human Cells. *Chemical Research in Toxicology* **2014**, 27 (4), 480-482.

61. Kang, H.; Konishi, C.; Kuroki, T.; Huh, N., Detection of O6-methylguanine, O4-methylthymine and O4-ethylthymine in human liver and peripheral blood leukocyte DNA. *Carcinogenesis* **1995**, 16 (6), 1277-80.

62. De Bont, R.; van Larebeke, N., Endogenous DNA damage in humans: a review of quantitative data. *Mutagenesis* **2004**, 19 (3), 169-185.

63. Tricker, A. R., N-nitroso compounds and man: sources of exposure, endogenous formation and occurrence in body fluids. *Eur J Cancer Prev* **1997**, 6 (3), 226-268.

Supporting Information

for

Chemical mechanism of O^6 -carboxymethyldeoxyguanosine formation from azaserine and abundance in cells

Susanne M. Geisen[†], Nora Escher[†], Claudia M.N. Aloisi[†], Shana J. Sturla^{†}*

[†]Department of Health Science and Technology, ETH Zurich, 8092 Zurich, Switzerland

*Corresponding author: Shana J. Sturla, Email: shana.sturla@hest.ethz.ch

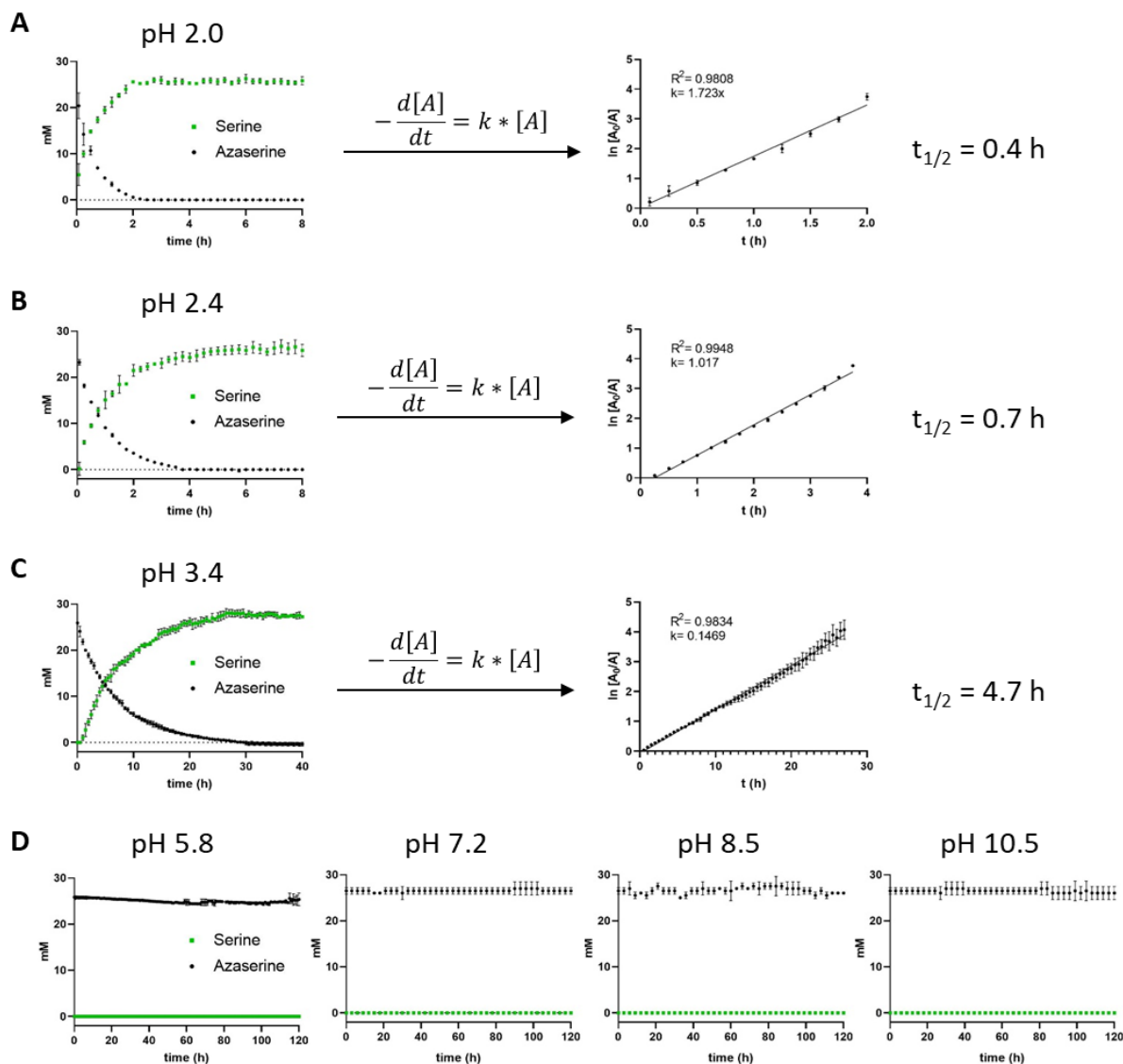


Figure S1. Acid-promoted hydrolysis of L-azaserine. Hydrolysis of L-azaserine to L-serine at **A** pH 2, $t_{1/2}=0.4$ h **B** pH 2.4, $t_{1/2}=0.7$ h. and **C** pH 3.4, $t_{1/2}=4.7$ h. Hydrolysis of L-azaserine was modeled as a reaction of pseudo first order and half-life ($t_{1/2}$) calculated with the following equations: $\frac{\ln[A_0]}{\ln[A]} = kt$, $t_{1/2} = \frac{\ln 2}{k}$ where $[A_0]$ =starting concentration of L-azaserine (mM), $[A]$ =concentration of L-azaserine at t (mM), k =slope (1/h), ($n=3$). **D** No hydrolysis of L-azaserine L-serine was observed when pH was 5.8, 7.2, 8.5 and 10.5 over 120 h ($n=2$).

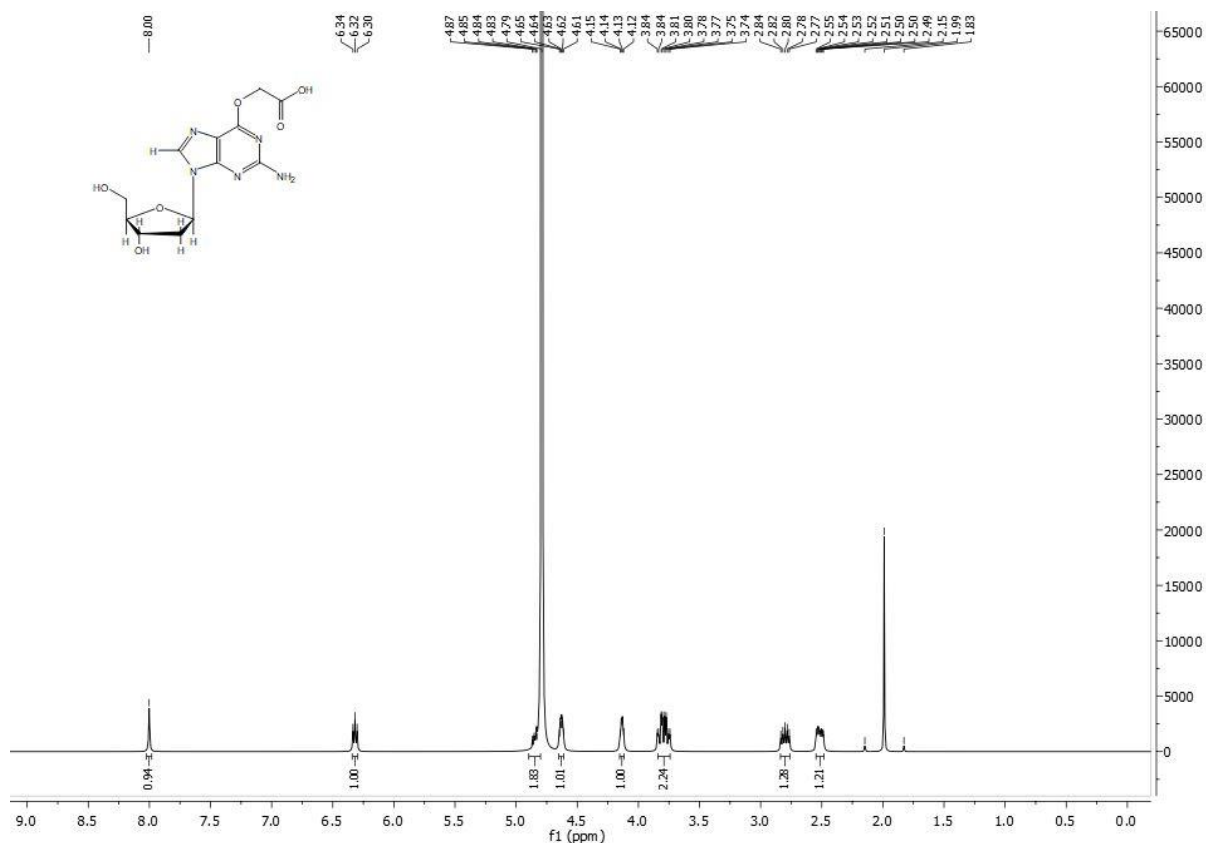


Figure S2. ^1H NMR (400 MHz, Deuterium Oxide) of $O^6\text{-CMdG}$ as standard for quantification by nanoLC-ESI-HRMS². $O^6\text{-CMdG}$: δ 8.00 (s, 1H, Ar-H), 6.32 (t, $J = 6.9$ Hz, 1H, 1'-H), 4.87 – 4.83 (m, 2H, O-CH₂), 4.63 (dt, $J = 6.5, 3.4$ Hz, 1H, 4'-H), 4.14 (q, $J = 3.8$ Hz, 1H, 3'-H), 3.79 (qd, $J = 12.5, 4.2$ Hz, 2H, 5'-H), 2.80 (dt, $J = 13.9, 6.8$ Hz, 1H, 2'-H), 2.52 (ddd, $J = 14.1, 6.4, 3.7$ Hz, 1H, 2'-H).

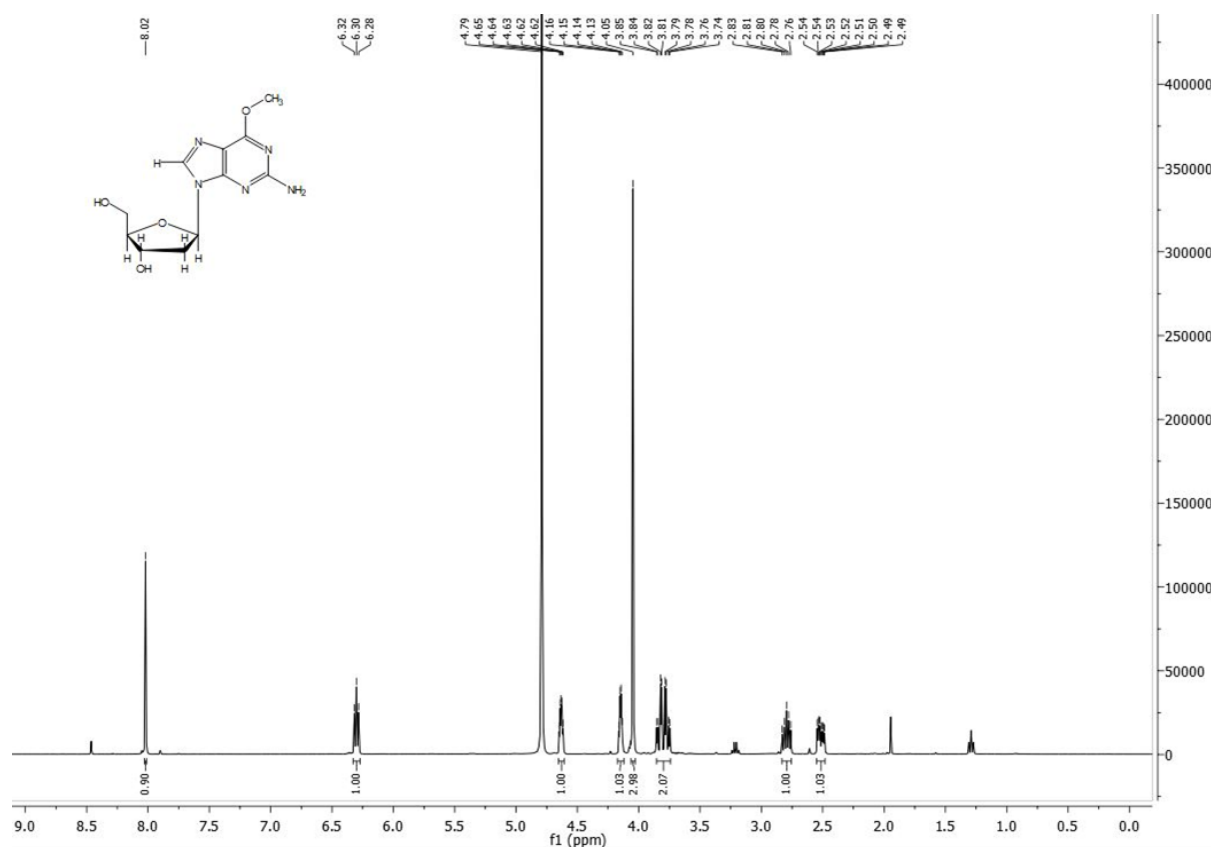


Figure S3. ^1H NMR (400 MHz, Deuterium Oxide) of O^6 -MedG as standard for quantification by nanoLC-ESI-HRMS². O^6 -MedG: δ 8.02 (s, 1H, Ar-H), 6.30 (t, J = 6.9 Hz, 1H, 1'-H), 4.63 (dt, J = 6.1, 3.1 Hz, 1H, 4'-H), 4.15 (q, J = 3.5 Hz, 1H, 3'-H), 4.05 (s, 3H, O-CH₃), 3.80 (qd, J = 12.6, 3.9 Hz, 2H, 5'-H), 2.80 (dt, J = 13.9, 6.8 Hz, 1H, 2'-H), 2.52 (ddd, J = 14.0, 6.2, 3.3 Hz, 1H, 2'-H).

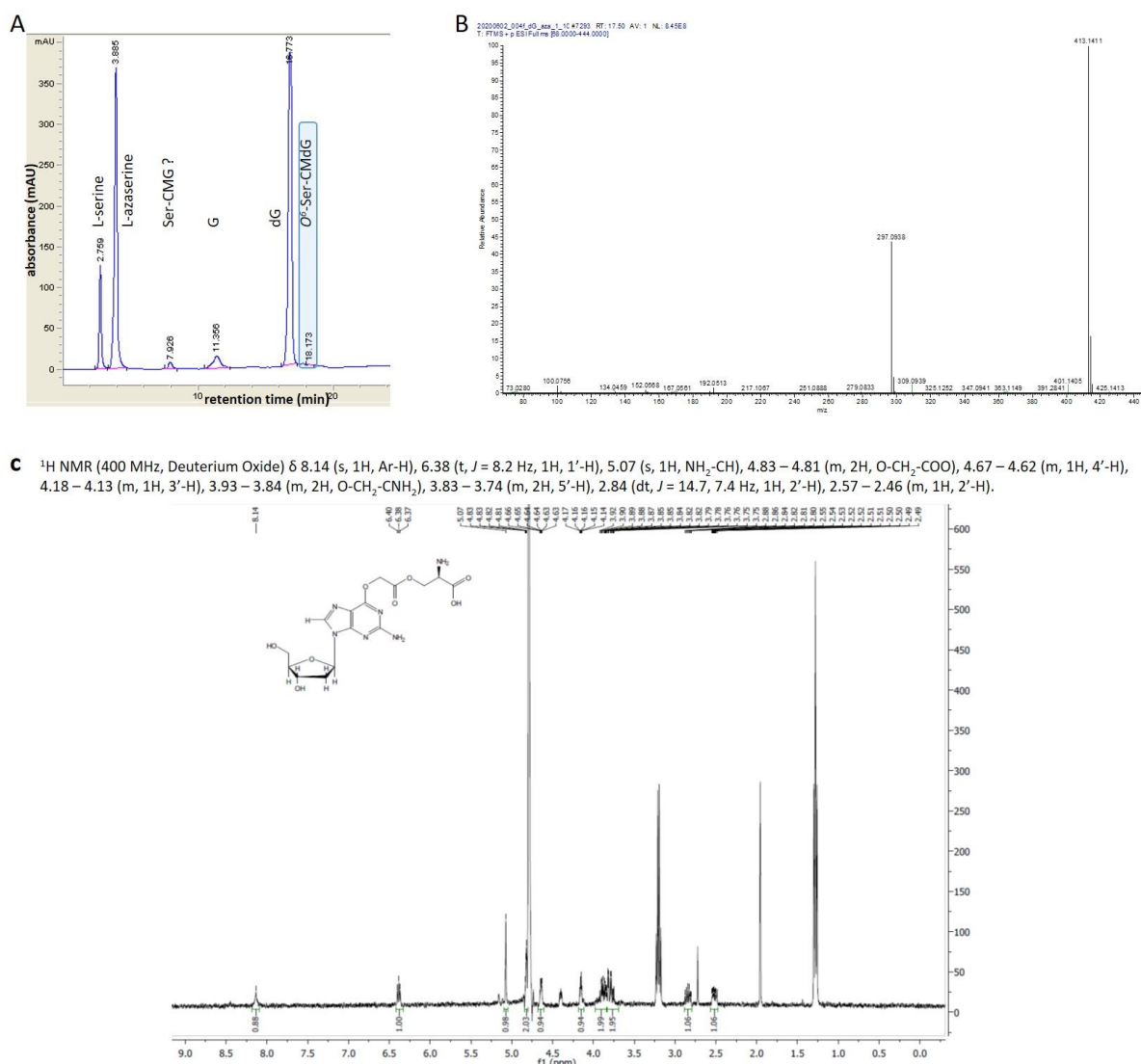


Figure S4. Characterization of O^6 -Ser-CMdG. **A.** A representative liquid chromatography chromatogram at $\lambda=210$ nm of a dG azaserine reaction mixture in water after 102 h. The peak at retention time of 18.7 min was collected for further characterization. **B.** NanoLC-ESI-HRMS on an Orbitrap FusionTM LumosTM (Thermo Scientific, Waltham, Massachusetts) characterization of the peak isolated by liquid chromatography. Most intense peak is m/z 413.1411 $[\text{M}+\text{H}]^+$ being identical to the calculated m/z for an O^6 -Ser-CMdG intermediate (413.1421), second intense peak is 297.0938 $[\text{M}+\text{H}]^+$, being identical to the calculated m/z of a O^6 -Ser-CMG intermediate (297.0947) most likely from loss of deoxyribose during the ionization process. **C.** ^1H NMR of the isolated compound confirming the O^6 -Ser-CMdG structure.

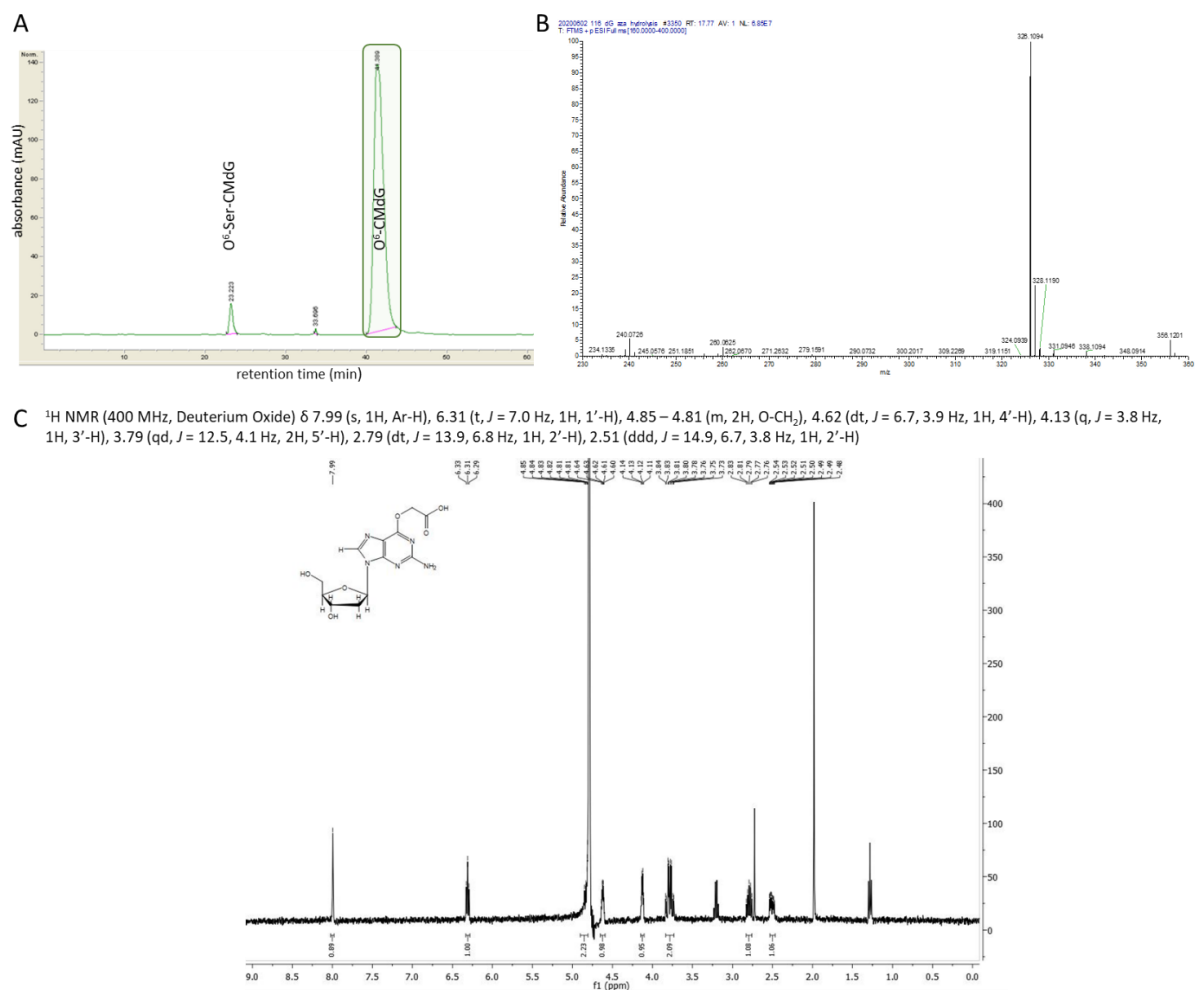


Figure S5. Characterization of the decomposition product of O^6 -Ser-CMdG. **A.** A representative liquid chromatography chromatogram at $\lambda=280$ nm of O^6 -Ser-CMdG after 30 h in D_2O . O^6 -Ser-CMdG (22.2 min) is not completely hydrolyzed. The peak at retention 41.3 min was collected for further characterization. **B.** NanoLC-ESI-HRMS characterization of the peak isolated by liquid chromatography. Most intense peak is m/z 326.1094 $[M+H]^+$ being identical to the calculated m/z for O^6 -CMdG (326.1101) **C.** ^1H NMR of the isolated compound confirming the O^6 -CMdG structure.

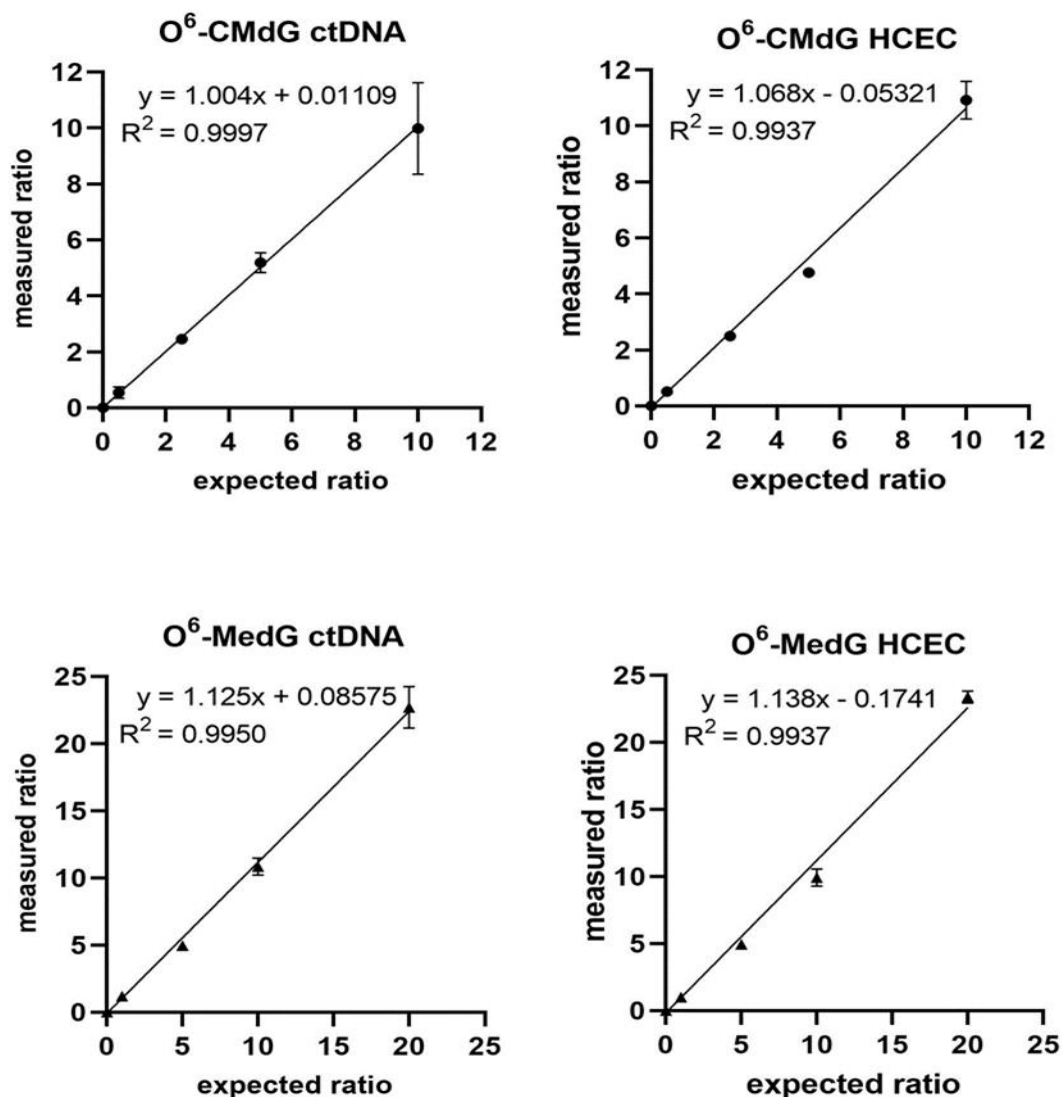


Figure S6. Validation results for the quantification of *O*⁶-CMdG and *O*⁶-MedG by nanoLC-ESI-HRMS². 0.01-200 nM *O*⁶-CMdG and *O*⁶-MedG were spiked in ctDNA (15 μg) or isolated DNA (15 μg) from unexposed HCEC cells followed by sample preparation and analysis as described. Results were plotted as measured ratio of analyte /internal standards over expected ratio of analyte/internal standard. Reasonable linearity was achieved for the analysis of *O*⁶-CMdG and *O*⁶-MedG in matrix.

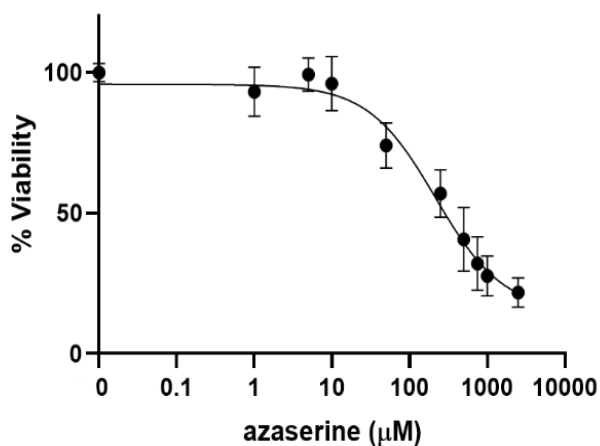


Figure S7. Viability of HCEC cells exposed to azaserine. Cells were exposed to 0, 1, 10, 50, 250, 750, 1000 and 2500 μM azaserine for 120 h and cell viability was determined by CellTiterGlo. Cell viability is expressed in % to un-exposed control cells (100 % viability) (mean ± SD, n=3). When exposed to 500 μM azaserine, concentration chosen for time-dependent adduct level measurement (Figure 7), 40 % of cells were viable after 120 h. Data were fitted in a nonlinear curve using the function [Inhibitor] vs response of GraphPad (R^2 was 0.92). EC50 was calculated to be 220 μM.

Chapter 3: A combination of direct reversion and excision repair in cells reduces the mutagenic effects of DNA carboxymethylation

Manuscript in preparation

Claudia M.N. Aloisi, Nora A. Escher, Susanne M. Geisen, Hyun S. Kim, Jung E. Yeo, Orlando D. Schärer, Shana J. Sturla*

Aloisi C.M.N. designed the studies, synthesized O^6 -CMG containing phosphoramidites and oligonucleotides, produced circular DNA for NER assay, performed EMSA and carried out cell-based studies and DNA extraction. Escher N.A. carried out cell-based studies, DNA extraction, and produced circular DNA for NER assay. Geisen S.M. performed sample preparation and mass spectrometry analysis of genomic DNA from exposed cells. Kim H.S. and Yeo J.E. assisted in EMSA and performed NER assay. Aloisi C.M.N., Escher N.A. and Geisen S.M. interpreted data. Aloisi C.M.N., Schärer O.D. and Sturla S.J. conceived the research. Aloisi C.M.N., Geisen S.M., Schärer O.D. and Sturla S.J. wrote the manuscript.

A combination of direct reversion and excision repair in cells reduces the mutagenic effects of DNA carboxymethylation

Claudia M.N. Aloisi¹, Nora A. Escher¹, Susanne M. Geisen¹, Hyun S. Kim², Jung E. Yeo², Orlando D. Schärer², Shana J. Sturla^{1*}

¹Laboratory of Toxicology, Institute of Food Nutrition and Health, Swiss Federal Institute of Technology, 8092 Zürich, Switzerland

²Ulsan National Institute of Science and Technology, Ulsan, Korea

*Correspondence to Prof. Shana J. Sturla, Email: sturlas@ethz.ch

3.1 Abstract

*O*⁶-alkylguanines are some of the most mutagenic forms of damage to genomic DNA and are a molecular initiating event in chemical carcinogenesis. The occurrence of *O*⁶-carboxymethylguanine (*O*⁶-CMG) in particular has been linked to meat consumption and hypothesized to contribute to the development of colorectal cancer. However, the cellular fate of *O*⁶-CMG is poorly characterized and the literature on repair mechanisms that protect cells from *O*⁶-CMG mutagenicity is contradictory. With the present work, we unravelled a longstanding question in DNA repair concerning the identification of how cells target and remove *O*⁶-CMG. We found that cells deficient in either *O*⁶-methylguanine-DNA methyltransferase enzyme or nucleotide excision repair machinery accumulate *O*⁶-CMG DNA adducts and are, therefore, more sensitive to carboxymethylating agents, mutating at a higher rate. The findings of this work advance our understanding of the relationship between *O*⁶-CMG DNA damage, repair and DNA mutation.

3.2 Introduction

DNA is continuously damaged by endogenous cellular events and exogenous environmental agents. In response to the DNA damage, a complex network of proteins is activated to sense and repair the damage.¹ To overcome the blockage to replication, damage can also be tolerated and bypasses at the expense of introducing mutations in the DNA, increasing the likelihood of carcinogenesis when cancer driver genes are affected.

*O*⁶-alkyl-guanines (*O*⁶-alkylGs) are mutagenic DNA adducts that have been linked to the development of cancer.²⁻⁴ *O*⁶-alkylGs are formed by exposure to endogenous and exogenous alkylating agents such as N-nitroso compounds (NOCs)⁵ and anticancer drugs such as temozolomide that decompose into alkyl-diazonium cations.⁶ Common exogenous sources of NOCs and of their precursors to humans are drugs,⁷ tobacco smoke,⁷ red and processed meat.⁸ NOCs precursors include nitrogenous dietary compounds that can be converted to NOCs through nitrite-derived nitrosation,⁹ a reaction favoured in the acidic gastric environment.¹⁰

Particularly relevant to dietary factors and digestion processes, *O*⁶-carboxymethylguanine (*O*⁶-CMG) has been detected in human colorectal DNA,¹¹ and its formation has been associated with meat consumption.^{8, 12} Therefore, *O*⁶-CMG has been hypothesized to be a potential molecular initiating event in the development of colorectal cancer (CRC) linked to diets high in meat.¹³ *O*⁶-CMG DNA adduct is highly mutagenic and the mutational spectrum induced by a carboxymethylating agent in the cancer-relevant gene *p53* resembled the one measured in CRC and stomach cancer tissues.¹⁴ Studies interrogating the fidelity of replication past *O*⁶-CMG performed *in vitro*¹⁵⁻¹⁷ and *in vivo* in bacteria¹⁸ have shown that T can be incorporated opposite *O*⁶-CMG instead of A, providing a basis for its mutagenicity and a potential cause-effect relationship with carcinogenesis.

While the structural and mechanistic basis of *O*⁶-CMG mutagenicity has been investigated, there is a lack of knowledge of how *O*⁶-CMG is eliminated from genomic DNA to alleviate the rise of mutations, with only few studies hinting at a role of *O*⁶-methylguanine-DNA methyltransferase (MGMT) and nucleotide excision repair (NER) in the repair of *O*⁶-CMG.¹⁹⁻

²¹ MGMT is an alkyl transferase that can directly remove the methyl group from O^6 -MeG DNA.²²⁻²⁴ The human MGMT gene shares homology with other species including rodents, and analogously to humans, mice deficient in MGMT were hypersensitive to methylating agents and showed increased tumorigenesis.²⁵⁻²⁸ The level of MGMT was a reliable predictor of sensitivity of human tumors to treatment with the alkylating agent temozolomide.^{29, 30} In contrast to repair by MGMT, which is mediated by a single enzyme, NER involves the concerted function of several factors, and it is made of two sub-pathways, global genome (GG) and transcription coupled (TC)-NER, which differ in the step of lesion recognition. GG-NER is initiated by XPC-RAD23B that recognizes DNA duplex distorting lesions, and TC-NER is initiated by the stalling of transcribing RNA polymerase with the help of CSB.

The carcinogen azaserine is used to form O^6 -CMG in cells and it was shown to induce DNA mutations.³¹ Bacteria and yeast cells deficient in NER genes showed hypersensitivity and increased mutation rate following azaserine exposure.³²⁻³⁴ Karran and colleagues exposed human cell lines with DNA repair defects to azaserine and found that NER-deficient cells were sensitive to the treatment.²¹ By contrast, deficiencies in other repair pathways including MGMT did not influence cell survival,²¹ in line with previous observation that purified bacterial MGMT were not able to remove the carboxymethyl- group from O^6 -CMG-oligonucleotides.¹⁹ Given the well-established role of MGMT in repairing O^6 -MeG, the activity of MGMT towards O^6 -CMG was readdressed in 2013, and O^6 -CMG was found to be a competent substrate of the purified human MGMT.²⁰ However, evidence that MGMT repairs O^6 -CMG in cells was not established. Overall, studies addressing the cellular fate of O^6 -CMG DNA damage are critically missing or contradictory.

In this work, we aimed to resolve the relative contribution of NER and MGMT to O^6 -CMG persistence and mutagenicity. We found that the carboxymethylating agent azaserine was more toxic and significantly more mutagenic in cells depleted of MGMT or deficient in NER proteins. The exposure to azaserine in repair-defective cells resulted in a higher number of O^6 -CMG adducts, suggesting the accumulation of DNA adducts as a potential cause of DNA mutations. Studies are ongoing to better characterize the involvement of NER proteins in the repair of O^6 -CMG. With the present studies, we answer a longstanding question regarding the role of repair pathways in the cellular accumulation of O^6 -CMG and how DNA repair deficiencies contribute to the rise of DNA mutations, in a repair- and drug dose-dependent manner.

3.3 Results

Reduced MGMT function sensitizes cells to carboxymethylating agent azaserine

Given the lack of consensus in the literature concerning whether MGMT repairs carboxymethylated DNA in cells, we aimed to test the cellular impact of MGMT-inhibition on cellular phenotype induced by azaserine. Previously, cell survival in response to azaserine has been employed to identify DNA repair pathways responsible to remove azaserine-induced DNA damage, and particularly O^6 -CMG.²¹ However, azaserine toxicity can also result from other activities of the drug in the cell, such as the inhibition of nucleotide synthesis.³⁵ Therefore, we reinvestigated the contribution of MGMT repair to azaserine mutagenicity. We employed the HPRT assay for the measurement of mutagenicity, which has been extensively performed on rodent cells.³⁶⁻³⁹ We therefore employed CHO cells in our studies, as they were more suitable in our studies than human cells (not shown). To assess the contribution of MGMT, we chemically depleted V79-4 cells of MGMT by treatment with O^6 -benzylguanine (O^6 -BnG), a well-established MGMT-inhibitor.^{40, 41} In the absence of treatment with additional agents, a dose of up to 60 μ M of O^6 -BnG was not toxic (Fig. S1A), and this was the maximal dose used in our studies in V79-4 cells. To confirm the activity on MGMT of O^6 -BnG at the chosen concentration, we measured the level of O^6 -MeG lesions by mass spectrometry upon treatment with the methylating agent MNNG, and compared to those formed when cells were pre-treated with O^6 -BnG (Fig. S.2A).⁴²

To measure the effect of influence of MGMT on azaserine cytotoxicity, we exposed V79-4 cells to azaserine (0-5 μ M) and to O^6 -BnG (0, 40 μ M) for 24 h and measured cell viability after 2 days of incubation in drug-free media. We found that cell survival of V79-4 cells was reduced when cells were exposed to O^6 -BnG in addition to azaserine (Fig. 1A, top). Cells were counted directly after exposure and every 24 h for 3 days. By allowing cells to grow after exposure to azaserine, the difference in cell number associated with MGMT-proficiency was enhanced and better measurable. The resulting curve of cell growth was lower for cells that were treated with both O^6 -BnG and azaserine, suggesting that MGMT-inhibition effectively diminished the number of cells (Fig. 1A, bottom).

Having observed that MGMT-inhibition increased the sensitivity of V79-4 cells to azaserine, we asked whether a similar phenotype could be observed in human cells. We measured azaserine cytotoxicity upon MGMT-inhibition in HCEC cells, an immortalized but normal diploid human colon epithelium cell line,^{43, 44} a model for healthy colon tissue.⁴⁵ We exposed HCEC cells to azaserine (0-5 mM) and to O^6 -BnG (50 μ M) for 24 h and measured cell viability after 3 days of incubation in drug-free media. We found reduced in cells depleted of MGMT by exposure to O^6 -BnG (Fig. 1 B, top). Similarly to what observed for V79-4 cells, the number of was significantly reduced by MGMT-inhibition (Fig. 1 B, bottom).

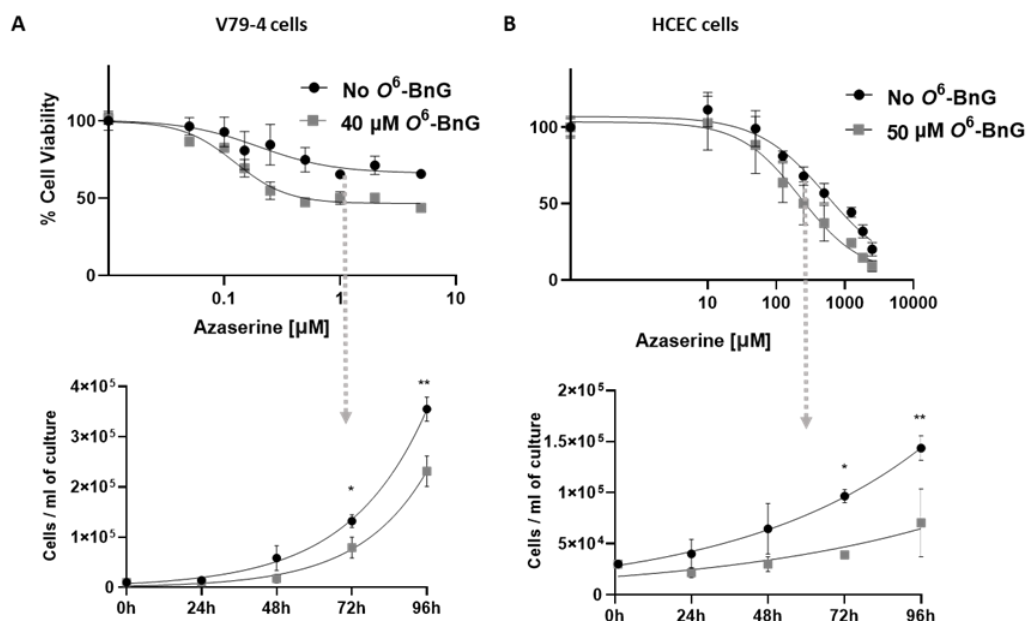


Figure 1. Cell viability and cell proliferation upon exposure to azaserine. V79-4 (A), HCEC (B) cells were pre-conditioned for 2 h with O^6 -BnG (40 μ M for V79-5; 50 μ M for HCEC), followed by exposure to azaserine (0-5 μ M for V79-4; 0-5 mM for HCEC) for 24 h. Cell viability (top graphs) was measured by CellTiter-Glo assay, 2 or 3 days after 24 h-exposure. To measure cell proliferation (bottom graphs), cells were counted immediately after exposure (24 h) to azaserine (1 μ M for V79-5 and 200 μ M for HCEC; concentration indicated by dashed arrow) and O^6 -BnG, or after 1 day (48 h), 2 days (72 h) or 3 days (96 h). Data were represented using GraphPad Prism 8. Cell viability data were fit in a nonlinear regression curve, using a dose-response function; cell proliferation data were fit in an exponential curve, using a growth equation. Error bars indicate standard deviation. Experiments were performed in triplicates, each with three technical replicates. Two-way ANOVA with Sidak's multiple comparison test was performed to compare proliferation between +/- O^6 -BnG at each time point (* p <0.05, ** p <0.01).

Reduced MGMT function enhances azaserine mutagenicity in cells

Having established the influence of MGMT on the sensitivity of cells to azaserine, we anticipated a potentially more significant and relevant impact on mutagenicity due to the cause-effect relationship of DNA adducts with mutation. We performed the HPRT mutagenicity assay in V79-4 rodent cells exposed to azaserine and depleted of MGMT-activity by exposure to O^6 -BnG. Ethyl methansulfonate (EMS) was employed as a positive control (Fig. S3). Preliminary tests were performed to identify the concentration of azaserine to test (Fig. S3) and the time of exposure. Final conditions consisted in 24 h-treatment, one week-incubation to express mutations, and one week-incubation in selection media to select mutants generated by the treatment.

We found that azaserine was mutagenic in V79-4 cells, and that mutagenicity was dose-dependent (Fig. 2A, black bars: 0; 0.5; 2 μ M azaserine). O^6 -BnG instead was not mutagenic at the tested concentrations (Fig.2B, black bars), but significantly increased azaserine mutagenicity (Fig. 2B). The enhanced mutagenicity of azaserine upon MGMT-inhibition

suggests that the depletion of MGMT could result in the accumulation and persistence of azaserine-induced O^6 -CMG adducts, and give rise to mutations.

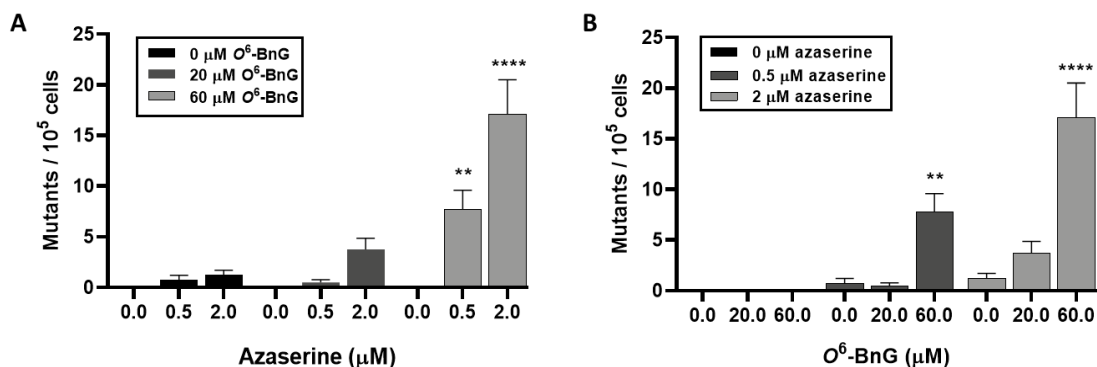


Figure 2. Mutagenicity in V79-4 cells exposed to azaserine and O^6 -BnG. V79-4 cells were exposed to O^6 -BnG (0, 20, 60 μM) followed by azaserine (0, 0.5, 2 μM). HPRT assay was performed as described and mutant colonies were counted manually after two weeks. Data were represented using GraphPad Prism 8. Graphs A and B represent the same data, with significance values calculated by comparing to azaserine-unexposed (A) or to O^6 -BnG-unexposed (B) samples. Statistical significance was obtained by performing two-way ANOVA with a Tukey post hoc test (*p<0.05, **p<0.01, ***p<0.001, ****p<0.0001). Significance is relative to unexposed control for each set of data.

Accumulation of O^6 -CMdG adducts and mutations in V79-4 cells depend on azaserine dose and on MGMT level

To test the hypothesis that the increase in mutagenicity observed upon MGMT-inhibition is due to the persistence of O^6 -CMG adducts, levels in azaserine-exposed cells as a function of O^6 -BnG exposure were measured by mass spectrometry. V79-4 cells were exposed to O^6 -BnG (60 μM) for 2 h and azaserine (0 or 2 μM) for 24 h; DNA was extracted from cells, hydrolysed enzymatically and purified for mass spectrometry analysis. Unexposed samples were prepared as controls and to define the background level of O^6 -CMdG. Although azaserine can induce both O^6 -MeG and O^6 -CMG, it was previously reported that O^6 -MeG is formed at around 10 or 20-fold lower level than O^6 -CMG, depending on the cell line.⁴⁶ Furthermore, the phenotype (e.g. mutagenicity) induced by azaserine or by its analogue diazoacetate is usually ascribed to O^6 -CMG, as it differs greatly from the phenotype of O^6 -MeG or from the one induced by methylating agents.^{14, 21}

The level of O^6 -CMdG adducts in azaserine-exposed cells increased with the dose of drug and with the degree of MGMT-inhibition ((Fig. 3A), mirroring the levels of mutations measured via HPRT assay (Fig. 2 and repeated in Fig. 3B). The positive correlation between the level of lesions and mutations in the HPRT gene supports a potential causative role of DNA mutations by O^6 -CMG. No adducts were detected in unexposed control cells, suggesting that, in V79-4 cells, O^6 -CMG does not represent a prevalent DNA damage under physiological conditions. In MGMT-proficient cells (Fig. 3A black bars; 0 μM O^6 -BnG), exposure to 0.5 μM azaserine resulted in no detectable O^6 -CMdG adduct levels, while exposure to 2 μM azaserine induced low levels of O^6 -CMdG (ca. 2-3 lesions per 10⁷ nucleotides).

Pre-conditioning with O^6 -BnG (Fig. 3A dark and light grey bars; 20 and 60 μ M O^6 -BnG) and the consequent competitive inhibition of MGMT resulted in a higher number of O^6 -CMdG adducts, also quantifiable in cells exposed to 0.5 μ M azaserine. Similarly to the rise of mutations, the most significant increase in O^6 -CMdG levels compared to unexposed cells was measured after cells with the highest level of MGMT-inhibition were exposed to the highest azaserine concentration (2 μ M). Decreased MGMT repair proficiency resulted in the accumulation of O^6 -CMdG adducts, suggesting a pivotal role of MGMT in protecting cells against O^6 -CMG mutagenicity.

Considering the putative involvement of MGMT in the clearance of O^6 -CMG, MGMT-inhibition is expected to cause a stable persistence of O^6 -CMG over time. To assess the cellular repair rate for O^6 -CMG and the impact of MGMT on time-dependent O^6 -CMG-removal, we are planning to measure O^6 -CMdG adduct levels following exposure to azaserine and including varying recovery time points. Adduct levels over time will be compared to levels assessed in MGMT-inhibited cells.

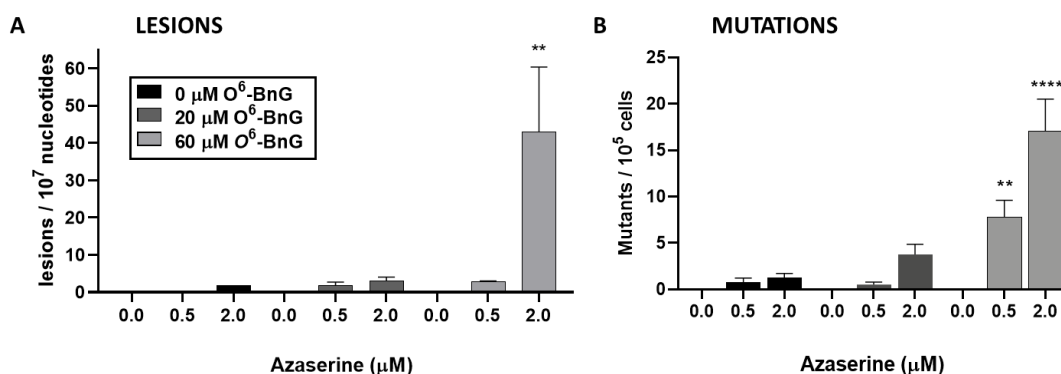


Figure 3. Level of O^6 -CMdG lesions upon exposure to azaserine and O^6 -BnG. V79-4 cells were pre-conditioned with O^6 -BnG (0, 20, 60 μ M) for 2 h, followed by a 24 h-exposure to azaserine (0, 0.5, 2 μ M). DNA was extracted and samples processed for O^6 -CMdG-analysis by nanoLC-ESI-hrMS² as described in *Chapter 2*. The number of adducts is normalized to sample nucleotides content. Experiments were performed three times and mean values are represented, with error bars indicating SEM. (A) Azaserine-induced mutagenicity in V79-4 (Fig. 2) is reported here for comparison (B). Statistical significance was obtained by performing two-way ANOVA with a Tukey post hoc test (**p<0.01, ****p<0.0001, ****p<0.0001). Significance is relative to untreated control for each set of data

Overall, we found that the inhibition of MGMT sensitizes mammalian cells to carboxymethylation, results in the accumulation of O^6 -CMdG and increases the rise of mutations. Thereby, with the presented studies on MGMT-inhibition, we established that MGMT has a significant impact on the cellular response to azaserine.

Considering the general lack of studies regarding the repair of O^6 -CMG in cell studies, and that our findings on MGMT contradict a previous work where MGMT deficiency had no significant impact on human cell sensitivity to azaserine,²¹ future effort should focus on testing the role of other repair pathways in removing O^6 -CMG from the DNA. In particular, NER is known to repair O^6 -alkylG DNA damage in lower organisms,^{33, 47-49} and was

previously suggested to have a protective role in response to carboxymethylation in human cells.²¹ Therefore, we were interested in confirming and further characterizing the role of NER in response to azaserine and to *O*⁶-CMG DNA damage.

NER-deficiency sensitizes cells to azaserine

To test the impact of cellular deficiencies in NER repair on azaserine phenotype, we compared the cell viability upon azaserine exposure in cells deficient in NER protein to wild type (WT) with NER-activity. We employed CHO rodent cells: CHO UV20 (ERCC1-deficient) cells and CHO UV20 cells transduced with a lentiviral vector expressing wild-type *hERCC1*, therefore “WT” in the NER function. ERCC1-XPF is an NER endonuclease, responsible for the incision 5' to the lesion, necessary for the excision of a short DNA strand containing the lesion. We exposed CHO cells to increasing concentrations of azaserine (0-10 μ M) for 24 h and measured cell viability after 2 days of incubation in drug-free media. As response to azaserine-exposure, cell survival was lower in CHO UV20 repair deficient cells, when compared to CHO WT cells (Fig. 4A). Noteworthy, no significant difference between CHO WT and CHO UV20 survival upon exposure to azaserine was recorded when measuring cell viability directly after the 24 h-treatment (Fig. S3), suggesting that the time of measurement is critical when investigating the impact of DNA damage and the role of cellular repair pathways, as observed for other cells (Fig. 1, top graphs).

Combined NER-deficiency and MGMT-inhibition do not further sensitize cells to azaserine

Having observed significant changes in cellular response to azaserine when MGMT or NER are depleted separately, we were interested whether the simultaneous impairment of both repair pathways could have an additive effect on increased cellular sensitivity to azaserine. Therefore, we exposed CHO cells, WT and UV20, to increasing concentrations of azaserine (0-10 μ M) and to a sub-toxic (Fig. S1) dose of *O*⁶-BnG (20 μ M). While CHO WT cells were more sensitive to azaserine when also *O*⁶-BnG was included, viability of CHO UV20 cells was independent from *O*⁶-BnG exposure (Fig. 4B). The observation that the depletion of MGMT had no measurable effect on azaserine cytotoxicity in NER-deficient cells might be due to experimental limitations (e.g. high variability of the signal), or to saturation of azaserine toxic properties, or indicate no further dependence of azaserine toxicity on repair proficiency. Further studies need to be conducted to establish more directly what is the combined impact of NER and MGMT in response to azaserine and azaserine-induced DNA damage.

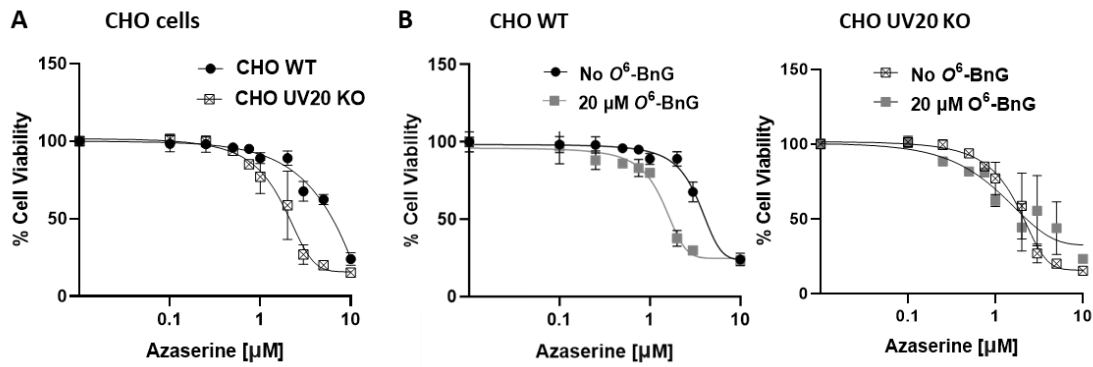


Figure 4. Cell viability upon exposure to azaserine and O^6 -BnG. CHO WT and CHO UV20 KO cells were treated for 24 h with increasing concentrations of azaserine (0-10 μ M) (A) or pre-conditioned with O^6 -BnG (20 μ M) followed by azaserine exposure (B). Cell viability was measured by CellTiter-Glo assay after two days. Data were represented using GraphPad Prism 8. Cell viability data were fit in a nonlinear regression curve, using a dose-response function. Error bars indicate standard deviation. Experiments were performed three independent times, each with three technical replicates

NER-deficiency enhances azaserine-mutagenicity

Given the higher the sensitivity of NER-deficient CHO cells to azaserine toxicity, we anticipated a potentially similar impact on mutagenicity. To test the contribution of NER in azaserine mutagenicity, HPRT assay was performed in CHO WT and CHO UV20 cells exposed to azaserine for 24 h. We found that azaserine was mutagenic in CHO cells at the highest dose tested (2 μ M), and that NER-deficient CHO cells were significantly more mutated than the CHO WT cells upon exposure to azaserine (Fig. 5), despite the variability in the level of mutants counted per dish that can be a limitation intrinsic of the HPRT assay. Noteworthy, the mutagenic concentration of 2 μ M azaserine corresponded to around 50% viability in CHO cells (Fig. 4A). Instead, the sub-toxic dose of 0.75 μ M of azaserine, which causes only 10% reduction of viability in CHO cells (Fig. 4A), was not mutagenic.

Combined NER-deficiency and MGMT-inhibition significantly enhance azaserine-induced mutagenicity

In this work, we established an increase of azaserine mutagenicity induced separately by MGMT-inhibition and by NER-deficiency in cells, which is likely caused by the accumulation of unrepaired DNA damage. Thus, we were interested to assess the combined impact of the two pathways on azaserine mutagenicity. Therefore, we pre-conditioned CHO cells, WT and UV20, with O^6 -BnG (20 μ M) followed by azaserine exposure (0, 0.75, 2 μ M) for 24 h. We found that when MGMT was inhibited by O^6 -BnG, azaserine was generally more mutagenic in CHO cells, inducing mutants also at the lower dose of 0.75 μ M. Remarkably, the increase induced in NER-deficient CHO UV20 cells was significantly higher than the increase induced in CHO WT cells. Additionally, the difference between CHO UV20 and CHO WT *hprt* mutants is less than 3-fold when cells are exposed to 2 μ M azaserine and no O^6 -BnG (Fig. 5, black and dark grey bars), but it reaches a difference of almost 10-fold when MGMT is inhibited (Fig. 5, light grey and white bars). Thus, we wondered whether

MGMT and NER repair pathways could have a synergistic protective role towards azaserine-induced mutagenicity.

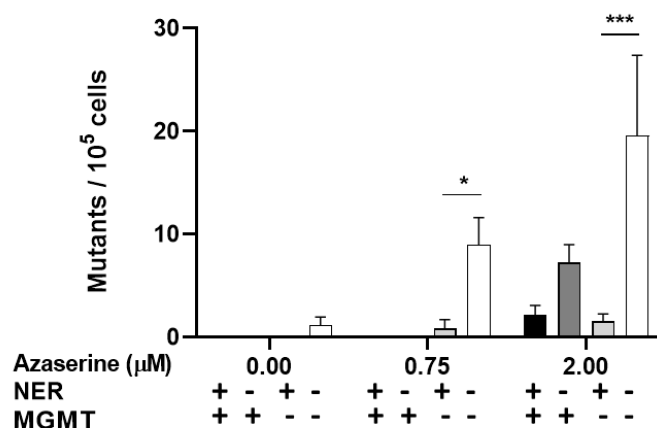


Figure 5. Mutagenicity in CHO WT (WT) and CHO UV20 KO (KO) cells exposed to azaserine and *O*⁶-BnG. CHO WT (NER +) and CHO UV20 KO (NER -) cells were pre-conditioned with 20 μM *O*⁶-BnG (MGMT -) or 0 μM *O*⁶-BnG (MGMT +) and exposed to increasing concentrations of azaserine (0, 0.75, 2 μM) for 24 h. HPRT assay was performed as described and mutant colonies were counted manually after two weeks. Data were represented using GraphPad Prism 8. Statistical significance was calculated by performing two-way ANOVA with a Tukey post hoc test (*p<0.05, **p<0.01, ***p<0.001, ****p<0.0001). Significance is shown among selected bars.

Noteworthy, some albeit low mutagenicity was measured for the first time in the absence of azaserine (negative control) when MGMT was inhibited in CHO NER deficient cells. Due to the absence of any mutagen, we reasoned that mutations might have arisen from mutagenic endogenous damage, from which the cell is left particularly unprotected when both NER and MGMT repair pathways are absent or defective. Because neither MGMT nor NER separate depletion was sufficient to give rise to mutations in CHO cells, we reasoned that either (1) MGMT- or NER-dependent mutagenicity arising from endogenous damage is individually below the limit of detection of the HPRT assay, or (2) that MGMT and NER might have a synergistic role towards endogenous damage. Although the former hypothesis is likely, especially given the low frequency of mutants observed in the untreated CHO UV20 KO + *O*⁶-BnG samples, more effort should be invested to interrogate a putative relationship between MGMT and NER in DNA damage repair and specifically for the case of *O*⁶-CMG adduct.

Accumulation of *O*⁶-CMdG adducts in CHO cells is azaserine dose-dependent and partially dependent on cellular repair capacity

To test the hypothesis that the increase in mutagenicity observed in NER-deficient cells (Fig. 5) is due to the persistence of adducts, *O*⁶-CMdG adduct levels in azaserine-exposed cells were measured by mass spectrometry and evaluated with regard to NER and MGMT-activity (Fig. 6 A-B). CHO cells were exposed to azaserine (0-5 μM) and co-exposed to *O*⁶-BnG (0, 20 μM) for 24 h. Unexposed samples were prepared as controls and to define the background level of *O*⁶-CMdG. For all drug conditions, we measured a consistently higher

level of O^6 -CMdG adducts in KO CHO cells when compared to WT cells and independent of MGMT activity; however, at the lowest concentration of azaserine (0.75 μ M), the increase in level adducts is only mild. Furthermore, the level of adducts is significantly different to untreated cells. Indeed, differently from what was observed in V79-4 cells, both WT and KO CHO cells presented detectable O^6 -CMdG in the absence of any drug treatment. Although physiological levels of O^6 -CMdG have been previously reported elsewhere,⁵⁰ their presence hinders the comparison among cells when exposed to low levels of azaserine. Therefore, we included a higher dose to the ones tested in the HPRT assay, i.e 5 μ M.

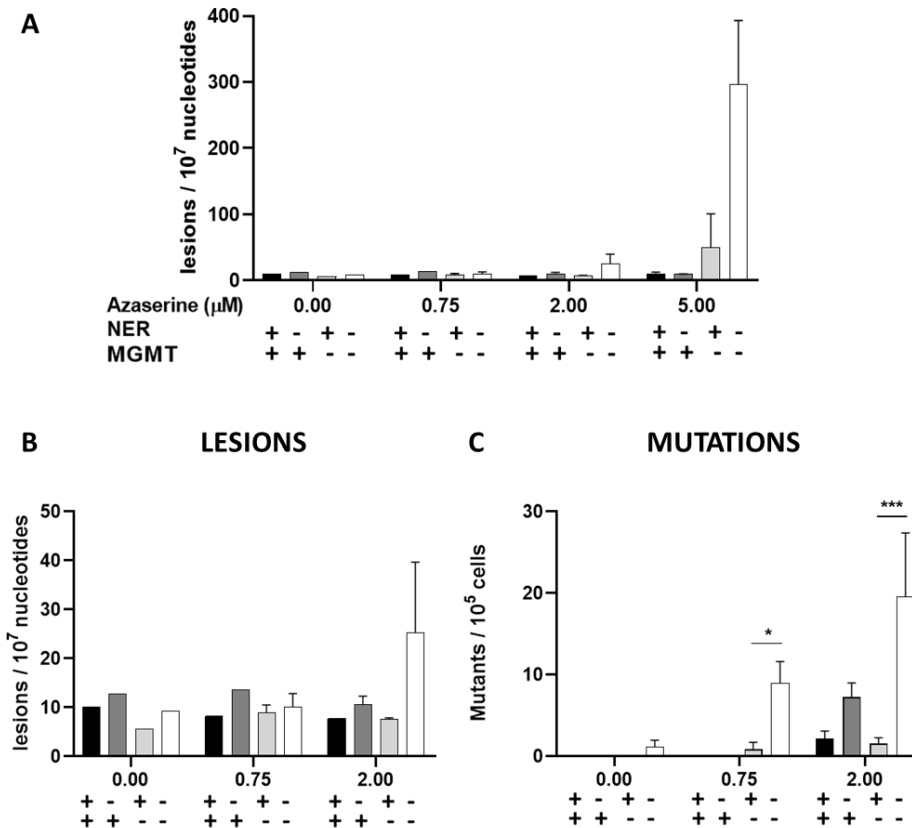


Figure 6. O^6 -CMdG levels upon exposure to azaserine and O^6 -BnG. CHO cells were pre-conditioned with O^6 -BnG (0, 20 μ M) and exposed for 24 h to increasing concentrations of azaserine (0, 0.75, 2 μ M). DNA was extracted and samples processed for O^6 -CMdG-analysis by nanoLC-ESI-hrMS² as described in Chapter 2. The number of adducts is normalized to sample nucleotides content. Experiments were performed two times. (A-B) Azaserine-induced mutagenicity in CHO cells (Fig. 5) is reported here for comparison (C). Data were represented using GraphPad Prism 8. Statistical significance was calculated by performing two-way ANOVA with a Tukey post hoc test (* p <0.05, ** p <0.01, *** p <0.001. Significance is shown among selected bars

When exposed to 5 μ M of azaserine, the depletion of MGMT induced a 5-fold increase of O^6 -CMdG adducts in WT CHO cells (Fig 6A light grey vs. black bar) and, remarkably, a 30-fold increase in KO CHO cells (Fig 6A white vs. dark grey bar). When MGMT was functional and cells were not co-exposed to O^6 -BnG, we did not measure a different level between NER WT and KO cells (Fig 6A black vs. dark grey bar). However, when MGMT was depleted, NER deficient cells presented 6 times more lesions than NER proficient cells (Fig 6A light

grey vs. white bar). A similar outcome is also measured when cells were exposed to 2 μ M azaserine, where a difference in adduct level between NER WT and KO cells is only measured when MGMT is inhibited. The apparently different degree of sensitivity of the measurement of mutations vs. adducts is not surprising, as the HPRT assay is performed on selected mutant cells. Indeed, despite the need of a higher azaserine concentration in CHO cells when measuring O^6 -CMdG lesions compared to mutations (Fig. 6B vs. C), both experiments similarly suggested that NER and MGMT pathways contribute to the repair of O^6 -CMG in cells, potentially in a non-additive manner.

Functionality of NER proteins in O^6 -CMG DNA recognition and repair

Data collected from cell survival assays, mutagenicity and adduct level measurements in this work suggest that NER and MGMT have a mutual influence in O^6 -CMG removal and protection from toxic and, especially, mutagenic properties. Despite hinting at the same conclusion, the outcome of mutagenicity assay and adduct accumulation in CHO cells exposed to azaserine were not in agreement for the low concentrations of azaserine. These discrepancies are likely due to the fact that adduct accumulation is a short-term phenotype, while mutations represent a long-term effect to azaserine exposure. Therefore, a direct comparison of conditions is not easily achieved. However, it motivated us to evaluate O^6 -CMG removal on a biochemical level, especially with reference to the NER machinery. The role of the isolated MGMT enzyme in reversing O^6 -CMG has been shown.^{19, 20} However, to our knowledge, similar investigations have not been performed with NER proteins. Thus, we performed biochemical assays with isolated NER proteins to assess whether the NER complex has the potential to recognize and excise O^6 -CMG from a DNA strand.

To test the binding of purified XPC-RAD23B protein (damage recognition factor of global genome NER) to O^6 -CMG DNA, we performed EMSA experiments. We synthesized a 24mer oligonucleotide containing O^6 -CMG and annealed it to a fluorescently labelled complementary strand (Fig. S4). As negative and positive controls for binding, we prepared respectively undamaged (G) dsDNA, and dsDNA containing a well-established NER target, namely acetylaminofluorene (AAF).⁵¹ We incubated the different samples of dsDNA with XPC-RAD23B at increasing concentrations, and we assessed the binding of the protein to the dsDNA by resolving samples on a denaturing gel and imaging for the fluorescent DNA (Fig. S4). When dsDNA was bound to XPC-RAD23B, a shift of signal towards the top of the gel is recorded (as DNA bound to a protein runs slower through a gel). We found that dsDNA containing O^6 -CMG bound to XPC-RAD23B at lower concentrations of the protein compared to the undamaged DNA, and at slightly lower concentrations when compared to the positive control AAF (Fig. 7). However, because XPC binds strongly to DNA even when not containing NER targets, the difference in signal shift is mild. For this reason, when performing EMSA analysis with XPC-RAD23B, unlabelled DNA is normally introduced as competitor for binding.⁵¹ By engaging with XPC-RAD23B and subtracting it from binding to other unmodified DNA, the presence of a competitor makes a difference in binding between non-NER targets and potential NER targets more easily detectable. In future studies, we propose to include a competitor when performing EMSA experiments.

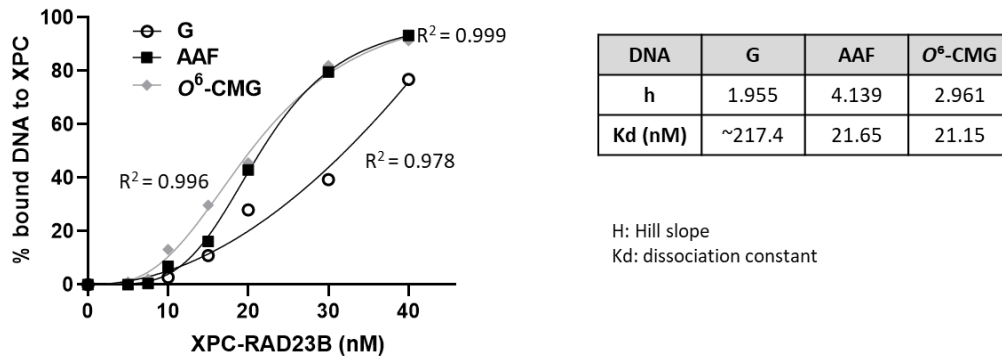


Figure 7. XPC-RAD23B binding to damaged and undamaged DNA. XPC-RAD23B at increasing concentrations (0-40 nM) was incubated with Cy5-labeled DNA: undamaged DNA (G, negative control) or DNA containing AAF adduct (positive control) or O⁶-CMG (here, oligo-O⁶-CMG-12 was used). Reactions were resolved on a denaturing gel and the shift of Cy5-labeled DNA signal (upper bands in Fig. S4 C) from untreated samples (0 nM XPC-RAD23B) was an indication of binding of the dsDNA to XPC-RAD23B. Band intensity was quantified on Image Lab software. The relative fraction of unbound DNA (lower bands, Fig. S4 C) was normalized as follows: 100*[unbound DNA] / ([unbound DNA] + [bound DNA]) and plotted on GraphPad Prism 8. The resulting sigmoid curves were fit using the Hill equation on GraphPad Prism 8 and K_d values (table) were obtained from the half-maximal binding point.

To test the capability of the NER machinery to recognize, bind and excise a region of DNA containing O⁶-CMG, we performed a cell-free NER assay, by using purified NER proteins or cellular extracts, combined with DNA containing O⁶-CMG, and assessing the excision of a short oligonucleotide containing O⁶-CMG via [α -32P] DNA end-labelling. We produced circular dsDNA containing O⁶-CMG by extending 24mer O⁶-CMG oligonucleotides (both oligo-O⁶-CMG-10 and oligo-O⁶-CMG-12 were used) annealed to a complementary region on circular ssDNA, which was produced in XL1 blue E.Coli cells, infected with helper phage R408. We used dsDNA containing a G-AAF adduct as positive control for NER excision. Samples containing either G-AAF or O⁶-CMG were incubated with HeLa extracts, or with NER proteins +/- XPA, pivotal for the proceeding of repair after damage recognition. We found that under none of the tested conditions DNA containing O⁶-CMG was excised. Instead, the positive control G-AAF was excised in all cases, except when XPA was not present. (Fig. 8) Preliminary data obtained from the NER assay disagree with both EMSA and cell-based studies, and suggest no involvement of the NER proteins in removing O⁶-CMG. In future experiments, the NER assay will be repeated, and factors such as MGMT or others proteins that might be crucial for NER activation or recognition will be included in the mix of purified proteins. In the case of employing the HeLa extracts, western blot of MGMT and other relevant factors should be performed to confirm their presence (the level of mRNA for MGMT in HeLa cells is on a middle-high;52 however, the actual amount of translated MGMT is not known). While being a powerful and robust tool to test the excision of damaged DNA by NER, the NER assay is based on a cell-free system and is restricted to the factors and conditions tested. Thus, more and more direct evidence of NER role in cells should be collected.

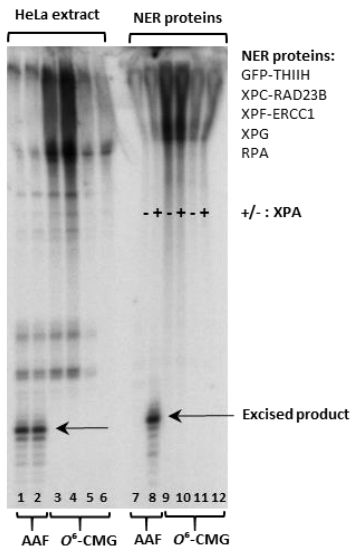


Figure 8. Interaction of O^6 -CMG in plasmid DNA with NER factors. Samples 1-2, 7-8 consisted of G-AAF; samples 3-4, 9-10 of oligo- O^6 -CMG-10 and samples 5-6, 11-12 of oligo- O^6 -CMG-12. Samples 1-6 were incubated with HeLa extract for 45 min at 30°C; samples 7-12 were incubated with NER proteins (except XPA for samples 7, 9 and 11) for 90 min at 30 °C. After incubation with either HeLa extract or NER proteins, all samples were detected by annealing to a complementary oligonucleotide with a 5'-GpGpGpG overhang, which served as a template for end-labelling with [α - 32 P]-dCTP with sequenase. The reaction products were resolved on a denaturing polyacrylamide gel and imaged using a Phosphorimager.

3.4 Discussion and Future studies

Mechanisms of DNA damage repair are pivotal to ensure cellular stability, and their disruption has been associated with adverse biological outcomes, particularly cell death,⁵³⁻⁵⁵ rise of mutations at the DNA and cancer.⁵⁶⁻⁵⁸ Thus, the contribution to mutagenesis and carcinogenesis of DNA damage that can be replicated depends on the cellular capacity to repair that damage. However, the identity and the cellular impact of the repair that targets some mutagenic DNA adducts is not known or well-characterized, hindering our understanding of how mutations arise and our ability to assess the increased risk associated with the exposure to certain chemicals.

*O*⁶-CMG is a mutagenic DNA adduct to which humans can be exposed upon red and processed meat consumption,^{4, 8, 11, 12} and that has been hypothesized to drive the development of colorectal cancer.¹³ However, it not yet clear what cellular pathways specialized in repairing *O*⁶-CMG prevent from its accumulation and alleviate *O*⁶-CMG-induced mutagenicity. Few studies have been carried out to address this question, and only one was performed in human cells. Furthermore, results were contradictory, making our current knowledge of *O*⁶-CMG repair elusive.

In the present study, we investigated how the phenotype of *O*⁶-CMG induced by the carboxymethylating agent azaserine in cells is affected by NER and MGMT repair pathways, for which contradictory evidences have been obtained regarding *O*⁶-CMG repair.^{20, 21} We found that azaserine was significantly more toxic in mammalian cells depleted of MGMT. We measured mutagenicity via a phenotypic assay and observed that azaserine was mutagenic in rodent cells in a dose-dependent manner. In particular, mutagenicity was low at sub-toxic concentrations but the number of induced mutants significantly increased when MGMT was inhibited. Similarly, to confirm and further characterize NER repair of *O*⁶-CMG, we employed cells with defined deficiencies in NER and measured cell viability and mutant occurrence upon azaserine exposure. Impaired NER-capacity sensitized cells to both azaserine toxicity and mutagenicity, hinting at a role of NER in removal of *O*⁶-CMG. However, preliminary results from cell-free assays show that NER proteins were not proficient at excising *O*⁶-CMG, although the NER lesion recognition factor XPC could bind to *O*⁶-CMG more strongly than to undamaged DNA. We reasoned that some factors that are not NER but needed for *O*⁶-CMG repair might have been missing in the experimental set-up of the NER assay and that some more testing is required. Finally, when we measured mutagenicity in cells depleted of both, MGMT and NER, we obtained an increased rate of mutants, significantly higher than when MGMT and NER were depleted individually, and higher than their sum. Although more concentrations of azaserine and *O*⁶-BnG need to be tested (experiments ongoing) to define whether the combined effect of MGMT and NER depletion on mutagenicity is simply additive and not synergistic, we reasoned that the increased mutagenicity might derive from a cooperative or cross-dependent relationship between MGMT and NER.

Previous work performed with yeast and bacterial alkyltransferase-like (ATL) proteins, which are homologous of MGMT but lack of transferase activity,^{33, 47-49} showed how ATL

proteins serve as signalling factors of O^6 -alkylG to the NER pathway, by binding to O^6 -alkylGs and making the adducts easily detectable by NER. Although ATLs have not been found in higher eukaryotes yet, studies on ATLs signalling function raises the questions of whether alkyltransferases such as MGMT might have a similar role of cross-communication between repair pathways in the presence of O^6 -CMG in higher organisms, in addition to its transferase activity.

With the present work, we unravelled a longstanding question in DNA repair concerning the identification of how cells remove O^6 -CMG and that that inadequate removal of this adduct gives rise to mutations. Both NER and MGMT function to alleviate O^6 -CMG detrimental consequences in cells, providing a clear resolution concerning previously conflicting evidence. Our findings are also further consistent with results from a recent study suggesting that MGMT and NER are the major cellular pathways proficient at repairing other O^6 -alkylG adducts.⁵⁹ The major open question remaining concerns the mechanism for how NER and MGMT target O^6 -CMG, in a potentially concerted manner, and whether other as yet unidentified factors or repair pathways might be involved. These findings advance our understanding of the relationship between O^6 -CMG DNA damage and mutation, paving the way for the further study of mutagenicity and cancer etiology. The outcome of this research expands fundamental knowledge of DNA repair, and for the risk assessment for drugs or dietary products, especially to account for individuals with impaired repair due to genetic conditions or drug treatment.

3.5 Material and Methods

Synthesis of O^6 -CMG phosphoramidite and oligonucleotide

Oligonucleotide sequences were (24mer) 5'- CTATTACCGXCYCCACATGTCAGC -3'; where X, Y = G in unmodified oligo-G; X = O^6 -CMG, Y = G in O^6 -CMG-modified oligo- O^6 -CMG-10; X = G, Y = O^6 -CMG in O^6 -CMG-modified oligo- O^6 -CMG-12. Unmodified oligo-G and its sequence-complementary oligonucleotide were purchased by IDT (Iowa, USA). O^6 -CMG-modified oligos were synthesized by solid-phase DNA synthesis on a Mermade 4 DNA synthesizer (Bioautomation Corporation; Texas, USA) in trityl-on mode on a 1- μ mol scale. Universal Q SynBaseTM CPG support columns and natural nucleotide phosphoramidites from Link Technologies Ltd. (Lanarkshire, Scotland, UK) were used, and O^6 -CMG phosphoramidite was obtained as previously reported.¹⁷ Oligonucleotide deprotection was carried out by treatment with 0.4 M NaOH (200 μ l) at RT overnight, and with 33% aqueous ammonium hydroxide (500 μ l) at RT for 24 hours. Residual ammonium was let evaporate, trityl-cleavage and oligonucleotide desalting were performed on reverse-phase C18 Sep-Pak cartridges (Waters; Massachusetts, USA) following the manufacturer's protocol and using 4 % trifluoroacetic acid for trityl cleavage. The oligonucleotides were dried under reduced pressure and purified by reverse phase HPLC using an Agilent eclipse XDB C-18 5 μ M 4.6 x 150 mm column. The mobile phase consisted of 50 mM triethylammonium acetate (TEAA) and acetonitrile (ACN). The flow rate was set to 1.0 ml/min with a mobile phase starting at from 10-40% ACN over 25 min, increasing to 50% ACN from 25.1 to 29 min, and equilibrated from 29.1-33 min at 10% ACN. Fractions corresponding to the desired oligonucleotides were collected, lyophilized and re-suspended in DNase/RNase free water.

The DNA concentrations were measured by UV absorbance on Nanodrop spectrophotometer (ThermoFisher; Massachusetts, USA).

Electrophoretic Mobility Shift Assay (EMSA)

EMSA assay was performed on oligo-*O*⁶-CMG-10 and oligo-*O*⁶-CMG-12, annealed with a Cy5-labeled complementary strands and incubated with NER protein XPC-RAD23B (0 - 40 nM) as previously reported.⁶⁰ Oligo-G and oligo-AAF-12 (5'-CTATTACCGXCYCCACATGTCAGC-3'; X= G, Y = AAF) were used respectively as negative and positive control for binding. AAF-modified oligo was synthesized as previously reported.⁵¹ The reaction mixtures were loaded onto a native 5% polyacrylamide gel pre-equilibrated with 0.5× TBE buffer and run at 4 °C for 1 h at 20 mA. Gels were imaged using a Typhoon 9400 Imager (Amersham Biosciences; Little Chalfont, UK). Band intensity was quantified on Image Lab software (Bio-Rad; California, USA). The relative fraction of unbound DNA was normalized as follows: $100 * [\text{unbound DNA}] / ([\text{unbound DNA}] + [\text{bound DNA}])$ and plotted on GraphPad Prism 8.

***O*⁶-CMG-single stranded circular DNA production and NER assay**

Single stranded circular DNA was generated from p98 (with a *NarI* site engineered into pBlusscript II SK+) as previously described.⁵¹ The oligonucleotides oligo-*O*⁶-CMG-10 and oligo-*O*⁶-CMG-12 (100 pmol) were 5'-phosphorylated by incubation with 20 units of T4 PNK and 2 mM ATP at 37 °C for 2 h. After annealing with 30 pmol of single-stranded p98, the mixture was incubated with dNTPs (800 μM), T4 DNA polymerase (90 units), and T4 DNA ligase (100 units) to generate the covalently closed circular DNA containing a single *O*⁶-CMG adduct. The closed circular DNA was purified by cesium chloride/ethidium bromide density gradient centrifugation, followed by consecutive butanol extractions to remove the ethidium bromide, and finally concentrated on a Centricon YM-30 (Millipore, Massachusetts, USA). The *in vitro* NER assay was performed as previously described,^{51, 60} using either HeLa cell extract (2 μL of 21 mg/ml), or NER purified proteins. The reaction products were visualized using a Phosphorimager, Typhoon 9400 (Amersham Biosciences; Little Chalfont, UK). The relative repair efficiency of each substrate was normalized to a nonspecific band and quantified by the Image Quant TL program from Amersham Biosciences.

Cell strains and culture conditions

V79-4 cells were purchased from ATCC (Virginia, USA). HCEC-1CT cell lines were kindly provided by Prof J.W. Shay (University of Texas, USA).^{43, 44} CHO UV20 (ERCC1-deficient) and CHO UV20 transduced with a lentiviral vector expressing wild-type *hERCC1* were donated by Prof R. Kanaar (Erasmus Medical Center, Netherlands). HAP1 cells were purchased from Horizon Discovery (Waterbeach, UK). All cells were maintained as monolayers in 10-cm dishes in a humidified, 5% CO₂ atmosphere at 37 °C. All culture media except the one for HCEC cells were supplemented with 10% FCS and 1% penicillin-streptomycin and were: DMEM (V79-4, CHO cells), IMDM (HAP1 cells). Media for HCEC cells consisted in 80% DMEM and 20% M199 Earle, supplemented with 2% of Hyclone serum, 25 ng/l epidermal growth factor, 1 μg/l hydrocortisone, 10 μg/l insulin, 2 μg/l transferrin, 50 μg/l gentamycin, 0.9 ng/l sodium selenite. All materials for cell culture were purchased from Invitrogen (California, USA).

Cytotoxicity assay

Cells were seeded in 96-well plates (2×10^3 per well for V79-4 cells, 3×10^3 per well for CHO cells, 4×10^3 per well for HCEC cells, 10×10^3 per well for HAP1 cells) and exposed to solutions of test compounds (compound and concentrations indicated in the relevant figures) with final concentration of 0.1% of DMSO. Cells were exposed to TritonX (Sigma) for positive control, and with 0.1% DMSO for negative control. After 24 h azaserine-exposure, cells were washed and drug-free medium was added. Cell survival was measured after further 2 days using CellTiter-Glo assay (Promega; Wisconsin, USA) following the manufacturer's instructions.⁶¹ The days of post-incubation were selected upon measurement of cell proliferation over 4 days in cells exposed to azaserine or to azaserine and O^6 -BnG. Each data set was acquired in triplicate for each of three or more experiments and the averaged luminescence values of the drug-treated cells were normalized to those of DMSO-treated cells (assigned as 100% viability). Data were analysed and plotted using GraphPad Prism (GraphPad Software Inc.; California, USA).

Mutagenicity (HPRT) assay

HPRT assay was performed on V79-4 and CHO cells with a protocol adapted from elsewhere.⁶² Cells were seeded in 30-cm dishes (5×10^5 cells per dish). Pre-existing *hprt*⁻ mutants were cleansed by incubating cells in medium supplemented with hypoxanthine, aminopterin and thymidine (HAT). After three days, HAT medium was removed and replaced by normal DMEM medium and left for 24h. Cells were reseeded in 10-cm dishes (10^5 cells per dish) and one 10-cm dish was prepared for each condition to test. Cells were let attach overnight. Cells were pre-conditioned for 2 h with O^6 -BnG (0 – 60 μ M for V79-4, 0 – 20 μ M for CHO) following by exposure to azaserine (0 – 2 μ M for V79-4, 0 – 1.25 μ M for CHO) for 24 h. DMSO final concentration was 0.06%. Cells for positive control were exposed to 1.7 or 3.5 mM ethyl methane sulfonate (EMS). After time of exposure, culture medium was changed with fresh drug-free DMEM medium. Cells were let grow for 7 days, and medium was changed every three days. Per each condition, cells were reseeded in four 10-cm dishes (2×10^5 cells per dish) in selective medium containing 10 μ g/ml of 6-thioguanine (6-TG), and in two 6-cm dishes (300 cells per dish) in normal DMEM medium for plating efficiency (PE) calculations. All cells were incubated for 14 days, and medium was changed every 4 days (for the four selection dishes, fresh medium contained always 6-TG). After 14-days of *hprt*⁻ mutants selection, cells were stained with 50 % Giemsa staining solution (v/v) in methanol. Clones were counted manually and normalized to the PE in the case of CHO WT and KO, for which PE was the most different. Data were analyzed and plotted on GraphPad Prism (GraphPad Software Inc.; California, USA). Statistical significances of differences relative to control were calculated using two-way ANOVA with a Tukey post hoc test (* $p < 0.05$, ** $p < 0.01$, *** $p < 0.001$, **** $p < 0.0001$).

Mass Spectrometric quantitation of O^6 -MedG and O^6 -CMdG

O^6 -MedG and O^6 -CMdG adduct levels were measured in DNA from cells pre-conditioned with O^6 -BnG (0 or 60 μ M for V79-4; 0 or 20 μ M for CHO) for 2 h, followed by a 24 h-exposure with azaserine (0 or 2 μ M for both V79-4 and CHO cells). To confirm MGMT-inhibition, O^6 -MedG adduct level were measured in cells exposed to MNNG (30 μ M for V79-

4 and CHO; 10 μ M for HCEC) +/- O^6 -BnG. DNA was extracted using QIAamp DNA Mini Kit (Qiagen; Germany) following manufacturer's instructions⁶³ and enzymatically hydrolyzed in the presence of isotopically labelled internal standards, D_3 - O^6 -MedG and $^{15}N_5$ - O^6 -CMdG (100 fmol and 200 fmol respectively) as described in *Chapter 2*. Following further sample clean-up by solid phase extraction, samples were analyzed by nanoLC-ESI-hrMS² as described in *Chapter 2*. PRM scanning in positive ionization mode is performed based on the following transitions for O^6 -MedG, D_3 - O^6 -MedG and O^6 -CMdG, $^{15}N_5$ - O^6 -CMdG respectively: m/z 282.1195 to 166.0722, m/z 285.1384 to 169.0911 and m/z 326.1096 to 210.0622, m/z 331.0946 to 215.0472. MS instrument control and data acquisition are performed using Xcalibur (version 4.0, ThermoFisher Scientific).

Acknowledgments

We acknowledge and thank Xuan Li for preliminary testing of HPRT assay, and Jiyoung Park for support with the cell culture.

3.6 References

1. Giglia-Mari, G.; Zotter, A.; Vermeulen, W., DNA damage response. *Cold Spring Harb Perspect Biol* **2011**, *3* (1), a000745.
2. Yarosh, D. B., The role of O⁶-methylguanine-DNA methyltransferase in cell survival, mutagenesis and carcinogenesis. *Mutation research* **1985**, *145* (1-2), 1-16.
3. Margison, G. P.; Santibanez Koref, M. F.; Povey, A. C., Mechanisms of carcinogenicity/chemotherapy by O⁶-methylguanine. *Mutagenesis* **2002**, *17* (6), 483-7.
4. O⁶-methylguanine in blood leucocyte DNA: an association with the geographic prevalence of gastric cancer and with low levels of serum pepsinogen A, a marker of severe chronic atrophic gastritis. *Carcinogenesis* **1994**, *15* (9), 1815-20.
5. Harrison, K. L.; Jukes, R.; Cooper, D. P.; Shuker, D. E., Detection of concomitant formation of O⁶-carboxymethyl- and O⁶-methyl-2'-deoxyguanosine in DNA exposed to nitrosated glycine derivatives using a combined immunoaffinity/HPLC method. *Chem Res Toxicol* **1999**, *12* (1), 106-11.
6. Roos, W. P.; Batista, L. F.; Naumann, S. C.; Wick, W.; Weller, M.; Menck, C. F.; Kaina, B., Apoptosis in malignant glioma cells triggered by the temozolomide-induced DNA lesion O⁶-methylguanine. *Oncogene* **2007**, *26* (2), 186-97.
7. Bennett, R. A.; Pegg, A. E., Alkylation of DNA in rat tissues following administration of streptozotocin. *Cancer research* **1981**, *41* (7), 2786-90.
8. Lewin, M. H.; Bailey, N.; Bandaletova, T.; Bowman, R.; Cross, A. J.; Pollock, J.; Shuker, D. E.; Bingham, S. A., Red meat enhances the colonic formation of the DNA adduct O⁶-carboxymethyl guanine: implications for colorectal cancer risk. *Cancer Res* **2006**, *66* (3), 1859-65.
9. Mirvish, S. S., Role of N-nitroso compounds (NOC) and N-nitrosation in etiology of gastric, esophageal, nasopharyngeal and bladder cancer and contribution to cancer of known exposures to NOC. *Cancer Lett* **1995**, *93* (1), 17-48.
10. Leaf, C. D.; Wishnok, J. S.; Tannenbaum, S. R., Mechanisms of endogenous nitrosation. *Cancer Surv* **1989**, *8* (2), 323-34.
11. Hall, C. N.; Badawi, A. F.; O'Connor, P. J.; Saffhill, R., The detection of alkylation damage in the DNA of human gastrointestinal tissues. *Br J Cancer* **1991**, *64* (1), 59-63.
12. Vanden Bussche, J.; Hemeryck, L. Y.; Van Hecke, T.; Kuhnle, G. G.; Pasmans, F.; Moore, S. A.; Van de Wiele, T.; De Smet, S.; Vanhaecke, L., O⁶-carboxymethylguanine DNA adduct formation and lipid peroxidation upon in vitro gastrointestinal digestion of haem-rich meat. *Mol Nutr Food Res* **2014**, *58* (9), 1883-96.
13. Cross, A. J.; Ferrucci, L. M.; Risch, A.; Graubard, B. I.; Ward, M. H.; Park, Y.; Hollenbeck, A. R.; Schatzkin, A.; Sinha, R., A large prospective study of meat consumption and colorectal cancer risk: an investigation of potential mechanisms underlying this association. *Cancer research* **2010**, *70* (6), 2406-14.
14. Gottschalg, E.; Scott, G. B.; Burns, P. A.; Shuker, D. E., Potassium diazoacetate-induced p53 mutations in vitro in relation to formation of O⁶-carboxymethyl- and O⁶-methyl-2'-deoxyguanosine DNA adducts: relevance for gastrointestinal cancer. *Carcinogenesis* **2007**, *28* (2), 356-62.
15. Raz, M. H.; Dexter, H. R.; Millington, C. L.; van Loon, B.; Williams, D. M.; Sturla, S. J., Bypass of Mutagenic O⁶-Carboxymethylguanine DNA Adducts by Human Y- and B-Family Polymerases. *Chem Res Toxicol* **2016**, *29* (9), 1493-503.
16. Wu, J.; Wang, P.; Li, L.; Williams, N. L.; Ji, D.; Zahurancik, W. J.; You, C.; Wang, J.; Suo, Z.; Wang, Y., Replication studies of carboxymethylated DNA lesions in human cells. *Nucleic Acids Res* **2017**, *45* (12), 7276-7284.
17. Raz, M. H.; Sandell, E. S.; Patil, K. M.; Gillingham, D. G.; Sturla, S. J., High Sensitivity of Human Translesion DNA Synthesis Polymerase kappa to Variation in O(6)-Carboxymethylguanine Structures. *ACS Chem Biol* **2019**, *14* (2), 214-222.
18. Wang, P.; Leng, J.; Wang, Y., DNA replication studies of N-nitroso compound-induced O⁶-alkyl-2'-deoxyguanosine lesions in Escherichia coli. *J Biol Chem* **2019**, *294* (11), 3899-3908.
19. Shuker, D. E.; Margison, G. P., Nitrosated glycine derivatives as a potential source of O⁶-methylguanine in DNA. *Cancer Res* **1997**, *57* (3), 366-9.
20. Senthong, P.; Millington, C. L.; Wilkinson, O. J.; Marriott, A. S.; Watson, A. J.; Reamtong, O.; Evers, C. E.; Williams, D. M.; Margison, G. P.; Povey, A. C., The nitrosated bile acid DNA lesion O⁶-carboxymethylguanine is a substrate for the human DNA repair protein O⁶-methylguanine-DNA methyltransferase. *Nucleic Acids Res* **2013**, *41* (5), 3047-55.
21. O'Driscoll, M.; Macpherson, P.; Xu, Y. Z.; Karran, P., The cytotoxicity of DNA carboxymethylation and methylation by the model carboxymethylating agent azaserine in human cells. *Carcinogenesis* **1999**, *20* (9), 1855-62.

22. Hermisson, M.; Klumpp, A.; Wick, W.; Wischhusen, J.; Nagel, G.; Roos, W.; Kaina, B.; Weller, M., O⁶-methylguanine DNA methyltransferase and p53 status predict temozolomide sensitivity in human malignant glioma cells. *J Neurochem* **2006**, *96* (3), 766-76.
23. Martin, L.; Marples, B.; Coffey, M.; Lawler, M.; Hollywood, D.; Marignol, L., Recognition of O⁶MeG lesions by MGMT and mismatch repair proficiency may be a prerequisite for low-dose radiation hypersensitivity. *Radiat Res* **2009**, *172* (4), 405-13.
24. Kawate, H.; Ihara, K.; Kohda, K.; Sakumi, K.; Sekiguchi, M., Mouse methyltransferase for repair of O⁶-methylguanine and O⁴-methylthymine in DNA. *Carcinogenesis* **1995**, *16* (7), 1595-602.
25. Tsuzuki, T.; Sakumi, K.; Shiraishi, A.; Kawate, H.; Igarashi, H.; Iwakuma, T.; Tominaga, Y.; Zhang, S.; Shimizu, S.; Ishikawa, T.; et al., Targeted disruption of the DNA repair methyltransferase gene renders mice hypersensitive to alkylating agent. *Carcinogenesis* **1996**, *17* (6), 1215-20.
26. Iwakuma, T.; Sakumi, K.; Nakatsuru, Y.; Kawate, H.; Igarashi, H.; Shiraishi, A.; Tsuzuki, T.; Ishikawa, T.; Sekiguchi, M., High incidence of nitrosamine-induced tumorigenesis in mice lacking DNA repair methyltransferase. *Carcinogenesis* **1997**, *18* (8), 1631-5.
27. Sakumi, K.; Shiraishi, A.; Shimizu, S.; Tsuzuki, T.; Ishikawa, T.; Sekiguchi, M., Methylnitrosourea-induced tumorigenesis in MGMT gene knockout mice. *Cancer research* **1997**, *57* (12), 2415-8.
28. Shiraishi, A.; Sakumi, K.; Sekiguchi, M., Increased susceptibility to chemotherapeutic alkylating agents of mice deficient in DNA repair methyltransferase. *Carcinogenesis* **2000**, *21* (10), 1879-83.
29. van Niflerik, K. A.; van den Berg, J.; van der Meide, W. F.; Ameziane, N.; Wedekind, L. E.; Steenberg, R. D.; Leenstra, S.; Lafleur, M. V.; Slotman, B. J.; Stalpers, L. J.; Sminia, P., Absence of the MGMT protein as well as methylation of the MGMT promoter predict the sensitivity for temozolomide. *Br J Cancer* **2010**, *103* (1), 29-35.
30. Bobola, M. S.; Alnoor, M.; Chen, J. Y.; Kolstoe, D. D.; Silbergeld, D. L.; Rostomily, R. C.; Blank, A.; Chamberlain, M. C.; Silber, J. R., O⁶-methylguanine-DNA methyltransferase activity is associated with response to alkylating agent therapy and with MGMT promoter methylation in glioblastoma and anaplastic glioma. *BBA Clin* **2015**, *3*, 1-10.
31. Iyer, V. N.; Szybalski, W., Mutagenic effect of azaserine in relation to azaserine resistance in *Escherichia coli*. *Science* **1959**, *129* (3352), 839-40.
32. Aramini, J. M.; Tubbs, J. L.; Kanugula, S.; Rossi, P.; Ertekin, A.; Maglaqui, M.; Hamilton, K.; Ciccocanti, C. T.; Jiang, M.; Xiao, R.; Soong, T. T.; Rost, B.; Acton, T. B.; Everett, J. K.; Pegg, A. E.; Tainer, J. A.; Montelione, G. T., Structural basis of O⁶-alkylguanine recognition by a bacterial alkyltransferase-like DNA repair protein. *J Biol Chem* **2010**, *285* (18), 13736-41.
33. Wilkinson, O. J.; Latypov, V.; Tubbs, J. L.; Millington, C. L.; Morita, R.; Blackburn, H.; Marriott, A.; McGown, G.; Thorncroft, M.; Watson, A. J.; Connolly, B. A.; Grasby, J. A.; Masui, R.; Hunter, C. A.; Tainer, J. A.; Margison, G. P.; Williams, D. M., Alkyltransferase-like protein (At1) distinguishes alkylated guanines for DNA repair using cation-pi interactions. *Proc Natl Acad Sci U S A* **2012**, *109* (46), 18755-60.
34. Kubitschek, H. E.; Sepanski, R. J., Azaserine: survival and mutation in *Escherichia coli*. *Mutat Res* **1982**, *94* (1), 31-8.
35. Sartorelli, A. C.; Booth, B. A., Inhibition of the synthesis of thymine nucleotides by azaserine. *Mol Pharmacol* **1967**, *3* (1), 71-80.
36. Nestmann, E. R.; Brillinger, R. L.; Gilman, J. P.; Rudd, C. J.; Swierenga, S. H., Recommended protocols based on a survey of current practice in genotoxicity testing laboratories: II. Mutation in Chinese hamster ovary, V79 Chinese hamster lung and L5178Y mouse lymphoma cells. *Mutation research* **1991**, *246* (2), 255-84.
37. Schweikl, H.; Schmalz, G., Glutaraldehyde-containing dentin bonding agents are mutagens in mammalian cells in vitro. *J Biomed Mater Res* **1997**, *36* (3), 284-8.
38. Schweikl, H.; Schmalz, G.; Rackebrandt, K., The mutagenic activity of unpolymerized resin monomers in *Salmonella typhimurium* and V79 cells. *Mutation research* **1998**, *415* (1-2), 119-30.
39. Follmann, W.; Lucas, S., Effects of the mycotoxin ochratoxin A in a bacterial and a mammalian in vitro mutagenicity test system. *Arch Toxicol* **2003**, *77* (5), 298-304.
40. Dolan, M. E.; Pegg, A. E., O⁶-benzylguanine and its role in chemotherapy. *Clin Cancer Res* **1997**, *3* (6), 837-47.
41. Konduri, S. D.; Ticku, J.; Bobustuc, G. C.; Sutphin, R. M.; Colon, J.; Isley, B.; Bhakat, K. K.; Srivenugopal, K. S.; Baker, C. H., Blockade of MGMT expression by O⁶ benzyl guanine leads to inhibition of pancreatic cancer growth and induction of apoptosis. *Clin Cancer Res* **2009**, *15* (19), 6087-95.
42. Abdel-Fattah, R.; Glick, A.; Rehman, I.; Maiberger, P.; Hennings, H., Methylation of the O⁶-methylguanine-DNA methyltransferase promoter suppresses expression in mouse skin tumors and varies with the tumor induction protocol. *Int J Cancer* **2006**, *118* (3), 527-31.
43. Zhang, L.; Kim, S.; Jia, G.; Buhmeida, A.; Dallol, A.; Wright, W. E.; Fornace, A. J.; Al-Qahtani, M.; Shay, J. W., Exome Sequencing of Normal and Isogenic Transformed Human Colonic Epithelial Cells (HCECs) Reveals Novel Genes Potentially Involved in the Early Stages of Colorectal Tumorigenesis. *BMC Genomics* **2015**, *16 Suppl 1*, S8.

44. Roig, A. I.; Eskiocak, U.; Hight, S. K.; Kim, S. B.; Delgado, O.; Souza, R. F.; Spechler, S. J.; Wright, W. E.; Shay, J. W., Immortalized epithelial cells derived from human colon biopsies express stem cell markers and differentiate in vitro. *Gastroenterology* **2010**, *138* (3), 1012-21.e1-5.
45. Erzinger, M. M.; Bovet, C.; Hecht, K. M.; Senger, S.; Winiker, P.; Sobotzki, N.; Cristea, S.; Beerenwinkel, N.; Shay, J. W.; Marra, G.; Wollscheid, B.; Sturla, S. J., Sulforaphane Preconditioning Sensitizes Human Colon Cancer Cells towards the Bioreductive Anticancer Prodrug PR-104A. *PLoS One* **2016**, *11* (3), e0150219.
46. Yu, Y.; Wang, J.; Wang, P.; Wang, Y., Quantification of Azaserine-Induced Carboxymethylated and Methylated DNA Lesions in Cells by Nanoflow Liquid Chromatography-Nanoelectrospray Ionization Tandem Mass Spectrometry Coupled with the Stable Isotope-Dilution Method. *Anal Chem* **2016**, *88* (16), 8036-42.
47. Tubbs, J. L.; Latypov, V.; Kanugula, S.; Butt, A.; Melikishvili, M.; Kraehenbuehl, R.; Fleck, O.; Marriott, A.; Watson, A. J.; Verbeek, B.; McGown, G.; Thorncroft, M.; Santibanez-Koref, M. F.; Millington, C.; Arvai, A. S.; Kroeger, M. D.; Peterson, L. A.; Williams, D. M.; Fried, M. G.; Margison, G. P.; Pegg, A. E.; Tainer, J. A., Flipping of alkylated DNA damage bridges base and nucleotide excision repair. *Nature* **2009**, *459* (7248), 808-13.
48. Latypov, V. F.; Tubbs, J. L.; Watson, A. J.; Marriott, A. S.; McGown, G.; Thorncroft, M.; Wilkinson, O. J.; Senthong, P.; Butt, A.; Arvai, A. S.; Millington, C. L.; Povey, A. C.; Williams, D. M.; Santibanez-Koref, M. F.; Tainer, J. A.; Margison, G. P., At11 regulates choice between global genome and transcription-coupled repair of O⁶-alkylguanines. *Molecular cell* **2012**, *47* (1), 50-60.
49. Tomaszowski, K. H.; Aasland, D.; Margison, G. P.; Williams, E.; Pinder, S. I.; Modesti, M.; Fuchs, R. P.; Kaina, B., The bacterial alkyltransferase-like (eATL) protein protects mammalian cells against methylating agent-induced toxicity. *DNA Repair (Amst)* **2015**, *28*, 14-20.
50. Yu, Y.; Wang, J.; Wang, P.; Wang, Y., Quantification of Azaserine-Induced Carboxymethylated and Methylated DNA Lesions in Cells by Nanoflow Liquid Chromatography-Nanoelectrospray Ionization Tandem Mass Spectrometry Coupled with the Stable Isotope-Dilution Method. *Analytical Chemistry* **2016**, *88* (16), 8036-8042.
51. Gillet, L. C.; Alzeer, J.; Scharer, O. D., Site-specific incorporation of N-(deoxyguanosin-8-yl)-2-acetylaminofluorene (dG-AAF) into oligonucleotides using modified 'ultra-mild' DNA synthesis. *Nucleic Acids Res* **2005**, *33* (6), 1961-9.
52. (CCLE), B. I. C. C. L. E., <https://portals.broadinstitute.org/ccle/page?gene=MGMT>. **2019**.
53. Surova, O.; Zhivotovsky, B., Various modes of cell death induced by DNA damage. *Oncogene* **2013**, *32* (33), 3789-97.
54. Bhupapadu Sunkesula, S. R.; Swain, U.; Babu, P. P., Cell death is associated with reduced base excision repair during chronic alcohol administration in adult rat brain. *Neurochemical research* **2008**, *33* (6), 1117-28.
55. Borrás-Fresneda, M.; Barquinero, J. F.; Gomolka, M.; Hornhardt, S.; Rossler, U.; Armengol, G.; Barrios, L., Differences in DNA Repair Capacity, Cell Death and Transcriptional Response after Irradiation between a Radiosensitive and a Radioresistant Cell Line. *Sci Rep* **2016**, *6*, 27043.
56. Chatterjee, N.; Walker, G. C., Mechanisms of DNA damage, repair, and mutagenesis. *Environ Mol Mutagen* **2017**, *58* (5), 235-263.
57. Foresta, M.; Izzotti, A.; La Maestra, S.; Micale, R.; Poggi, A.; Vecchio, D.; Frosina, G., Accelerated repair and reduced mutagenicity of DNA damage induced by cigarette smoke in human bronchial cells transfected with E.coli formamidopyrimidine DNA glycosylase. *PLoS One* **2014**, *9* (1), e87984.
58. Moore, J. M.; Correa, R.; Rosenberg, S. M.; Hastings, P. J., Persistent damaged bases in DNA allow mutagenic break repair in Escherichia coli. *PLoS genetics* **2017**, *13* (7), e1006733.
59. Du, H.; Wang, P.; Li, L.; Wang, Y., Repair and translesion synthesis of O (6)-alkylguanine DNA lesions in human cells. *J Biol Chem* **2019**, *294* (29), 11144-11153.
60. Yeo, J. E.; Khoo, A.; Fagbemi, A. F.; Schäfer, O. D., The efficiencies of damage recognition and excision correlate with duplex destabilization induced by acetylaminofluorene adducts in human nucleotide excision repair. *Chem Res Toxicol* **2012**, *25* (11), 2462-8.
61. Kuhn, K. S.; Muscaritoli, M.; Wischmeyer, P.; Stehle, P., Glutamine as indispensable nutrient in oncology: experimental and clinical evidence. *European Journal of Nutrition* **2010**, *49* (4), 197-210.
62. Klein, C. B.; Broday, L.; Costa, M., Mutagenesis assays in mammalian cells. *Curr Protoc Toxicol* **2001**, Chapter 3, Unit3.3.
63. Gong, J.; Sturla, S. J., A synthetic nucleoside probe that discerns a DNA adduct from unmodified DNA. *Journal of the American Chemical Society* **2007**, *129* (16), 4882-3.

Supporting Information
for

**A combination of direct reversion and excision repair in cells
reduces the mutagenic effects of DNA carboxymethylation**

Claudia M.N. Aloisi¹, Nora A. Escher¹, Susanne M. Geisen¹, Hyun S. Kim², Jung E. Yeo²,
Orlando D. Schärer², Shana J. Sturla^{1*}

¹Laboratory of Toxicology, Institute of Food Nutrition and Health, Swiss Federal Institute of
Technology, 8092 Zürich, Switzerland

²Ulsan National Institute of Science and Technology, Ulsan, Korea

*Correspondence to Prof. Shana J. Sturla, Email: sturlas@ethz.ch

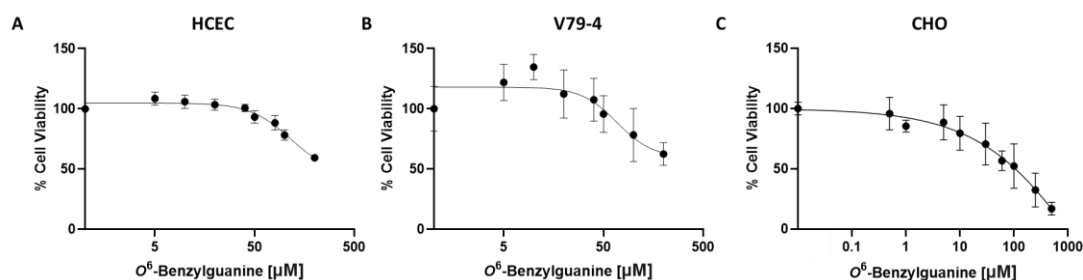


Figure S1. O^6 -BnG toxicity in HCEC, V79-4 and CHO cells. HCEC (A), V79-4 (B) and CHO cells (C) were exposed for 24 h to increasing concentrations of O^6 -BnG. Cell viability was measured by CellTiter-Glo. Data were represented using GraphPad Prism 8. Cell viability data were fit in a nonlinear regression curve, using a dose-response function. Error bars indicate standard deviation. Experiments in duplicates, each time in technical triplicates.

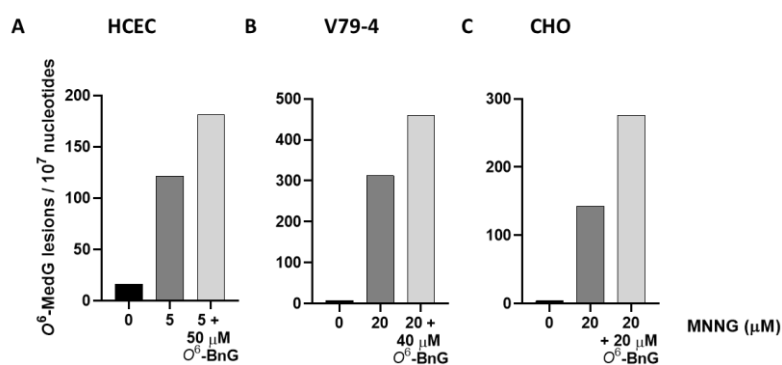


Figure S2. Level of O^6 -MedG lesions upon exposure to MNNG and O^6 -BnG. HCEC (A), V79-4 (B) and CHO cells (C) were exposed for 4 h to MNNG, after pre-conditioning with O^6 -BnG. DNA was extracted from the cells and enzymatically hydrolysed to nucleosides, O^6 -MedG was purified by solid phase extraction and detected by mass spectrometry. The number of detected lesions is normalized to the overall nucleotides content. Experiments were performed two independent times.

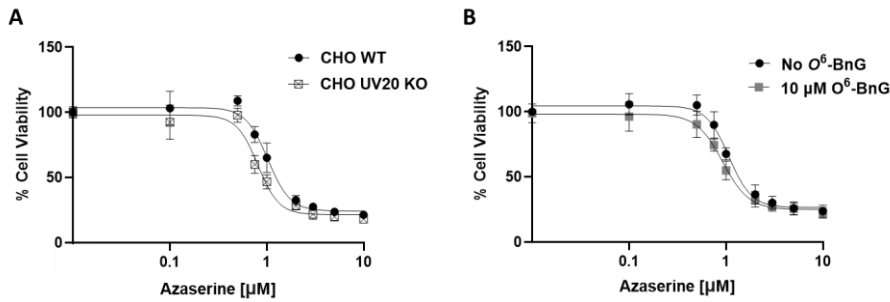


Figure S3. Viability of CHO cells after 24 h exposure to azaserine. CHO WT and UV20 KO cells were exposed to increasing concentrations of azaserine (A). CHO WT cells \pm pre-conditioning with 10 μ M O^6 -BnG were exposed to increasing concentrations of azaserine (B). Viability was measured directly after 24 h-exposure using CellTiter-Glo assay. Data from at least three independent experiments, each performed in triplicates, were averaged and fit in a nonlinear regression curve, using a dose-response function on GraphPad Prism 8. Error bars indicate standard deviation

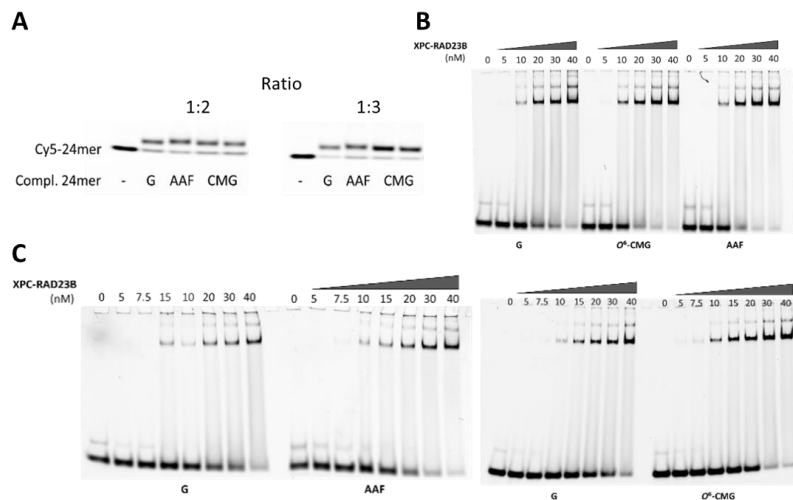


Figure S4. Annealing of oligonucleotides and EMSA for binding of XPC-RAD23B to O⁶-CMG. To prepare dsDNA for EMSA, undamaged (G) and damaged (oligo-AAF-12, oligo-O⁶-CMG-10 and oligo-O⁶-CMG-12) 24mer oligonucleotides were annealed to a complementary Cy5-labeled 24mer strand, in a ratio 1:2 or 1:3 (A). Homogenous annealing through the four samples was evaluated by imaging of samples run on a denaturing gel. (B-C) Undamaged (G) and damaged (oligo-AAF-12 and oligo-O⁶-CMG-12) 24mer oligonucleotides annealed to Cy5-labelled 24mer were incubated with increasing concentrations of XPC-RAD23B protein. Reactions were resolved on a denaturing gel, and binding of the protein to the dsDNA was evaluated by quantification of the intensity of the upper bands using ImageLab software. Data obtained from gels in (C) are plotted in Fig. 4.

Chapter 4. The role of *O*⁶-methylguanine-DNA methyltransferase in the repair of the mutagenic DNA lesion *O*⁶-carboxymethyl-guanine in human colon epithelial cells

Manuscript in preparation

Döhning J., Geisen S.M., Kostka T., Stornetta A., Christmann M., Shay J.W., Empl M. T., Sturla S.J., Steinberg P.

Döhning J. performed cell studies and comet assay, evaluated and interpreted data and participated in writing. Geisen S.M. performed mass spectrometry analysis, evaluated and interpreted data, and participated in writing. Kostka T. performed cell studies and participated in writing. Stornetta A. performed mass spectrometry analysis, and evaluated and interpreted data. Christmann M. performed MGMT-activity assay and evaluated and interpreted data. Shay J.W. generated the HCEC cell line. Empl M.T., Sturla S.J. and Steinberg P. conceived of research, interpreted data, and wrote the manuscript.

The role of O⁶-methylguanine-DNA methyltransferase in the repair of the mutagenic DNA lesion O⁶-carboxymethylguanine in human colon epithelial cells

Manuscript in preparation

Döhring J.¹, Geisen S.M.², Kostka T.¹, Stornetta A.², Empl M.T.¹, Christmann M.³, Shay J.W.⁴, Sturla S.J.², Steinberg P.^{1,5,*}

¹ Institute for Food Toxicology, University of Veterinary Medicine Hannover, 30173 Hannover, Germany

² Laboratory of Toxicology, Institute of Food Nutrition and Health, Swiss Federal Institute of Technology, 8092 Zürich, Switzerland

³ Institute of Toxicology, University Medical Center Mainz, 55131 Mainz Germany

⁴ Department of Cell Biology, University of Texas Southwestern Medical Center, Dallas, TX 75390-9039, USA

⁵ Current address: Max Rubner-Institute, Federal Research Institute of Nutrition and Food, 76131 Karlsruhe, Germany

* To whom correspondence should be addressed. Tel: +49 721 6625201; Fax: +49 721 6625111; Email: Pablo.steinberg@mri.bund.de

Short title: Repair of CMG adducts by MGMT in human colon cells

4.1 Abstract

A diet rich in red and processed meat leads to an increased endogenous formation of nitroso compounds (NOCs), which are able to alkylate the DNA of gastrointestinal tract cells, resulting in the formation of pro-mutagenic DNA lesions. DNA adducts occurring at the O^6 -position, such as O^6 -carboxymethylguanine (O^6 -CMG) and O^6 -methylguanine (O^6 -MeG), of guanine are usually repaired by the enzyme O^6 -methylguanine-DNA methyltransferase (MGMT). Although well documented in the case of the O^6 -Med adduct, the ability of MGMT to repair the O^6 -CMG adduct is currently open to debate. To address this question, immortalized normal diploid human colon epithelial cells (HCECs) lacking MGMT activity were established and exposed to the carboxymethylating agent azaserine. Subsequently, cell viability was analyzed by means of the CellTiterGlo[®] assay, genotoxicity by the alkaline comet assay and O^6 -CMG formation by high-resolution tandem mass spectrometry (hrMS/MS). When compared to the wild type cell line, cell viability decreased and genotoxicity notably increased in MGMT-deficient cells, and these cells were unable to repair the azaserine-induced O^6 -CMG adducts. We further validate the results via chemical inhibition of MGMT followed by nucleoside analysis with nano-LC-ESI-hrMS², allowing for detection of O^6 -CMG adducts in MGMT proficient cells. In conclusion, we show for the first time that MGMT activity protects normal human colon epithelial cells against the cytotoxic and genotoxic effects of a carboxymethylating agent and is indeed involved in the repair of the pro-mutagenic DNA lesion O^6 -CMG in these cells.

Keywords: Colorectal cancer, DNA adducts, O^6 -carboxymethyldeoxyguanosine, O^6 -methylguanine DNA methyltransferase, DNA adduct repair

Abbreviations: HCECs, immortalized normal diploid human colon epithelial cells; hrMS/MS, high-resolution tandem mass spectrometry; IARC, International Agency for Research on Cancer; MGMT, O^6 -methylguanine-DNA methyltransferase, NER, nuclear excision repair; NOCs, nitroso compounds; O^6 -MedG, O^6 -methyldeoxyguanosine; O^6 -CMdG, O^6 -carboxymethyldeoxyguanosine

4.2 Introduction

Colorectal cancer (CRC) is one of the most frequent cancers worldwide, with genetic and environmental factors (alcohol, tobacco and diet) contributing to the development of this disease.¹⁻³ In this context, the International Agency for Research on Cancer (IARC) recently classified processed meat as a group 1 carcinogen and red meat as probably carcinogenic to humans (group 2A).⁴ The consumption of red meat is known to stimulate the formation of nitroso compounds (NOCs) in the gut⁵ and the amount of NOCs formed increases with the amount of ingested red meat.⁶⁻⁷ It has been postulated that these NOCs can lead to the alkylation of guanine at the *O*⁶-position, resulting in the formation of the pro-mutagenic DNA lesions *O*⁶-methylguanine (*O*⁶-MeG) and *O*⁶-carboxymethylguanine (*O*⁶-CMG).⁸ In fact, Lewin *et al.* showed that *O*⁶-CMG adducts were detectable in exfoliated cells present in faeces of volunteers having consumed a high amount of red meat and that the amount of fecal NOCs correlated positively with the percentage of cells staining positive for *O*⁶-CMG.⁸ At the time, Lewin *et al.* hypothesized that *O*⁶-CMG adducts were not repaired, and that the formation of these adducts, along with other related and potentially not repaired adducts, could lead to gene mutations and, subsequently, to the development of CRC, i.e. a cascade of molecular events that could explain the association of red meat consumption with the development of CRC.

The enzyme *O*⁶-methylguanine-DNA methyltransferase (MGMT) repairs *O*⁶-MeG adducts by transferring the methyl group from guanine to its active site. This reaction results in the inactivation and subsequent degradation of MGMT.⁹⁻¹⁰ Shuker *et al.* reported that MGMT present in extracts of the human lung fibroblast cell line MRC-5 did not remove *O*⁶-CMdG adducts from DNA and postulated that this might be the only alkyl adduct type that is not repaired by MGMT.¹¹ Moreover, it was suggested that this adduct might only be repaired by nucleotide excision repair (NER).¹² In contrast, it was recently shown in a cell-free system that *O*⁶-CMG-containing oligodeoxyribonucleotides effectively inactivate MGMT, thereby indicating that this type of adduct can act as a substrate for this enzyme.¹³

It is well known that *O*⁶-CMdG adducts are pro-mutagenic DNA lesions, which lead to both GC→AT transition and GC→TA transversion mutations in genes known to play a role in the development of human CRC.¹⁴⁻¹⁶ The aim of the present study was therefore to investigate whether MGMT is able to repair *O*⁶-CMG adducts in HCECs.¹⁷ Therefore, we evaluated cytotoxicity, DNA adduct levels and DNA strand breaks in HCEC cells with and without MGMT activity after treatment with the carboxymethylating agent azaserine. MGMT activity was reduced via shRNA silencing and via chemical inhibition by the well-established inhibitor *O*⁶-benzylguanine (*O*⁶-BG).¹⁸⁻¹⁹ DNA adduct levels were detected by mass spectrometry with two different approaches: nucleobase quantification of *O*⁶-MeG and *O*⁶-CMG on an LTQ-Orbitrap for the adduct levels in cells with silenced MGMT and nucleoside analysis for the quantification of *O*⁶-methyldeoxyguanosine (*O*⁶-MedG) and *O*⁶-carboxymethyldeoxyguanosine (*O*⁶-CMdG) on an LUMOS instrument in cells with chemical inhibition of MGMT. The implications of the results obtained herein are discussed in the context of human CRC development.

4.3 Material and methods

Materials

If not stated otherwise, all materials were purchased from Sigma Aldrich (Schnelldorf, Germany). All solvents used for HPLC and MS analysis were > 99.9% purity.

Cell culture

HCEC cells (clone 1CT) were kindly provided by Prof. J. Shay (Department of Cell Biology, Southwestern Medical Center, University of Texas, Dallas, USA).¹⁷ Cells were cultured under hypoxic (i.e. for colon epithelial cells physiological) conditions (2% O₂, 5% CO₂, 37 °C) on Primaria[®] plates (Corning, Kaiserslautern, Germany) in DMEM GlutaMax mixed 4:1 with 199 medium (Thermo Fisher Scientific, Darmstadt, Germany). Medium was supplemented with 2% HyClone[™] Cosmic Calf[™] serum (GE Healthcare, Hamburg, Germany) as well as the following growth supplements: 25 ng/ml human epidermal growth factor, 1 µg/ml hydrocortisone, 10 µg/ml bovine pancreas insulin, 2 µg/ml transferrin, 5 nM sodium selenite and 50 µg/ml gentamycin sulfate.

HT-29 cells were purchased from the American Type Culture Collection (ATCC, Manassas, VA) and culture medium consisted of DMEM (Biochrom, Berlin, Germany) supplemented with 10% fetal bovine serum (Biochrom), 2 mM L-glutamine (Biochrom), 100 U/ml penicillin and 100 g/ml streptomycin (Biochrom). BALB/c-3T3 cells were kindly provided by Dr. A. Poth (Dr. Knoell Consult, Mannheim, Germany) and cultured in DMEM/Ham's F-12 medium (Biochrom) supplemented with 5% FCS, 2 mM L-glutamine, 100 U/mL penicillin/100 g/mL streptomycin (all from Biochrom). HT-29 as well as BALB/c-3T3 cells were cultivated in polystyrene flasks/dishes (TPP, Trasadingen, Switzerland) and incubated at 37 °C, 95% relative humidity and 5% CO₂.

Azaserine exposure in MGMT⁻ and WT cells

A 75 mM azaserine stock solution was prepared by dissolving azaserine (Santa Cruz Biotechnology, Heidelberg, Germany) in sterilized distilled water. Subconfluent cells were washed with preheated PBS and incubated with 75 µM azaserine in cell culture medium for 4 or 24 h. Unexposed cells served as background control. For DNA adduct quantification, the cells were pelleted immediately after the azaserine treatment and stored at -80 °C until further analysis.

Measurement of nucleobase adducts in MGMT⁻ and WT cells

DNA Extraction

DNA was extracted from azaserine-exposed HCEC WT and HCEC MGMT⁻ cells by using the DNA Isolation Kit for Cells and Tissues (Roche, Rotkreuz, Switzerland) according to the instructions of the manufacturer. Then, DNA was dissolved in 0.1 M formic acid (500 µl, pH 2) and spiked with 2 pmol of isotope-labeled O⁶CD₃G. Hydrolysis of DNA was achieved by heating the samples at 80°C for 1 h. Upon hydrolysis, samples were cooled down to room temperature and neutralized with 1 N NaOH. Samples were then filtered through a Centrifree[®] Ultrafiltration Device (MW cut-off= 30,000; Merck Millipore, Dublin, Ireland). An aliquot (20 µl) of each sample was used for the analysis of adenine by ultra performance

liquid chromatography (UPLC). A reaction mixture containing all the solutions except DNA served as negative control. Samples were acidified with 0.1 N HCl (800 µl) and purified by solid-phase extraction (SPE) on an OASIS MCX ion exchange cartridge (30 µm particle size; Waters, Milford, MA). After conditioning and equilibration of the cartridge with 1 ml methanol (MeOH) and 1 ml 0.1 N HCl, samples were loaded on the cartridge, which was then washed with 1 ml 0.1 N HCl and 1 ml MeOH, and finally eluted with 1 ml 5% MeOH/ammonia solution. The eluted fractions were subsequently evaporated to dryness and re-suspended in 5 µl of a 0.1% trifluoroacetic acid solution. All steps of the sample preparation were performed in silanized glass vials.

DNA adduct measurement by hrMS/MS

Liquid chromatography separation was performed on a Dionex RSLCnano UPLC system (Thermo Fisher Scientific, Dublin, CA) equipped with a 1 µl injection loop. One microliter of each sample was injected onto a capillary column (75 µm ID, 20 cm length, 10 µm orifice) prepared by hand-packing a commercially available fused-silica emitter (New Objective, Woburn, MA) with Hydro RP C18-bonded separation medium (Phenomenex, Torrance, CA). The flow rate was set at 300 nl/min and 0% acetonitrile (ACN) for 3.5 min followed by switching of the injection port to remove the injection loop from the flow path and a 13-min linear gradient to 20% ACN. This step was followed by a 0.5 min gradient to 90% ACN with an increased flow rate of 900 nl/min and a 1-min hold. The flow composition was then returned to 0% ACN and the column was re-equilibrated for 7 min at 900 nl/min. The mass spectrometric analysis was performed by nanoelectrospray ionization with an LTQ-Orbitrap Elite mass spectrometer (Thermo Scientific, Waltham, MA). The source voltage was set to 2.2 kV. The capillary temperature was 350°C, and the S-Lens RF level was set to 50%. Adducts were quantified by detection of O⁶-MeG at m/z 166.1 [M + H]⁺ → m/z 134.0461 [M - CH₄O + H]⁺, D₃-O⁶-MeG at m/z 169.1 → m/z 134.0461 [M - CHD₃O + H]⁺ and O⁶-CMG at 210.1 [M + H]⁺ → m/z 152.0567 [G + H]⁺ with accurate mass monitoring of the fragment ions at 5 ppm mass accuracy utilizing the Orbitrap detector. Higher energy collisional dissociation fragmentation with a collision energy of 60% was used for all events, 1.5 amu isolation widths for O⁶-MeG and D₃-O⁶-MeG, and a 3 amu isolation width for O⁶-CMG. Data was collected using a resolution setting of 15,000 (at m/z 400) with an actual resolution of 25,000 (at m/z 134 and 152). Calibration curves were calculated from injections of solutions containing increasing concentrations of O⁶-MeG or O⁶-CMG and a fixed concentration of D³-O⁶-MeG, by assuming that any effect on quantitation due to recovery and ion suppression when measuring O⁶-CMG adducts is accounted for by the deuterated O⁶-MeG internal standard.

MGMT-inhibition and azaserine exposure in HCEC cells

A 100 mM azaserine stock solution was prepared by dissolving azaserine (Santa Cruz Biotechnology, Heidelberg, Germany) in sterilized distilled water. HCEC WT cells were pre-conditioned for 4 h with 50 µM O⁶-BG to inhibit MGMT, while repair proficient WT cells were pre-conditioned with 0.1% DMSO as control. Media was removed, and cells ± MGMT were exposed to 0, 50 or 100 µM azaserine for 24 or 48 h. 50 µM O⁶-BG were added to the medium after 24 h of azaserine incubation to ensure MGMT-inhibition over long time exposure. Absence of MGMT was confirmed by Western Blot. For DNA adduct

quantification, the cells were pelleted immediately after the azaserine treatment and stored at -80 °C until further analysis.

Measurement of nucleoside adducts in HCEC cells with and without MGMT-inhibition

DNA was extracted from cell pellets using the DNA isolation kit for cells and tissue (Roche, Rotkreuz, Switzerland) according to the instructions of the manufacturer.²⁰ Then, DNA was further processed as described in *Chapter 1*. In short, internal standards were added and DNA was enzymatically digested to nucleobases. DNA was quantified via deoxyguanosine (dG) content by reversed phase liquid chromatography and samples were further processed by solid phase extraction for nano-liquid chromatography electrospray ionization high-resolution tandem mass spectrometry (nanoLC-ESI-hrMS²). *O*⁶-MedG and *O*⁶-CMdG levels were expressed as lesions/10⁷ nucleotides.

Data analysis

Data from at least three independent experiments were statistically analyzed, unless otherwise indicated. Statistical evaluation was conducted using Prism v. 6.04 (GraphPad, La Jolla, CA, USA) as specifically indicated in each figure and table caption, and *p*-values < 0.05 were considered statistically significant.

4.4 Results

Characterization of HCEC MGMT⁻ cells

The goal of this study was to determine whether MGMT acts on *O*⁶-CMG. The strategy involved first creating a human colon epithelial cell line with silenced MGMT with the aim of evaluating the persistence of DNA adducts in these cells. MISSION[®] small hairpin RNA (shRNA) sequences against MGMT cloned into pLKO.1 containing a puromycin resistance gene (puro vector) was used, to produce HCEC cells with a stable transduction of the MGMT gene, termed HCEC MGMT⁻. As analyzed by RT-qPCR, there was a 70% reduction of MGMT expression and decreased MGMT activity to 0.55 fmol/mg protein, a ~230-fold lower activity than that measured in the HCEC WT cells (Table 1). To determine whether the transduction process or the MGMT deficiency as such led to any alterations in cell growth, several growth-related parameters were analyzed. The population doubling time (PDL) was only slightly increased (21.57 h [HCEC WT] vs. 24.34 h [HCEC MGMT⁻]) (Figure 1A); no decrease in cell-cell contact inhibition (Figure 1B) and no increase in anchorage-independent growth were observed in HCEC cells following MGMT silencing (Figure 1C).

Cell line	MGMT expression ^a (%)	MGMT activity ^b (fmol/mg protein)
HCEC WT	100 ± 7	129 ± 7
HCEC MGMT ⁻	30 ± 5	0.55 ± 0.38

Table 1. MGMT expression and activity analysis in HCEC WT and HCEC MGMT⁻ cells. ^aDetermined by RT-qPCR with the following primers: GAPDH-up: 5'-CATGAGAAGTATGACAACAG-3', GAPDH-low: 5'-ATGAGTCCTTCCACGATA-3', ACTB-up: 5'-TGGCATCCACGAACTACC-3', ACTB-low: 5'-GTGTTGGCGTACAGGTCTT-3', MGMT-up: 5'-AATCACTTCTCCGAATTTTCAC-3', MGMT-low: 5'-CTCTTCACCATCCCGTTT-3'. MGMT expression was normalized to the expression of glyceraldehyde 3-phosphate dehydrogenase and β-actin and expressed in relation to the unexposed control. Values represent the mean ± SD of duplicate experiments. ^bMGMT activity determined as previously described.²¹⁻²²

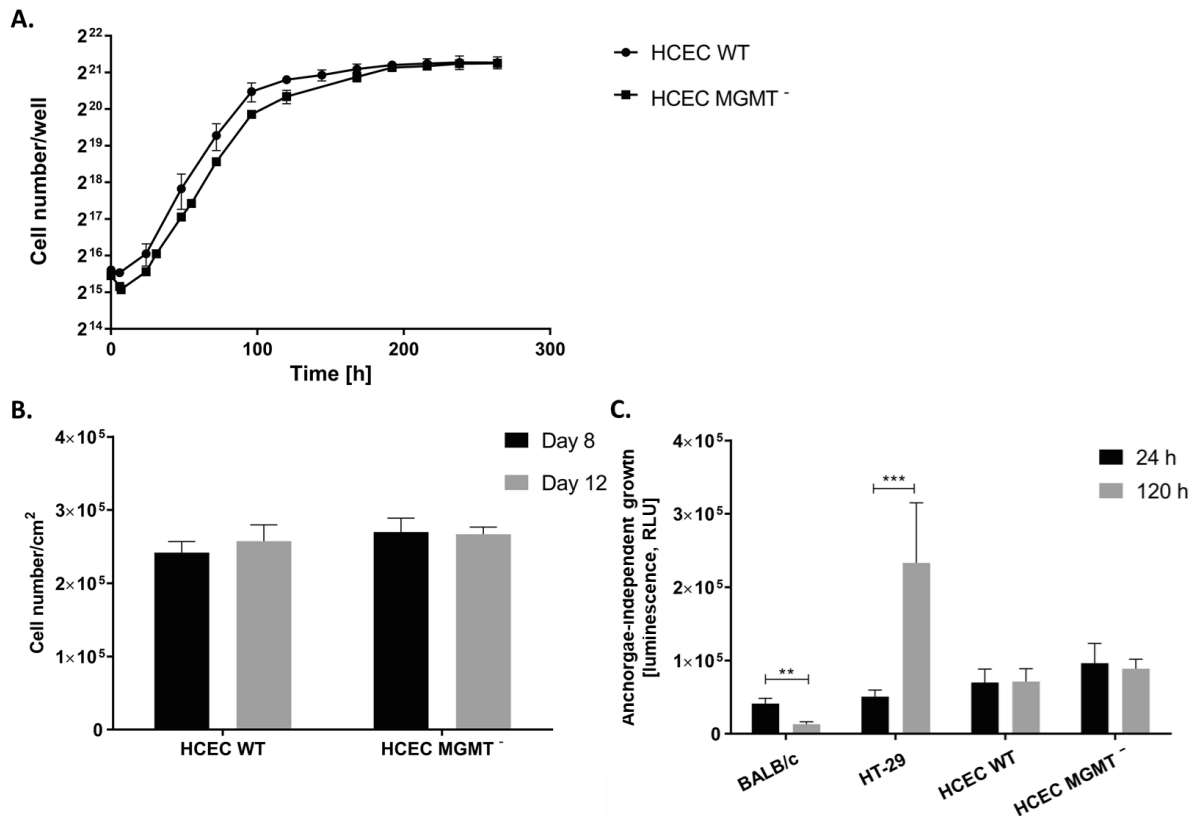


Figure 1. Characterization of the growth behavior of HCEC WT and HCEC MGMT⁻ cells. **A:** Determination of the population doubling level (PDL). Cells were plated in 6-well plates at a density of 4×10^4 cells/well and counted by trypan blue exclusion test in a Neubauer chamber every 24 h for 12 days with medium replacement every three days. The PDL was calculated using the following formula for the evaluation performed three times, each measured in triplicate: $PDL = T \frac{\ln 2}{\ln(\frac{Xe}{Xb})}$ (T = incubation time, Xe = cell number at the end of the incubation period, Xb = cell number at the beginning of the incubation period). **B:** Determination of the saturation density after the cells reached confluence (day 8) as well as

four days later (day 12). The saturation density of the cells was determined by seeding 1×10^5 cells/well in 6-well plates and then counting their number after the cells had reached 100% confluence (day 8) as well as four days later (day 12). Cell culture medium was replaced every three days. **C:** Analysis of anchorage-independent growth using the GILA assay. The “growth in low attachment” (GILA) assay²³ was used to measure the anchorage-independent growth of the cells. Briefly, 1,000 cells/well were seeded in triplicate onto ultra low-attachment plates (Corning, Kaiserslautern, Germany). After 24 and 120 h, cellular growth was quantified by measuring the ATP levels in the permeabilized cells with the CellTiter-Glo[®] luminescent assay (Promega, Mannheim, Germany) according to the instructions of the manufacturer.²⁴ BALB/c-3T3 and HT-29 cells served as negative and positive controls, respectively. In all four cases each value represents the mean \pm SD of three independent experiments. The statistical analysis was performed by using an unpaired *t*-test with Welch’s correction (all cell lines compared to the positive control [HT-29 cells] as well as HCEC WT cells tested against HCEC MGMT⁻ cells). * $p \leq 0.05$; ** $p \leq 0.01$; *** $p \leq 0.001$; **** $p \leq 0.0001$. RLU: relative luminescence units.

Increased cytotoxicity and genotoxicity in HCEC MGMT⁻ cells after prolonged exposure to azaserine

Following the characterization of HCEC MGMT⁻ cells, we were interested in whether suppression of MGMT sensitizes cells towards exposure of azaserine as carboxymethylating agent. Therefore, we assessed cytotoxicity and genotoxicity in HCEC WT and HCEC MGMT⁻ cells after short and long term azaserine exposure. A 4 h exposure with increasing concentrations of azaserine did not lead to a decrease in cell viability in HCEC WT and HCEC MGMT⁻ cells (Figure 2). In contrast, a 24 h incubation led to a concentration dependent decrease in cell viability in both cell lines, whereby the effect was significantly more pronounced in the HCEC MGMT⁻ cells compared to HCEC WT cells (Figure 2). The extent of genotoxicity induced by azaserine in HCEC WT and HCEC MGMT⁻ cells was measured by a modified alkaline comet assay. As shown in Figure 3, unexposed HCEC WT and HCEC MGMT⁻ cells showed a similar basal level of DNA damage (0 h), while exposure to azaserine led to a time-dependent increase of the tail intensity in HCEC MGMT⁻ cells, but not in HCEC WT cells.

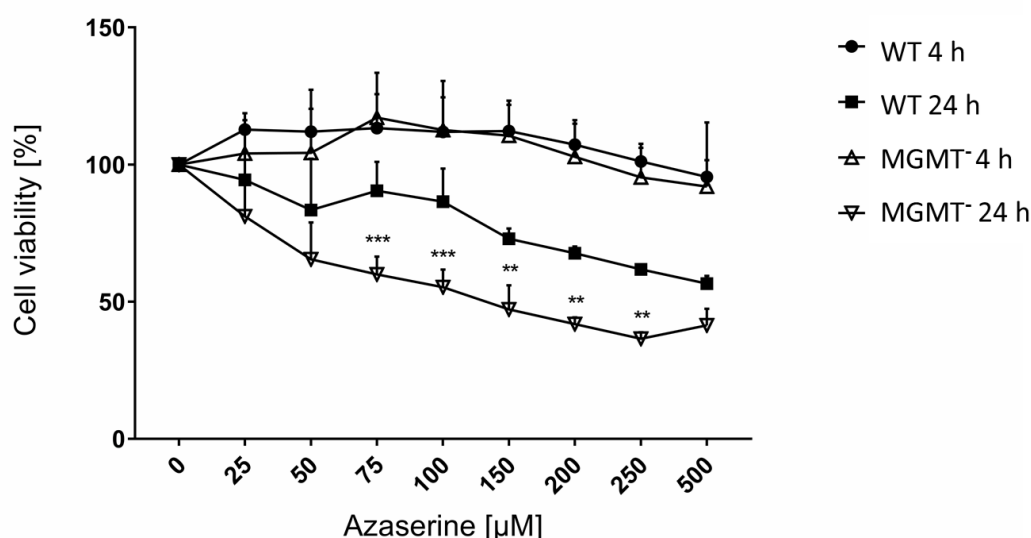


Figure 2. Viability of HCEC WT and HCEC MGMT⁻ cells exposed to increasing concentrations of azaserine for 4 or 24 h. The azaserine-induced cytotoxicity was determined by using the CellTiter-Glo[®]-Luminescent Cell Viability assay (Promega) according to the instructions of the manufacturer.²⁴ Shown is the mean \pm SD of four independent experiments. The statistical analysis was performed by using a two-way ANOVA with Bonferroni's multiple comparisons test (HCEC WT cells tested against HCEC MGMT⁻ cells); **: $p < 0.01$; ***: $p < 0.001$.

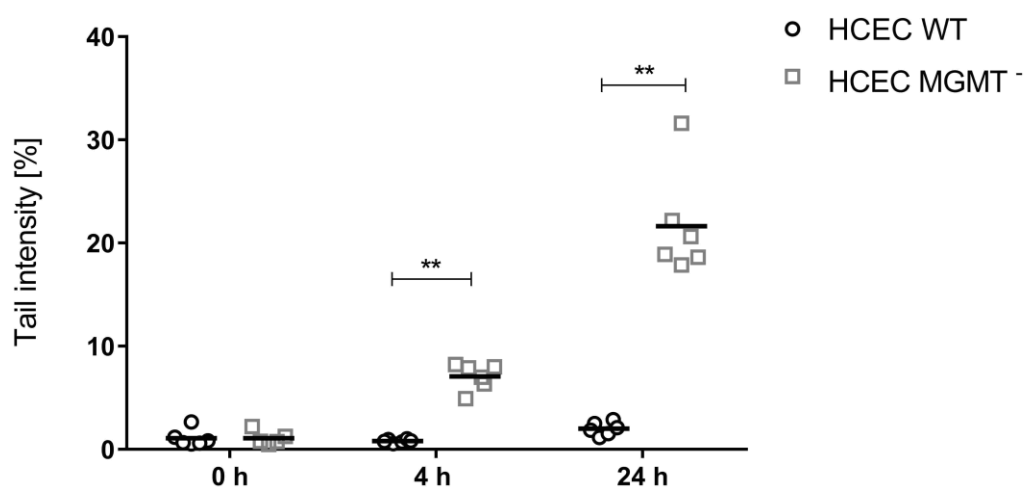


Figure 3. DNA strand breaks in HCEC WT and HCEC MGMT⁻ cells after azaserine exposure. DNA strand breaks and alkali-labile sites were analyzed after exposure of cells to 75 μ M azaserine for 4 or 24 h using a slightly modified alkaline comet assay procedure according to Singh et al.²⁵ Briefly, after treatment the cells were detached and counted, resuspended in pre-heated 0.7% low melt agarose (Promega) and applied to slides that were precoated with agarose (1% regular melt agarose [Promega]). Thereafter, the cells were lysed overnight at 4 °C. Subsequently, DNA unwinding was achieved by incubating the slides in an electrophoresis buffer (300 mM NaOH, 2 mM EDTA, pH > 13) for 40 min, followed by an electrophoresis for 25 min (1 V/cm, 290-300 mA, 4°C). Finally, the slides were neutralized in PBS and DNA was stained with propidium iodide (15 μ g/mL). DNA damage was quantified by using an Axiovert 200M fluorescence microscope (Zeiss, Jena, Germany) and the Comet Assay III software (Version 3; Perceptive Instruments, Bury St Edmunds, UK). Fifty comets per slide and five independent experiments per treatment were analyzed. The tail intensity of

the comets (in %) is shown as the median of a minimum of five independent experiments. Significant differences between the cell lines were analyzed by applying the Mann-Whitney U-test (** $p \leq 0.01$).

Elevated O^6 -MeG and O^6 -CMG levels in MGMT⁻ cells after azaserine exposure

Having characterized cellular responses of colon epithelial cells to azaserine, we were interested to test whether the increased sensitivity of the cells was related with a persistence of azaserine-induced adduct levels. Thus, O^6 -MeG and O^6 -CMG levels in HCEC WT and HCEC MGMT⁻ cells were analyzed after exposure to azaserine by the hrMS/MS method for simultaneous quantification of the base adducts on an LTQ-Orbitrap. The O^6 -MeG levels in HCEC WT cells exposed to azaserine for 4 or 24 h were similar to those in unexposed HCEC WT cells, while the O^6 -MeG level in HCEC MGMT⁻ cells exposed to azaserine for 24 h strongly increased (up to 6.3 fmoles O^6 -MeG/ μ g DNA; Figure 4A). No O^6 -CMG adducts were detected in unexposed or azaserine-exposed HCEC WT cells, whereas the O^6 -CMG levels were strongly enhanced in HCEC MGMT⁻ cells (up to 53.9 fmoles O^6 -CMG/ μ g DNA; Figure 4B). Interestingly, elevated adduct levels were only visible after 24 h, but not after 4 h azaserine-exposure. Thus, while MGMT is known to repair O^6 -MeG, elevated levels of O^6 -CMG in MGMT-deficient cells suggest MGMT to be involved in the repair this alkylated dG adduct as well.

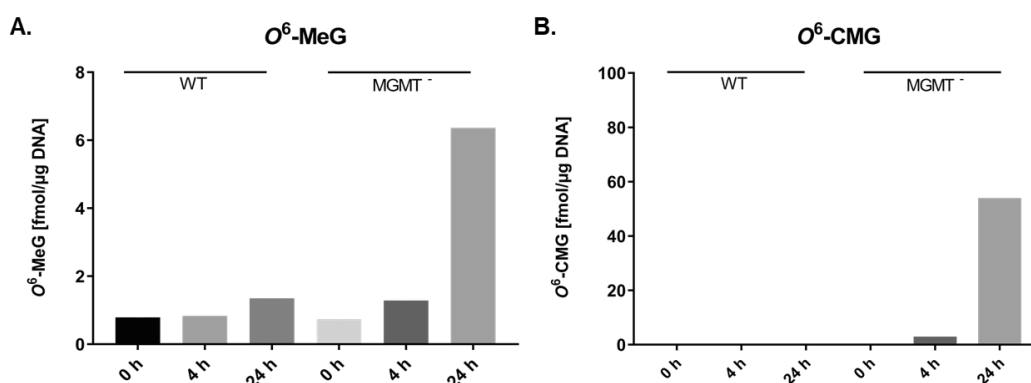


Figure 4. Quantification of O^6 -MeG (A) and O^6 -CMG adducts (B) in HCEC WT and HCEC MGMT⁻ cells exposed to 75 μ M azaserine for 4 or 24 h. The mean of two independent experiments per treatment group is shown.

Chemical inhibition of MGMT results in persistence of *O*⁶-MedG and *O*⁶-CMdG adducts in azaserine-exposed HCEC cells

The complete absence of *O*⁶-CMG levels in WT cells after exposure to azaserine was not expected, therefore we wanted to address more closely the observations by using a potentially more robust MGMT-depletion strategy, and also using a more sensitive analysis approach. To overcome limitations of the nucleobase analysis used to evaluate MGMT⁻ cells (Figure 4), we established a nano-ESI-hrMS² methodology (described in Chapter 2) to analyze the nucleoside forms of the adducts, i.e. *O*⁶-MedG and *O*⁶-CMdG, in azaserine-exposed HCEC cells pre-conditioned with *O*⁶-BG, a highly effective MGMT inhibitor.¹⁸⁻¹⁹ By this approach, *O*⁶-MedG levels in azaserine-exposed HCEC cells were similar to unexposed control cells with maximum adduct levels being 3.1 ± 3.0 lesions/ 10^7 nucleotides (100 μ M, 48 h; Figure 5). In HCEC cells pre-conditioned with *O*⁶-BG, the level of *O*⁶-MedG increased with azaserine concentration from 0 to 100 μ M, from 0.6 ± 0.5 to 7.4 ± 0.5 lesions/ 10^7 nucleotides after 24 h, and from 0.2 ± 0.3 to 25.8 ± 10.8 lesions/ 10^7 nucleotides after 48 h. After treatment with 100 μ M azaserine, *O*⁶-MedG levels were significantly higher in HCEC cells with MGMT inhibition, with a maximum fold increase in MGMT-proficient cells of 8.3 (100 μ M, 48 h; adduct levels of 3.0 in MGMT-proficient vs 25.8 ± 10.8 lesions/ 10^7 nucleotides in MGMT-inhibited). Persistence of *O*⁶-MedG in MGMT-inhibited cells was expected as MGMT is well known to be involved in the repair of this adduct.²⁵⁻²⁶ Thereby, results from *O*⁶-MedG demonstrate that repair by MGMT can be reflected in elevated adduct levels after long time azaserine-exposure of MGMT-inhibited cells.

We then addressed repair of *O*⁶-CMdG by MGMT, where preliminary results suggested that MGMT acts on this adduct as well. *O*⁶-CMdG levels in HCEC cells were similar after exposure to 50 and 100 μ M azaserine for 24 or 48 h, and as anticipated, *O*⁶-CMdG levels were higher than *O*⁶-MeG level. The maximum *O*⁶-CMdG levels were 54.7 ± 31.5 lesions/ 10^7 nucleotides (100 μ M azaserine, 48 h). Furthermore, in HCEC cells pre-conditioned with the MGMT inhibitor *O*⁶-BG, *O*⁶-CMdG adduct levels increased with increasing azaserine concentration (55.5 ± 19.0 vs 137.6 ± 26.3 lesions/ 10^7 nucleotides after 24 h and 77.0 ± 8.5 vs 131.4 ± 13.3 lesions/ 10^7 nucleotides after 48 h), and were significantly higher in the presence of the inhibitor. The maximum fold increase in *O*⁶-CMdG levels was 3.2 (100 μ M azaserine, 24 h; adduct levels of 42.7 ± 32.9 vs 137.6 ± 26.3 lesions/ 10^7 nucleotides). Summarizing, not only *O*⁶-MedG but also *O*⁶-CMdG adducts persisted in MGMT-inhibited cells, but maximum fold increase to MGMT-proficient cells was minor when compared to *O*⁶-MedG. Therefore, the results demonstrate that MGMT is involved in the repair of *O*⁶-CMdG, but less effective than for *O*⁶-MedG.

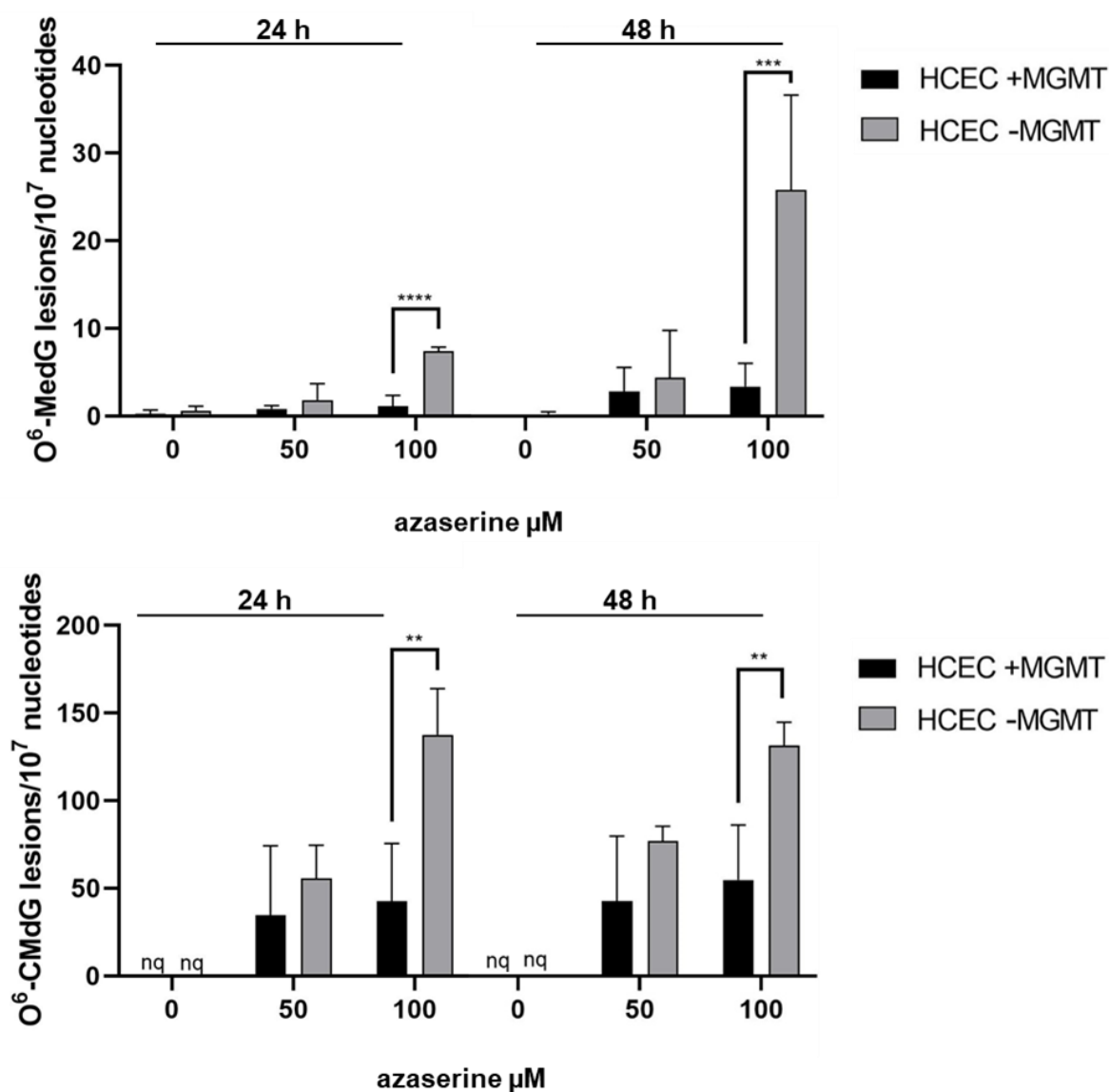


Figure 5. Impact of MGMT inhibition on levels of *O*⁶-MedG adducts (A) and *O*⁶-CMdG adducts (B) in HCEC cells. Cells were pre-conditioned for 4 h with 50 μM *O*⁶-BG or 0.1% DMSO, followed by 24 or 48 h azaserine exposure (0, 50, 100 μM). Data are mean ± SD of three independent experiments per condition. P-values were calculated with two-way ANOVA and Sidak's multiple comparison test (**p < 0.01, ***p < 0.001, ****p < 0.0001).

4.5 Discussion

MGMT is known to repair the pro-mutagenic DNA lesion O^6 -MeG but its activity on O^6 -CMG is unknown, as results from previous studies concerning O^6 -CMG repair by MGMT were not conclusive.^{13,11} Therefore, the aim of this study was to address this open question by directly evaluating the impact of MGMT activity on O^6 -CMG levels in cultured cells. We first established a human colon epithelial cell line with reduced MGMT activity (HCEC MGMT⁻) via shRNA silencing. Upon exposure to azaserine, MGMT-lacking cells showed decreased cell viability, increased genotoxicity and were not able to repair azaserine-induced O^6 -CMG adducts. For cells in which the suppression of MGMT function was achieved by shRNA silencing, nucleobase adduct levels were measured by a hrMS/MS approach on an LTQ-Orbitrap. O^6 -CMG levels strongly persisted in HCEC MGMT⁻ cells after prolonged exposure to azaserine, but no O^6 -CMG adduct levels could be detected in HCEC, presumably related to technical limitations of the nucleobase approach, including poor chromatographic retention and the inability to distinguish DNA from RNA adducts. To overcome these limitations, we developed a nanoLC-ESI-hrMS² method for the quantification of nucleoside adducts. This approach was also sufficiently sensitive to detect O^6 -CMdG in HCEC WT cells. In addition to introducing a new analytical approach, we also tested chemical inhibition of MGMT with O^6 -BG to exclude the possibility that shRNA silencing may spuriously influence the azaserine uptake pathway in HCEC cells. Thus, as a positive control, HCEC cells pre-conditioned with O^6 -BG were observed to retain up to 8.4-fold higher O^6 -MedG adduct levels compared to control cells consisted with well-known MGMT-mediated adduct removal.²⁵ Moreover, we observed that O^6 -CMdG adduct levels in cells that were pre-conditioned to inhibit MGMT function were also higher, but only up to 3.2-fold. The results suggest that MGMT indeed contributes to O^6 -CMdG repair in cells, but less effectively than for O^6 -MedG.

These results are consistent with the finding that MGMT has a broad substrate specificity for O^6 -alkyl adducts, but the reaction rate decreases for increasing alkyl lengths.²⁷⁻²⁸ MGMT removes alkylating damage from guanine by transferring the alky group to a cysteine residue, most likely via attack of the thiolate anion on the alky group. O^6 -CMG can be negatively charged under physiological conditions, which might be a steric hindrance for MGMT to bind to the damage, thereby explaining reduced repair activity of MGMT on O^6 -CMdG. Also, contributions of other pathways may not be excluded. For example, it was suggested that O^6 -CMdG adducts could also be repaired by the nucleotide excision repair (NER) pathway as the lymphoblastoid cell line GM2345, which is defective in NER, was hypersensitive to the toxic effects of azaserine.¹² On the other hand, the same cells with a DNA mismatch repair deficiency remained unaffected. Involvement of NER in the repair of O^6 -CMG is further highlighted by NER-defective *E. coli* UvrA mutants being sensitive towards azaserine.²⁹ Taken together, results suggest that a dynamic combination of MGMT and NER, may be involved in the repair of the O^6 -CMG adducts. The related bulky O^6 -alkyl-G adduct O^6 -[4-oxo-4-(3-pyridyl)butyl]guanine has indeed been shown to be repaired by MGMT³⁰ as well as by NER.³¹ Thus, further research addressing the potential interplay of MGMT and NER in the repair of O^6 -CMG is needed.

Nevertheless, the effectiveness of MGMT in reducing O^6 -CMG levels may explain in part its association with reduced colorectal cancer risk. For example, single *MGMT* polymorphisms resulting in diminished repair activity may predispose humans to colorectal cancer.³²⁻³³ Additionally, low MGMT activity or inactivation of *MGMT* by promotor hypermethylation in colorectal tissue is associated with the high frequency of GC→AT transition mutation in the proto-oncogene *KRAS*.^{34,35} Finally, reduced MGMT activity in human colorectal adenomas leads to GC→AT transition mutations in *KRAS* in a population exposed to methylating agents.³⁶ In about 50 % of colorectal cancer patients, GC → TA transversion and GC → AT transition mutations are found in *KRAS*.³⁷ Further, GC → AT transition and GC → TA transversion mutations were found to be the predominant mutations in the p53 gene of colorectal cancer patients and a similar mutation spectra was induced by a carboxymethylating agent.¹⁴ While O^6 -MeG is known to almost exclusively induce GC→AT transition mutations,³⁸⁻³⁹ O^6 -CMG was found to result in misincorporation of adenine and thymine during translesion synthesis (TLS), thereby providing fundamental evidence for O^6 -CMG adducts being responsible for dominant GC → AT transition and GC → TA transversion mutations found in colorectal cancer.⁴⁰⁻⁴¹ If one takes into account the results of the present study and those in previous reports, MGMT seems to play a crucial role as a potential tumor suppressor gene in protecting cancer driver genes from DNA base methylation and carboxymethylation, thereby preventing the subsequent development of colorectal cancer.

In conclusion, we demonstrated that MGMT depletion leads to decreased cell viability, increased genotoxicity and increased O^6 -CMG and O^6 -MeG adduct levels after azaserine exposure. Persistence of O^6 -CMdG and O^6 -MedG adduct levels was further verified after chemical inhibition of MGMT, providing evidence that MGMT is involved in the repair of pro-mutagenic O^6 -CMG adducts. Further research is needed to elucidate if other repair pathways contribute to the repair of O^6 -CMG.¹² Also, to link adduct levels with genotoxicity, the comet assay will be performed in HCEC cells with chemical inhibition of MGMT, conditions for which we could quantify O^6 -CMdG adduct levels in MGMT-proficient HCEC cells. We will include methyl methanesulfonate (MMS) as a negative control and N-methyl-N-nitrosourea (MNU) as a positive control with higher induction of O^6 -methylguanine⁴² to confirm that increased genotoxicity is related to O^6 -alkylguanine adducts and not to the more frequently induced N⁷-guanine adduct. Thus, the data presented here lend support to the hypothesis that highly active MGMT in colon epithelial cells confers protection against colorectal carcinogenesis initiated by exposure to methylating and carboxymethylating agents such as NOCs that are present in the diet.⁸

Funding

Deutsche Forschungsgemeinschaft (grant number STE 493/21-1).

Conflict of Interest Statement

None declared.

4.6 References

1. Kune, G. A.; Vitetta, L., Alcohol-Consumption and the Etiology of Colorectal-Cancer - a Review of the Scientific Evidence from 1957 to 1991. *Nutrition and Cancer* **1992**, *18* (2), 97-111.
2. Nagao, M.; Sugimura, T., Carcinogenic factors in food with relevance to colon cancer development. *Mutation research* **1993**, *290* (1), 43-51.
3. Heineman, E. F.; Zahm, S. H.; McLaughlin, J. K.; Vaught, J. B., Increased Risk of Colorectal-Cancer among Smokers - Results of a 26-Year Follow-up of Us Veterans and a Review. *International Journal of Cancer* **1994**, *59* (6), 728-738.
4. Bouvard, V.; Loomis, D.; Guyton, K. Z.; Grosse, Y.; Ghissassi, F. E.; Benbrahim-Tallaa, L.; Guha, N.; Mattock, H.; Straif, K., Carcinogenicity of consumption of red and processed meat. *The Lancet Oncology* **2015**, *16* (16), 1599-1600.
5. Bingham, S. A.; Pignatelli, B.; Pollock, J. R. A.; Ellul, A.; Malaveille, C.; Gross, G.; Runswick, S.; Cummings, J. H.; O'Neill, I. K., Does increased endogenous formation of N-nitroso compounds in the human colon explain the association between red meat and colon cancer? *Carcinogenesis* **1996**, *17* (3), 515-523.
6. Bingham, S. A.; Hughes, R.; Cross, A. J., Effect of white versus red meat on endogenous N-nitrosation in the human colon and further evidence of a dose response. *Journal of Nutrition* **2002**, *132* (11), 3522s-3525s.
7. Hughes, R.; Cross, A. J.; Pollock, J. R.; Bingham, S., Dose-dependent effect of dietary meat on endogenous colonic N-nitrosation. *Carcinogenesis* **2001**, *22* (1), 199-202.
8. Lewin, M. H.; Bailey, N.; Bandaletova, T.; Bowman, R.; Cross, A. J.; Pollock, J.; Shuker, D. E. G.; Bingham, S. A., Red Meat Enhances the Colonic Formation of the DNA Adduct O⁶-Carboxymethyl Guanine: Implications for Colorectal Cancer Risk. *Cancer research* **2006**, *66* (3), 1859-1865.
9. Xu-Welliver, M.; Pegg, A. E., Degradation of the alkylated form of the DNA repair protein, O(6)-alkylguanine-DNA alkyltransferase. *Carcinogenesis* **2002**, *23* (5), 823-30.
10. Srivenugopal, K. S.; Yuan, X. H.; Friedman, H. S.; Ali-Osman, F., Ubiquitination-dependent proteolysis of O6-methylguanine-DNA methyltransferase in human and murine tumor cells following inactivation with O6-benzylguanine or 1,3-bis(2-chloroethyl)-1-nitrosourea. *Biochemistry* **1996**, *35* (4), 1328-34.
11. Shuker, D. E. G.; Margison, G. P., Nitrosated Glycine Derivatives as a Potential Source of O⁶-Methylguanine in DNA. *Cancer research* **1997**, *57* (3), 366.
12. O'Driscoll, M.; Macpherson, P.; Xu, Y.-Z.; Karran, P., The cytotoxicity of DNA carboxymethylation and methylation by the model carboxymethylating agent azaserine in human cells. *Carcinogenesis* **1999**, *20* (9), 1855-1862.
13. Senthong, P.; Millington, C. L.; Wilkinson, O. J.; Marriott, A. S.; Watson, A. J.; Reamtong, O.; Evers, C. E.; Williams, D. M.; Margison, G. P.; Povey, A. C., The nitrosated bile acid DNA lesion O6-carboxymethylguanine is a substrate for the human DNA repair protein O6-methylguanine-DNA methyltransferase. *Nucleic Acids Research* **2013**, *41* (5), 3047-55.
14. Gottschalg, E.; Scott, G. B.; Burns, P. A.; Shuker, D. E., Potassium diazoacetate-induced p53 mutations in vitro in relation to formation of O6-carboxymethyl- and O6-methyl-2'-deoxyguanosine DNA adducts: relevance for gastrointestinal cancer. *Carcinogenesis* **2007**, *28* (2), 356-62.
15. Gay, L. J.; Mitrou, P. N.; Keen, J.; Bowman, R.; Naguib, A.; Cooke, J.; Kuhnle, G. G.; Burns, P. A.; Luben, R.; Lentjes, M.; Khaw, K. T.; Ball, R. Y.; Ibrahim, A. E.; Arends, M. J., Dietary, lifestyle and clinicopathological factors associated with APC mutations and promoter methylation in colorectal cancers from the EPIC-Norfolk study. *The Journal of Pathology* **2012**, *228* (3), 405-15.
16. Johnson, W. W., Cytochrome P450 inactivation by pharmaceuticals and phytochemicals: Therapeutic relevance. *Drug Metabolism Reviews* **2008**, *40* (1), 101-147.
17. Roig, A. I.; Eskiocak, U.; Hight, S. K.; Kim, S. B.; Delgado, O.; Souza, R. F.; Spechler, S. J.; Wright, W. E.; Shay, J. W., Immortalized Epithelial Cells Derived From Human Colon Biopsies Express Stem Cell Markers and Differentiate In Vitro. *Gastroenterology* **2010**, *138* (3), 1012-1021.e5.
18. Dolan, M. E.; Pegg, A. E., O6-benzylguanine and its role in chemotherapy. *Clinical cancer research : an official journal of the American Association for Cancer Research* **1997**, *3* (6), 837-47.
19. Dolan, M. E.; Pegg, A. E.; Dumenco, L. L.; Moschel, R. C.; Gerson, S. L., Comparison of the inactivation of mammalian and bacterial O6-alkylguanine-DNA alkyltransferases by O6-benzylguanine and O6-methylguanine. *Carcinogenesis* **1991**, *12* (12), 2305-9.
20. https://www.sigmaaldrich.com/content/dam/sigma-aldrich/docs/Roche/General_Information/1/dna-isolation-kit-for-cells-and-tissues.pdf. Roche online protocol.
21. Preuss, I.; Haas, S.; Eichhorn, U.; Eberhagen, I.; Kaufmann, M.; Beck, T.; Eibl, R. H.; Dall, P.; Bauknecht, T.; Hengstler, J.; Wittig, B. M.; Dippold, W.; Kaina, B., Activity of the DNA repair protein O6-methylguanine-DNA methyltransferase in human tumor and corresponding normal tissue. *Cancer detection and prevention* **1996**, *20* (2), 130-6.

22. Fahrner, J.; Frisch, J.; Nagel, G.; Kraus, A.; Dorsam, B.; Thomas, A. D.; Reissig, S.; Waisman, A.; Kaina, B., DNA repair by MGMT, but not AAG, causes a threshold in alkylation-induced colorectal carcinogenesis. *Carcinogenesis* **2015**, *36* (10), 1235-44.
23. Rotem, A.; Janzer, A.; Izar, B.; Ji, Z.; Doench, J. G.; Garraway, L. A.; Struhl, K., Alternative to the soft-agar assay that permits high-throughput drug and genetic screens for cellular transformation. *Proceedings of the National Academy of Sciences of the United States of America* **2015**, *112* (18), 5708-13.
24. <https://ch.promega.com/-/media/files/resources/protocols/technical-bulletins/0/celltiter-glo-luminescent-cell-viability-assay-protocol.pdf>. *Promega online protocol*.
25. Pegg, A. E.; Byers, T. L., Repair of DNA containing O6-alkylguanine. *FASEB journal : official publication of the Federation of American Societies for Experimental Biology* **1992**, *6* (6), 2302-10.
26. Pegg, A. E., Repair of O(6)-alkylguanine by alkyltransferases. *Mutat Res* **2000**, *462* (2-3), 83-100.
27. Kaina, B.; Christmann, M.; Naumann, S.; Roos, W. P., MGMT: Key node in the battle against genotoxicity, carcinogenicity and apoptosis induced by alkylating agents. *DNA repair* **2007**, *6* (8), 1079-1099.
28. Choi, J. Y.; Chowdhury, G.; Zang, H.; Angel, K. C.; Vu, C. C.; Peterson, L. A.; Guengerich, F. P., Translesion synthesis across O6-alkylguanine DNA adducts by recombinant human DNA polymerases. *The Journal of biological chemistry* **2006**, *281* (50), 38244-56.
29. Kubitschek, H. E.; Sepanski, R. J., Azaserine: survival and mutation in Escherichia coli. *Mutat Res* **1982**, *94* (1), 31-8.
30. Wang, L.; Spratt, T. E.; Liu, X. K.; Hecht, S. S.; Pegg, A. E.; Peterson, L. A., Pyridyloxobutyl adduct O6-[4-oxo-4-(3-pyridyl)butyl]guanine is present in 4-(acetoxymethylnitrosamino)-1-(3-pyridyl)-1-butanone-treated DNA and is a substrate for O6-alkylguanine-DNA alkyltransferase. *Chem Res Toxicol* **1997**, *10* (5), 562-7.
31. Li, L.; Perdigo, J.; Pegg, A. E.; Lao, Y.; Hecht, S. S.; Lindgren, B. R.; Reardon, J. T.; Sancar, A.; Wattenberg, E. V.; Peterson, L. A., The influence of repair pathways on the cytotoxicity and mutagenicity induced by the pyridyloxobutylation pathway of tobacco-specific nitrosamines. *Chem Res Toxicol* **2009**, *22* (8), 1464-72.
32. Loh, Y. H.; Mitrou, P. N.; Bowman, R.; Wood, A.; Jeffery, H.; Luben, R. N.; Lentjes, M. A.; Khaw, K. T.; Rodwell, S. A., MGMT Ile143Val polymorphism, dietary factors and the risk of breast, colorectal and prostate cancer in the European Prospective Investigation into Cancer and Nutrition (EPIC)-Norfolk study. *DNA repair* **2010**, *9* (4), 421-8.
33. Lu, Y.; Cao, M.; Gao, K.; Jiang, J.; Shi, X., The role of O(6)-methylguanine-DNA methyltransferase polymorphisms in colorectal cancer susceptibility: a meta analysis. *International journal of clinical and experimental medicine* **2015**, *8* (1), 791-799.
34. Jackson, P. E.; Hall, C. N.; O'Connor, P. J.; Cooper, D. P.; Margison, G. P.; Povey, A. C., Low O6-alkylguanine DNA-alkyltransferase activity in normal colorectal tissue is associated with colorectal tumours containing a GC→AT transition in the K-ras oncogene. *Carcinogenesis* **1997**, *18* (7), 1299-302.
35. Esteller, M.; Toyota, M.; Sanchez-Cespedes, M.; Capella, G.; Peinado, M. A.; Watkins, D. N.; Issa, J. P.; Sidransky, D.; Baylin, S. B.; Herman, J. G., Inactivation of the DNA repair gene O6-methylguanine-DNA methyltransferase by promoter hypermethylation is associated with G to A mutations in K-ras in colorectal tumorigenesis. *Cancer research* **2000**, *60* (9), 2368-71.
36. Lees, N. P.; Harrison, K. L.; Hall, C. N.; Margison, G. P.; Povey, A. C., Reduced MGMT activity in human colorectal adenomas is associated with K- ras GC→AT transition mutations in a population exposed to methylating agents. *Carcinogenesis* **2004**, *25* (7), 1243-1247.
37. Jančík, S.; Drábek, J.; Radzioch, D.; Hajdúch, M., Clinical Relevance of KRAS in Human Cancers. *Journal of Biomedicine and Biotechnology* **2010**, *2010*, 150960.
38. Loechler, E. L.; Green, C. L.; Essigmann, J. M., In vivo mutagenesis by O6-methylguanine built into a unique site in a viral genome. *Proceedings of the National Academy of Sciences* **1984**, *81* (20), 6271-6275.
39. Pauly, G. T.; Moschel, R. C., Mutagenesis by O6-Methyl-, O6-Ethyl-, and O6-Benzylguanine and O4-Methylthymine in Human Cells: Effects of O6-Alkylguanine-DNA Alkyltransferase and Mismatch Repair. *Chemical Research in Toxicology* **2001**, *14* (7), 894-900.
40. Ráz, M. H.; Dexter, H. R.; Millington, C. L.; van Loon, B.; Williams, D. M.; Sturla, S. J., Bypass of Mutagenic O(6)-Carboxymethylguanine DNA Adducts by Human Y- and B-Family Polymerases. *Chem Res Toxicol* **2016**, *29* (9), 1493-503.
41. Wu, J.; Wang, P.; Li, L.; Williams, N. L.; Ji, D.; Zahurancik, W. J.; You, C.; Wang, J.; Suo, Z.; Wang, Y., Replication studies of carboxymethylated DNA lesions in human cells. *Nucleic Acids Research* **2017**, *45* (12), 7276-7284.
42. Wyatt, M. D.; Pittman, D. L., Methylating agents and DNA repair responses: Methylated bases and sources of strand breaks. *Chemical research in toxicology* **2006**, *19* (12), 1580-1594.

Chapter 5: Immunological and mass spectrometry-based approaches to determine thresholds of the mutagenic DNA adduct *O*⁶-methylguanine in vivo

Reprinted with permission from

Alexander Kraus, Maureen McKeague, Nina Seiwert, Georg Nagel, Susanne M. Geisen, Nathalie Ziegler, Ioannis A. Trantakis, Bernd Kaina, Adam D. Thomas, Shana J. Sturla, Jörg Fahrer, *Archives of Toxicology* (2019) 93:559–572

Copyright © 2019 Springer

The publication is available at Springer Nature via

<https://link.springer.com/article/10.1007%2Fs00204-018-2355-0>

Kraus A., Seiwert N., and Nagel G performed the immunological experiments, cell culture, and animal studies and analyzed the data. McKeague M. and Geisen S.M. performed the mass spectrometry experiments and analyzed data. Ziegler N. and Trantakis I.A. developed the mass spectrometry method. Kaina B., Thomas A.D., Sturla S.J., Fahrer J., conceived of research, and interpreted data. All authors contributed to writing the manuscript.



Immunological and mass spectrometry-based approaches to determine thresholds of the mutagenic DNA adduct *O*⁶-methylguanine in vivo

Alexander Kraus¹ · Maureen McKeague² · Nina Seiwert^{1,3} · Georg Nagel¹ · Susanne M. Geisen² · Nathalie Ziegler² · Ioannis A. Trantakis² · Bernd Kaina¹ · Adam D. Thomas⁴ · Shana J. Sturla² · Jörg Fahrer^{1,3}

Received: 21 July 2018 / Accepted: 8 November 2018 / Published online: 16 November 2018
© Springer-Verlag GmbH Germany, part of Springer Nature 2018

Abstract

N-nitroso compounds are alkylating agents, which are widespread in our diet and the environment. They induce DNA alkylation adducts such as *O*⁶-methylguanine (*O*⁶-MeG), which is repaired by *O*⁶-methylguanine-DNA methyltransferase (MGMT). Persistent *O*⁶-MeG lesions have detrimental biological consequences like mutagenicity and cytotoxicity. Due to its pivotal role in the etiology of cancer and in cytotoxic cancer therapy, it is important to detect and quantify *O*⁶-MeG in biological specimens in a sensitive and accurate manner. Here, we used immunological approaches and established an ultra performance liquid chromatography–tandem mass spectrometry (UPLC–MS/MS) to monitor *O*⁶-MeG adducts. First, colorectal cancer (CRC) cells were treated with the methylating anticancer drug temozolomide (TMZ). Immunofluorescence microscopy and an immuno-slot blot assay, both based on an adduct-specific antibody, allowed for the semi-quantitative, dose-dependent assessment of *O*⁶-MeG in CRC cells. Using the highly sensitive and specific UPLC–MS/MS, TMZ-induced *O*⁶-MeG adducts were quantified in CRC cells and even in peripheral blood mononuclear cells exposed to clinically relevant TMZ doses. Furthermore, all methodologies were used to detect *O*⁶-MeG in wildtype (WT) and MGMT-deficient mice challenged with the carcinogen azoxymethane. UPLC–MS/MS measurements and dose–response modeling revealed a non-linear formation of hepatic and colonic *O*⁶-MeG adducts in WT, whereas linear *O*⁶-MeG formation without a threshold was observed in MGMT-deficient mice. Collectively, the UPLC–MS/MS analysis is highly sensitive and specific for *O*⁶-MeG, thereby allowing for the first time for the determination of a genotoxic threshold upon exposure to *O*⁶-methylating agents. We envision that this method will be instrumental to monitor the efficacy of methylating chemotherapy and to assess dietary exposures.

Keywords *O*⁶-methylguanine · *O*⁶-methylguanine-DNA methyltransferase (MGMT) · Alkylating agents · Ultra performance liquid chromatography–tandem mass spectrometry · Thresholds

Alexander Kraus and Maureen McKeague contributed equally.

Electronic supplementary material The online version of this article (<https://doi.org/10.1007/s00204-018-2355-0>) contains supplementary material, which is available to authorized users.

✉ Jörg Fahrer
Joerg.Fahrer@pharma.med.uni-giessen.de

¹ Department of Toxicology, University Medical Center, 55131 Mainz, Germany

² Department of Health Sciences and Technology, ETH Zurich, 8092 Zurich, Switzerland

³ Rudolf Buchheim Institute of Pharmacology, Justus Liebig University Giessen, 35392 Giessen, Germany

⁴ Centre for Research in Biosciences, University of the West of England, Bristol BS16 1QY, UK

Introduction

Genotoxic *N*-nitroso compounds (NOC) are widespread in our diet and the environment. They are found in processed meat and fish, beer, cosmetics and cigarette smoke (Fahrer and Kaina 2013). Furthermore, NOC are formed endogenously in the stomach and the large intestine by nitrosation of amino acids (Fahrer and Kaina 2013). These harmful compounds cause DNA alkylation and thereby generate a plethora of DNA adducts, such as *N*-methylpurines and *O*⁶-methylguanine (*O*⁶-MeG) (Fu et al. 2012). *O*⁶-MeG is repaired by the suicide enzyme *O*⁶-methylguanine-DNA methyltransferase (MGMT) in a damage reversal reaction by transferring the methyl group from *O*⁶-MeG onto a cysteine residue located in its active site (Daniels et al. 2004). The

S-methylation of MGMT leads to its inactivation and concomitant degradation by the ubiquitin–proteasome pathway (Xu-Welliver and Pegg 2002). Interestingly, a number of compounds modulate the MGMT level and its transferase activity. Antioxidants such as *N*-acetyl cysteine and the polyphenol curcumin were shown to increase MGMT activity (Niture et al. 2007), whereas the disulfide compound and dietary supplement α -lipoic acid (LA) was identified as a natural MGMT inhibitor (Dörsam and Fahrner 2016; Göder et al. 2015). Importantly, persistent O^6 -MeG lesions have detrimental biological consequences including mutagenicity and carcinogenicity (Kaina et al. 2007). Apart from that, O^6 -MeG has also cytotoxic potential due to the downstream generation of DNA double-strand breaks (DSBs) (Mojas et al. 2007; Ochs and Kaina 2000; Quiros et al. 2010).

NOC-related compounds such as dimethylhydrazine and its metabolite azoxymethane (AOM) are frequently used in rodents to initiate colon carcinogenesis through induction of O^6 -MeG and other alkylated DNA bases (Neufert et al. 2007). Alkylating agents also play an important role in cancer chemotherapy due to their induction of cytotoxic DSBs, resulting mainly from subsequent replications over O^6 -MeG. These methylating anticancer drugs include temozolomide (TMZ) and dacarbazine (DTIC), which are both triazine compounds used for the treatment of high-grade glioma and malignant melanoma (Kaina et al. 2010).

Thus, understanding the basis of O^6 -MeG formation and how its repair is regulated are critical in broad biological questions, ranging from fundamental mechanisms of mutagenesis to creating strategies to overcome clinical resistance to cancer therapeutics. However, gaining a functional and quantitative picture of how much O^6 -MeG is in genomic DNA from cells and tissues remains difficult. Immunological assays for detection of O^6 -MeG have been developed that are based upon a monoclonal antibody against the adduct (Seiler et al. 1993). This O^6 -MeG antibody has been used to visualize the DNA lesion in fixed cultured cells and organs, e.g., liver and colon, by immunofluorescence microscopy (Fahrner et al. 2015; Seiler et al. 1993). In addition, the antibody has been successfully employed for immuno-slot blot (ISB) analysis of O^6 -MeG lesions in genomic DNA extracted from cells and tissue (Fahrner et al. 2015; Mikhed et al. 2016; Stephanou et al. 1996), and an ELISA-related assay, in which single-stranded (ss) DNA fragments with O^6 -MeG were captured by the antibody followed by the detection of the ssDNA (Georgiadis et al. 2011). Complementary to immunoassay strategies, DNA adducts have been measured in diverse sample matrices by liquid chromatography combined with tandem mass spectrometry (LC–MS/MS). This approach was successfully used to quantify O^6 -MeG in lung and liver DNA ($\geq 50 \mu\text{g}$) from rats chronically exposed to 10 ppm of the tobacco-specific nitrosamine 4-(methylnitrosamino)-1-(3-pyridyl)-1-butanone (NNK),

which worked with fresh-frozen and formalin-fixed paraffin-embedded tissue (Guo et al. 2016; Upadhyaya et al. 2009). By means of LC–MS/MS, the formation of O^6 -MeG was also monitored in calf thymus DNA and genomic DNA (100 μg) from colorectal cancer cells challenged in vitro with potassium diazoacetate at mM doses (Vanden Bussche et al. 2012).

Here, we performed a head-to-head comparison of these methods and examined the scope of each method for measuring O^6 -MeG adducts in both cells and tissues isolated from animals exposed to the anticancer drug TMZ and the colonotropic carcinogen AOM. Our data illustrated that both immunofluorescence (IF) and immuno-slot blot (ISB) assay permitted the time- and dose-dependent detection of O^6 -MeG in CRC cells in a semi-quantitative manner, but are limited in sensitivity as illustrated in colon tissue exposed to low AOM doses. The UPLC–MS/MS approach was demonstrated to be highly sensitive and specific, allowing for the quantification of O^6 -MeG adducts in CRC cells and peripheral blood mononuclear cells (PBMCs) at clinically relevant TMZ doses. Furthermore, the dose–response curve of AOM-induced O^6 -MeG formation was assessed by mass spectrometry in liver and colon tissue of mice differing in their MGMT repair status. Using hockey stick dose–response modeling, our data revealed, for the first time, a genotoxic threshold for O^6 -MeG formation in vivo, resulting from MGMT repair activity.

Materials and methods

Material

All solutions were made with deionized water (18.2 M Ω , resistivity). O^6 -methyl- d_3 -guanine (O^6 -Me- d_3 -G) was from Toronto Research Chemicals (Toronto, Canada). O^6 -MeG, ammonium hydroxide (ACS Reagent 28–30%), hydrochloric acid (ACS Reagent 37%), and acetic acid (HPLC grade) were purchased from Sigma-Aldrich (Buchs, Switzerland). Guanine was obtained from Acros Organics (New Jersey, USA) and Strata-X polymeric columns (30 μm) were from Phenomenex (Torrance, USA). Methanol (HPLC Gradient Grade) was bought at VWR (Dietikon, Switzerland).

Cell culture

HCT116 colorectal cancer cells were kindly provided by Dr. Bert Vogelstein (John Hopkins University, Baltimore, USA). HCT116 cells were cultured in DMEM (Life Technologies, Darmstadt, Germany) supplemented with 10% FCS and antibiotics (100 U/mL penicillin and 100 $\mu\text{g}/\text{mL}$ streptomycin). PBMCs (peripheral blood mononuclear cells) were isolated from buffy coat by density centrifugation as described previously (Heylmann and Kaina 2016). Buffy coat from human

healthy donors was provided by the blood transfusion center at University Medical Center, Mainz, Germany. Blood samples were layered on Histopaque (Sigma-Aldrich, Deisenhofen, Germany) and centrifuged at 2500 rpm for 35 min at RT without the brake. PBMCs (lymphocytes, monocytes) were collected, transferred to a 50 ml tube and resuspended in wash buffer (2 mM EDTA in PBS with 0.5% bovine serum albumin). Cells were pelleted by centrifugation and washed three times in wash buffer. Finally, cells were resuspended in X-VIVO 15 medium (Lonza, Basel, Switzerland) and transferred into six well plates.

Animal experiments

Mgmt-null (*MGMT*^{-/-}) mice on a C57BL/6 background were described previously (Bugni et al. 2009; Glassner et al. 1999). Eight to 14 weeks old *MGMT*^{-/-} and C57BL/6 wildtype (WT) mice were used. All mouse strains were obtained from the in-house animal breeding facility at University Medical Center, Mainz, Germany. Animal experiments were approved by the government of Rhineland-Palatinate and the Animal Care and Use Committee of the University Medical Center, Mainz, Germany. All animal studies were performed in agreement with the German federal law and the guidelines for the protection of animals. Azoxymethane (AOM; Sigma, Deisenhofen, Germany) solution was prepared as described previously and administered by intraperitoneal injection at doses up to 10 mg/kg body weight (bw) (Fahrer et al. 2015). Animals were then sacrificed after 24 h. Colon and liver tissues were harvested, carefully rinsed with ice-cold PBS and either snap-frozen in liquid nitrogen or fixed in 4% neutral-buffered formaldehyde solution (Roti@-Histofix; Carl Roth, Karlsruhe, Germany). For subsequent histological analysis, fixed tissue was embedded in paraffin and stored at room temperature awaiting immunological analysis as detailed below.

Immunofluorescence detection of *O*⁶-MeG adducts

HCT116 cells (2×10^5 cells per well) were seeded onto cover slips and allowed to adhere overnight. The medium was replaced by fresh medium and the cells were then pre-incubated with the specific *MGMT* inhibitor *O*⁶-benzylguanine (*O*⁶-BG; 10 μ M; Sigma-Aldrich, Deisenhofen, Germany) for 2 h. Temozolomide (TMZ; kind gift of Dr. Geoffrey P. Margison, Manchester, UK) was added (0 to 1000 μ M) and cells were incubated for another 2 h. Following aspiration of the medium, cells were washed with pre-warmed phosphate-buffered saline (PBS) and fixed with ice-cold methanol for 15 min at -20 °C. After two washing steps with PBS, RNA was digested with a mixture of RNase A (200 μ g/ml) and RNase T (50 U/ml) for 10 min at 37 °C. Cells were washed with PBS followed by Proteinase K (20 μ g/ml) digestion for

10 min at 37 °C. Cells then were washed with 0.2% glycine in PBS for 10 min and cover slips were transferred into a humid chamber. Unspecific binding sites were blocked with 5% BSA in PBS for 45 min at RT. Subsequently, the samples were incubated with a primary mouse antibody against *O*⁶-MeG (diluted 1:2000 in 1% BSA in tris-buffered saline-tween 20 (TBS-T); #SQX-SQM003.1, Axxora, Farmingdale, USA) overnight at 4 °C. After several washing steps with TBS-T and PBS, the samples were incubated with an appropriate secondary antibody (Goat-anti-Mouse-Alexa Fluor 488, diluted 1:400 in 1% BSA/PBS, Life Technologies) for 2 h at RT under light exclusion. After several washing steps with TBS-T and PBS, the nuclei were counterstained with TO-PRO-3 (diluted 1:100 in PBS, Life Technologies, Darmstadt, Germany) for 15 min at RT. Finally, the cover slips were coated with Vectashield® (Linaris, Dossenheim, Germany) medium and transferred onto a microscope slide. The samples were analyzed by confocal microscopy with a Zeiss Axio Observer.Z1 microscope equipped with a LSM710 laser-scanning unit (Zeiss, Oberkochen, Germany). Images were acquired with ZEN software and processed with ImageJ (NIH, USA). The mean *O*⁶-MeG intensity per nucleus was assessed with ImageJ (at least ten sections with 100 nuclei/treatment, $n \geq 3$) and data were evaluated using GraphPad Prism 7.0 software.

Isolation of genomic DNA from cells and tissue

HCT116 cells (4×10^6) were seeded into 10 cm dishes and grown overnight. Cells were then incubated in fresh medium and *O*⁶-BG was added as described above. After 2 h, cells were treated with increasing doses of TMZ as indicated and harvested. To extract the genomic DNA, cells were resuspended in 300 μ l Tris-EDTA buffer supplemented with 0.1% Triton X-100 and RNase A (30 μ g/ml). After incubation for 1.5 h at RT, proteinase K (20 μ g/ml) and 1% SDS were added and incubated overnight at 48 °C. In the next step, 700 μ l phenol/chloroform/isoamyl alcohol (Carl Roth, Karlsruhe, Germany) was added. The samples were briefly vortexed and centrifuged for 5 min at 20,000g. The upper aqueous layer was transferred into a new reaction tube and extracted again with 700 μ l phenol/chloroform/isoamyl alcohol. Following centrifugation, the upper aqueous layer was transferred to a new reaction tube and supplemented with 750 μ l 90% ethanol and 1 M NH_4OAc to precipitate the DNA for 1 h at 4 °C. The samples were then centrifuged for 45 min at 20,000g and 4 °C. The supernatant was discarded and the DNA pellets were washed with 1 ml 70% EtOH. Following centrifugation at 20,000g and 4 °C for 15 min, the supernatant was discarded and the remaining DNA pellets were dissolved in 50–100 μ l TE buffer. The samples were gently vortexed and put on ice. Finally, the DNA content

and purity were determined with a NanoDrop 2000 (Thermo Scientific, Dreieich, Germany).

PBMCs (6×10^6 ; approximately 70% T-lymphocytes) in 2.5 ml X-Vivo 15 medium were exposed to increasing doses of TMZ (50 to 1000 μM) for 2 h at 37 °C. PBMCs were then transferred into tubes, washed with PBS and centrifuged for 5 min at 300g. The supernatant was discarded and the pellets were resuspended in PBS. The cell suspension was centrifuged at 600g for 5 min and pellets were processed to isolate genomic DNA as described above.

To isolate genomic DNA from mouse tissue, snap-frozen colon and liver (~20 mg) were homogenized with a pestle and samples were processed as described above.

Immuno-slot blot assay (ISB) of O^6 -MeG adducts

A previously established immuno-slot blot assay (Göder et al. 2015) was used to determine O^6 -MeG adduct levels in genomic DNA extracted from TMZ-treated HCT116 cells or AOM-treated animals. First, 500 ng DNA in TE buffer was denatured by heating for 10 min at 99 °C. 50 μl of 2 M ammonium acetate were then added and samples were vortexed followed by their immediate vacuum aspiration onto a positively charged nylon membrane (GE Healthcare, Munich, Germany). The membrane was fixed for 90 min at 90 °C and incubated for 60 min with blocking buffer (5% dry milk in TBS-T). Subsequently, the membrane was incubated with a primary mouse antibody against O^6 -MeG (diluted 1:500 in 1% BSA in TBS-T) overnight at 4 °C. After several washing steps with TBS-T, the membrane was incubated with a secondary peroxidase-coupled antibody (G- α -M-HRP, diluted 1:2000 in blocking buffer; Santa Cruz Biotechnology, Heidelberg, Germany) for 1 h at RT. After several washing steps with TBS-T, O^6 -MeG adducts were visualized by enhanced chemoluminescence detection using Western Lightning® Plus-ECL (Perkin Elmer, Rodgau, Germany). Densitometric evaluation of blots was conducted by Adobe Photoshop CS5 and analyzed by GraphPad Prism 7.0 software.

Immunohistochemistry (IHC)

Formalin-fixed, paraffin-embedded (FFPE) colon and liver tissues from AOM-treated mice were sectioned at 5 μm and processed for immunohistochemistry as reported (Fahrer et al. 2015). Tissue sections were incubated at 60 °C for 30 min in a drying oven, then deparaffinized in xylene and rinsed in graded ethanol solutions. Following several washing steps, the sections were immersed in pre-heated antigen retrieval solution (DAKO, Hamburg, Germany) for 30 min in a steamer. The samples were allowed to cool for 15 min at RT and washed several times in PBS. This process was followed by a permeabilization step in 0.4% Triton X-100 in

PBS for 5 min at RT. Sections were then rinsed in PBS and RNA digestion was performed for 1 h at 37 °C using both RNase A (200 $\mu\text{g}/\text{ml}$) and RNase T (50 U/ml).

After alkaline unwinding of the DNA for 5 min, the sections were carefully washed in PBS and incubated with pepsin (60 $\mu\text{g}/\text{ml}$) 30 min at 37 °C. Thereafter, the sections were washed with PBS and incubated with proteinase K (20 $\mu\text{g}/\text{ml}$) for 30 min at 37 °C. Following another washing step with 0.2% glycine-PBS, the sections were incubated for 2 h with blocking solution (DAKO, Hamburg, Germany) at RT. The sections were then treated with an O^6 -MeG antibody (1:100, diluted in 2% BSA in PBS) overnight at 4 °C. After several washing steps in PBS-0.1% Tween, the samples were incubated with the appropriate secondary antibody (G- α -M-Alexa 488, 1:500 diluted in 2% BSA in PBS/0.2% Triton X-100; Life Technologies, Darmstadt, Germany) for 2 h at RT. The sections were then rinsed thoroughly with PBS-0.1% Tween and a nuclear staining was performed using TO-PRO-3 (1:100 in PBS) for 30 min at RT. Slides were mounted with Vectashield® medium and analyzed by confocal microscopy with a Zeiss Axio Observer.Z1 microscope equipped with a LSM710 laser-scanning unit (Zeiss, Oberkochen, Germany). Images were processed with ImageJ version 1.45 (NIH, USA).

LC-MS/MS analysis of O^6 -MeG adducts

DNA hydrolysis

All DNA samples were measured on a Nanodrop 1000 (PecLab, Rodgau, Germany). The total number of nucleotides present was calculated based on the average base pair molecular weight of 650 g/mol. The number of guanine residues was calculated assuming 21% guanine in the mouse genome, and 20.5% in the human genome (Ruvinsky and Graves 2005). A minimum of 10 μg of DNA was transferred to new Eppendorf DNA LoBind microcentrifuge tubes and concentrated to dryness by vacuum centrifugation. Samples were resuspended and thoroughly vortexed in 500 μL of a 0.1 M HCl solution spiked with 2 nM of the internal standard (IS), O^6 -Me- d_3 -G. To release the purines from the DNA, each sample was heated for 2 h at 70 °C. Samples were cooled at RT for at least 10 min followed by a 20 s centrifugation pulse at 1000g. Each sample was neutralized with 15 μL of 15% aqueous ammonium hydroxide (NH_4OH) and vortexed.

Confirmation of DNA hydrolysis

30 μL from each DNA sample was removed for HPLC analysis to verify complete release of guanine. Quantification of guanine was carried out on an Agilent Technologies 1200 Series HPLC (Santa Clara, CA) with a UV-visible detector.

The method was adapted from Roy et al. (2013). To monitor absorbance, the diode array detector was set to 270 nm and the reference was set to 360 nm.

Chromatography was performed with a Luna C18 Column (5 µm, 100 Å, 4.6 × 250 mm) from Phenomenex (Torrance, CA). Mobile phase A was water and mobile phase B was methanol. The flow rate was 1 mL/min and the column temperature was not controlled. 8 µL of sample was injected and separated as follows: 1% B for 3 min, 1–10% B linear gradient for 7 min, a wash at 85% B for 3 min, and re-equilibration at 1% B for 7 min (20 min total run time). Guanine eluted at a retention time of 8.7 min. Samples were analyzed in duplicate.

A calibration curve for guanine (2–100 µM) was prepared in a 0.1 M HCl, 0.03% NH₄OH solution. The amount of guanine in each sample was calculated on the basis of guanine peak area, slope of the calibration curve, and fraction of the total volume injected. The percent recovery of guanine was calculated using the guanine measured by HPLC compared to the theoretical amount calculated from the Nanodrop measurement. All samples yielded between 80–120% recovery of released guanine.

Adduct enrichment

Solid phase extraction (SPE) columns (Strata-X 33 µm, 30 mg/1 mL) were preconditioned with two 1 mL washes with methanol, followed by three separate washes of 1 mL water each. The entire remaining sample (485 µL) was loaded onto a column for enrichment and purification. Each column was then washed with 600 µL water, then 600 µL of 3% methanol. Elution was performed by adding 600 µL of 60% methanol. The entire eluent was recovered and vacuum centrifuged to dryness in 250 µL conical glass HPLC inserts. Samples were stored at –20 °C. Immediately prior to LC–MS/MS analysis, samples were thawed, reconstituted in 20 µL water, and sonicated for 10 min.

LC–ESI–MS/MS

Samples were analyzed by LC–MS/MS using a nanoAcquity UPLC system (Waters, Milford, CA) and Agilent tandem quadrupole mass spectrometer (LCQ Vantage, Thermo Scientific, Waltham, MA) with an electrospray ionization source (ESI). Mass spectrometry ionization parameters were optimized by tuning the instrument with 1 µM *O*⁶-MeG, *O*⁶-d3-MeG, and G by direct injection. The ESI source was set in positive ion mode with the following parameters: capillary temperature, 270 °C; spray voltage, 3000 V; sheath gas pressure, 25; ion sweep gas pressure, 0; aux gas pressure, 5; Q2 CID gas pressure, 1.5 mTorr; collision gas, argon; scan width, m/z 0.01; scan time, 0.1 s. Optimal collision energies for each transition are in Table 1.

Table 1 SRM transitions for *O*⁶-MeG and *O*⁶-d3-MeG identification and quantification

	Quantification		Qualification	
	SRM transition	Collision energy (V)	SRM transition	Collision energy (V)
Guanine	152.1 → 135.1	26	152.1 → 110.1	26
<i>O</i> ⁶ -MeG	166.1 → 149.0	16	166.1 → 67.1	30
<i>O</i> ⁶ -d3-MeG	169.1 → 152.0	16	169.1 → 107.0	26

Chromatography was performed with a Synergi 4 µm Polar-RP column (Phenomenex 80 Å 150 × 0.5 mm). Mobile phases were sonicated for 15 min prior to the run. Mobile phase A was water with 0.05% acetic acid, phase B was methanol, and the flow rate was 10 µL/min at the column temperature was set to 40 °C. The autosampler was cooled to 4 °C, a seal wash was performed every 30 min, and the injection volume was 1 µL. Samples were separated as follows: 0% B for 1 min, 1–40% B gradient for 14 min, 99% B for 5 min, and re-equilibrate for 15 min. The eluent was directed to the MS between 2 min and 14 min, otherwise the eluent was diverted to the waste. *O*⁶-MeG and *O*⁶-d3-MeG eluted at 9.8 min. The single reaction monitoring (SRM) transitions that were monitored are listed in Table 1. Xcalibur software (Thermo) was used for data acquisition and processing.

Calibration curves

A series of eight different *O*⁶-MeG standards of known concentration (0.5, 1, 2.5, 5, 10, 25, 40, 50 nM) was prepared. A fresh 20 µL aliquot of each prepared standard was concentrated to dryness by vacuum centrifugation and resuspended in 500 µL of a 0.1 M HCl solution spiked with 2 nM of the IS as above. Thermal acid hydrolysis and SPE were performed in the same way as the DNA samples. Standards were reconstituted with 20 µL water for LC–MS/MS analysis. Each calibrated standard was measured in triplicate. Standards were prepared and analyzed immediately prior to analysis. The peak area ratio was determined for each standard by dividing the peak area of the standard by the peak area of the IS. Data were fitted to a straight line by least squares (ordinary) in GraphPad Prism 7.0.

Adduct quantification

Each sample was first injected once into the MS to ensure they were within the linear range. For samples that were higher than the standard curve, a 1:10 dilution was performed in water. For samples where the *O*⁶-MeG was lower than the standard curve, the injection volume was increased to 4 µL or was analyzed using a nanoAcquity UPLC M-class

system (Waters, Milford, CA) and tandem quadrupole mass spectrometer (TSQ Quantiva, Thermo Scientific, Waltham, MA) with an electrospray ionization source (ESI) using the same ionization parameters and chromatography. Relative standard deviation of the technical triplicates was less than 20%. The peak area ratio was determined for each sample by dividing the peak area for *O*⁶-MeG by the peak area for *O*⁶-d3-MeG. The amount of *O*⁶-MeG in each sample was calculated on the basis of the peak area ratio, the slope of the calibration curve, and the fraction of the total volume injected. Adduct levels are reported as adducts per 10⁷ total nucleotides.

Statistics

Experiments were performed independently three times, unless otherwise stated. Figures show representative images. Values are depicted as mean ± standard errors of the mean (SEM) using GraphPad Prism 7.0 Software. Statistical analysis was performed using two-sided Student's *t* test and statistical significance was defined as *p* < 0.05.

Hockey stick dose–response modelling

Dose–response modeling was performed as described (Lutz and Lutz 2009) using R software (version 3.3.1) (R Development Core Team 2013). The lower confidence interval of the threshold dose is also reported. It should be noted that confidence intervals of < 0 lacks statistical significance for a threshold.

Results

In this study, levels of *O*⁶-MeG resulting from exposure to either the anticancer drug TMZ or the colonotropic carcinogen AOM were evaluated in CRC cells and different murine tissues (i.e., liver and colon) by a combination of qualitative immunological assays and quantitative mass spectrometry (Fig. 1a). AOM requires metabolic activation by the hepatic enzyme CYP2E1 to generate a reactive methylating agent (Neufert et al. 2007). TMZ, on the other hand, spontaneously decomposes at neutral pH to deliver a methyl group (Zhang et al. 2012). Both chemicals give rise to DNA reactive

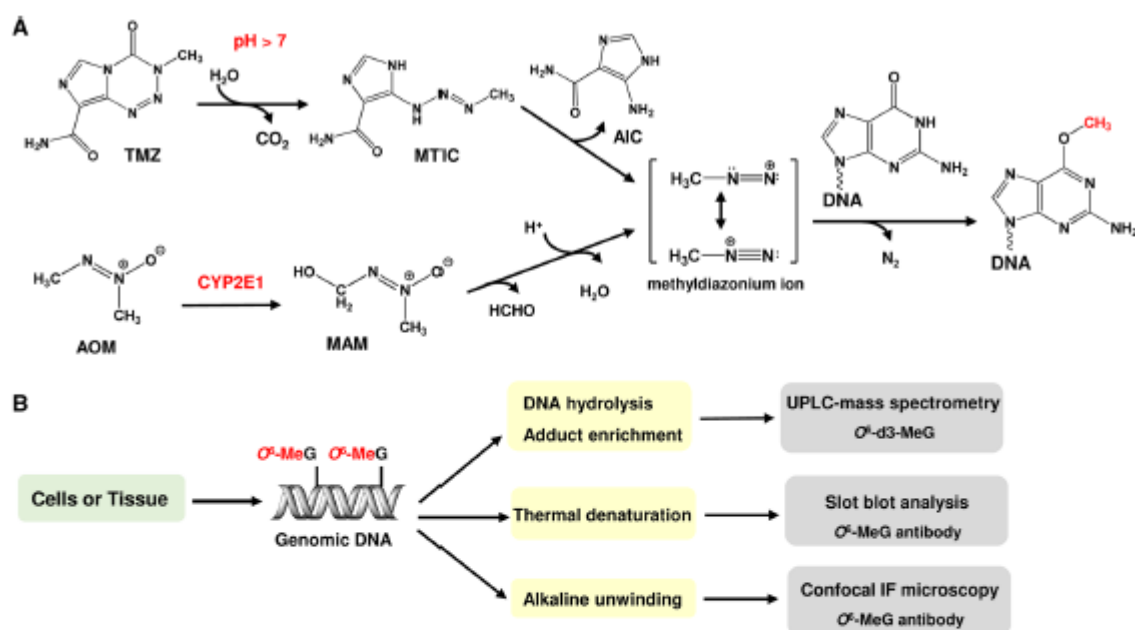


Fig. 1 Formation of *O*⁶-MeG DNA adducts and their analysis by qualitative and quantitative methods. **a** Formation of *O*⁶-MeG DNA adducts by alkylating agents. The anticancer drug temozolomide (TMZ) decomposes spontaneously to methyl-(triazen-1-yl) imidazole-4-carboxamide (MTIC) in aqueous solutions at pH > 7 (top panel). This instable intermediate gives rise to 5-aminoimidazole-4-carboxamide (AIC) and diazomethane, which then reacts with nucleophilic centers in DNA, thereby forming *O*⁶-MeG DNA adducts. The colo-

notropic carcinogen azoxymethane (AOM), which is chemically related with *N*-nitroso compounds, requires metabolic activation by hepatic CYP2E1 to methylazoxymethanol (MAM). Subsequently, this compound undergoes decomposition to diazomethane as DNA methylating agent (bottom panel). MAM is also biliary excreted as glucuronic acid conjugate and thereby reaches the colorectum, where it also generates diazomethane (not shown). **b** Analysis of *O*⁶-MeG in cells and tissues. Please refer to the main text for further explanations

methylidiazonium ions that induce the minor lesion *O*⁶-MeG among other DNA methylation adducts. The workflow of sample processing and subsequent analysis is depicted in Fig. 1b.

Time-dependent formation of *O*⁶-MeG in cells challenged with TMZ

First, we investigated the induction and persistence of *O*⁶-MeG in a time-dependent manner over 24 h. To this end, HCT116 CRC cells were pre-incubated with *O*⁶-BG for 2 h to inactivate MGMT and then challenged with TMZ for up to 24 h. Confocal IF microscopy showed a time-dependent formation of *O*⁶-MeG with a peak after 4 h, which persisted up to 14 h after exposure to TMZ (Fig. 2a, b). After 24 h, the *O*⁶-MeG level declined, presumably because of resynthesis of MGMT or lesion dilution resulting from cell division. To quantify the adducts, we used

stable isotope dilution mass spectrometry. The results showed a similar time course of *O*⁶-MeG accumulation as compared to the IF analysis (Fig. 2c). 4 h after treatment with 500 μM TMZ, the basal *O*⁶-MeG level (~2 lesions per 10⁷ nucleotides) increased to 116 *O*⁶-MeG adducts per 10⁷ nucleotides. After 24 h, the *O*⁶-MeG content decreased to 58 adducts per 10⁷ nucleotides, which is still considerably higher than in untreated control cells. Representative chromatograms for *O*⁶-MeG measurements in TMZ-treated HCT116 cells are also shown (SI, Fig. 1). To illustrate the intrinsic MGMT repair capacity in HCT116 cells, cells were incubated in the absence or presence of the MGMT inhibitor *O*⁶-BG and challenged with 500 μM TMZ (Fig. 2d). Mass spectrometry revealed a slightly higher, yet not statistically significant *O*⁶-MeG level following TMZ treatment in cells pre-treated with the MGMT inhibitor (74 versus 56 adducts per 10⁷ nucleotides), indicating the protection mediated by MGMT against TMZ-induced *O*⁶-MeG in HCT116 cells.

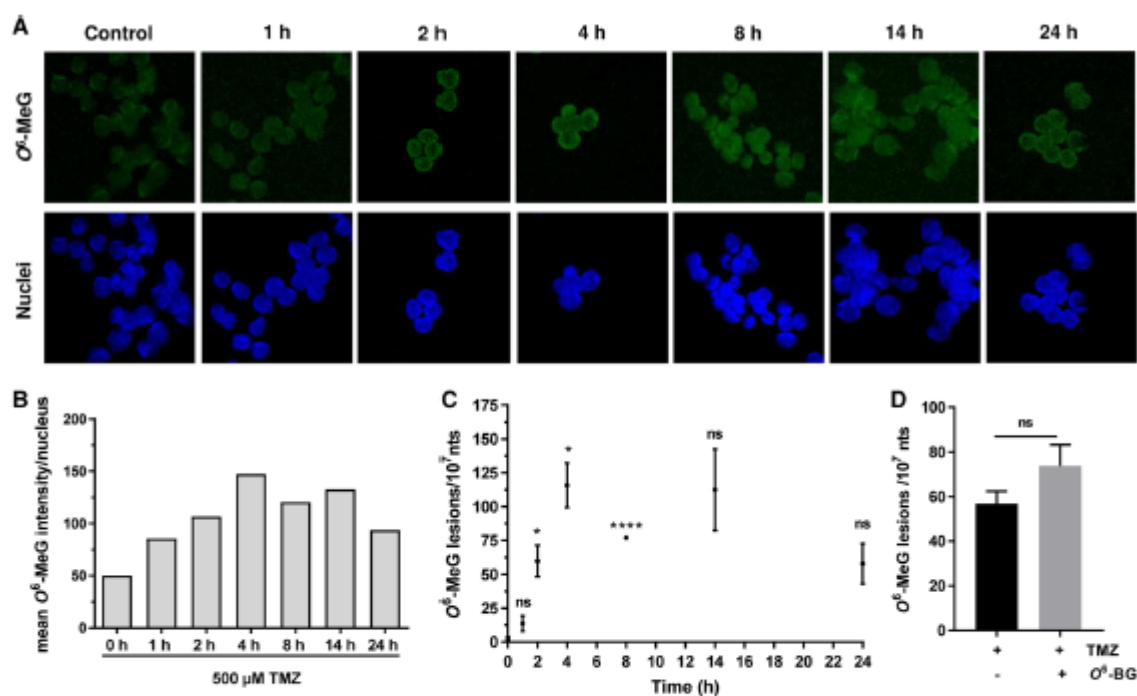


Fig. 2 Analysis of *O*⁶-MeG induction and persistence in CRC cells using immunofluorescence and mass spectrometry. **a** HCT116 cells were pre-treated with the MGMT inhibitor *O*⁶-Benzylguanine (*O*⁶-BG) for 2 h and then exposed to the anticancer drug TMZ (500 μM) and incubated for up to 24 h. Representative images are shown. *O*⁶-MeG (green) and nuclei (blue). **b** Determination of the mean staining intensity by ImageJ. **c** Mass spectrometry-based detection of *O*⁶-MeG in HCT116 cells treated as described in **a**. Genomic DNA

was isolated and *O*⁶-MeG levels were determined with mass spectrometry using an isotope-labeled internal standard. Data are depicted as mean ± SEM (*n* = 3). ****, *p* < 0.0001; *, *p* < 0.05; *ns* not significant. **d** Induction of *O*⁶-MeG adducts by 500 μM TMZ with or without pre-treatment with the MGMT inhibitor *O*⁶-BG. Number of *O*⁶-MeG lesions were assessed by mass spectrometry. Data are shown as mean ± SEM (*n* = 3). *ns* not significant. (Color figure online)

Dose-dependent induction of O^6 -MeG in cells challenged with TMZ

To monitor the dose-dependent formation of O^6 -MeG adducts, HCT116 cells were pre-incubated with the pharmacological inhibitor O^6 -BG to block MGMT activity. The cells were then exposed to increasing doses of TMZ (0–1000 μ M) for 2 h, fixed and processed. O^6 -MeG was specifically labeled with an antibody followed by confocal microscopy (Fig. 3). As expected, O^6 -MeG displayed exclusive nuclear localization. TMZ, at 100 μ M, caused a moderate, significant rise in the O^6 -MeG level relative to the untreated control (Fig. 3a–c). At higher dose levels, O^6 -MeG levels increased dose dependently (Fig. 3a–c). Subsequently, we compared the sensitivity of the ISB assay with mass spectrometry-based analysis of O^6 -MeG

adducts in genomic DNA from TMZ-treated HCT116 cells. By means of the ISB assay, we were able to detect a dose-dependent O^6 -MeG DNA adduct formation, reaching statistical significance only at doses \geq 500 μ M TMZ (Fig. 4a, b). Doses up to 250 μ M were hardly distinguishable from the background level (Fig. 4b). In contrast, UPLC–MS/MS revealed a significant rise in O^6 -MeG at a lower dose of 100 μ M TMZ with 13 adducts per 10^7 nucleotides, while the baseline level without TMZ treatment was low (2.5 adducts per 10^7 nucleotides) (Fig. 4c). This clearly demonstrates the higher sensitivity and specificity of the mass spectrometry-based approach. It is interesting to note that we were also able to measure O^6 -MeG in PBMC following in vitro treatment with 100 μ M TMZ (SI Table 1). This experiment was conducted without the MGMT inhibitor O^6 -BG, i.e., in the presence of intrinsic MGMT repair activity.

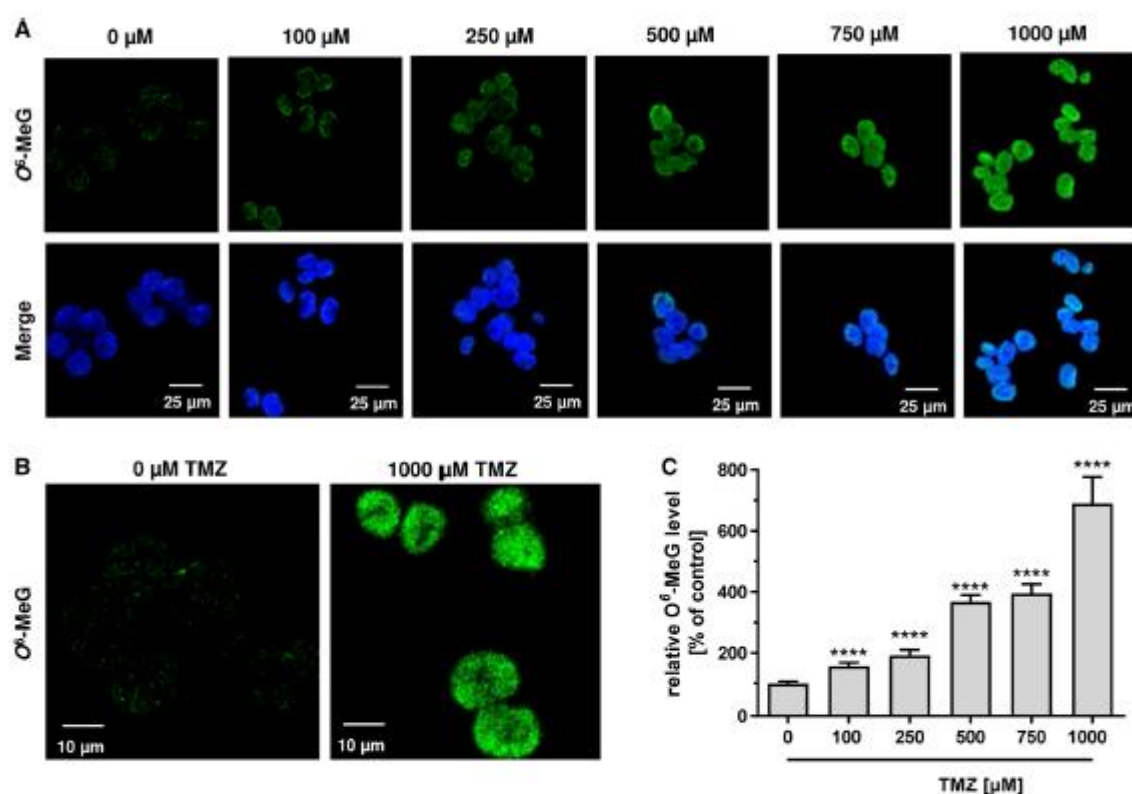


Fig. 3 Detection of O^6 -MeG adducts in CRC cells by immunofluorescence. **a** HCT116 cells were pre-incubated for 2 h with O^6 -benzylguanine to block cellular MGMT repair activity. Cells were then treated with increasing doses of the S_N1 -alkylating anticancer drug temozolomide (TMZ; 0–1000 μ M) for 2 h to allow for damage induction. Representative images acquired by confocal microscopy are

shown. O^6 -MeG (green) and nuclei (blue). **b** Magnification showing pan-nuclear localization of O^6 -MeG adducts. **c** Quantitative evaluation of dose-response samples. Data are presented as mean + SEM ($n=3$, ≥ 10 sections per sample). ****, $p<0.0001$. (Color figure online)

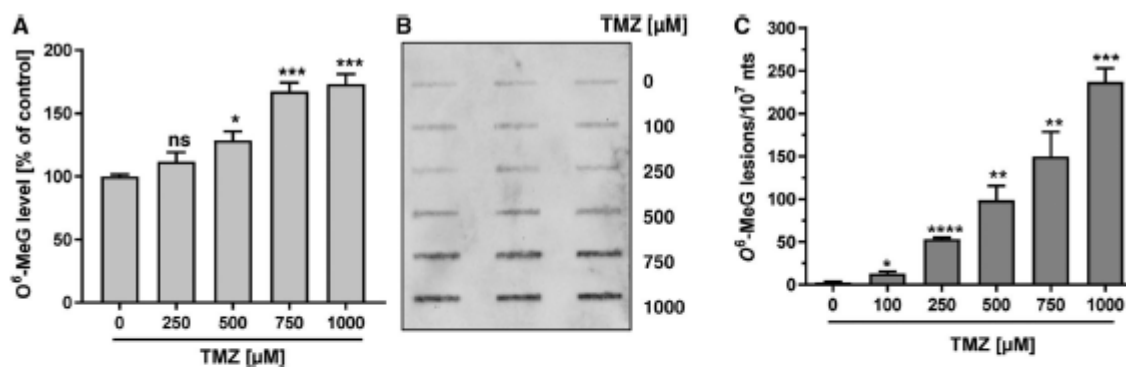


Fig. 4 Analysis of dose-dependent *O*⁶-MeG adduct formation in CRC cells by immune slot blot detection versus mass spectrometry. **a** HCT 116 cells were pre-incubated with the MGMT inhibitor *O*⁶-benzylguanine (*O*⁶-BG) for 2 h and then challenged with increasing doses of the anticancer drug TMZ (0–1000 µM) for additional 2 h. *O*⁶-MeG adducts were determined in isolated genomic DNA by an immune

slot blot approach. Data are depicted as mean ± SEM (*n* = 3). ***, *p* < 0.001; *, *p* < 0.05; ns not significant. **b** Representative immunoslot blot **c** Cells were treated as described in **a** and genomic DNA was isolated. The number of *O*⁶-MeG lesions per 10⁷ nucleotides (nts) was obtained by mass spectrometry. Data are given as mean ± SEM (*n* = 3). ****, *p* < 0.0001; ***, *p* < 0.001; **, *p* < 0.005; *, *p* < 0.05

Assessment of *O*⁶-MeG in tissue of AOM-treated mice and impact of MGMT

Having extensively characterized the dose- and time-dependent formation of *O*⁶-MeG in CRC cells, we switched to a mouse model using B6/J wildtype (WT) and transgenic, MGMT-deficient mice (MGMT^{-/-}). The animals were exposed to AOM, which is a well-established colonotropic carcinogen. AOM requires metabolic activation in the liver and the colorectum, involving an interplay of hepatic cytochrome P450 2E1 (CYP2E1)- and UDP-glucuronosyl-transferase (UGT)-dependent metabolism together with β-glucuronidase activity from gut bacteria (Neufert et al. 2007). AOM was administered by intraperitoneal injection in doses ranging from 0 to 10 mg/kg bw and animals were sacrificed after 24 h to isolate genomic DNA from liver and colorectal tissue. *O*⁶-MeG levels were already assessed in our previous work using the ISB technique (Fahrer et al. 2015). Both genotypes displayed a dose-dependent formation of hepatic *O*⁶-MeG adducts, with significant higher levels in MGMT knockout mice that lack methyl transferase activity towards *O*⁶-MeG (Fahrer et al. 2015). In colorectal tissue, no differences in *O*⁶-MeG levels were detected in WT mice challenged with up to 10 mg/kg AOM, while a dose-dependent increase was observed in MGMT-deficient mice using the ISB assay (SI Fig. 2a, b). Next, the liver samples were analyzed by mass spectrometry, resulting in dose-dependent generation of *O*⁶-MeG as a function of the repair phenotype (Fig. 5a, c). It should be stressed that *O*⁶-MeG levels were about twofold higher in MGMT^{-/-} as compared to WT animals at doses of 3 and 5 mg AOM/kg bw (SI Fig. 3a), reaching

statistical significance only for 5 mg. Finally, we studied *O*⁶-MeG formation in colorectal tissue, which is pivotal for DNA alkylation-triggered colorectal carcinogenesis. Intriguingly, UPLC–MS/MS revealed *O*⁶-MeG induction (6 adducts per 10⁷ nucleotides) at the lowest tested AOM dose (3 mg AOM/kg bw) in WT animals, which was tremendously augmented (60 adducts per 10⁷ nucleotides) at the highest AOM dose (10 mg/kg bw) (Fig. 5e). In stark contrast, MGMT^{-/-} animals displayed a dose-dependent and almost linear formation of *O*⁶-MeG adducts (16, 35, 81 adducts per 10⁷ nucleotides, respectively) (Fig. 5g). Side-by-side comparison of the induced *O*⁶-MeG lesions in colorectal tissue showed significantly higher levels in MGMT^{-/-} versus WT animals at AOM doses ≤ 5 mg/kg bw (SI Fig. 3b).

Dose–response modeling of *O*⁶-MeG adducts and threshold analysis

We performed hockey stick dose–response modeling (Lutz and Lutz 2009) on the in vivo data following ISB and MS quantification of *O*⁶-MeG adducts to identify a potential threshold dose and assess the dose–response relationship (Fig. 5b, d, f, h). We only identified a threshold dose using UPLC–MS/MS quantification, but not via ISB (SI Fig. 4). Interestingly, the threshold dose of 1.9 mg/kg bw and 4.8 mg/kg bw AOM in the respective liver and colon of WT mice was absent in the MGMT-deficient genotype (Table 2), indicating a change in dose–response relationship from sub-linear to linear when MGMT-mediated repair of *O*⁶-MeG is lacking.

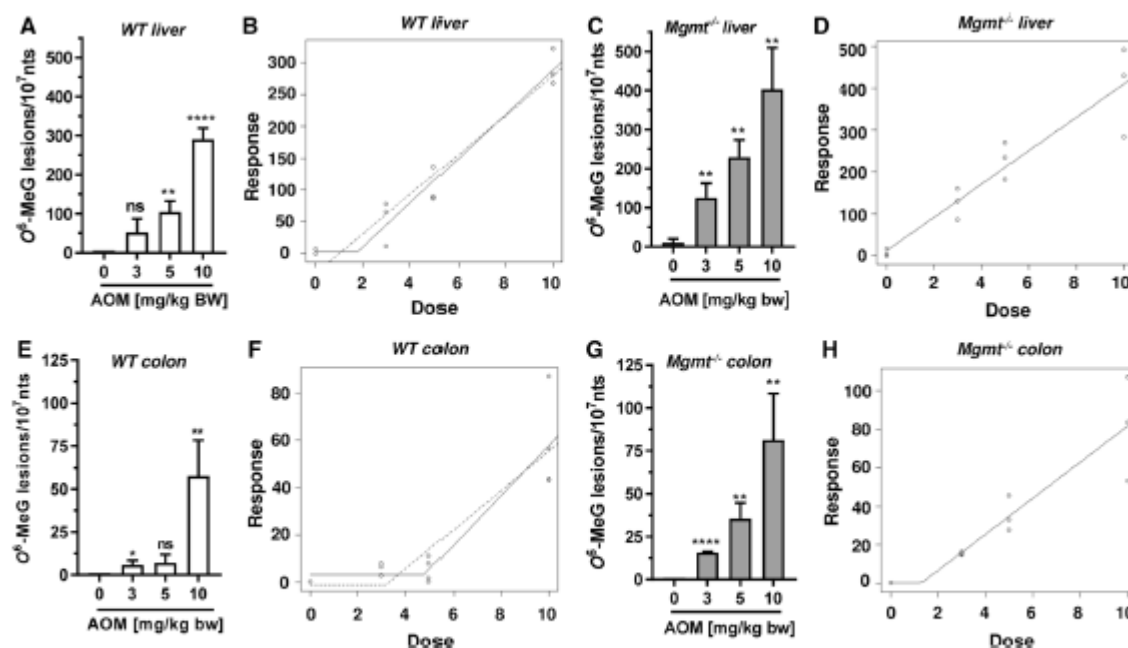


Fig. 5 Analysis of the dose-dependent O^6 -MeG formation in liver and colorectal tissue of MGMT-proficient and -deficient mice. Mass spectrometry-based determination of hepatic (a, c) and colonic (e, g) O^6 -MeG lesions in isolated genomic DNA of WT and MGMT $^{-/-}$ mice. Data with 10 mg AOM/kg bw has been reported previously by our group (Dörsam et al. 2018). Data is shown as mean + SEM ($n=3$ per dose and genotype). ****, $p<0.0001$; ***, $p<0.001$; **, $p<0.005$;

*, $p<0.05$; ns not significant (as compared to the respective control treated with 0 mg AOM/kg bw). Dose–response modeling to elucidate the threshold dose for O^6 -MeG formation in liver (b, d) and colorectal (f, h) tissue of WT and MGMT $^{-/-}$ mice. Solid line shows the best fit of the model. The broken line shows the 90% lower confidence interval of the threshold dose for those dose–responses where linearity can be rejected

Discussion

The present work provides a characterisation of currently available techniques to detect and quantify O^6 -MeG adducts in cells and murine tissues, with a focus on their sensitivity and specificity. Furthermore, the approaches were applied to determine genotoxic thresholds using the hockey stick

dose–response modeling. First, we showed that IF microscopy allows for the time- and dose-dependent detection of O^6 -MeG in cells treated with the methylating antineoplastic drug TMZ. The procedure itself is relatively fast and not expensive, but includes critical steps such as the unwinding of DNA at alkaline pH, during which the cells can detach. Furthermore, the O^6 -MeG antibody caused some background signal, which is particularly prominent in tissue samples (SI Fig. 5). The digestion of proteins and RNA are further essential steps to yield specific, nuclear staining of O^6 -MeG. This method has been employed to detect O^6 -MeG in cells and in tissue, particularly liver and colon tissues (Fahrer et al. 2015; Nyskohus et al. 2013), as it offers the advantage to visualize damage induction in distinct cell types and regions within a given tissue. Using confocal microscopy, we could demonstrate the spatial formation of O^6 -MeG adducts in liver lobuli, with the highest damage induction in hepatocytes around the central hepatic vein, while no adducts were formed in the periportal field [SI Fig. 5 and (Fahrer et al. 2015)]. Interestingly, O^6 -MeG staining can also be combined with the detection of γ H2AX, an established marker for DNA DSBs (Fahrer et al. 2014;

Table 2 Threshold dose analysis of in vivo samples

Sample	Assay	Threshold dose (mg/kg bw)	Lower CI (mg/kg bw)
WT liver	ISB	–	–
MGMT $^{-/-}$ liver	ISB	–	–
WT liver	UPLC–MS/MS	1.93	0.78
MGMT $^{-/-}$ liver	UPLC–MS/MS	–	–
WT colon	UPLC–MS/MS	4.78	3.20
MGMT $^{-/-}$ colon	UPLC–MS/MS	1.32	0.00

CI Confidence intervals

Kinner et al. 2008), in paraffin-embedded liver tissue (Fahrer et al. 2015). The IF-based method proved also to be useful for monitoring the time-dependent induction and removal of *O*⁶-MeG adducts in colon crypts of rats treated with up to 15 mg AOM/kg bw (Nyskohus et al. 2013). However, IF is a semi-quantitative method and offers moderate sensitivity as compared to mass spectrometry, which was revealed mainly during the analysis of tissue samples. For example, our UPLC–MS/MS approach detected *O*⁶-MeG in liver tissue of WT mice at low AOM doses (Fig. 5), whereas IF microscopy did not (Fahrer et al. 2015).

Second, we employed the ISB assay to detect *O*⁶-MeG adducts in genomic DNA isolated from cells and tissues exposed to methylating agents. The ISB assay allows for the direct comparison of multiple samples (up to 48) on the same membrane, requiring only a little amount of DNA (≤ 500 ng). Furthermore, it is a very fast and inexpensive method. We showed a dose-dependent *O*⁶-MeG generation in cells challenged with TMZ, however with only moderate sensitivity. Nevertheless, *O*⁶-MeG adducts were monitored in liver DNA from WT and MGMT-deficient mice exposed to low dose levels of AOM (3 mg/kg bw). It also should be mentioned that the effect of the different DNA repair phenotype, i.e., MGMT proficiency and MGMT deficiency, was clearly visible here. In support of its rather moderate sensitivity, no AOM-dependent formation of *O*⁶-MeG was detectable in DNA isolated from colorectal tissue of WT animals using the ISB assay (SI Fig. 2). The method has also been applied to measure *O*⁶-MeG and *O*⁶-ethylguanine in human lymphocytes exposed to methylnitrosurea (MNU) and ethylnitrosurea (ENU), respectively, at the mM dose range (0.5–4 mM) *in vitro* (Jiao et al. 2007; Stephanou et al. 1996), confirming the limited sensitivity of ISB. This drawback is also attributable to the background signal, which is observed in untreated control samples.

Third, we applied UPLC–MS/MS to quantify *O*⁶-MeG adduct levels in human cells and murine tissue samples (liver and colon). This approach was highly sensitive and superior to the other antibody-based methods (IF and ISB) throughout our experiments. While former studies using HPLC–MS/MS required moderate to high amounts of DNA (50 μ g up to 1 mg) (Upadhyaya et al. 2009; Vanden Bussche et al. 2012; Zhang et al. 2006), we have optimized the sample cleanup and subsequent analysis, reducing the amount of DNA needed to below 10 μ g. Our UPLC–MS/MS approach is highly sensitive and permitted the detection of *O*⁶-MeG in colorectal tissue of WT mice challenged with only 3 mg/kg bw AOM. This method was also instrumental for our very recent study dealing with the impact of the DNA repair protein PARP-1 on alkylation-induced colorectal carcinogenesis (Dörsam et al. 2018).

Mass spectrometry revealed moderate differences in *O*⁶-MeG levels following TMZ treatment in the presence

or absence of the MGMT inhibitor *O*⁶-BG, which were however not statistically significant. This finding could be attributable to several factors. First, HCT116 cells display only moderate MGMT activity (Göder et al. 2015), whereas other CRC cells such as HT29 have a fourfold higher MGMT activity (Tomaszowski et al. 2015). Less *O*⁶-BG is thus required to inhibit the cellular MGMT pool in HCT116 cells, attenuating the effects particularly at a high TMZ dose of 500 μ M. Second, it is conceivable that the catalytic Cys residue of MGMT is directly alkylated by TMZ, which could also overshadow the *O*⁶-BG-mediated inhibition. In support of this notion, a previous study indicated that the S_N2 alkylating agent methyl iodide and, at higher doses, the S_N1 alkylating agent MNU directly alkylate MGMT in cell extracts (Oh et al. 1996). Third, the TMZ exposure time used for this experiment (2 h) might be not ideal, bearing in mind that *O*⁶-MeG induction by TMZ peaks after 4 h (Fig. 2c).

Intriguingly, our measurements revealed a linear, dose-dependent accumulation of adducts in MGMT-deficient mice, whereas adduct levels exhibited non-linearity in WT animals, and the threshold analysis supports this result (Table 2). We found threshold doses of AOM in the liver and colon of treated mice at 1.93 mg/kg bw and 4.78 mg/kg bw, respectively. The liver has higher basal levels of the AOM activating enzyme, CYP2E1, than in the colon (Rosenberg and Mankowski 1994). We could therefore hypothesize that more AOM is activated in the liver and able to react with DNA, accounting for the lower threshold dose than in the colon. Caution is urged however, as the dose–responses look sub-linear (due to vastly higher adduct levels at the highest dose) as opposed to threshold, particularly in the colon (Fig. 5). However, the difference in threshold dose between the repair phenotypes is intriguing and supports a mechanistic basis for the observed threshold doses (Fahrer et al. 2015; Thomas et al. 2013).

Moreover, it is hypothesized that detoxifying processes can prevent genotoxin activation, subsequent DNA reaction and adduct formation and, therefore, contribute to a non-linear DNA adduct relationship (Thomas et al. 2015). The half-life of the DNA adducts (governed by their removal by repair enzymes, such as MGMT) may influence the relationship observed depending on the time following treatment when the adducts were quantified. The influence of DNA repair is evidenced in the absence of threshold doses in the MGMT-deficient phenotype. While this data is limited and firm conclusions on the dose–responses are difficult to draw, it is interesting to speculate particularly, as in this instance, the relationships correlate to our mechanistic understanding of DNA damage induction and repair. This is consistent with our previous study dealing with the impact of DNA repair on the dose–response relationship in alkylation-induced colorectal carcinogenesis (Fahrer et al. 2015) and illustrates that

Table 3 Features of the different analytical techniques used for O^6 -MeG detection

	Immunofluorescence	Immuno-slot blot	UPLC–mass spectrometry
Required sample	≤ 50,000 cells	250–500 ng DNA	≥ 5 µg DNA
Sensitivity	Moderate	Moderate	High
Specificity	Moderate	Moderate	High
Throughput	Moderate	High	Low

initial DNA adduct levels may be correlated with later onset of tumorigenesis.

Using this mass spectrometry-based approach, O^6 -MeG formation was also quantitatively assessed in PBMCs isolated from healthy human volunteers following in vitro treatment with the anticancer drug TMZ. This experiment was conducted without the MGMT inhibitor O^6 -BG, i.e., in the presence of intrinsic MGMT activity that amounts to about 105 fmoI/10⁶ PBMCs (Janssen et al. 2001). Interestingly, significant levels of O^6 -MeG were detected at a dose of 100 µM TMZ, which is comparable to the plasma concentration that can be achieved in patients after oral administration of the drug (Britten et al. 1999; Hammond et al. 1999). It can be envisioned that O^6 -MeG induced by methylating anticancer drugs such as TMZ and DTIC could be monitored in peripheral blood cells as clinical pharmacodynamic biomarker in the future, comparable to γ H2AX and poly(ADP-ribose) as proposed elsewhere (Redon et al. 2010). This will assist in stratifying patients and monitoring therapeutic efficacy in personalized medicine, an approach that is also amenable to other DNA-damaging anticancer drugs, including cisplatin and cyclophosphamide (Stornetta et al. 2017). The advantages and disadvantages of each method used here are summarized in Table 3.

Very recently, novel strategies have been developed to detect O^6 -MeG in a sequence-specific context. To this end, artificial nucleotides (benzimidazole-derived 2'-deoxynucleoside-5'-O-triphosphates) have been synthesized, which are incorporated into DNA opposite O^6 -MeG by an engineered KlenTaq DNA polymerase (Wyss et al. 2016; Betz et al. 2017). Novel hybridization probes based on an oligonucleotide with nucleoside analogues conjugated to gold nanoparticles have also been used to successfully detect O^6 -MeG within a mutational hotspot in the *KRAS* oncogene (Trantakis et al. 2016). These chemical approaches may open a new avenue to measure O^6 -MeG levels in a sequence-specific manner at single base resolution instead of assessing the global O^6 -MeG load in genomic DNA.

In summary, the UPLC–MS/MS approach allowed for the quantitative, sensitive and specific detection of critical O^6 -MeG adducts in cells and tissue. This technique was further pivotal for the determination of threshold levels for O^6 -MeG

adducts, which were caused by the repair enzyme MGMT. We envision that this method will be instrumental to monitor the therapeutic efficacy of alkylating anticancer drugs and to assess dietary and environmental exposure to O^6 -MeG-inducing agents.

Acknowledgements This work was supported by the University Medical Center Mainz (MAIFOR), the German Research Foundation (DFG-FA 1034/3-1 and DFG-KA724/29-1) and the Swiss National Science Foundation (156280). We are indebted to Dr. Daniel Heylmann (Department of Toxicology, University Medical Center, Mainz, Germany) for isolating PBMCs from buffy coat. We are also grateful to Dr. Bert Vogelstein (John Hopkins University, Baltimore, USA) for providing HCT116 cells, to Dr. Leona D. Samson (MIT, Boston, USA) for providing MGMT knockout animals, and to Dr. Geoffrey P. Margison (University of Manchester, UK) for providing TMZ. We also thank the FGCZ Functional Genomics Center Zürich (FGCZ) for LC–MS/MS assistance.

Compliance with ethical standards

Conflict of interest The authors declare no conflict of interest.

References

- Betz K, Nilforoushan A, Wyss LA, Diederichs K, Sturla SJ, Marx A (2017) Structural basis for the selective incorporation of an artificial nucleotide opposite a DNA adduct by a DNA polymerase. *Chem Commun* 53:12704–12707
- Britten CD, Rowinsky EK, Baker SD et al (1999) A Phase I and pharmacokinetic study of temozolomide and cisplatin in patients with advanced solid malignancies. *Clin Cancer Res* 5(7):1629–1637
- Bugni JM, Meira LB, Samson LD (2009) Alkylation-induced colon tumorigenesis in mice deficient in the Mgmt and Msh6 proteins. *Oncogene* 28(5):734–741. <https://doi.org/10.1038/ncr.2008.426>
- Daniels DS, Woo TT, Luu KX et al (2004) DNA binding and nucleotide flipping by the human DNA repair protein AGT. *Nat Struct Mol Biol* 11(8):714–720. <https://doi.org/10.1038/nsmb791>
- Dorsam B, Fahrer J (2016) The disulfide compound alpha-lipoic acid and its derivatives: a novel class of anticancer agents targeting mitochondria. *Cancer Lett* 371(1):12–19. <https://doi.org/10.1016/j.canlet.2015.11.019>
- Dorsam B, Seiwert N, Foersch S et al (2018) PARP-1 protects against colorectal tumor induction, but promotes inflammation-driven colorectal tumor progression. *Proc Natl Acad Sci USA* 115(17):E4061–E4070. <https://doi.org/10.1073/pnas.1712345115>
- Fahrer J, Kaina B (2013) O^6 -methylguanine-DNA methyltransferase in the defense against N-nitroso compounds and colorectal cancer. *Carcinogenesis* 34(11):2435–2442. <https://doi.org/10.1093/carcin/bgt275>
- Fahrer J, Huelsenbeck J, Jaurich H et al (2014) Cytotoxic distending toxin (CDT) is a radiomimetic agent and induces persistent levels of DNA double-strand breaks in human fibroblasts. *DNA Repair* 18:31–43. <https://doi.org/10.1016/j.dnarep.2014.03.002>
- Fahrer J, Frisch J, Nagel G et al (2015) DNA repair by MGMT, but not AAG, causes a threshold in alkylation-induced colorectal carcinogenesis. *Carcinogenesis* 36(10):1235–1244. <https://doi.org/10.1093/carcin/bgv114>
- Fu D, Calvo JA, Samson LD (2012) Balancing repair and tolerance of DNA damage caused by alkylating agents. *Nat Rev Cancer* 12(2):104–120. <https://doi.org/10.1038/nrc3185>

- Georgiadis P, Kaila S, Makedonopoulou P et al (2011) Development and validation of a new, sensitive immunochemical assay for O(6)-methylguanine in DNA and its application in a population study. *Cancer Epidemiol Biomarkers Prev* 20(1):82–90. <https://doi.org/10.1158/1055-9965.EPI-10-0788>
- Glassner BJ, Weeda G, Allan JM et al (1999) DNA repair methyltransferase (Mgmt) knockout mice are sensitive to the lethal effects of chemotherapeutic alkylating agents. *Mutagenesis* 14(3):339–347
- Göder A, Nagel G, Kraus A et al (2015) Lipoic acid inhibits the DNA repair protein O⁶-methylguanine-DNA methyltransferase (MGMT) and triggers its depletion in colorectal cancer cells with concomitant autophagy induction. *Carcinogenesis* 36(8):817–831. <https://doi.org/10.1093/carcin/bgv070>
- Guo J, Yun BH, Upadhyaya P et al (2016) Multiclass carcinogenic DNA adduct quantification in formalin-fixed paraffin-embedded tissues by ultraperformance liquid chromatography-tandem mass spectrometry. *Anal Chem* 88(9):4780–4787. <https://doi.org/10.1021/acs.analchem.6b00124>
- Hammond LA, Eckardt JR, Baker SD et al (1999) Phase I and pharmacokinetic study of temozolomide on a daily-for-5-days schedule in patients with advanced solid malignancies. *J Clin Oncol* 17(8):2604–2613. <https://doi.org/10.1200/JCO.1999.17.8.2604>
- Heylmann D, Kaina B (2016) The gammaH2AX DNA damage assay from a drop of blood. *Sci Rep* 6:22682. <https://doi.org/10.1038/srep22682>
- Janssen K, Eichhorn-Grombacher U, Schlink K, Nitzsche S, Oesch F, Kaina B (2001) Long-time expression of DNA repair enzymes MGMT and APE in human peripheral blood mononuclear cells. *Arch Toxicol* 75(5):306–312
- Jiao L, Chang P, Fircozi PF, Lai D, Abbruzzese JL, Li D (2007) Polymorphisms of phase II xenobiotic-metabolizing and DNA repair genes and in vitro N-ethyl-N-nitrosourea-induced O⁶-ethylguanine levels in human lymphocytes. *Mutat Res* 627(2):146–157. <https://doi.org/10.1016/j.mrgentox.2006.11.001>
- Kaina B, Christmann M, Naumann S, Roos WP (2007) MGMT: key node in the battle against genotoxicity, carcinogenicity and apoptosis induced by alkylating agents. *DNA Repair* 6(8):1079–1099. <https://doi.org/10.1016/j.dnarep.2007.03.008>
- Kaina B, Margison GP, Christmann M (2010) Targeting O(6)-methylguanine-DNA methyltransferase with specific inhibitors as a strategy in cancer therapy. *Cell Mol Life Sci* 67(21):3663–3681. <https://doi.org/10.1007/s00018-010-0491-7>
- Kinner A, Wu W, Staudt C, Iliakis G (2008) Gamma-H2AX in recognition and signaling of DNA double-strand breaks in the context of chromatin. *Nucleic Acids Res* 36(17):5678–5694. <https://doi.org/10.1093/nar/gkn550>
- Lutz WK, Lutz RW (2009) Statistical model to estimate a threshold dose and its confidence limits for the analysis of sublinear dose-response relationships, exemplified for mutagenicity data. *Mutat Res* 678(2):118–122. <https://doi.org/10.1016/j.mrgentox.2009.05.010>
- Mikhed Y, Fahrer J, Oelze M et al (2016) Nitroglycerin induces DNA damage and vascular cell death in the setting of nitrate tolerance. *Basic Res Cardiol* 111(4):52. <https://doi.org/10.1007/s00395-016-0571-4>
- Mojas N, Lopes M, Jiricny J (2007) Mismatch repair-dependent processing of methylation damage gives rise to persistent single-stranded gaps in newly replicated DNA. *Genes Dev* 21(24):3342–3355. <https://doi.org/10.1101/gad.455407>
- Neufert C, Becker C, Neurath MF (2007) An inducible mouse model of colon carcinogenesis for the analysis of sporadic and inflammation-driven tumor progression. *Nat Protoc* 2(8):1998–2004. <https://doi.org/10.1038/nprot.2007.279>
- Niture SK, Velu CS, Smith QR, Bhat GJ, Srivenugopal KS (2007) Increased expression of the MGMT repair protein mediated by cysteine prodrugs and chemopreventative natural products in human lymphocytes and tumor cell lines. *Carcinogenesis* 28(2):378–389. <https://doi.org/10.1093/carcin/bgl155>
- Nyskohus LS, Watson AJ, Margison GP et al (2013) Repair and removal of azoxymethane-induced O⁶-methylguanine in rat colon by O⁶-methylguanine DNA methyltransferase and apoptosis. *Mutat Res* 758(1–2):80–86. <https://doi.org/10.1016/j.mrgentox.2013.10.001>
- Ochs K, Kaina B (2000) Apoptosis induced by DNA damage O⁶-methylguanine is Bcl-2 and caspase-9/3 regulated and Fas/caspase-8 independent. *Cancer Res* 60(20):5815–5824
- Oh HK, Teo AK, Ali RB et al (1996) Conformational change in human DNA repair enzyme O⁶-methylguanine-DNA methyltransferase upon alkylation of its active site by SN1 (indirect-acting) and SN2 (direct-acting) alkylating agents: breaking a “salt-link”. *Biochemistry* 35(38):12259–12266. <https://doi.org/10.1021/bi9603635>
- Quiros S, Roos WP, Kaina B (2010) Processing of O⁶-methylguanine into DNA double-strand breaks requires two rounds of replication whereas apoptosis is also induced in subsequent cell cycles. *Cell Cycle* 9(1):168–178
- R Development Core Team (2013) R: A language and environment for statistical computing. R Foundation for Statistical Computing, Vienna
- Redon CE, Nakamura AJ, Zhang YW et al (2010) Histone gamma-H2AX and poly(ADP-ribose) as clinical pharmacodynamic biomarkers. *Clin Cancer Res* 16(18):4532–4542. <https://doi.org/10.1158/1078-0432.CCR-10-0523>
- Rosenberg DW, Mankowski DC (1994) Induction of cyp2e-1 protein in mouse colon. *Carcinogenesis* 15(1):73–78
- Roy L, Harrell CC, Ryan AS, Thorsteinsson T, Sancilio FD (2013) Development and validation of a single hplc method for analysis of purines in fish oil supplements. *Food Nutr Sci* 4(12):1255–1259. <https://doi.org/10.4236/fns.2013.412160>
- Ruvinsky A, Graves JAM (2005) Mammalian genomics. CABI Pub., Wallingford
- Seiler F, Kirstein U, Eberle G, Hochleitner K, Rajewsky MF (1993) Quantification of specific DNA O-alkylation products in individual cells by monoclonal antibodies and digital imaging of intensified nuclear fluorescence. *Carcinogenesis* 14(9):1907–1913
- Stephanou G, Vlastos D, Vlachodimitropoulos D, Demopoulos NA (1996) A comparative study on the effect of MNU on human lymphocyte cultures in vitro evaluated by O⁶-mdG formation, micronuclei and sister chromatid exchanges induction. *Cancer Lett* 109(1–2):109–114
- Stornetta A, Zimmermann M, Cimino GD, Henderson PT, Sturla SJ (2017) DNA Adducts from anticancer drugs as candidate predictive markers for precision medicine. *Chem Res Toxicol* 30(1):388–409. <https://doi.org/10.1021/acs.chemrestox.6b00380>
- Thomas AD, Jenkins GJ, Kaina B et al (2013) Influence of DNA repair on nonlinear dose-responses for mutation. *Toxicol Sci* 132(1):87–95. <https://doi.org/10.1093/toxsci/kfs341>
- Thomas AD, Fahrer J, Johnson GE, Kaina B (2015) Theoretical considerations for thresholds in chemical carcinogenesis. *Mutat Res Rev Mutat Res* 765:56–67. <https://doi.org/10.1016/j.mrrrev.2015.05.001>
- Tomaszowski KH, Schirmacher R, Kaina B (2015) Multidrug efflux pumps attenuate the effect of MGMT inhibitors. *Mol Pharm* 12(11):3924–3934. <https://doi.org/10.1021/acs.molpharmac.5b00341>
- Trantakis IA, Nilforoushan A, Dahlmann HA, Stauble CK, Sturla SJ (2016) In-gene quantification of O(6)-methylguanine with elongated nucleoside analogues on gold nanoprobles. *J Am Chem Soc* 138(27):8497–8504. <https://doi.org/10.1021/jacs.6b03599>
- Upadhyaya P, Lindgren BR, Hecht SS (2009) Comparative levels of O⁶-methylguanine, pyridyloxobutyl-, and pyridylhydroxybutyl-DNA adducts in lung and liver of rats treated chronically with the tobacco-specific carcinogen

- 4-(methylnitrosamino)-1-(3-pyridyl)-1-butanone. *Drug Metab Dispos* 37(6):1147–1151. <https://doi.org/10.1124/dmd.109.027078>
- Vanden Bussche J, Moore SA, Pasmans F, Kuhnle GG, Vanhaecke L (2012) An approach based on ultra-high pressure liquid chromatography-tandem mass spectrometry to quantify O6-methyl and O6-carboxymethylguanine DNA adducts in intestinal cell lines. *J Chromatogr A* 1257:25–33. <https://doi.org/10.1016/j.chroma.2012.07.040>
- Wyss LA, Nilforoushan A, Williams DM, Marx A, Sturla SJ (2016) The use of an artificial nucleotide for polymerase-based recognition of carcinogenic O6-alkylguanine DNA adducts. *Nucleic Acids Res* 44(14):6564–6573. <https://doi.org/10.1093/nar/gkw589>
- Xu-Welliver M, Pegg AE (2002) Degradation of the alkylated form of the DNA repair protein, O(6)-alkylguanine-DNA alkyltransferase. *Carcinogenesis* 23(5):823–830
- Zhang F, Bartels MJ, Pottenger LH, Gollapudi BB, Schisler MR (2006) Simultaneous quantitation of 7-methyl- and O6-methylguanine adducts in DNA by liquid chromatography-positive electrospray tandem mass spectrometry. *J Chromatogr B Analyt Technol Biomed Life Sci* 833(2):141–148. <https://doi.org/10.1016/j.jchromb.2006.01.035>
- Zhang J, Stevens MF, Bradshaw TD (2012) Temozolomide: mechanisms of action, repair and resistance. *Curr Mol Pharmacol* 5(1):102–114

Supplementary Information

Supplementary Figure S1

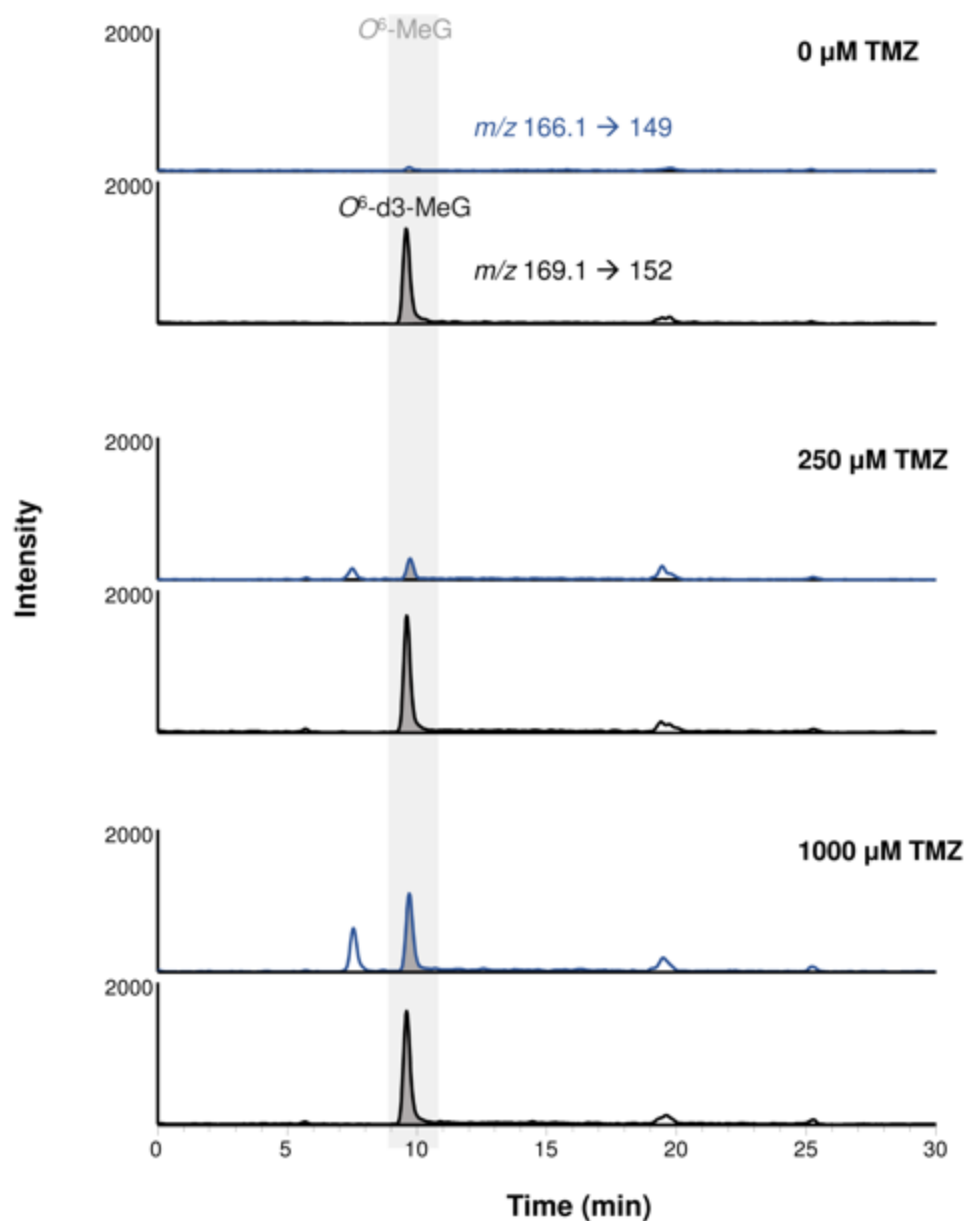


Figure S1: Representative selective (SRM) chromatograms of HCT116 cells exposed to increasing doses of temozolomide (TMZ). Top panel: m/z 166.1 \rightarrow 149; O^6 -MeG is eluted at 9.8 min. Bottom panel: m/z 169.1 \rightarrow 152; isotope-labeled O^6 -MeG standard is eluted at 9.8 min.

Supplementary Figure S2

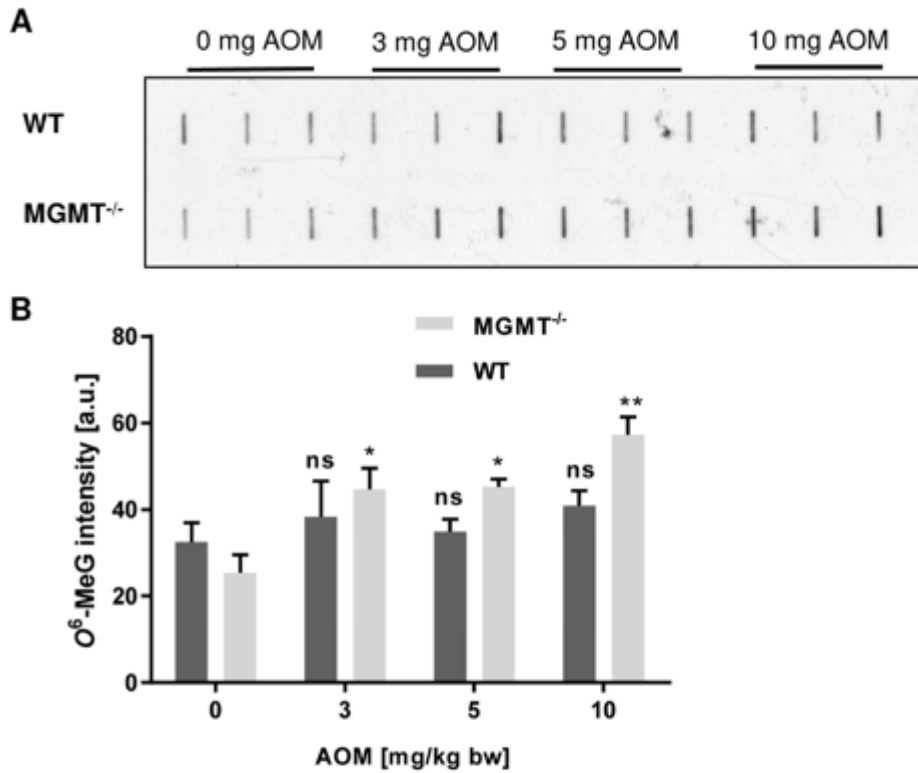


Figure S2: Immuno-slot blot (ISB) analysis of O^6 -MeG in genomic colon DNA of WT and MGMT deficient mice. **A** Animals were treated with increasing doses of AOM (0–10 mg/kg bw; $n = 3$ per dose and genotype) and sacrificed after 48 h. Genomic DNA was isolated from colon tissue and analyzed by ISB. **B** O^6 -MeG levels were calculated in relation to PBS-treated control mice (0 mg AOM/kg bw) and are presented as mean + SEM. **, $p < 0.005$; *, $p < 0.05$; n.s. not significant (as compared to the respective genotype control treated with 0 mg AOM/kg bw).

Supplementary Figure S3

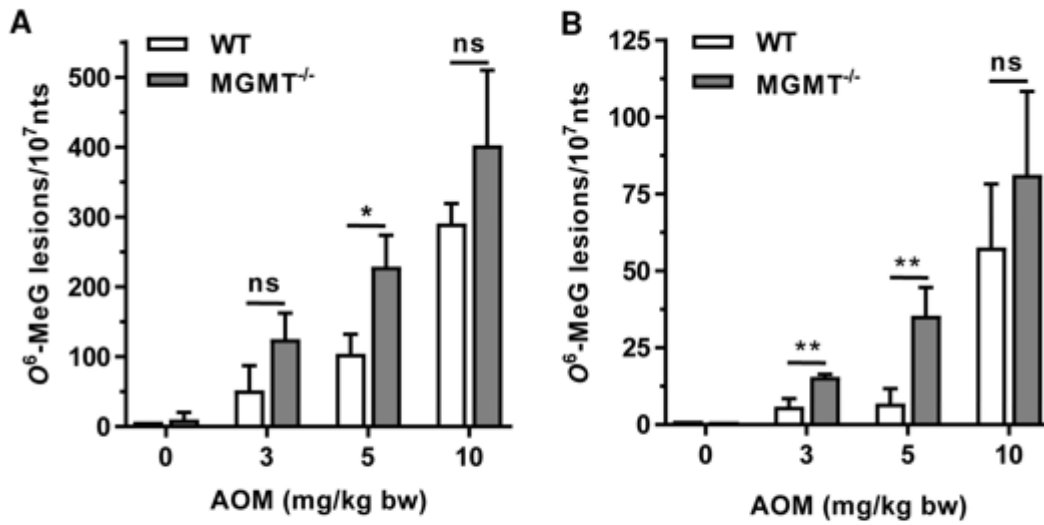


Figure S3: Dose-dependent *O*⁶-MeG formation in liver and colorectal tissue of WT and MGMT^{-/-} mice. A and B Determination of hepatic and colonic *O*⁶-MeG lesions in isolated genomic DNA by mass spectrometry. Data with 10 mg/kg AOM has been reported previously by our group (Dörsam et al. 2018). Data is shown as mean + SEM (n = 3 per dose and genotype). **, p < 0.01; *, p < 0.05.; n.s. not significant.

Supplementary Figure S4

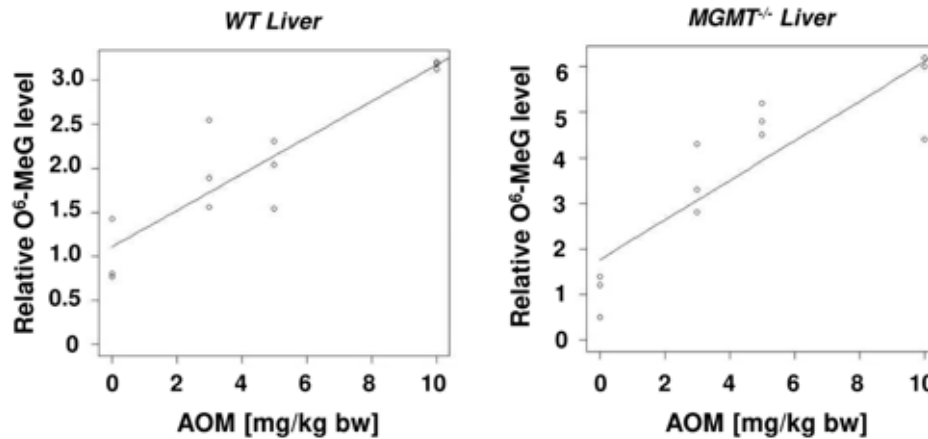


Figure S4: Dose-response modeling of hepatic *O*⁶-MeG formation assessed by immuno-slot blot (ISB) analysis. ISB data of hepatic *O*⁶-MeG formation in AOM-treated WT and MGMT^{-/-} animals were reported previously by our group (Fahrer et al. 2015). Dose-response modeling was performed to elucidate the putative threshold dose for AOM-induced *O*⁶-MeG in WT and MGMT-deficient mice. Solid line shows the best fit of the model, indicating linearity.

Supplementary Figure S5

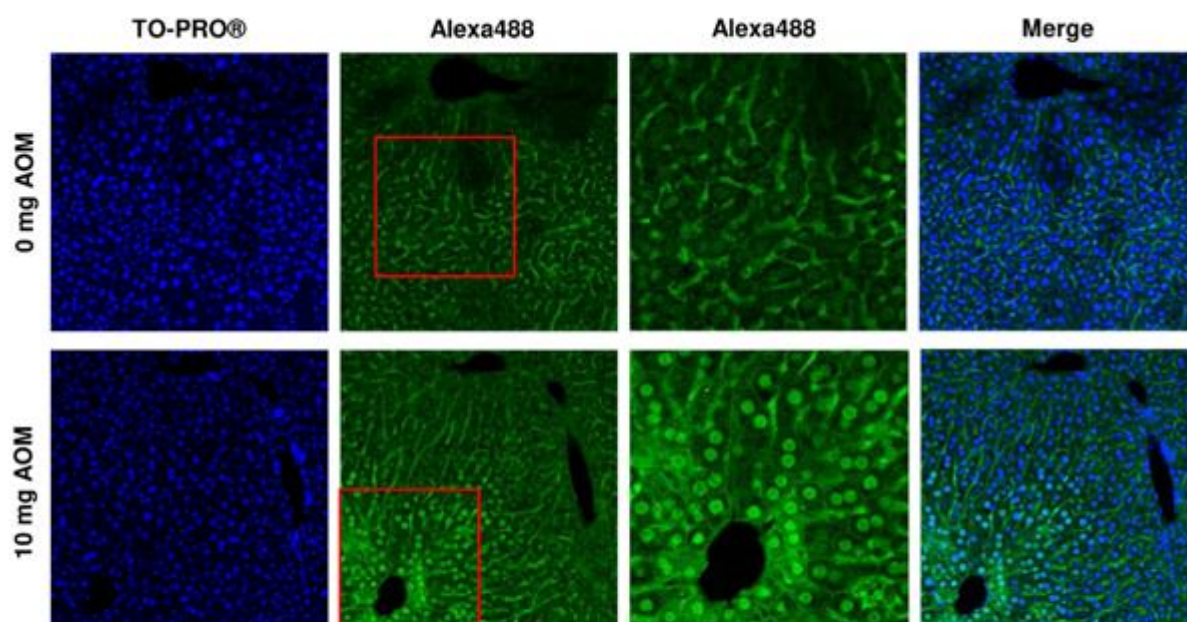


Figure S5: Detection of AOM-induced O^6 -MeG DNA adducts in liver tissue. *Mgmt*^{-/-} animals were challenged with AOM (0 or 10 mg/kg bw) and sacrificed after 24 h. Paraffin-embedded liver tissue was sectioned at 5 μ m and stained with an O^6 -MeG antibody together with an Alexa488-coupled secondary antibody (green). Nuclei were counterstained with TO-PRO-3 (blue). Samples were then analyzed by confocal microscopy. Red box indicates enlarged image section.

Supplementary Table S1

PBMCs	O^6 -MeG lesions/ 10^7 nts
0 μ M TMZ	20
50 μ M TMZ	19
100 μ M TMZ	40
250 μ M TMZ	91
500 μ M TMZ	615
1000 μ M TMZ	212

Table S1: Formation of O^6 -MeG in peripheral blood mononuclear cells (PBMCs). PBMCs were exposed *in vitro* to increasing doses of the methylating anticancer drug temozolomide (TMZ) for 2 h. Genomic DNA was isolated and processed for UPLC-MS/MS analysis as described in materials and methods.

Chapter 6: Summary and Outlook

N-Nitroso compounds (NOCs) are known human carcinogens due to their potential to alkylate DNA leading to replication-associated mutagenesis. Among the DNA adducts formed from NOC exposure, those arising from alkylation of the oxygen in the DNA base guanine include *O*⁶-methyldeoxyguanosine (*O*⁶-MedG) and *O*⁶-carboxymethyldeoxyguanosine (*O*⁶-CMdG), which are highly mutagenic and potentially carcinogenic.¹⁻⁵ The mutation spectra in the cancer relevant p53 gene of stomach and colorectal cancer patients matches the one induced by the carboxymethylating agent KDA, implicating carboxymethylation of DNA in the initiation of both cancer types.⁶ Further, during translesion synthesis of *O*⁶-CMdG, misincorporation of thymine and adenine occurs, providing a mechanism for the origin of the mutation spectra.⁷⁻⁸ NOC-induced carcinogenesis is further supported by molecular epidemiology data demonstrating the occurrence of *O*⁶-CMdG and *O*⁶-MedG in blood and tissue samples from high meat consumption and colorectal cancer patients.⁹⁻¹³ Thus NOC exposure from meat consumption is characterized as a carcinogen hazard, however, risk assessment on the basis of NOC exposure and biological consequences is lacking and requires quantitative biomarkers concerning internal exposure and knowledge of how they are impacted by genetic background.¹⁴⁻¹⁶

A goal of this thesis was to characterize the chemical basis of NOC-induced *O*⁶-CMdG adduct formation to improve the understanding of biological factors that govern the balance of DNA adduct formation and removal in cells. Further, phenotypic responses to NOC-induced DNA damage was elucidated and key factors mediating cellular susceptibility towards NOC exposure evaluated. Improved understanding of cellular response upon NOC exposure is anticipated to help establish biomarker-based strategies for risk assessment and for predicting individual susceptibility based on assessment of exposure and/or activity of critical damage response factors. Three main further directions suggested from this research concern enzymatic studies addressing NOC decomposition and uptake, repair studies elucidating a potential interplay of pathways in *O*⁶-CMdG repair and dose-response studies for *O*⁶-CMdG and carboxymethylating agents with regard to genotoxic thresholds mediated by repair pathways. Finally, of these further studies would be enabled by the sensitive and specific mass spectrometric analysis approaches that have been established and applied in this research.

Mechanism of *O*⁶-alkylguanine formation

The mechanism of NOC-induced DNA adduct formation relies on spontaneous decomposition of nitrosamides and CYP450-activated alpha-hydroxynitrosamines to yield alkylating agents via monoalkynitrosamines and alkyldiazonium ions.¹⁷ Indeed, *O*⁶-CMdG formation via the intermediate diazoacetate was demonstrated for nitrosated glycine under physiological conditions,¹⁸ but overall evidence for diazoacetate as the intermediate in *O*⁶-CMdG formation is lacking. Azaserine, a diazo-compound that can be considered as the active decomposition product of NOCs, was chosen as a model compound to study NOC-induced adduct formation.

The chemical mechanism of azaserine-induced *O*⁶-CMdG formation was characterized, revealing for the first time the formation of *O*⁶-Ser-CMdG as an intermediate accessible by

direct reaction of L-azaserine with DNA. O^6 -Ser-CMdG spontaneously degrades to the biologically relevant adduct O^6 -CMdG (Chapter 2). Furthermore, azaserine-induced O^6 -CMdG and O^6 -MedG formation in cells followed a linear dose-response relationship with maximal levels being reached after 48 h of L-azaserine exposure. These data and the bioanalysis strategies established to obtain it critically support the use of L-azaserine as a model compound to study NOC exposure in carcinogenesis research. Enzymatic β -elimination of L-azaserine has also been proposed to occur in cells but a corresponding enzyme could never be identified.¹⁹⁻²⁰ Since we did not detect the O^6 -Ser-CMdG intermediate in cells, the enzymatic decomposition warrants further investigation, e.g. by using cell lysates in the reaction mixture of dG and azaserine. Preliminary results by nanoLC-ESI-hrMS² showed no detectable analyte peaks, probably due to high background of the matrix. For MS-based analysis, the cell lysate samples require further clean-up, e.g. molecular weight filtration, or analysis by HPLC would be preferable to test for enzymatic intermediates of L-azaserine that subsequent can result in O^6 -CMdG and O^6 -MedG formation.

Another process that remains unclear is the role of enzymatic pathways in O^6 -MedG formation from carboxymethylating NOCs. As a chemical mechanism, O^6 -MedG formation via decarboxylation of NOC decomposition intermediates has been suggested,¹ and our data support this hypothesis. However, enzymatic O^6 -MedG formation from L-azaserine has never been addressed. The role of enzymatic pathways in L-azaserine induced DNA adduct formation is further supported by studies demonstrating weak mutagenicity for D-azaserine.²¹

Finally, cellular uptake of L-azaserine warrants further investigation. Reduced mutagenicity of D-azaserine could be explained by diminished uptake compared to L-azaserine as active transport via amino acid transporters has been suggested for L-azaserine²²⁻²³ and is further supported by L-azaserine acting as an antagonist for cellular glutamine-dependent amidotransferases.²⁴⁻²⁶ Cellular uptake studies have to be carefully evaluated as amino acids, present in the cell culture media to maintain cells, may alter L-azaserine dependent uptake.

The results from the studies proposed here will provide new knowledge concerning susceptibility towards L-azaserine. As L-azaserine represents a model compound to study NOCs, results might enable to predict susceptibility towards NOC exposure based on individual activity of enzymes involved in compound activation and cellular uptake of active intermediates.

Repair of the pro-mutagenic O^6 -carboxymethylguanine adduct

Next to formation, also current knowledge concerning O^6 -CMG repair is limited. MGMT and NER are discussed to act on O^6 -CMdG, thereby preventing from its genotoxic effects.²⁷⁻³² Evaluation of the cellular response to carboxymethylating agents from the perspective of their relationship with O^6 -CMdG levels demonstrated that decreased cell viability and higher mutation rates occur when MGMT is depleted and that increased mutagenicity is associated with an accumulation of O^6 -CMdG adducts (Chapter 3, 4). MGMT-inhibited cells revealed an increase in adduct levels of 8.4-fold for O^6 -MedG and 3.2-fold for O^6 -CMdG adduct levels compared to MGMT-proficient cells, suggesting that MGMT indeed contributes to O^6 -CMdG repair in cells, but less effectively than for O^6 -MedG. Further, the potential involvement of NER in the cellular response to O^6 -CMdG was assessed in NER-deficient cells, revealing decreased cell viability and higher mutation rates upon exposure to azaserine. Interestingly,

mutagenicity and O^6 -CMdG adduct levels were significantly increased upon inhibition of MGMT in NER-deficient cells, suggesting an interactive function of both repair pathways in cellular response upon NOC-exposure. Summarizing, results demonstrated a pivotal role of both MGMT and NER in the cellular response to O^6 -CMdG. Moreover, persistence of O^6 -CMdG adducts due to inactive repair resulted in increased mutagenicity, supporting a causative role of DNA adducts in the rise of mutations.

Future studies are warranted to address the interplay of MGMT and NER. Studies in yeast and bacteria suggest alkyltransferases, homologous to MGMT but without transferase activity, to signal for the NER pathway by binding to the O^6 -alkylguanine damages.³³⁻³⁴ The potential role of MGMT in signalling for NER in mammalian cells has yet to be elucidated. Performing cell-free NER repair assays on O^6 -CMG-containing oligodeoxyribonucleotides, also in the presence of human MGMT protein will help to elucidate a potential interplay and can be extended to assess the involvement of other DNA repair pathways. As our data demonstrates that MGMT acts on O^6 -CMdG, but less effectively than for O^6 -MeG, establishing repair kinetics for the removal of O^6 -CMdG by MGMT only will help to understand the interplay and regulation of other repair pathways in O^6 -CMdG-removal.

Repair-activity mediates dose-response relationship

Knowledge on O^6 -CMdG repair pathways is also crucial in risk assessment of NOC exposure, as DNA repair pathways are discussed to be responsible for a non-linear dose response of genotoxic chemicals,^{35,36,37-38} as demonstrated e.g. for the NOC methylnitrosourea for which a no observed genotoxic effect level (NOGEL) dependent on MGMT-activity could be established.³⁹⁻⁴¹ DNA adducts as biomarker of exposure are considered to become a valuable tool in genotoxic risk assessment as their quantitative assessment accounts for activating and detoxifying processes of a genotoxic chemical.^{35, 36, 37-38} Risk assessment based on low DNA adduct levels is expected to benefit from advances in LC-MS technologies enabling the detection of endogenous level.⁴²

Applying such a sensitive LC-MS approach to monitor O^6 -MeG formation in colon and hepatic tissue in MGMT-deficient and WT mice challenged with different concentrations of the methylating agent azoxymethane (AOM) allowed us to establish genotoxic thresholds in the presence of active repair as a detoxifying process (*Chapter 5*). Dose-response relationships in MGMT-inhibited colorectal cancer cells were further established by applying different analytical approaches for O^6 -MeG monitoring. IF microscopy and ISB allowed for semi-quantitative, dose-dependent assessment of O^6 -MeG after exposure of cells to the methylating anticancer drug temozolomide (TMZ). Only LC-MS/MS based assessment of O^6 -MeG levels in mice allowed for the establishment of the genotoxic threshold upon exposure to AOM. The LC-MS/MS based strategy further enabled O^6 -MeG detection in blood cells exposed *in vitro* to clinically relevant concentrations of TMZ. Quantifying drug-adduct levels in blood samples of patients is envisioned to improve personalized anticancer therapy by monitoring and predicting drug response.⁴³ LC-MS/MS based strategies for quantifying DNA damage in biological samples have excellent sensitivity and selectivity compared to other available detection methods, and recent advances also allow for sensitive untargeted analysis of DNA adducts.^{36, 42, 44-45} Therefore, the use of LC-MS/MS is envisioned to be instrumental for biomonitoring studies of drug efficacy and exposure to alkylating agents. The identification of MGMT-activity to be responsible for genotoxic thresholds in O^6 -MeG

formation supports the use of personal risk assessment strategies based on MGMT polymorphisms and will improve the understanding of quantitative data in genotoxic risk assessment.³⁹⁻⁴¹ The existence of genotoxic thresholds for O^6 -CMdG formation upon MGMT and/or NER depletion is of interest, too, especially with regard to the established correlation of O^6 -CMdG levels with mutagenicity, highlighting its importance for biological consequences and its use as a biomarker in risk assessment strategies (*Chapter 3*). Results from these studies might help risk assessment of NOC exposure and meat intake on the onset of colorectal cancer.

6.1 References

1. Harrison, K. L.; Jukes, R.; Cooper, D. P.; Shuker, D. E. G., Detection of Concomitant Formation of O6-Carboxymethyl- and O6-Methyl-2'-deoxyguanosine in DNA Exposed to Nitrosated Glycine Derivatives Using a Combined Immunoaffinity/HPLC Method. *Chemical Research in Toxicology* **1999**, *12* (1), 106-111.
2. Harrison, K. L.; Fairhurst, N.; Challis, B. C.; Shuker, D. E. G., Synthesis, Characterization, and Immunochemical Detection of O6-(Carboxymethyl)-2'-deoxyguanosine: A DNA Adduct Formed by Nitrosated Glycine Derivatives. *Chemical Research in Toxicology* **1997**, *10* (6), 652-659.
3. Montesano, R.; Pegg, A. E.; Margison, G. P., Alkylation of DNA and carcinogenicity of N-nitroso compounds. *Journal of toxicology and environmental health* **1980**, *6* (5-6), 1001-8.
4. Warren, J. J.; Forsberg, L. J.; Beese, L. S., The structural basis for the mutagenicity of O⁶-methyl-guanine lesions. *Proceedings of the National Academy of Sciences* **2006**, *103* (52), 19701-19706.
5. Swann, P. F., Why do O6-alkylguanine and O4-alkylthymine miscode? The relationship between the structure of DNA containing O6-alkylguanine and O4-alkylthymine and the mutagenic properties of these bases. *Mutat Res* **1990**, *233* (1-2), 81-94.
6. Gottschalg, E.; Scott, G. B.; Burns, P. A.; Shuker, D. E. G., Potassium diazoacetate-induced p53 mutations in vitro in relation to formation of O6 -carboxymethyl- and O6 -methyl-2'-deoxyguanosine DNA adducts: relevance for gastrointestinal cancer. *Carcinogenesis* **2007**, *28* (2), 356-362.
7. Wu, J.; Wang, P.; Li, L.; Williams, N. L.; Ji, D.; Zahurancik, W. J.; You, C.; Wang, J.; Suo, Z.; Wang, Y., Replication studies of carboxymethylated DNA lesions in human cells. *Nucleic Acids Research* **2017**, *45* (12), 7276-7284.
8. Ráz, M. H.; Dexter, H. R.; Millington, C. L.; van Loon, B.; Williams, D. M.; Sturla, S. J., Bypass of Mutagenic O(6)-Carboxymethylguanine DNA Adducts by Human Y- and B-Family Polymerases. *Chem Res Toxicol* **2016**, *29* (9), 1493-503.
9. Bussche, J. V.; Hemeryck, L. Y.; Van Hecke, T.; Kuhnle, G. G. C.; Pasmans, F.; Moore, S. A.; Van de Wiele, T.; De Smet, S.; Vanhaecke, L., O6-carboxymethylguanine DNA adduct formation and lipid peroxidation upon in vitro gastrointestinal digestion of haem-rich meat. *Molecular Nutrition & Food Research* **2014**, *58* (9), 1883-1896.
10. Lewin, M. H.; Bailey, N.; Bandaletova, T.; Bowman, R.; Cross, A. J.; Pollock, J.; Shuker, D. E. G.; Bingham, S. A., Red Meat Enhances the Colonic Formation of the DNA Adduct O⁶-Carboxymethyl Guanine: Implications for Colorectal Cancer Risk. *Cancer research* **2006**, *66* (3), 1859-1865.
11. Hall, C. N.; Badawi, A. F.; O'Connor, P. J.; Saffhill, R., The detection of alkylation damage in the DNA of human gastrointestinal tissues. *Br J Cancer* **1991**, *64* (1), 59-63.
12. O6-methylguanine in blood leucocyte DNA: an association with the geographic prevalence of gastric cancer and with low levels of serum pepsinogen A, a marker of severe chronic atrophic gastritis. The EUROGAST Study Group. *Carcinogenesis* **1994**, *15* (9), 1815-20.
13. Hemeryck, L. Y.; Decloedt, A. I.; Vanden Bussche, J.; Geboes, K. P.; Vanhaecke, L., High resolution mass spectrometry based profiling of diet-related deoxyribonucleic acid adducts. *Analytica Chimica Acta* **2015**, *892*, 123-131.
14. Turesky, R. J., Mechanistic Evidence for Red Meat and Processed Meat Intake and Cancer Risk: A Follow-up on the International Agency for Research on Cancer Evaluation of 2015. *Chimia* **2018**, *72* (10), 718-724.
15. Bouvard, V.; Loomis, D.; Guyton, K. Z.; Grosse, Y.; Ghissassi, F. E.; Benbrahim-Tallaa, L.; Guha, N.; Mattock, H.; Straif, K., Carcinogenicity of consumption of red and processed meat. *The Lancet Oncology* **2015**, *16* (16), 1599-1600.
16. Cross, A. J.; Ferrucci, L. M.; Risch, A.; Graubard, B. I.; Ward, M. H.; Park, Y.; Hollenbeck, A. R.; Schatzkin, A.; Sinha, R., A Large Prospective Study of Meat Consumption and Colorectal Cancer Risk: An Investigation of Potential Mechanisms Underlying this Association. *Cancer research* **2010**, *70* (6), 2406-2414.
17. Guttenplan, J. B., Effects of pH and Structure on the Mutagenic Activity of N-Nitroso Compounds. In *Genotoxicology of N-Nitroso Compounds*, Rao, T. K.; Lijinsky, W.; Epler, J. L., Eds. Springer US: Boston, MA, 1984; pp 59-90.
18. Cupid, B. C.; Zeng, Z.; Singh, R.; Shuker, D. E. G., Detection of O6-Carboxymethyl-2'-deoxyguanosine in DNA Following Reaction of Nitric Oxide with Glycine and in Human Blood DNA Using a Quantitative Immunoslot Blot Assay. *Chemical Research in Toxicology* **2004**, *17* (3), 294-300.
19. Jacquez, J. A.; Sherman, J. H., Enzymatic Degradation of Azaserine. *Cancer research* **1962**, *22* (1 Part 1), 56.
20. Rosenkrantz, H.; Sprague, R.; Schaeppi, U.; Pittillo, R. T.; Cooney, D. A.; Davis, R. D., The stoichiometric fate of azaserine metabolized in vitro by tissues from azaserine-treated dogs and mice. *Toxicology and Applied Pharmacology* **1972**, *22* (4), 607-620.

21. Staiano, N.; Everson, R. B.; Cooney, D. A.; Longnecker, D. S.; Thorgeirsson, S. S., Mutagenicity of d- and l-azaserine, 6-diazo-5-oxo-l-norleucine and N-(N-methyl-N-nitroso-carbamyl)-l-ornithine in the Salmonella test system. *Mutation Research/Genetic Toxicology* **1980**, *79* (4), 387-390.
22. Jacquez, J. A., Active transport of O-diazoacetyl-L-serine and 6-diazo-5-oxo-L-norleucine in Ehrlich ascites carcinoma. *Cancer research* **1957**, *17* (9), 890-6.
23. Pine, E. K., Concentrative Uptake of Azaserine by Neoplastic Plasma Cells and Lymphocytes2. *JNCI: Journal of the National Cancer Institute* **1958**, *21* (5), 973-984.
24. Bennett, L. L.; Schabel, F. M.; Skipper, H. E., Studies on the mode of action of azaserine. *Archives of Biochemistry and Biophysics* **1956**, *64* (2), 423-436.
25. Lyons, S. D.; Sant, M. E.; Christopherson, R. I., Cytotoxic mechanisms of glutamine antagonists in mouse L1210 leukemia. *Journal of Biological Chemistry* **1990**, *265* (19), 11377-81.
26. Henderson, J. F.; Lepage, G. A.; McIver, F. A., Observations on the action of azaserine in mammalian tissues. *Cancer research* **1957**, *17* (6), 609-12.
27. Senthong, P.; Millington, C. L.; Wilkinson, O. J.; Marriott, A. S.; Watson, A. J.; Reamtong, O.; Eyers, C. E.; Williams, D. M.; Margison, G. P.; Povey, A. C., The nitrosated bile acid DNA lesion O6-carboxymethylguanine is a substrate for the human DNA repair protein O6-methylguanine-DNA methyltransferase. *Nucleic Acids Research* **2013**, *41* (5), 3047-55.
28. O'Driscoll, M.; Macpherson, P.; Xu, Y.-Z.; Karran, P., The cytotoxicity of DNA carboxymethylation and methylation by the model carboxymethylating agent azaserine in human cells. *Carcinogenesis* **1999**, *20* (9), 1855-1862.
29. Du, H.; Wang, P.; Li, L.; Wang, Y., Repair and translesion synthesis of O6-alkylguanine DNA lesions in human cells. *Journal of Biological Chemistry* **2019**, *294* (29), 11144-11153.
30. Bronstein, S. M.; Skopek, T. R.; Swenberg, J. A., Efficient repair of O6-ethylguanine, but not O4-ethylthymine or O2-ethylthymine, is dependent upon O6-alkylguanine-DNA alkyltransferase and nucleotide excision repair activities in human cells. *Cancer research* **1992**, *52* (7), 2008-11.
31. Wang, L.; Spratt, T. E.; Liu, X. K.; Hecht, S. S.; Pegg, A. E.; Peterson, L. A., Pyridyloxobutyl adduct O6-[4-oxo-4-(3-pyridyl)butyl]guanine is present in 4-(acetoxymethylnitrosamino)-1-(3-pyridyl)-1-butanone-treated DNA and is a substrate for O6-alkylguanine-DNA alkyltransferase. *Chem Res Toxicol* **1997**, *10* (5), 562-7.
32. Li, L.; Perdigo, J.; Pegg, A. E.; Lao, Y.; Hecht, S. S.; Lindgren, B. R.; Reardon, J. T.; Sancar, A.; Wattenberg, E. V.; Peterson, L. A., The influence of repair pathways on the cytotoxicity and mutagenicity induced by the pyridyloxobutylation pathway of tobacco-specific nitrosamines. *Chem Res Toxicol* **2009**, *22* (8), 1464-72.
33. Tubbs, J. L.; Latypov, V.; Kanugula, S.; Butt, A.; Melikishvili, M.; Kraehenbuehl, R.; Fleck, O.; Marriott, A.; Watson, A. J.; Verbeek, B.; McGown, G.; Thorncroft, M.; Santibanez-Koref, M. F.; Millington, C.; Arvai, A. S.; Kroeger, M. D.; Peterson, L. A.; Williams, D. M.; Fried, M. G.; Margison, G. P.; Pegg, A. E.; Tainer, J. A., Flipping of alkylated DNA damage bridges base and nucleotide excision repair. *Nature* **2009**, *459* (7248), 808-813.
34. Latypov, V. F.; Tubbs, J. L.; Watson, A. J.; Marriott, A. S.; McGown, G.; Thorncroft, M.; Wilkinson, O. J.; Senthong, P.; Butt, A.; Arvai, A. S.; Millington, C. L.; Povey, A. C.; Williams, D. M.; Santibanez-Koref, M. F.; Tainer, J. A.; Margison, G. P., At11 regulates choice between global genome and transcription-coupled repair of O(6)-alkylguanines. *Mol Cell* **2012**, *47* (1), 50-60.
35. Himmelstein, M. W.; Boogaard, P. J.; Cadet, J.; Farmer, P. B.; Kim, J. H.; Martin, E. A.; Persaud, R.; Shuker, D. E. G., Creating context for the use of DNA adduct data in cancer risk assessment: II. Overview of methods of identification and quantitation of DNA damage. *Critical Reviews in Toxicology* **2009**, *39* (8), 679-694.
36. Chang, Y.-J.; Cooke, M. S.; Hu, C.-W.; Chao, M.-R., Novel approach to integrated DNA adductomics for the assessment of in vitro and in vivo environmental exposures. *Archives of Toxicology* **2018**, *92* (8), 2665-2680.
37. Hartwig, A.; Arand, M.; Epe, B.; Guth, S.; Jahnke, G.; Lampen, A.; Martus, H.-J.; Monien, B.; Rietjens, I. M. C. M.; Schmitz-Spanke, S.; Schriever-Schwemmer, G.; Steinberg, P.; Eisenbrand, G., Mode of action-based risk assessment of genotoxic carcinogens. *Archives of Toxicology* **2020**, *94* (6), 1787-1877.
38. Ji, Z.; LeBaron, M. J.; Schisler, M. R.; Zhang, F.; Bartels, M. J.; Gollapudi, B. B.; Pottenger, L. H., Dose-Response for Multiple Biomarkers of Exposure and Genotoxic Effect Following Repeated Treatment of Rats with the Alkylating Agents, MMS and MNU. *Mutagenesis* **2016**, *31* (3), 297-308.
39. Bevan, R. J.; Harrison, P. T. C., Threshold and non-threshold chemical carcinogens: A survey of the present regulatory landscape. *Regulatory Toxicology and Pharmacology* **2017**, *88*, 291-302.
40. Thomas, A. D.; Jenkins, G. J. S.; Kaina, B.; Bodger, O. G.; Tomaszowski, K.-H.; Lewis, P. D.; Doak, S. H.; Johnson, G. E., Influence of DNA Repair on Nonlinear Dose-Responses for Mutation. *Toxicological Sciences* **2013**, *132* (1), 87-95.
41. Klapacz, J.; Pottenger, L. H.; Engelward, B. P.; Heinen, C. D.; Johnson, G. E.; Clewell, R. A.; Carmichael, P. L.; Adeleye, Y.; Andersen, M. E., Contributions of DNA repair and damage response pathways

to the non-linear genotoxic responses of alkylating agents. *Mutation Research/Reviews in Mutation Research* **2016**, 767, 77-91.

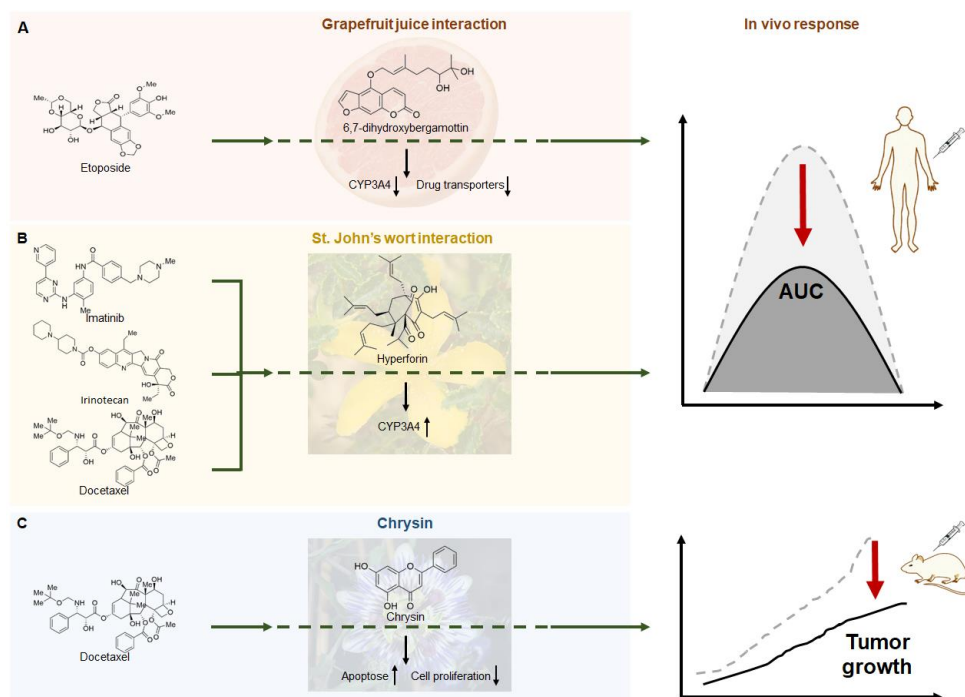
42. Balbo, S.; Turesky, R. J.; Villalta, P. W., DNA Adductomics. *Chemical Research in Toxicology* **2014**, 27 (3), 356-366.

43. Stornetta, A.; Zimmermann, M.; Cimino, G. D.; Henderson, P. T.; Sturla, S. J., DNA Adducts from Anticancer Drugs as Candidate Predictive Markers for Precision Medicine. *Chem Res Toxicol* **2017**, 30 (1), 388-409.

44. Balbo, S.; Hecht, S. S.; Upadhyaya, P.; Villalta, P. W., Application of a high-resolution mass-spectrometry-based DNA adductomics approach for identification of DNA adducts in complex mixtures. *Anal Chem* **2014**, 86 (3), 1744-52.

45. Liu, S.; Wang, Y., Mass spectrometry for the assessment of the occurrence and biological consequences of DNA adducts. *Chemical Society reviews* **2015**, 44 (21), 7829-7854.

Appendix I: Can foods or herbs alter the bioavailability of chemotherapy drugs?



Reprinted with permission from

Geisen S.M. and Sturla S.J., Can foods or herbs alter the bioavailability of chemotherapy drugs? *ACS Pharmacol. Transl. Sci.* **2019**, 2, 143–146

Copyright © 2019 American Chemical Society

The Publication is available at ACS via <https://pubs.acs.org/doi/10.1021/acspsci.9b00007>

Geisen S.M. and Sturla S.J. wrote the manuscript.

Can Foods or Herbs Alter the Bioavailability of Chemotherapy Drugs?

Susanne M. Geisen¹ and Shana J. Sturla^{1*}

Department of Health Sciences and Technology, ETH Zurich, Schmelzbergstrasse 9, 8092 Zurich, Switzerland

Among cancer patients the use of complementary and alternative medicine to treat disease-related depression, alleviate side effects, or even improve therapeutic efficacy varies between 29% in Europe to 87% in the US.^{1,2} These medicines comprise supplements, vitamins, minerals and herbs, special foods, and diets as well as massage and spiritual therapy. While vitamins and minerals are the most common complementary and alternative medicines used by cancer patients, herbal supplements rank second. Half of the time, there may be a known risk for a drug interaction, but only around one-third of patients may inform their doctor about the use of these agents.¹ Some can contain pharmacologically active compounds with the potential to alter the bioavailability of cancer drugs by influencing, for example, drug-metabolizing enzymes or transporters.

Interactions arising from concomitant use of bioactive alternatives and conventional chemotherapy could alter plasma levels of active drugs and influence therapeutic efficacy.^{3,4} There are a large number of *in vitro* studies exploring the possible benefits of combining herbal components with anticancer agents, fewer *in vivo* studies, and very limited clinical data addressing efficacy and safety of combinations. Three illustrative examples include grapefruit juice, St. John's wort and chrysin. Highlighting these examples provides a viewpoint on the current understanding and underscores pharmacological concepts relevant to a range of combinations currently used by patients or that may arise with new therapeutics.

■ GRAPEFRUIT JUICE AND ETOPOSIDE

Grapefruit juice is probably the most familiar basis of food-drug interactions, arising from well-known influences on oral cholesterol-lowering drugs and selective serotonin reuptake inhibitors on the basis of irreversible inhibition of intestinal cytochrome P450 3A4 (CYP3A4).^{5–7} *In vitro* microsomal and clinical studies revealed that furanocoumarins, including 6,7-dihydroxybergamottin (Figure 1), are the bioactive constituents in grapefruit juice responsible for intestinal CYP3A4 inhibition.^{6,8} The topoisomerase II inhibitor etoposide (Figure 1), a first line treatment for small cell lung cancer, also applied in refractory testicular tumors and leukemia, is also mainly metabolized by CYP3A4, and to a lesser extent CYP1A2 and CYP2E1.^{9,10} Thus, inhibition of intestinal CYP3A4 by orally administered grapefruit juice has been hypothesized to result in reduced, presystemic etoposide metabolism.

On the basis of furanocoumarin inhibition of CYP3A4, and the relevance of this enzyme to etoposide activity, drinking grapefruit juice with etoposide administration may result in increased bioavailability of the orally administered drug. In a randomized crossover study six cancer patients were treated

sequentially with etoposide either as intravenous infusion, orally, or orally 15 min after drinking grapefruit juice.¹¹ While the area under the curve (AUC) was highest for intravenous infusion, there was a decrease of 26% in the AUC for orally administered etoposide when it was given after grapefruit juice, suggesting decreased etoposide bioavailability for the combination. This influence might be explained by the inhibition of intestinal uptake transporters after grapefruit juice consumption as demonstrated in cell and other clinical studies, and suggests a relevant impact of a food on chemotherapy drug bioavailability.^{6,12}

■ ST. JOHN'S WORT AND IMATINIB, DOCETAXEL, AND IRINOTECAN

St. John's wort (SJW) is a perennial plant the extracts of which from the flowering portion have been used over decades in Europe and the US to treat depression, anxiety, and sleeping disorders. In 2002, a population study in the US revealed that 14% of participants took weekly herbal supplements for improving general health with the fourth most common being SJW.¹³ SJW was shown to be a potent inducer of CYP3A4 in human hepatocytes and in healthy volunteers.^{14,15} The bioactive compound hyperforin (Figure 1) appears to be responsible for SJW mediated CYP3A4-induction.¹⁶ Like grapefruit juice, but in the opposite direction, there is clinical evidence suggesting that CYP3A4-mediated drug metabolism increased, and therefore bioavailability decreased, after taking high-hyperforin extracts.^{17,18}

Imatinib (Figure 1) is a specific tyrosine kinase inhibitor used in targeted anticancer therapy of advanced Philadelphia chromosome positive leukemia and gastrointestinal stromal tumors.¹⁹ It is mainly metabolized by CYP3A4 to N-desmethylimatinib with a potency similar to imatinib.²⁰ The pharmacokinetic profile of oral imatinib before and after oral long-term administration of SJW extract in healthy volunteers exhibited a decrease in the AUC for imatinib of 30% and an apparent oral clearance increase of 43%.²¹ A similar significant reduction in imatinib bioavailability after long-term intake of SJW was also observed in which the imatinib AUC decreased by 32% after SJW administration.²² These findings indicate the potential for a clinically relevant interaction between SJW and imatinib, and the product information for imatinib by the European Medicines Agency now reflects this. SJW is listed as a substance that may decrease imatinib plasma concentrations significantly and increase the risk of therapy failure, therefore avoiding concomitant use is suggested.²³

Received: January 23, 2019

Published: February 7, 2019

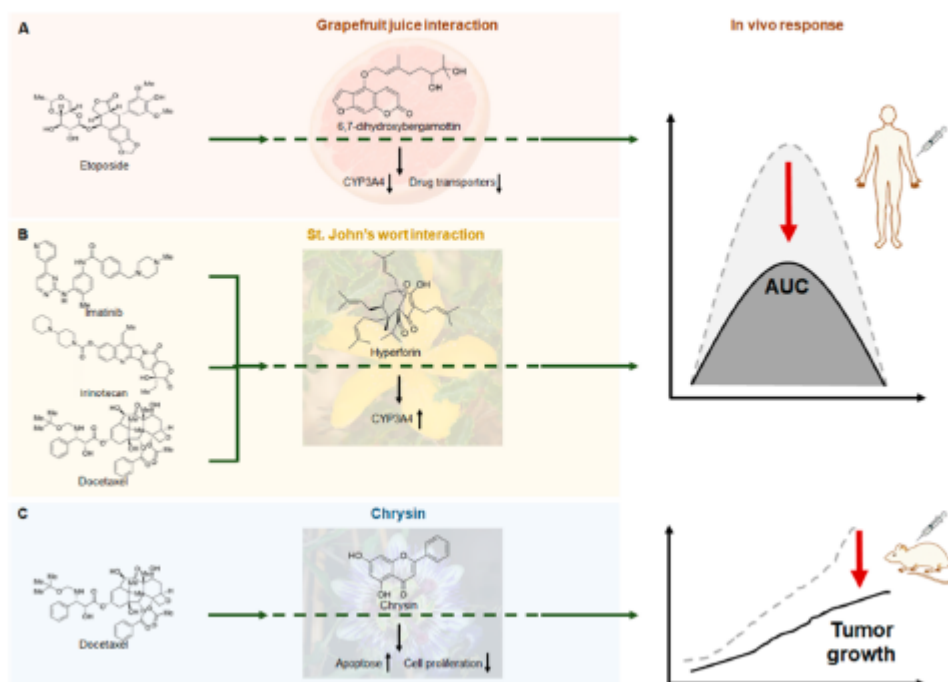


Figure 1. Clinically observed pharmacokinetics-based food/herb–drug interactions for grapefruit juice (A) and St. John's wort (B) in cancer patients and potential interactions for chrysin (C) in anticancer treatment.

A significant decrease in bioavailability after SJW administration was also evident for intravenous docetaxel (Figure 1),²⁴ an anticancer drug widely used for breast, lung, and ovarian carcinomas.²⁵ Docetaxel is a microtubule stabilizer mainly metabolized by CYP3A4 and CYP3A5 to oxidized metabolites with reduced anticancer efficacy observed in cell lines and mice.²⁶ In human hepatocytes, decreased docetaxel plasma concentration after hyperforin exposure at physiological concentrations promoted docetaxel-metabolism.²⁷ In line with this observation, in cancer patients, after oral long-term intake of SJW, the docetaxel AUC decreased by 12%.²⁴ Interestingly, fewer docetaxel-related side effects were observed but the sample size was very small. Thus, while the reduced therapeutic levels associated with SJW suggest a combined use of docetaxel and SJW should be avoided, further studies are anticipated to explore the potential for reducing side effects.

Another anticancer drug with significant clinical SJW interactions is the topoisomerase I inhibitor irinotecan (Figure 1). It is metabolized by CYP3A4 to the more active 7-ethyl-10-hydroxycamptothecin (SN-38);²⁸ therefore, increased CYP3A4 activity could result in undertreatment of patients due to lowered bioavailability of the active drug metabolite. In cancer patients, SJW led to a 42% decrease in SN-38-plasma levels of the intravenously delivered drug.²⁹ This observation suggests possible compromised antitumor activity, however myelosuppression was substantially reduced for the combination, an observation requiring further studies to explore whether this alleviation is only due to lowered bioavailability of the active drug metabolite or if other mechanisms contribute.

A number of examples suggest a real potential for relevant herb–drug interactions generally;^{30,31} however, alterations in CYP activity were generally absent after short-term SJW.^{15,31} The relevance of herbal therapy regimen dependency for the interaction of SJW with irinotecan could also be demonstrated in experimental animals wherein short-term (3 days) SJW treatment did not alter the pharmacokinetics of irinotecan and SN-38, but long-term (14 days) SJW resulted in 34.2% reduced AUC for SN-38 along with significantly increased clearance.³² In addition, coadministration resulted in less body weight loss, significantly reduced the severity score for early and late onset diarrhea ($p < 0.05$) and reduced hematological toxicities. The alleviated side effects could be related to drug pharmacokinetics, but in a follow-up study, it was demonstrated that SJW–irinotecan coadministration was accompanied by the reduction of pro-inflammatory cytokines and intestinal epithelium apoptosis, compared to the irinotecan-only treated control.³³ These data illustrate the need for research on herbal active ingredients and their mode of action.

■ CHRYSIN AND IRINOTECAN OR DOCETAXEL

Chrysin (Figure 1) is a naturally occurring flavone present in plant extracts from *Passiflora caerulea* and in honey and is commonly used as an herbal supplement to boost testosterone levels.^{34,35} On the basis of observations in intestinal cells, it is hypothesized that taking chrysin supplements may induce the metabolic enzyme uridine diphosphate glucuronosyltransferase 1A1 (UGT1A1) in the gastrointestinal mucosa.³⁶ This up-regulation could not be confirmed in mice heterozygous for the human *UGT1* locus,³⁷ an observation in line with *in vivo* data for the topoisomerase I inhibitor irinotecan, which is

inactivated by UGT1A1-mediated glucuronidation.²⁸ Oral chrysin cotreatment did not alter the pharmacokinetics of intravenous irinotecan in colorectal cancer patients compared to historical controls.³⁸ However, the low rate of diarrhea observed in this study raised the hypothesis that chrysin may reduce the severity of delayed diarrhea, although this needs to be further investigated. The opposing results for chrysin observed *in vitro* and *in vivo* could be based on the low systemic bioavailability of orally administered chrysin, as demonstrated *in vitro* in caco-2 and Hep2G cells and confirmed in healthy volunteers.^{39,40} Most likely, extensive presystemic intestinal and hepatic glucuronidation and sulfation limit possible chrysin interaction to the intestine.³⁹ This offers a potential explanation for the observed reduction in severity of irinotecan-induced diarrhea while plasma levels were not affected by cotreatment with chrysin.

Recently it was shown that chrysin itself suppresses tumor growth of melanoma cells *in vitro* and in mice.⁴¹ Anticancer activity of chrysin was also demonstrated in breast and lung cell lines and could be confirmed in animal models.³⁴ Underlying mechanisms involve decrease in cell proliferation, induction of apoptosis, and reduction of inflammation.⁴² Also, chrysin has the potential to increase antitumor activity of anticancer drugs and to alleviate side effects.^{34,42} Co-exposure of cells to chrysin and docetaxel resulted in increased induction of apoptosis and in a respective xenograft model, the combination was more efficient in delaying tumor growth and reducing the size of tumors.⁴³ In addition, a docetaxel-induced inflammation indicator, paw edema, was reduced by 25% when chrysin was administered orally before intravenous docetaxel treatment. Clinical evidence demonstrating anticancer activity of chrysin is missing and the relevance of these findings needs to be considered critically considering the low systemic bioavailability of chrysin.

CONCLUSIONS AND OUTLOOK

Herbal supplements are largely used among cancer patients, but clinical evidence for their effects on anticancer drugs is limited. Clinically relevant combinations mainly result in lowered bioavailability of active drug metabolites potentially risking under-treatment in cancer patients.^{11,21,22,24,29} For SJW and docetaxel or irinotecan, *in vitro* results corresponded with *in vivo* responses in animals and patients.^{24,27,29,32} While this observation certainly cannot be generalized, it provides a case to suggest the potential relevance of addressing *in vitro* observations of possible compounds that interfere with drug metabolism.⁴⁴ On the other hand, *in vitro*, chrysin increases UGT1A1 levels, but this induction could not be confirmed in animals and patients presumably due to the low bioavailability of the orally administered herb.^{36,38–40} Bioavailability of an herbal active constituent should be carefully evaluated to draw significant conclusions on potential interactions. Chrysin and grapefruit juice drug interactions seemed to be limited to the intestine.^{11,38} SJW can also modulate hepatic CYP enzymes and clinically significant interactions for intravenous^{24,28} and orally administered drugs.^{21,22}

While there is extensive pharmacokinetic data for herb-drug interactions, there is limited evidence addressing side effects and mechanisms beyond metabolism.^{24,29,38} Reduction of side effects might be explained by reduced drug-bioavailability for herb-drug cotreatment or other mechanisms.^{33,43} Furthermore, herbal supplements have chemoprevention activity or are synergistic with conventional drugs while alleviating side

effects.^{42,45} Thus, there is a need during the development of new drugs and therapeutic strategies for continued attention to potential combination effects. Critical aspects include induction and inhibition of metabolizing enzymes, efflux and influx transporters, detailed knowledge of herbal bioactive ingredients, altered molecular signaling pathways, the translational relevance of possible adverse interactions, and even the possibility for beneficial relationships.

AUTHOR INFORMATION

ORCID

Susanne M. Geisen: 0000-0002-9394-0274

Shana J. Sturla: 0000-0001-6808-5950

Notes

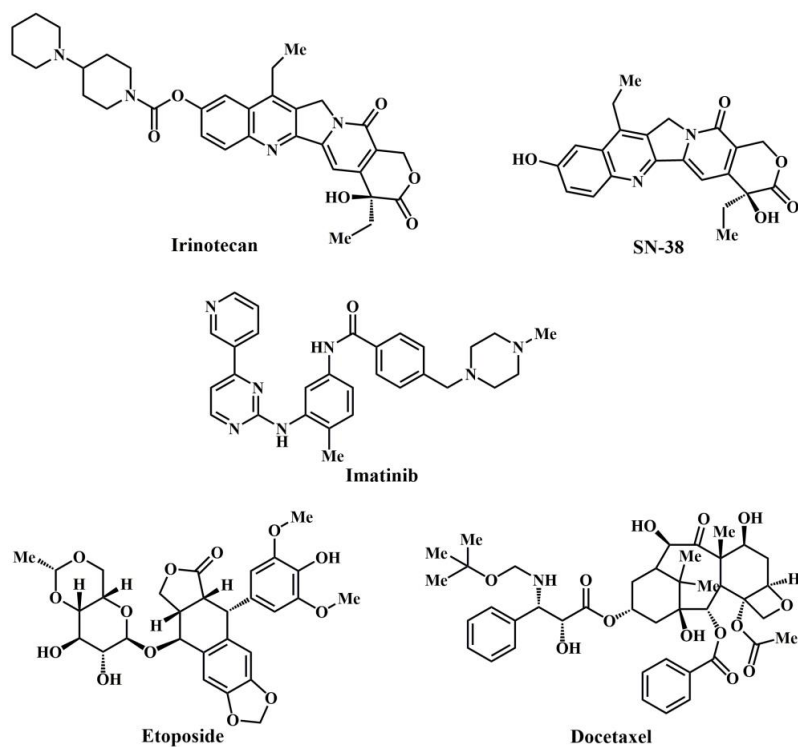
The authors declare no competing financial interest.

REFERENCES

- (1) Firkins, R., Eisfeld, H., Keinki, C., Buentzel, J., Hochhaus, A., Schmidt, T., and Huebner, J. (2018) The use of complementary and alternative medicine by patients in routine care and the risk of interactions. *J. Cancer Res. Clin. Oncol* 144, 551–557.
- (2) Judson, P. L., Abdallah, R., Xiong, Y., Elbert, J., and Lancaster, J. M. (2017) Complementary and Alternative Medicine Use in Individuals Presenting for Care at a Comprehensive Cancer Center. *Integr. Cancer Ther.* 16, 96–103.
- (3) Gorman, G. S., Coward, L., Darby, A., and Rasberry, B. (2013) Effects of herbal supplements on the bioactivation of chemotherapeutic agents. *J. Pharm. Pharmacol.* 65, 1014–1025.
- (4) Meijerman, I., Beijnen, J. H., and Schellens, J. H. M. (2006) Herb-drug interactions in oncology: Focus on mechanisms of induction. *Oncologist* 11, 742–752.
- (5) Bailey, D. G., Dresser, G., and Arnold, J. M. O. (2013) Grapefruit–medication interactions: Forbidden fruit or avoidable consequences? *Can. Med. Assoc. J.* 185, 309–316.
- (6) Hanley, M. J., Cancalon, P., Widmer, W. W., and Greenblatt, D. J. (2011) The effect of grapefruit juice on drug disposition. *Expert Opin. Drug Metab. Toxicol.* 7, 267–286.
- (7) Low, K. S., Bailey, D. G., Fontana, R. J., Janardan, S. K., Adair, C. H., Fortlage, L. A., Brown, M. B., Guo, W., and Watkins, P. B. (1997) Grapefruit juice increases felodipine oral availability in humans by decreasing intestinal CYP3A protein expression. *J. Clin. Invest.* 99, 2545–2553.
- (8) Lian-qing, G., and Yasushi, Y. (2016) Inhibition of cytochrome P450 by furanocoumarins in grapefruit juice and herbal medicines. *Acta Pharmacol. Sin.* 25, 129–136.
- (9) Kawashiro, T., Yamashita, K., Zhao, X. J., Koyama, E., Tani, M., Chiba, K., and Ishizaki, T. (1998) A study on the metabolism of etoposide and possible interactions with antitumor or supporting agents by human liver microsomes. *J. Pharmacol. Exp. Ther.* 286, 1294–1300.
- (10) Lovett, B. D., Strumberg, D., Blair, I. A., Pang, S., Burden, D. A., Megonigal, M. D., Rappaport, E. F., Rebbeck, T. R., Osheroff, N., Pommier, Y. G., and Felix, C. A. (2001) Etoposide Metabolites Enhance DNA Topoisomerase II Cleavage near Leukemia-Associated MLL Translocation Breakpoints. *Biochemistry* 40, 1159–1170.
- (11) Reif, S., Nicolson, M. C., Bisset, D., Reid, M., Kloff, C., Jaehde, U., and McLeod, H. L. (2002) Effect of grapefruit juice intake on etoposide bioavailability. *Eur. J. Clin. Pharmacol.* 58, 491–494.
- (12) Glaeser, H., Bailey, D. G., Dresser, G. K., Gregor, J. C., Schwarz, U. I., McGrath, J. S., Jolicoeur, E., Lee, W., Leake, B. F., Tirona, R. G., and Kim, R. B. (2007) Intestinal Drug Transporter Expression and the Impact of Grapefruit Juice in Humans. *Clin. Pharmacol. Ther.* 81, 362–370.
- (13) Kaufman, D. W., Kelly, J. P., Rosenberg, L., Anderson, T. E., and Mitchell, A. A. (2002) Recent patterns of medication use in the ambulatory adult population of the United States: The slone survey. *JAMA* 287, 337–344.

- (14) Moore, L. B.; Goodwin, B.; Jones, S. A.; Wisely, G. B.; Serabjit-Singh, C. J.; Willson, T. M.; Collins, J. L.; and Kiewer, S. A. (2000) St. John's wort induces hepatic drug metabolism through activation of the pregnane X receptor. *Proc. Natl. Acad. Sci. U. S. A.* **97**, 7500–7502.
- (15) Markowitz, J. S.; DeVane, C. L.; Boulton, D. W.; Carson, S. W.; Nahas, Z.; and Risch, S. C. (2000) Effect of St. John's wort (*Hypericum perforatum*) on cytochrome P-450 2D6 and 3A4 activity in healthy volunteers. *Life Sci.* **66**, PL133–139.
- (16) Komoroski, B. J.; Zhang, S.; Cai, H.; Hutzler, J. M.; Frye, R.; Tracy, T. S.; Strom, S. C.; Lehmann, T.; Ang, C. Y.; Cui, Y. Y.; and Venkataraman, R. (2004) Induction and inhibition of cytochromes P450 by the St. John's wort constituent hyperforin in human hepatocyte cultures. *Drug Metab. Dispos.* **32**, 512–518.
- (17) Whitten, D. L.; Myers, S. P.; Hawrelak, J. A.; and Wohlmut, H. (2006) The effect of St. John's wort extracts on CYP3A: a systematic review of prospective clinical trials. *Br. J. Clin. Pharmacol.* **62**, 512–526.
- (18) Madabushi, R.; Frank, B.; Drewelow, B.; Derendorf, H.; and Butterweck, V. (2006) Hyperforin in St. John's wort drug interactions. *Eur. J. Clin. Pharmacol.* **62**, 225–233.
- (19) Iqbal, N., and Iqbal, N. (2014) Imatinib: A Breakthrough of Targeted Therapy in Cancer. *Chemother. Res. Pract.* **2014**, 357027.
- (20) Peng, B.; Lloyd, P.; and Schran, H. (2005) Clinical Pharmacokinetics of Imatinib. *Clin. Pharmacokinet.* **44**, 879–894.
- (21) Frye, R. F.; Fitzgerald, S. M.; Lagattuta, T. F.; Hruska, M. W.; and Egorin, M. J. (2004) Effect of St. John's wort on imatinib mesylate pharmacokinetics. *Clin. Pharmacol. Ther.* **76**, 323–329.
- (22) Smith, P.; Bullock, J. M.; Booker, B. M.; Haas, C. E.; Berenson, C. S.; and Jusko, W. J. (2004) The influence of St. John's Wort on the pharmacokinetics and protein binding of imatinib mesylate. *Pharmacotherapy* **24**, 1508–1514.
- (23) Summary of product characteristics. https://www.ema.europa.eu/documents/product-information/glivec-epar-product-information_en.pdf (accessed on 15.01.2019).
- (24) Goey, A. K. L.; Meijerman, I.; Rosing, H.; Marchetti, S.; Mergui-Roelvink, M.; Keessen, M.; Burgers, J. A.; Beijnen, J. H.; and Schellens, J. H. M. (2014) The Effect of St. John's Wort on the Pharmacokinetics of Docetaxel. *Clin. Pharmacokinet.* **53**, 103–110.
- (25) Herbst, R. S., and Khuri, F. R. (2003) Mode of action of docetaxel - a basis for combination with novel anticancer agents. *Cancer Treat. Rev.* **29**, 407–415.
- (26) Vuilhorgne, M.; Gaillard, C.; Sanderink, G. J.; Royer, L.; Monsarrat, B.; Dubois, J.; and Wright, M. (1994) Metabolism of Taxoid Drugs. In *Taxane Anticancer Agents* (Gunda, L., Georg, T. T. C., Ojima, I., and Vyas, D. M., Eds.), pp 98–110, American Chemical Society.
- (27) Komoroski, B. J.; Parise, R. A.; Egorin, M. J.; Strom, S. C.; and Venkataraman, R. (2005) Effect of the St. John's wort constituent hyperforin on docetaxel metabolism by human hepatocyte cultures. *Clin. Cancer Res.* **11**, 6972–6979.
- (28) Mathijssen, R. H. J.; van Alphen, R. J.; Verweij, J.; Loos, W. J.; Nooter, K.; Stoter, G.; and Sparreboom, A. (2001) Clinical Pharmacokinetics and Metabolism of Irinotecan (CPT-11). *Clin. Cancer Res.* **7**, 2182–2194.
- (29) Mathijssen, R. H.; Verweij, J.; de Bruijn, P.; Loos, W. J.; and Sparreboom, A. (2002) Effects of St. John's wort on irinotecan metabolism. *J. Natl. Cancer Inst.* **94**, 1247–1249.
- (30) Dresser, G. K.; Schwarz, U. I.; Wilkinson, G. R.; and Kim, R. B. (2003) Coordinate induction of both cytochrome P4503A and MDRI by St. John's wort in healthy subjects. *Clin. Pharmacol. Ther.* **73**, 41–50.
- (31) Wang, Z. Q.; Gorski, C.; Hamman, M. A.; Huang, S. M.; Lesko, L. J.; and Hall, S. D. (2001) The effects of St. John's wort (*Hypericum perforatum*) on human cytochrome P450 activity. *Clin. Pharmacol. Ther.* **70**, 317–326.
- (32) Hu, Z.; Yang, X.; Ho, P. C.-L.; Chan, E.; Chan, S. Y.; Xu, C.; Li, X.; Zhu, Y.-Z.; Duan, W.; Chen, X.; Huang, M.; Yang, H.; and Zhou, S. (2005) St. John's Wort Modulates the Toxicities and Pharmacokinetics of CPT-11 (Irinotecan) in Rats. *Pharm. Res.* **22**, 902–914.
- (33) Hu, Z.-P.; Yang, X.-X.; Chan, S. Y.; Xu, A.-L.; Duan, W.; Zhu, Y.-Z.; Sheu, F.-S.; Boelsterli, U. A.; Chan, E.; Zhang, Q.; Wang, J.-C.; Ee, P. L. R.; Koh, H. L.; Huang, M.; and Zhou, S.-F. (2006) St. John's wort attenuates irinotecan-induced diarrhea via down-regulation of intestinal pro-inflammatory cytokines and inhibition of intestinal epithelial apoptosis. *Toxicol. Appl. Pharmacol.* **216**, 225–237.
- (34) Mani, R., and Natesan, V. (2018) Chrysin: Sources, beneficial pharmacological activities, and molecular mechanism of action. *Phytochemistry* **145**, 187–196.
- (35) Maughan, R. J.; King, D. S.; and Lea, T. (2004) Dietary supplements. *J. Sports Sci.* **22**, 95–113.
- (36) Galijatovic, A.; Walle, U. K.; and Walle, T. (2000) Induction of UDP-glucuronosyltransferase by the flavonoids chrysin and quercetin in Caco-2 cells. *Pharm. Res.* **17**, 21–26.
- (37) Bonzo, J. A.; Bélanger, A.; and Tukey, R. H. (2007) The role of chrysin and the Ah receptor in induction of the human UGT1A1 gene in vitro and in transgenic UGT1 mice. *Hepatology* **45**, 349–360.
- (38) Tobin, P. J.; Beale, P.; Noney, L.; Liddell, S.; Rivory, L. P.; and Clarke, S. (2006) A pilot study on the safety of combining chrysin, a non-absorbable inducer of UGT1A1, and irinotecan (CPT-11) to treat metastatic colorectal cancer. *Cancer Chemother. Pharmacol.* **57**, 309–316.
- (39) Walle, T.; Otake, Y.; Brubaker, J. A.; Walle, U. K.; and Halushka, P. V. (2001) Disposition and metabolism of the flavonoid chrysin in normal volunteers. *Br. J. Clin. Pharmacol.* **51**, 143–146.
- (40) Walle, U. K.; Galijatovic, A.; and Walle, T. (1999) Transport of the flavonoid chrysin and its conjugated metabolites by the human intestinal cell line Caco-2. *Biochem. Pharmacol.* **58**, 431–438.
- (41) Sassi, A.; Maatouk, M.; El gueder, D.; Bréouich, I. M.; Abdelkefi-Ben Hatira, S.; Jemni-Yacoub, S.; Ghedira, K.; and Chekir-Ghedira, L. (2018) Chrysin, a natural and biologically active flavonoid suppresses tumor growth of mouse B16F10 melanoma cells: In vitro and In vivo study. *Chem-Biol. Interact.* **283**, 10–19.
- (42) Kasala, E. R.; Bodduluri, L. N.; Madana, R. M.; V. A. K.; Gogoi, R.; and Barua, C. C. (2015) Chemopreventive and therapeutic potential of chrysin in cancer: mechanistic perspectives. *Toxicol. Lett.* **233**, 214–225.
- (43) Lim, H.-K.; Kim, K. M.; Jeong, S.-Y.; Choi, E. K.; and Jung, J. (2017) Chrysin Increases the Therapeutic Efficacy of Docetaxel and Mitigates Docetaxel-Induced Edema. *Integr. Cancer Ther.* **16**, 496–504.
- (44) Venkataraman, R.; Komoroski, B.; and Strom, S. (2006) In vitro and in vivo assessment of herb drug interactions. *Life Sci.* **78**, 2105–2115.
- (45) You, M.-K.; Kim, H.-J.; Kook, J. H.; and Kim, H.-A. (2018) St. John's Wort Regulates Proliferation and Apoptosis in MCF-7 Human Breast Cancer Cells by Inhibiting AMPK/mTOR and Activating the Mitochondrial Pathway. *Int. J. Mol. Sci.* **19**, 966.

Appendix II: Clinical evidence for pharmacokinetics-based herb-drug interactions with chemotherapy drugs



Reprinted with permission from

Barozzi N., Geisen S.M. and Sturla S.J.

Manuscript in preparation

Barozzi N., Geisen S.M. and Sturla S. J. wrote the manuscript.

Clinical evidence for pharmacokinetics-based herb-drug interactions with chemotherapy drugs (Review)

Nadia Barozzi^{1,2,3}, Susanne M. Geisen², Shana J. Sturla²

¹Healthy4Life, P.O.Box 41 4009 Basel Switzerland

²Department of Health Science and Technology, ETH Zurich, 8092 Zurich, Switzerland

³School of Pharmacy, The University of Queensland, 4102 Brisbane, Australia

Correspondence to: Professor Shana J. Sturla, Laboratory of Toxicology, Department of Health Sciences and Technology, ETH Zürich, Schmelzbergstrasse 9, 8092 Zürich, sturlas@ethz.ch

Keywords

pharmacokinetics

metabolism

herbs

cancer chemotherapy

Abstract

Purpose: Cancer patients commonly take herbal supplements to limit side effects experienced from chemotherapy. Potential risks are associated with the possibility of altered therapeutic efficacy or safety due to altered drug pharmacokinetics. The purpose of this review is to summarize available clinical data concerning the effect of herbal co-administration on responses to single chemotherapy agents.

Method: A non-systematic PubMed search of commonly used herb, supplement or food products combined with chemotherapy drugs identified 12 clinical studies with pharmacokinetic data (4 drugs and 8 substances).

Results: Clinical data is available concerning the combined use of irinotecan with cannabis, milk thistle, St. Johns Wort (SJW), and chrysin; imatinib with SJW; etoposide with grapefruit juice; and docetaxel with cannabis, garlic, SJW and astragalus. While in many studies, there was no significant evidence for altered drug pharmacokinetics, 6 showed clinically relevant interactions, including irinotecan, imatinib and docetaxel with SJW, and etoposide with grapefruit juice. Typically there was decreased total drug exposure, while data concerning impacts on drug clearance were variable.

Conclusion: Although a large number of patients undergoing cancer chemotherapy use herbal supplements, clinical pharmacokinetics data for interactions are limited, and most involve very small sample sizes and outcomes that are inconclusive or show no evidence for interaction. Nonetheless, there does exist clinical evidence of altered drug exposures due to herb-drug combinations, suggesting that more clinical studies are warranted to create evidence-based understanding of clinically relevant herb-drug interactions.

Contents

1 Introduction

2 Search strategy and selection of examples addressed in this review

3 Irinotecan and combinations with cannabis, milk thistle, St. Johns Wort, and chrysin

4 Imatinib and combinations with St. John's Wort

5 Etoposide in combination with grapefruit juice

6 Docetaxel and combinations with cannabis, garlic, St. John's Wort and astragalus

7 Special considerations in herb-drug interactions and clinical studies

8 Conclusion

1. Introduction

Cancer chemotherapy can be extremely effective, but also can cause debilitating side effects. For this reason, many patients turn to dietary or herbal supplements with the goal of reducing side effects, addressing treatment-associated malnourishment or fatigue, or even to improve therapeutic efficacy (Akbulut 2011; Conklin 2000; Khurana et al. 2018). It has been estimated that up to 80% of cancer survivors have used a supplement, including herbal, mineral, vitamin or multivitamin supplements (Firkins et al. 2018; Gillett et al. 2012; Miller et al. 2008; Sparreboom et al. 2004a). The fact that most herbal or dietary supplements are natural compounds contributes to the notion that they are implicitly safe, and can be taken without consultation with a health care professional (Basheti 2017; Samojlik et al. 2013). Likewise, healthcare providers have limited evidence-based tools for making recommendations even if consulted and information on herb-drug interactions is not easily accessible on drug-databases.

Commonly used supplements may interact with cancer chemotherapy by altering pharmacokinetics, however, potentially reducing efficacy (Geisen and Sturla 2019). Plasma concentrations and bioavailability of many drugs, including chemotherapy agents, may be altered due to changes in the efficiencies of absorption, distribution, metabolism or elimination (Boullata and Armenti 2010). The function of predominant metabolic enzymes and drug transporters, i.e. cytochrome P450s, P-glycoprotein, uridine diphosphoglucuronosyl transferase, can impact herb-drug interactions (Gorman et al. 2013; Meijerman et al. 2006). Thus, herbs may alter cellular susceptibility to drugs by inducing relevant metabolic enzyme or transporter activity (Kesarwani K et al. 2013; Ruggiero et al. 2012; Singh and Malhotra 2004), and increased drug persistence can lead to greater adverse responses. Additionally, herbal supplements may change the physiological absorption of a drug by binding in the gastrointestinal tract and inhibiting and/or inducing modifications of the transport of the drug in the intestinal epithelium and liver (Boullata and Armenti 2010).

On the other hand, there is extensive, mostly pre-clinical and early phase clinical data suggesting possible benefits of combined use of herbal supplements during chemotherapy. These include aspects of processes related to ameliorating side effects, such as nausea, vomiting or lack of appetite (Zhang et al. 2018). Some products demonstrate anticancer activity against human cells, or attenuate angiogenesis (Aung et al. 2017; Kaur and Verma 2015; Singh et al. 2016). Furthermore, just as drug efficacy may be reduced due to metabolism, enhancements may result from increased function of drug-activating enzymes that transform pro-drugs into their active forms (Erzinger et al. 2016; Erzinger and Sturla 2011). However, situations when it is safe to concomitantly use herbal supplement during therapies with conventional medicines, especially in cancer patients, are not clearly defined (Ryan et al. 2012; Sontakke et al. 2003).

Lack of information and inconsistency of data supporting the clinical significance of herb-drug interactions makes it difficult to create recommendations and identify research priorities likely to impact relevant therapeutic scenarios. Clinical studies that integrate strategies to address the pharmacokinetic basis of potential herb-drug interactions may be most informative in this regard. Thus, the aim of this review is to provide an overview of the clinical evidence for potentially adverse effects or benefits of co-administration of herbal supplements with chemotherapy drugs. Presented here are the available clinical data assessing the safety and impact on pharmacokinetics of single chemotherapy agents when given in combination with herbal supplements are presented here. We expect that consolidated knowledge of these findings provide an informed perspective and context for what is now known and where further study is needed.

2. Search strategy and selection of examples addressed in this review

For this non-systematic literature review, a series of searches were performed using PubMed combining the name of chemotherapy agents from the national cancer institute website (NIH 2019) and the following list of herbs/supplements/related products utilized by cancer patients compiled based on studies assessing supplement utilization in the cancer population (Cheng et al. 2018; Emi et al. 2018; Qianlai and N. 2018):

Acai juice, Agaricus, Allium sativum, Aloe barbadensis/capensis, Aloe vera, Anastrozole, Annona muricata, Arnica gel, Ashwagandha, Astragalus, Atractylodes macrocephala, Bilberry, Black cohosh, Black vinegar, Blueberry, Chrysin, Camelia sinesis, Cannabis, Cat's claw, Chlorophyll, Chondroitin, Coenzyme Q10, Cranberry, Curcuma longa, Curcumin, Dandelion root, Dragon's blood, Echinacea, Fucoidan, Garlic, Ginger, Ginkgo biloba, Ginseng, Glucosamine, Glutamine, Grape seed extract, Green tea, Hawthorn, Hedyotis diffusa, Isoflavone, Lecithin, Lutein, Lycopene, Matricaria recutita, Melatonin, Milk thistle, Moringa oleifera, Mushroom extracts, Omega-3 fatty acids, Panax ginseng, Parsley, Peppermint oil, Pomegranate, Probiotics, Propolis, Protein supplement, Quercetin, Rhizoma rhei, Salvia miltiorrhiza, Saw palmetto, Scutellaria, Soy supplement, Spirulina, St. John's wort, Taraxacum mongolicum, Tart cherry, Turmeric, Uncaria tomentosa, Valeriana officinalis, Ziziphus spinosa. The results were refined using the term "interaction and/or pharmacokinetics." Studies involving mixtures of herbal products were excluded. The number of total results was not recorded, however, we refined the results to include clinical studies assessing the potential interaction of chemotherapy drugs and herbal supplements, and that included any monitoring of pharmacokinetics, resulting in 12 studies (Table 1) involving 4 drugs and 8 substances. Results were organized on the basis of the chemotherapy agents used.

3. Irinotecan

Irinotecan is a semi-synthetic derivative of camptothecin, a cytotoxic alkaloid derived from *Camptotheca Acuminata*, a plant historically used in traditional Chinese medicine to treat cancer (CPT-11, Figure 1) (Efferth T et al. 2007). Irinotecan is a topoisomerase I inhibitor, and is metabolized by cytochrome p450 3A4 (CYP3A4) and carboxylesterases to the more active form 7-ethyl-10-hydroxycamptothecin (SN-38, Figure 1) (Mathijssen et al. 2001). SN-38 is inactivated by uridine diphosphate glucuronosyltransferase 1A1 (UGT1A1)-mediated glucuronidation (Mathijssen et al. 2001). Both irinotecan and SN-38 are primarily cleared via hepatic metabolism and biliary excretion. Inhibition of drug metabolism by herbal supplements in patients treated with irinotecan has been hypothesized to reduce drug efficacy due to a decrease in levels of the active metabolite (Gorman et al. 2013). Therefore, studies assessing the influence of herbal supplements including cannabis, milk thistle, St John Wort (SJW) and Chrysin on drug metabolism in cancer patients undergoing irinotecan therapy have been conducted to clarify clinical implications of concurrent use.

Cannabis is an annual herbaceous plant in the Cannabaceae family and its primary active ingredient, namely delta-9-tetrahydrocannabinol (THC) (Ross et al. 2005) acts on the endocannabinoid system, a regulator of homeostatic mechanisms implicated in nociception, regulation of appetite, and stress (Hohmann and Suplita 2006; Panikashvili et al. 2005; van der Stelt and Di Marzo 2003). THC was approved by the Food and Drug administration (FDA) in 1986 to alleviate chemotherapy induced nausea and vomiting, to relieve pain, and stimulate appetite in cancer patients (Walsh 2003). Cannabis seems to modulate the activity of several hepatic CYP enzymes with most being inhibitory to CYP3A (Jaeger W. 1996) and P-glycoprotein (P-gp) (Zhu et al.

2006), but repeated administration could result in CYP3A induction (Bornheim and Correia 1990). A drug interaction crossover study was performed in twenty-four cancer patients to assess whether concurrent use of cannabis during anticancer therapies, including irinotecan, leads to clinically significant herb-drug interactions. Twelve patients were treated with irinotecan (600 mg, 1 h intravenous) on day 1 and 21 of a 24-day treatment course and starting from day 10 concomitant with medicinal cannabis (200 ml herbal tea, 1 g/l, 18% THC and 0.8% cannabidiol (CBD)) for 15 consecutive days (Engels et al. 2007). Cannabis administration did not significantly influence exposure to and clearance of irinotecan (Area under the curve extrapolated to infinity ($AUC_{0-\infty}$) 1.04; Confidence interval (CI), 0.96-1.11 and clearance (CL) 0.97; CI, 0.90-1.05, respectively), and therefore the use of cannabis appeared to have no significant effect on irinotecan disposition.

Milk thistle is a plant of the *Asteraceae* which is often used for liver disorders, loss of appetite and dyspepsia (Siegel and Stebbing 2013). The therapeutic parts of the plant are the seeds which contain silymarin (Siegel and Stebbing 2013), a complex mixture of active polyphenolic molecules believed to be responsible for the hepatoprotective effects (Chen et al. 2011). Data from *in vitro* studies with microsomes and hepatocytes suggested that milk thistle inactivates CYP3A4, CYP2C9, UGT1A1, UGT1A6, UGT1A9, and UGT2B7 enzymes (Beckmann-Knopp et al. 2000; Chrungoo et al. 1997; Sridar et al. 2004; Venkataramanan et al. 2000; Zuber et al. 2002) and increases the side effects of drugs metabolized by them (Mohamed and Frye 2011; Venkataramanan et al. 2000). Silybin, another milk thistle flavonoid was shown to downregulate CYP3A4 *in vitro* (Mooiman et al. 2013). Short-, and long-term administration of milk thistle (*Silybum marianum L.*) and its impact on irinotecan pharmacokinetics was investigated by van Erp et al. in 2007 (van Erp et al. 2005) for six cancer patients treated with irinotecan (125 mg/m², 1.5 h intravenous) weekly for 4 weeks. Four days before the second dose, patients received milk thistle (200 mg, orally, three times a day) for 12 consecutive days. Short-term or longer intake (4 vs. 12 days) of milk thistle had no significant impact on irinotecan clearance. Plasma concentrations of silybin were measured following milk thistle intake and appeared to be too low to influence the function of CYP3A4 or UGT1A1 in patients, indicating that milk thistle at the administered dose is unlikely to alter irinotecan metabolism *in vivo* (van Erp et al. 2005). Potential limitations in discerning the significance of the clinical observations are related to the limited sample size, no randomization and lack of a placebo arm or that the applied, manufacturer-recommended silybin dose may be too low to attain an effect. Nonetheless, the data suggest that the risk of adverse interactions between milk thistle and chemotherapeutic agents that are CYP3A4 or UGT1A1 substrates may be low (van Erp et al. 2005).

SJW is a perennial plant and widely used in Europe and the USA to treat depression, anxiety, and sleeping disorders (Sparreboom et al. 2004b). The two most common bioactive compounds of SJW are hyperforin and hypericin. SJW is a potent inducer of human CYP3A4 (Madabushi et al. 2006) and P-gp (Moore et al. 2000). In an unblinded, randomized, controlled crossover study conducted by Mathijssen et al. in 2002 the influence of SJW on plasma concentrations of SN-38 was assessed in five cancer patients. The subjects were treated with irinotecan (350 mg/m², 1.5 h intravenous) once every 3 weeks and SJW (300 mg tablet, three times a day) for 18 days (Mathijssen et al. 2002). Results indicated that when SJW was co-administered, the AUC of SN-38 decreased by 42% ($p=0.033$) relative to irinotecan alone. Furthermore, the AUC ratio of its CYP3A4-generated detoxification product 7-ethyl-10-[4-N-(5-aminopentanoic acid)-1-piperidino] carbonyloxy camptothecin (APC) was reduced by 28% (not statistically significant) (Mathijssen et al. 2002). In the case of the combination, comprised antitumor drug-activity could be the result of the lowered bioavailability of the active drug metabolite. Human studies addressing the effect of SJW on CYP-activity in healthy volunteers

demonstrated increased drug clearance linked with increased CYP3A-activity after long-term SJW administration (Dresser et al. 2003; Wang et al. 2001) However, after short-term SWJ administration, no effect on CYP activity was obvious (Markowitz et al. 2000; Wang et al. 2001). This data suggests that the effect of SJW on drug efficacy depends on therapy regimen and points out the critical need for more studies to establish a clear model for a safe combination strategy. Another factor to consider in herb-drug interactions is the concentration of active herb metabolite as SJW mediated induction of CYP3A is mainly found for high-hyperforin extracts ($\geq 10\text{mg/daily dose}$) (Whitten et al. 2006).

Chrysin is a naturally occurring flavone found in the passion flowers *Passiflora caerulea*, *Passiflora incarnate*, *Pleurotus ostreatus*, chamomile, and *Oroxylum indicum*, commonly used to boost testosterone levels. Chrysin is metabolized by CYP1A2 and appears to reduce of P-gp efflux pump activity (Gyemant et al. 2005). It has been hypothesized that chrysin could induce UGT1A1 in the gastrointestinal mucosa because chrysin was observed to up-regulate UGT1A1 expression in caco-2 cells (Galijatovic et al. 2000). Therefore the safety profile of irinotecan when given together with chrysin was investigated in an open-label pilot study (Tobin et al. 2006). In the study conducted by Tobin et al. in 2006, twenty-one patients with colorectal cancer received irinotecan (350 mg/m^2 , 1.5 h intravenous) once every 3 weeks, one week before and after cyrysin treatment (250 mg, orally, twice a days). They assessed levels of irinotecan and its metabolites SN-38, SN-38-glucuronidate and APC. No adverse responses that could be attributed to chrysin use were evident and no associations between pharmacokinetic parameters and clinical outcome were apparent (Tobin et al. 2006). Patient DNA was analyzed for genetic single nucleotide polymorphisms (SNPs) in UGT1A1, as UGT1A1*28 is associated with a reduced ability to deactivate SN-38 and diarrhea associated with CPT-11 therapy can be increased in patients with this polymorphism. However, no relationship was observed between severity of diarrhea and genotype. The low rate of diarrhea observed in this study raised the hypothesis that chrysin may reduce the severity of delayed diarrhea, but to our knowledge any therapeutic potential of this observation has not been realized.

4. Imatinib

Imatinib is a tyrosine-kinase inhibitor used in the treatment of multiple cancers (Figure 1) (Iqbal and Iqbal 2014). It inhibits the receptor C-kit and the Abelson murine Leukemia (ABL) kinases, including the BCR-ABL fusion protein. Imatinib was first approved by the US Food and Drug Administration in May 2001 to treat patients with advanced Philadelphia chromosome positive chronic myeloid leukemia. It is a targeted therapeutic agent, as BCR-ABL is uniquely expressed by leukemic cells and is essential for their survival (Iqbal and Iqbal 2014). Imatinib is mainly metabolized by CYP3A4 to N-desmethylimatinib with a potency similar to Imatinib (Peng et al. 2005). The drug is a potent competitive inhibitor of CYP2C9, CYP2D6, CYP3A4 and CYP3A5 in cultured human cells.

The impact of SJW as potent inducer of human CYP3A4 (Madabushi et al. 2006) on the disposition of imatinib and its metabolite N-desmethylimatinib was evaluated in an open-label study involving twelve healthy, non-smoking volunteers (Frye et al. 2004). The pharmacokinetic profile of imatinib (400 mg, orally), was assessed 0 to 72 h after imatinib administration before (day one) and during (day 15) the oral intake of SJW extract (300 mg, three times daily), taken from day four to 17. The AUC of imatinib decreased by 30%, ($p=0.0001$), and its apparent oral CL increased by 43% ($p=0.0001$). The half-life of imatinib was reduced during SJW administration as compared with imatinib alone ($p=0.0018$). While N-desmethylimatinib AUC was not affected by SJW, the corresponding maximum concentration (C_{max}) increased by 13% ($p=0.0272$). SJW co-

treatment led to a decrease in imatinib plasma concentrations in all subjects. These findings were consistent with results of previous drug interaction studies conducted with healthy volunteers, and also with *in vitro* data indicating that imatinib is primarily metabolized by CYP3A4 (Frye et al. 2004).

A significant reduced imatinib-bioavailability after long-term SJW administration was also observed by Smith et al 2004 in an open-labeled, cross-over study (Smith P et al. 2004). Ten healthy volunteers received imatinib (400 mg, orally) on day one and 48 h after two weeks of SJW-administration (300 mg, three times daily). The median AUC for imatinib decreased by 32% ($p=0.0001$), C_{max} by 29% ($p<0,01$), and half-life by 21%, ($p<0.01$). In both studies involving healthy volunteers, the decrease in imatinib plasma levels apparently resulting from co-administration with SJW is likely to be clinically relevant and could contribute to treatment failures. Also, the imatinib product information by the European Medicines Agency suggests that patients undergoing imatinib therapy should refrain from taking SJW and concomitant use of any drug that induces CYP3A may necessitate a higher imatinib dose to maintain clinical effectiveness (EMA accessed on 15.01.2019).

5. Etoposide

Etoposide is a derivate of podophyllotoxin, a non-alkaloid toxin lignan from the roots and rhizomes of *Podophyllum* species (Figure 1) (Xu et al. 2009). Etoposide belongs to the topoisomerase II inhibitor class of antineoplastic drugs, compounds that interrupt DNA replication and inhibit the re-annealing of double stranded DNA (Wang 2002). Etoposide is metabolized mainly by CYP3A4, and to a lesser extent CYP1A2 and CYP2E1, to the 3-demethylated product with similar potency at inhibiting topoisomerase II (Kawashiro et al. 1998; Lovett et al. 2001). The involvement of CYP3A4 in the metabolism of etoposide motivates investigation of the potential interactions with herbal supplements, for which there is high potential for modulating CYP3A4 function.

Grapefruit juice is a well-characterized inhibitor of intestinal CYP3A4 with the potential to interfere with pharmacokinetics from orally administered drugs (Bailey et al. 1998). The first grapefruit-drug interaction was discovered for felodipine, a calcium channel antagonist used to decrease blood pressure, where increased drug-bioavailability was linked to grapefruit juice reducing CYP3A4-levels in the intestine and thereby reducing pre-systemic felodipine metabolism (Bailey et al. 1991; Bailey et al. 1998). Since then, increased drug bioavailability along with increased side effects after grapefruit juice administration could also be demonstrated for further CYP3A4-metabolized drugs, among them anticancer agents, cardiovascular agents, central nervous system agents and anti-infective agents (Bailey et al. 1991; Bailey et al. 1998). The major active ingredients in grapefruit juice are furanocoumarins, which irreversibly inhibit intestinal CYP3A4. On the other side, flavonoids like naringin are responsible to inhibit organic anion transporting polypeptides (OATPs) and thereby reduce respective drug uptake when grapefruit juice is taken together (Bailey et al. 2013).

A randomized crossover study was conducted on six patients to evaluate the effect of co-administered grapefruit juice on the bioavailability of oral etoposide (Reif et al. 2002). It was expected that grapefruit juice would inhibit the etoposide metabolizing enzyme CYP3A4 leading to increased AUC of etoposide. Patients were treated sequentially with etoposide (50 mg) either as 1h intravenous infusion, orally with 100 ml water or orally 15 min after the intake of 100 ml of grapefruit juice on day 1, 4, and 8 of a 14-day treatment course. Serial blood samples were drawn before and 0.25, 1.5, 3, 6, 12, and 24 h after oral intake. The AUC for etoposide, after pretreatment with grapefruit juice, decreased by 26% on average in all patients compared to without grapefruit juice. Despite the very small sample size, the results suggested that grapefruit juice co-administration might lead

to a decrease in etoposide bioavailability contrasting results of other studies supporting that grapefruit juice reduces the clearance of drugs that are CYP3A4 substrates (Bailey et al. 1998; Kane and Lipsky 2000). One possible explanation for the observed effect may be an alteration of intestinal drug transporters (Glaeser et al. 2007). Further investigations are needed to elucidate the origin of effect of grapefruit juice co-administration on orally administered drugs and the interplay of CYP3A4 and drug transporter inhibition. Also, the clinical relevance of lowered etoposide bioavailability needs to be evaluated, considering that Lovett et al 2001 suggest similar potency for parent drug and CYP3A4-metabolized 3-demethylated etoposide (Lovett et al. 2001). This examples highlights the need for further research on active drug metabolites for a mechanism based understanding of clinically significant herb-drug interactions.

6. Docetaxel

Docetaxel is a widely used chemotherapy drug belonging to the drug class taxanes, derived from taxol, a natural product extracted from *Taxus brevifolia*, a rare variety of the Pacific yew tree (Figure 1) (Lee et al. 2012). It is anti-mitotic by promoting microtubulin assembly followed by stabilization of the polymer, resulting in cell cycle arrest and inhibition of cell proliferation (Herbst and Khuri 2003). It is mainly inactivated in the liver by CYP3A4- and CYP3A5- (Shou et al. 1998; Stanton et al. 2011) mediated hydroxylation (Stanton et al. 2011).

The relevance of cannabis as a CYP3A- (Jaeger W. 1996) and P-glycoprotein- (P-gp) (Zhu et al. 2006) inhibitor for the pharmacokinetics of docetaxel was tested in a drug interaction study in 12 cancer patients (Engels et al. 2007). Docetaxel (180 mg, 1 h intravenous) was given on day one and 22, while medicinal cannabis (200 ml of herbal tea, 1 g/l, 18% THC and 0.8% CBD, daily) was co-administered starting from day 10 for 15 consecutive days. Blood samples were taken 0.5 h before and up to 47 h after docetaxel administration to measure drug plasma levels. Pharmacokinetics for docetaxel did not change upon cannabis administration (docetaxel AUC 1.11, CI 0.94-1.28; CL 0.95, CI 0.82-1.08) and predominant side effects were not influenced. These results therefore did not suggest cannabis co-administration to affect docetaxel bioavailability.

Garlic is a common spice, yet oral formulations are taken to treat hypertension, diabetes mellitus, hepatotoxicity, cancer, and infections (Bayan et al. 2014). The therapeutic benefits of garlic seem to be associated to allicin, a compound claimed to have antiplatelet, ant proliferative and antibacterial (Bayan et al. 2014). Garlic can inhibit CYP2C9, CYP2C19, CYP3A4 and therefore, may interfere with the action of drugs metabolized by these enzymes (Foster et al. 2001; Hajda et al. 2010; Ho et al. 2010). The influence of garlic supplementation on the pharmacokinetic profile of docetaxel was evaluated prospectively by Cox et al in 2006. Their pharmacokinetic crossover study involved eleven women with metastatic breast cancer treated weekly with docetaxel (30 mg/m², 1 h intravenous) for three weeks and starting from day five to 17, a garlic supplement (600 mg orally, twice a day) was co-administered (Cox et al. 2006). Cycles were repeated every four weeks. Furthermore, two common CYP3A4 and CYP3A5 genetic polymorphisms were evaluated to determine whether genotyping may help predict interactions with docetaxel. The results of the study indicated that co-administering garlic with docetaxel did not significantly influence the pharmacokinetic profile of the drug. However, in an earlier study involving a different drug, saquinavir, Piscitelli et al. (2002) found that garlic supplements taken long term (25 days) impacted systemic exposure to the drug (Piscitelli et al. 2002). Saquinavir is also a CYP3A4 substrate, and in healthy volunteers, its AUC decreased by 51% (Piscitelli et al. 2002). A possible explanation for the contradicting results observed by Cox et al is that patients could eliminate docetaxel following exposure to CYP3A4-inhibitory components present in garlic through compensatory mechanisms. This explanation is

supported by the observation that docetaxel can also be metabolized by CYP2C8 (Komorowski et al. 2005), a function that seems not to be affected by garlic constituents. However, when polymorphisms were taken into account, it was observed that over the 12-day period, garlic decreased the CL of docetaxel in patients carrying a CYP3A5*1A allele, although this difference was not statistically significant ($p = 0.38$) (Cox et al. 2006). The results indicate that garlic supplementation does not appear to significantly affect the disposition of the CYP3A4-substrate drug docetaxel, but suggest more insights could be gained from genotyping drug-metabolizing enzymes as an integral part of herb-drug interaction studies.

SJW is a potent inducer of human CYP3A4 (Madabushi et al. 2006) and P-gp (Moore et al. 2000), with relevant pharmacokinetic interactions for the CYP3A4-dependent anticancer drugs irinotecan (Mathijssen et al. 2002) and imatinib (Frye et al. 2004; Smith P et al. 2004). In vitro studies suggest strong dependence of docetaxel-metabolism on CYP3A (Marre et al. 1996; Shou et al. 1998). Therefore the effect of SJW on the pharmacokinetic profile of docetaxel was investigated by Goey et al in 2014 (Goey et al. 2014). Ten cancer patients with various cancers including bladder, ovarian, non-small cell lung and ureteral cancer were treated with docetaxel (135 mg, 1 h intravenous) on day one and 22 of a 24-day treatment course, while SJW (300 mg, orally, three times daily) was taken starting from day seven for two weeks. Blood samples for characterizing docetaxel pharmacokinetic were taken after each docetaxel infusion. SJW supplementation resulted in a statistically significant 12% decrease in the AUC of docetaxel ($p = 0.045$), while the docetaxel CL increased significantly ($p = 0.045$). Considering the lowered incidence of docetaxel-related toxicities, these results suggest that combined use of docetaxel and SJW should be avoided to prevent potentially reduced efficacy. The effect could be even worse when docetaxel is administered orally as additional intestinal CYP3A4-induction might contribute to docetaxel metabolism.

Echinacea purpurea (*E. purpurea*) is an herbal supplement generally used to stimulate the immune system and to prevent the common cold and upper respiratory infections (EMA 2015). *E. purpurea* has been shown to induce cytochrome P450 3A4 (CYP3A4) both *in vitro* and in humans (Gorski et al. 2004; Hellum et al. 2007; Penzak et al. 2010). Therefore, Goey et al (2013) also explored whether *E. purpurea* affects the pharmacokinetics of the CYP3A4 substrate docetaxel in cancer patients (Goey et al. 2013). Ten cancer patients received docetaxel (135 mg, 60 min IV infusion) before the intake of a commercially available *E. purpurea* extract (20 oral drops three times daily) and 3 weeks later after a 14-day supplementation period with *E. purpurea*. In both cycles, pharmacokinetic parameters of docetaxel were analyzed (Goey et al. 2013). In this study, concomitant use of *E. purpurea* and docetaxel did not show a significant change in the pharmacokinetics of docetaxel. The finding from this study suggests that the used formulation of *E. purpurea* (95% aerial parts and 5% roots) may be combined safely with docetaxel.

Astragalus is an herb largely used in China for therapeutic purposes in diabetes mellitus, fatigue, for hepato- and immune-protective effects and to treat cardiovascular diseases (Auyeung et al. 2016). It contains many different active compounds such as flavonoids, saponins, and polysaccharides and one of the main active ingredients is astragaloside IV (Yu et al. 2005). *Astragalus membranaceus* appears to inhibit CYP3A4, therefore potentially interferes with pharmacokinetics of CYP3A-metabolized drugs (Lau et al. 2013). Jinfukang, an oral liquid formulation approved by the Chinese State Drug Administration for the treatment of non-small cell lung cancer, contains extracts of twelve botanicals including *Astragalus membranaceus*. In a single arm study conducted by Cassileth et al. 2009, the influence of Jinfukang on docetaxel pharmacokinetics was investigated in twenty-one patients with advanced non-small cell lung cancer after failed platinum-based chemotherapy

(Cassileth et al. 2009). Patients were treated with docetaxel (35 mg/m², intravenous) once weekly for three weeks followed by one week of rest. Jinfukang (75 ml/m², orally) was administered on day four to 28 of the chemotherapy cycle. There was wide variation in docetaxel pharmacokinetics across patients but no significant change in AUC and CL with Jinfukang co-administration. Thus, this study was inconclusive concerning a potential effect of Jinfukang co-administration on docetaxel pharmacokinetics. One potential confounding factor is the raw product itself. Even if the Jinfukang extract is standardized regarding its four major constituent botanicals, the concentration of active ingredient is not known. This indicates the importance of knowing concentrations of active components of herb supplements and their careful characterization and standardization.

7. Special considerations in herb-drug interactions and clinical studies

Clinical pharmacokinetics data for the interaction of herbal medicines with conventional pharmaceuticals in cancer patients is limited. Moreover, as evidenced by the examples described here, most data involve very small sample sizes resulting from often stringent inclusion criteria and high patient discontinuation, potentially not representing the usual treatment population. Recruiting larger samples can be costly, and it can be difficult to find patients willing to participate in such studies if not already familiar with herbal supplement use. Also, it cancer patients undergoing chemotherapy may be unwilling to be subject to additional tests or screening, especially requiring additional hospital visits or blood sample collection. For clinical trial sponsors, a solution might be the use of different media channels for attracting patient attention. Clinical trial advertisement is common in some countries, however, once patients have been recruited, follow-up visits are a challenge. Patients undergoing chemotherapy usually are in very poor condition and unwilling to travel to the study site resulting in incomplete data collection. A number of strategies have been evaluated to overcome barriers, such as financial assistance programs that include accommodations for patients and family during treatment, for trained health professionals to travel to the patient's home, or programs to motivate and educate patients about the value of clinical trials (Nipp et al. 2019)

In addition to patient-oriented limitations in recruitment, variability of study design limits direct comparison of results and some special considerations are necessary to improve study design for herb-drug interactions. First, for certain herbal products, good placebo equivalents can require particular effort to develop due to taste, odor, and color being sometimes difficult to mimic with inert ingredients. Cancer patients have heavily compromised health status and take many medications, thus multiple confounding factors make it difficult to assess the existence and causality of any herb-drug interaction, especially on a small sample of patients. Yet, the meaning of findings in healthy volunteers for cancer patients is unclear. Furthermore, the nature of the herbal medicines themselves, being derived from plant sources that vary in species, cultivating conditions, and concentration of bioactive constituents, can be a huge confounding factor. Variable extraction protocols and processing can alter the effects from even the same raw material and in processing, herbal extracts may become contaminated or contain impurities or toxicants (Ribnicky et al. 2008). Legal requirements that allow the implementation of good practices, tightly regulated for conventional medicine may be poorly controlled for plant products, generally sold as food supplements for which a regulatory framework may not exist (Sahoo et al. 2009). More stringent regulatory process may improve herbal products quality and safety amongst cancer patients.

To overcome challenges with regard to interaction studies and related research outcomes, it could be very helpful to introduce measurements for standardization of effect, e.g. plasma levels of herbal bioactive

constituent (Engels et al. 2007; van Erp et al. 2005). This approach is limited as often the active herbal ingredients(s) are not clearly defined. Thus, research to better identify active compounds in plants and understand mixture effects on pharmacology remains important (Lau et al. 2013; Whitten et al. 2006). Also, a common basis of herb-drug interactions is altered biotransformation by CYP450s, P-gp, UGT, and other drug-metabolizing enzymes (Shen 2008). Therefore, metabolic dependency of drug action should be actively explored to help predict and avoid potential adverse herb-drug interactions. Knowledge of drug-metabolism and active metabolites is important to predict therapy outcome and levels of active metabolites should be included in clinical studies to draw significant conclusion from pharmacokinetic studies on overall drug efficacy. Furthermore, the potential of polymorphisms in drug-metabolizing enzymes emphasized the importance of genotyping in pharmacogenomics strategies for guiding combination therapy. Only two studies presented here included genotyping of drug metabolizing enzymes and the results are not conclusive (Cox et al. 2006; Tobin et al. 2006), indicating knowledge about the specificity of particular enzymes or their overlapping function presents a challenge for effective study design.

Aside from basic research and clinical studies of herb-drug interactions, another important approach is the design of drugs with attention to avoiding metabolic pathway alerts. For example, the thiophene moiety present in certain drugs (e.g. tienilic acid, suprofen, and ticlopidine) is a structural alert due to several thiophene-containing drugs having been withdrawn from the market due to hepatotoxicity and nephrotoxicity associated with CYP inhibition. Therefore, better understanding of structural alerts and drug metabolism could avoid interactions and drug-induced toxicities in general.

8. Conclusion

Herbal products are largely used amongst cancer patients with the expectation of prolonging survival, improving quality of life, enhancing tumor response, or alleviating adverse events. Furthermore, many pre-clinical studies suggest possible benefits of concomitant use of herbal supplements during chemotherapy, but a perspective on the available clinical evidence supporting an evidence-based understanding regarding herbal product dosages, interactions, contraindications, and efficacy is largely lacking. This review of currently available clinical data suggests that combining certain herbal products and chemotherapy drugs may indeed lead to clinically significant herb-drug interactions, mainly resulting in lowered plasma levels of pharmacologically active drug metabolites. Notable results are the interaction of SJW and irinotecan (Mathijssen et al. 2002), imatinib (Frye et al. 2004; Smith P et al. 2004) and docetaxel (Goey et al. 2014) and the effect of grapefruit juice on etoposide (Reif et al. 2002), where pharmacokinetic data suggest to avoid the combination to prevent reduced drug efficacy.

Only a limited number of chemotherapy agents have been studied in the clinical setting to assess herb-drug interactions (table 1), and available data is derived from studies in which the sample size is often too small to draw significant conclusions. Herbal supplements may be beneficial in reducing side effects such as nausea, diarrhea and gastrointestinal discomforts, but considering the large number of people using herbal supplements, more clinical trials are worth performing to better understand potential risks. Pharmacodynamics in healthy volunteers can differ from ones obtained in cancer patients experiencing a multidrug regimen and heavy compromised health status. Also, duration of herb supplement intake may play a role for potential herb-drug interaction as indicated for irinotecan and SJW (Markowitz et al. 2000; Mathijssen et al. 2002). For better comparability of future clinical studies, treatment schedules should be standardized regarding therapy regimen

and herb supplement intake. In addition, introducing a clear measurement for the relief of side effects can elucidate if and how herbal supplements are beneficial for patients undergoing chemotherapy. Knowledge about drug metabolism, active components of drug and herbal supplement and their specificity to metabolizing enzymes is crucial for safe therapies.

One way to address the complexity of herb-drug interactions is the inclusion of metabolic biomarkers in clinical studies. To overcome limitations in study design, measurement of active drug (metabolite) and if known bioactive herbal constituent concentration in plasma would be beneficial. Moreover, screening patients for genetic polymorphisms of drug-metabolizing enzymes might be helpful elucidating and predicting herb-drug interactions (Cox et al. 2006).

Herbal supplements are often taken without consulting a healthcare professional. Improved knowledge regarding potential herb-drug interactions and their clinical consequences would enable care providers to accurately inform patients. Thus, besides gaining knowledge concerning herb-drug interactions, also the careful curation of databases containing clinically significant outcomes, like the Stockley's Herbal Medicines Interactions, is an important step forward (MedicinesComplete accessed on 26.01.2019). Further advances in knowledge surrounding this topic can help care providers and patients make informed decisions on the use of herbal supplements.

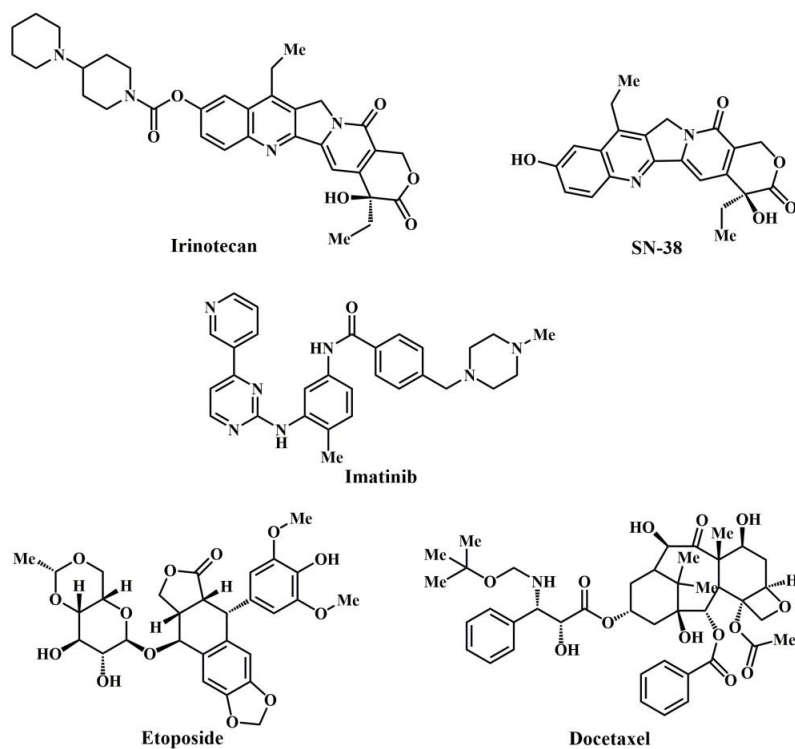


Figure 1. Chemical structures of selected drugs examined in combination with herbs in the clinic.

Table 1. Examples of clinical trials investigating herb-drug interactions in chemotherapy reviewed herein.

Drug	Herb	Number patients	Enzyme	Observations	Ref
Irinotecan	Cannabis	12 cancer patients	P-gp ^h CYP3A4 ⁱ	no significant effects on irinotecan-pharmacokinetics	(Engels et al. 2007)
Irinotecan	Milk thistle	6 cancer patients	CYP3A4 ⁱ	no significant effects on pharmacokinetics of Irinotecan, SN-38 ^e , SN-38G ^f	(van Erp et al. 2005)
Irinotecan	SJW ^g	5 cancer patients	CYP3A4 ⁱ	AUC ^a for SN-38 ^e decreased by 42% (p=0.033)	(Mathijssen et al. 2002)
Irinotecan	Chrysin	21 colorectal cancer patients	UGT1A1 ^j	no significant effects on pharmacokinetics of irinotecan, SN-38 ^e , SN-38G ^f (in comparison to historical controls), no relationship between UGT1A1 polymorphism and diarrhea	(Tobin et al. 2006)
Imatinib	SJW ^g	12 healthy volunteers	CYP3A4 ⁱ	Imatinib AUC ^a decreased by 30% (p<0.001), CL ^b increased by 43% (p<0.001), half-life and C _{max} ^d reduced (p<0.005), N-desmethylimatinib C _{max} ^d increased by 13% (p=0.0272), no effect on AUC ^a	(Frye et al. 2004)
Imatinib	SJW ^g	10 healthy volunteers	CYP3A4 ⁱ P-gp ^h	Imatinib AUC ^a reduced by 32% (p=0.0001), C _{max} ^d reduced by 29% (p=0.005), half-life reduced by 21% (p=0.0001)	(Smith P et al. 2004)
Etoposide	Grapefruit juice	6 lung cancer patients	CYP3A4 ⁱ P-gp ^h	AUC ^a decreased by 26%	(Reif et al. 2002)
Docetaxel	Cannabis	12 cancer patients	P-gp ^h CYP3A ⁱ	no significant effects on docetaxel-pharmacokinetics	(Engels et al. 2007)
Docetaxel	Garlic	11 breast cancer patients	CYP3A4 ⁱ CYP3A5	no significant effects on docetaxel-pharmacokinetics, AUC ^a ratio for day 15 to 1 increased for CYP3A5*A1/*A1 genotype (3 patients) compared to CYP3A5*3C/*3C genotype (6 patients)	(Cox et al. 2006)
Docetaxel	SJW ^g	10 cancer patients	CYP3A4 ⁱ	AUC ^a decreased by 11.6% (p=0.045), CL ^b increased by 13.3% (p=0.045), lowered incidence of doetaxel- related toxicities	(Goey et al. 2014)
Docetaxel	E. purpurea	10 cancer patients	CYP3A4 ⁱ	no significant effects on docetaxel-pharmacokinetics	(Goey et al. 2013)
Docetaxel	Jinfukang	21 NSC ^l lung cancer patients	CYP3A4 ⁱ	no significant effects on docetaxel-pharmacokinetics	(Cassileth et al. 2009)

^aAUC, area under the curve, ^bCL, clearance; ^cCI, Confidence Interval; ^dCmax, maximum concentration; ^eSN-38, 7-ethyl-10-hydroxycamptothecin; ^fSN-38G, SN-38-Glucuronidate, ^gSJW, St John's Wort; ^hP-gp, P-glycoprotein; ⁱCYP3A4, cytochrome p450 3A4; ^jUGT1A1, uridine diphosphoglucuronosyl transferase 1A1; ^kiv, intravenous; ^lnon-small cell (NSC).

References

- Akbulut G (2011) New perspective for nutritional support of cancer patients: Enteral/parenteral nutrition *Exp Ther Med* 2:675-684 doi:10.3892/etm.2011.247
- Aung TN, Qu Z, Kortschak RD, Adelson DL (2017) Understanding the Effectiveness of Natural Compound Mixtures in Cancer through Their Molecular Mode of Action *International Journal of Molecular Sciences* 18:656
- Auyeung KK, Han Q-B, Ko JK (2016) Astragalus membranaceus: A Review of its Protection Against Inflammation and Gastrointestinal Cancers *Am J Chin Med* 44:1-22 doi:10.1142/s0192415x16500014
- Bailey D, Spence J, Munoz C, Arnold JMO (1991) Interaction of citrus juices with felodipine and nifedipine *The Lancet* 337:268-269 doi:https://doi.org/10.1016/0140-6736(91)90872-M
- Bailey DG, Dresser G, Arnold JMO (2013) Grapefruit–medication interactions: Forbidden fruit or avoidable consequences? *Can Med Assoc J* 185:309-316 doi:10.1503/cmaj.120951
- Bailey DG, Malcolm J, Arnold O, David Spence J (1998) Grapefruit juice–drug interactions *Br J Clin Pharmacol* 46:101-110 doi:doi:10.1046/j.1365-2125.1998.00764.x
- Basheti RAlIA (2017) Herbal Medicine Use by People in Jordan: Exploring Beliefs and Knowledge of Herbalists and Their Customers. *J Biol Sci* 17:400-409 doi:10.3923/jbs.2017.400.409
- Bayan L, Koulivand PH, Gorji A (2014) Garlic: a review of potential therapeutic effects *Avicenna J Phytomed* 4:1-14
- Beckmann-Knopp S et al. (2000) Inhibitory effects of silibinin on cytochrome P-450 enzymes in human liver microsomes *Pharmacology & toxicology* 86:250-256
- Bornheim LM, Correia MA (1990) Selective inactivation of mouse liver cytochrome P-450III_A by cannabidiol *Mol Pharmacol* 38:319-326
- Boullata JI, Armenti VT (2010) *Handbook of drug-nutrient interactions*. 2nd edn. Humana Press,
- Cassileth BR et al. (2009) Safety and pharmacokinetic trial of docetaxel plus an Astragalus-based herbal formula for non-small cell lung cancer patients *Cancer Chemother Pharmacol* 65:67-71 doi:10.1007/s00280-009-1003-z
- Chen X-W, Serag ES, Sneed KB, Zhou S-F (2011) Herbal bioactivation, molecular targets and the toxicity relevance *Chem Biol Interact* 192:161-176 doi:https://doi.org/10.1016/j.cbi.2011.03.016
- Cheng Y-Y, Hsieh C-H, Tsai T-H (2018) Concurrent administration of anticancer chemotherapy drug and herbal medicine on the perspective of pharmacokinetics *Journal of Food and Drug Analysis* 26:S88-S95 doi:https://doi.org/10.1016/j.jfda.2018.01.003
- Chrungoo VJ, Reen RK, Singh K, Singh J (1997) Effects of silymarin on UDP-glucuronic acid and glucuronidation activity in the rat isolated hepatocytes and liver in relation to D-galactosamine toxicity *Indian journal of experimental biology* 35:256-263
- Conklin KA (2000) Dietary antioxidants during cancer chemotherapy: Impact on chemotherapeutic effectiveness and development of side effects *Nutr Cancer* 37:1-18 doi:10.1207/s15327914nc3701_1
- Cox MC et al. (2006) Influence of garlic (*Allium sativum*) on the pharmacokinetics of docetaxel *Clin Cancer Res* 12:4636-4640 doi:10.1158/1078-0432.ccr-06-0388

- Dresser GK, Schwarz UI, Wilkinson GR, Kim RB (2003) Coordinate induction of both cytochrome P4503A and MDRI by St John's wort in healthy subjects *Clin Pharm Ther* 73:41-50 doi:10.1067/mcp.2003.10
- Efferth T, Fu YJ, Zu YG, Schwarz G, Konkimalla VS, Wink M (2007) Molecular target-guided tumor therapy with natural products derived from traditional Chinese medicine *Curr Med Chem* 14:2024-2032
- EMA (2015) European Union herbal monograph on *Echinacea purpurea* (L.) Moench, herba recens Accessed May 13th 2019
- EMA (accessed on 15.01.2019) Glivec: EPAR- Summary for the public. European Medicines Agency. https://www.ema.europa.eu/documents/product-information/glivec-epar-product-information_en.pdf
- Emi A, Marie M, Masaru K, Tohru H (2018) Use of Supplements by Japanese Cancer Patients Receiving Outpatient Cancer Chemotherapy *The Journal of Alternative and Complementary Medicine* 24:1003-1006 doi:10.1089/acm.2018.0078
- Engels FK et al. (2007) Medicinal cannabis does not influence the clinical pharmacokinetics of irinotecan and docetaxel *Oncologist* 12:291-300 doi:10.1634/theoncologist.12-3-291
- Erzinger MM et al. (2016) Sulforaphane preconditioning sensitizes human colon cancer cells towards the bioreductive anticancer prodrug PR-104A *PLOS ONE* 11:10.1371/journal.pone.0150219 doi:10.1371/journal.pone.0150219
- Erzinger MM, Sturla SJ (2011) Bioreduction-mediated food-drug interactions: opportunities for oncology nutrition *Chimia* 65:411-415
- Firkins R, Eisfeld H, Keinki C, Buentzel J, Hochhaus A, Schmidt T, Huebner J (2018) The use of complementary and alternative medicine by patients in routine care and the risk of interactions *J Cancer Res Clin Oncol* 144:551-557 doi:10.1007/s00432-018-2587-7
- Foster BC et al. (2001) An in vitro evaluation of human cytochrome P450 3A4 and P-glycoprotein inhibition by garlic *Journal of pharmacy & pharmaceutical sciences : a publication of the Canadian Society for Pharmaceutical Sciences, Societe canadienne des sciences pharmaceutiques* 4:176-184
- Frye RF, Fitzgerald SM, Lagattuta TF, Hruska MW, Egorin MJ (2004) Effect of St John's wort on imatinib mesylate pharmacokinetics *Clin Pharm Ther* 76:323-329 doi:10.1016/j.clpt.2004.06.007
- Galijatovic A, Walle UK, Walle T (2000) Induction of UDP-glucuronosyltransferase by the flavonoids chrysin and quercetin in Caco-2 cells *Pharmaceutical research* 17:21-26
- Geisen SM, Sturla SJ (2019) Can Foods or Herbs Alter the Bioavailability of Chemotherapy Drugs? *ACS Pharmacology & Translational Science* doi:10.1021/acspsci.9b00007
- Gillett J, Ientile C, Hiscock J, Plank A, Martin JM (2012) Complementary and Alternative Medicine Use in Radiotherapy: What Are Patients Using? *J Altern Complement Med* 18:1014-1020 doi:10.1089/acm.2011.0334
- Glaeser H et al. (2007) Intestinal Drug Transporter Expression and the Impact of Grapefruit Juice in Humans *Clin Pharm Ther* 81:362-370 doi:10.1038/sj.clpt.6100056
- Goey AKL et al. (2013) The effect of *Echinacea purpurea* on the pharmacokinetics of docetaxel *British journal of clinical pharmacology* 76:467-474 doi:10.1111/bcp.12159
- Goey AKL et al. (2014) The Effect of St John's Wort on the Pharmacokinetics of Docetaxel *Clin Pharmacokinet* 53:103-110 doi:10.1007/s40262-013-0102-5

- Gorman GS, Coward L, Darby A, Rasberry B (2013) Effects of herbal supplements on the bioactivation of chemotherapeutic agents *J Pharm Pharmacol* 65:1014-1025 doi:10.1111/jphp.12055
- Gorski JC et al. (2004) The effect of echinacea (*Echinacea purpurea* root) on cytochrome P450 activity in vivo *Clin Pharmacol Ther* 75:89-100 doi:10.1016/j.clpt.2003.09.013
- Gyemant N, Tanaka M, Antus S, Hohmann J, Csuka O, Mandoky L, Molnar J (2005) In vitro search for synergy between flavonoids and epirubicin on multidrug-resistant cancer cells In vivo (Athens, Greece) 19:367-374
- Hajda J, Rentsch KM, Gubler C, Steinert H, Stieger B, Fattinger K (2010) Garlic extract induces intestinal P-glycoprotein, but exhibits no effect on intestinal and hepatic CYP3A4 in humans *European journal of pharmaceutical sciences : official journal of the European Federation for Pharmaceutical Sciences* 41:729-735 doi:10.1016/j.ejps.2010.09.016
- Hellum BH, Hu Z, Nilsen OG (2007) The Induction of CYP1A2, CYP2D6 and CYP3A4 by Six Trade Herbal Products in Cultured Primary Human Hepatocytes *Basic & Clinical Pharmacology & Toxicology* 100:23-30 doi:10.1111/j.1742-7843.2007.00011.x
- Herbst RS, Khuri FR (2003) Mode of action of docetaxel - a basis for combination with novel anticancer agents *Cancer Treat Rev* 29:407-415 doi:10.1016/S0305-7372(03)00097-5
- Ho BE, Shen DD, McCune JS, Bui T, Risler L, Yang Z, Ho RJ (2010) Effects of Garlic on Cytochromes P450 2C9- and 3A4-Mediated Drug Metabolism in Human Hepatocytes *Scientia pharmaceutica* 78:473-481 doi:10.3797/scipharm.1002-11
- Hohmann AG, Suplita RL (2006) Endocannabinoid mechanisms of pain modulation *The AAPS journal* 8:E693-E708 doi:10.1208/aapsj080479
- Iqbal N, Iqbal N (2014) Imatinib: A Breakthrough of Targeted Therapy in Cancer *Chemother Res Pract* 2014:357027 doi:10.1155/2014/357027
- Jaeger W. BL, Bornheim LM (1996) Inhibition of cyclosporine and tetrahydrocannabinol metabolism by cannabidiol in mouse and human microsomes *Xenobiotica; the fate of foreign compounds in biological systems* 26:275-284
- Kane GC, Lipsky JJ (2000) Drug-grapefruit juice interactions *Mayo Clinic proceedings Mayo Clinic* 75:933-942 doi:10.4065/75.9.933
- Kaur G, Verma N (2015) Nature curing cancer - review on structural modification studies with natural active compounds having anti-tumor efficiency *Biotechnol Rep (Amst)* 6:64-78 doi:10.1016/j.btre.2015.01.005
- Kawashiro T, Yamashita K, Zhao XJ, Koyama E, Tani M, Chiba K, Ishizaki T (1998) A study on the metabolism of etoposide and possible interactions with antitumor or supporting agents by human liver microsomes *J Pharmacol Exp Ther* 286:1294-1300
- Kesarwani K, Gupta R, Mukerjee A (2013) Bioavailability enhancers of herbal origin: An overview *Asian Pac J Trop Biomed* 3:253-266
- Khurana RK, Jain A, Jain A, Sharma T, Singh B, Kesharwani P (2018) Administration of antioxidants in cancer: debate of the decade *Drug Discovery Today* doi:https://doi.org/10.1016/j.drudis.2018.01.021
- Komoroski BJ, Parise RA, Egorin MJ, Strom SC, Venkataramanan R (2005) Effect of the St. John's wort constituent hyperforin on docetaxel metabolism by human hepatocyte cultures *Clinical cancer research : an official journal of the American Association for Cancer Research* 11:6972-6979 doi:10.1158/1078-0432.ccr-04-2488

- Lau C, Mooiman KD, Maas-Bakker RF, Beijnen JH, Schellens JHM, Meijerman I (2013) Effect of Chinese herbs on CYP3A4 activity and expression in vitro *J Ethnopharmacol* 149:543-549 doi:<https://doi.org/10.1016/j.jep.2013.07.014>
- Lee WL, Shiao JY, Shyur LF (2012) Taxol, Camptothecin and Beyond for Cancer Therapy. In: Shyur LF, Lau ASY (eds) *Recent Trends in Medicinal Plants Research*, vol 62. *Advances in Botanical Research*. Academic Press Ltd-Elsevier Science Ltd, London, pp 133-178. doi:10.1016/b978-0-12-394591-4.00008-8
- Lovett BD et al. (2001) Etoposide Metabolites Enhance DNA Topoisomerase II Cleavage near Leukemia-Associated MLL Translocation Breakpoints *Biochemistry* 40:1159-1170 doi:10.1021/bi002361x
- Madabushi R, Frank B, Drewelow B, Derendorf H, Butterweck V (2006) Hyperforin in St. John's wort drug interactions *Eur J Clin Pharmacol* 62:225-233 doi:10.1007/s00228-006-0096-0
- Markowitz JS, DeVane CL, Boulton DW, Carson SW, Nahas Z, Risch SC (2000) Effect of St. John's wort (*Hypericum perforatum*) on cytochrome P-450 2D6 and 3A4 activity in healthy volunteers *Life Sci* 66:PL133-139
- Marre F, Sanderink GJ, de Sousa G, Gaillard C, Martinet M, Rahmani R (1996) Hepatic biotransformation of docetaxel (Taxotere) in vitro: involvement of the CYP3A subfamily in humans *Cancer research* 56:1296-1302
- Mathijssen RH, Verweij J, de Bruijn P, Loos WJ, Sparreboom A (2002) Effects of St. John's wort on irinotecan metabolism *J Natl Cancer Inst* 94:1247-1249
- Mathijssen RHJ, van Alphen RJ, Verweij J, Loos WJ, Nooter K, Stoter G, Sparreboom A (2001) Clinical Pharmacokinetics and Metabolism of Irinotecan (CPT-11) *Clin Cancer Res* 7:2182-2194
- MedicinesComplete (accessed on 26.01.2019). <https://about.medicinescomplete.com/publication/stockleys-herbal-medicines-interactions-2/#updates>.
- Meijerman I, Beijnen JH, Schellens JHM (2006) Herb-drug interactions in oncology: Focus on mechanisms of induction *Oncologist* 11:742-752 doi:10.1634/theoncologist.11-7-742
- Miller P et al. (2008) Dietary supplement use among elderly, long-term cancer survivors *J Cancer Surviv* 2:138-148 doi:10.1007/s11764-008-0060-3
- Mohamed ME, Frye RF (2011) Effects of herbal supplements on drug glucuronidation. Review of clinical, animal, and in vitro studies *Planta Med* 77:311-321 doi:10.1055/s-0030-1250457
- Mooiman KD, Maas-Bakker RF, Moret EE, Beijnen JH, Schellens JH, Meijerman I (2013) Milk thistle's active components silybin and isosilybin: novel inhibitors of PXR-mediated CYP3A4 induction *Drug metabolism and disposition: the biological fate of chemicals* 41:1494-1504 doi:10.1124/dmd.113.050971
- Moore LB et al. (2000) St. John's wort induces hepatic drug metabolism through activation of the pregnane X receptor *Proc Natl Acad Sci U S A* 97:7500-7502 doi:10.1073/pnas.130155097
- NIH (2019) A to Z List of Cancer Drugs. <https://www.cancer.gov/about-cancer/treatment/drugs>. Accessed May 13th 2019
- Nipp RD, Hong K, Paskett ED (2019) Overcoming Barriers to Clinical Trial Enrollment *American Society of Clinical Oncology Educational Book*:105-114 doi:10.1200/edbk_243729
- Panikashvili D, Mechoulam R, Beni SM, Alexandrovich A, Shohami E (2005) CB1 cannabinoid receptors are involved in neuroprotection via NF- κ B inhibition *J Cereb Blood Flow Metab* 25:477-484 doi:10.1038/sj.jcbfm.9600047

- Peng B, Lloyd P, Schran H (2005) Clinical Pharmacokinetics of Imatinib Clin Pharmacokinet 44:879-894 doi:10.2165/00003088-200544090-00001
- Penzak SR et al. (2010) Echinacea purpurea significantly induces cytochrome P450 3A activity but does not alter lopinavir-ritonavir exposure in healthy subjects Pharmacotherapy 30:797-805 doi:10.1592/phco.30.8.797
- Piscitelli SC, Burstein AH, Welden N, Gallicano KD, Falloon J (2002) The effect of garlic supplements on the pharmacokinetics of saquinavir Clinical infectious diseases : an official publication of the Infectious Diseases Society of America 34:234-238 doi:10.1086/324351
- Qianlai L, N. AG (2018) Use of Dietary Supplements at a Comprehensive Cancer Center The Journal of Alternative and Complementary Medicine 24:981-987 doi:10.1089/acm.2018.0183
- Reif S, Nicolson MC, Bisset D, Reid M, Kloft C, Jaehde U, McLeod HL (2002) Effect of grapefruit juice intake on etoposide bioavailability Eur J Clin Pharmacol 58:491-494 doi:10.1007/s00228-002-0495-9
- Ribnicky DM, Poulev A, Schmidt B, Cefalu WT, Raskin I (2008) Evaluation of botanicals for improving human health The American journal of clinical nutrition 87:472S-475S
- Ross SA, ElSohly MA, Sultana GN, Mehmedic Z, Hossain CF, Chandra S (2005) Flavonoid glycosides and cannabinoids from the pollen of Cannabis sativa L Phytochemical analysis : PCA 16:45-48 doi:10.1002/pca.809
- Ruggiero A, Cefalo MG, Coccia P, Mastrangelo S, Maurizi P, Riccardi R (2012) The role of diet on the clinical pharmacology of oral antineoplastic agents European Journal of Clinical Pharmacology 68:115-122 doi:10.1007/s00228-011-1102-8
- Ryan JL et al. (2012) Ginger (Zingiber officinale) reduces acute chemotherapy-induced nausea: a URCC CCOP study of 576 patients Supportive care in cancer : official journal of the Multinational Association of Supportive Care in Cancer 20:1479-1489 doi:10.1007/s00520-011-1236-3
- Sahoo N, Choudhury K, Manchikanti P (2009) Manufacturing of biodrugs: need for harmonization in regulatory standards BioDrugs : clinical immunotherapeutics, biopharmaceuticals and gene therapy 23:217-229 doi:10.2165/11317110-000000000-00000
- Samojlik I, Mijatović V, Gavarić N, Krstin S, Božin B (2013) Consumers' attitude towards the use and safety of herbal medicines and herbal dietary supplements in Serbia International Journal of Clinical Pharmacy 35:835-840 doi:10.1007/s11096-013-9819-3
- Shen DD (2008) Casarett and Doull's Toxicology: The Basic Science of Poisons vol 7th Edition. McGraw-Hill,
- Shou M, Martinet M, Korzekwa KR, Krausz KW, Gonzalez FJ, Gelboin HV (1998) Role of human cytochrome P450 3A4 and 3A5 in the metabolism of taxotere and its derivatives: enzyme specificity, interindividual distribution and metabolic contribution in human liver Pharmacogenetics 8:391-401
- Siegel AB, Stebbing J (2013) Milk thistle: early seeds of potential Lancet Oncol 14:929-930 doi:10.1016/S1470-2045(13)70414-5
- Singh BN, Malhotra BK (2004) Effects of food on the clinical pharmacokinetics of anticancer agents - Underlying mechanisms and implications for oral chemotherapy Clinical Pharmacokinetics 43:1127-1156 doi:10.2165/00003088-200443150-00005
- Singh S, Sharma B, Kanwar SS, Kumar A (2016) Lead Phytochemicals for Anticancer Drug Development Frontiers in Plant Science 7 doi:10.3389/fpls.2016.01667

- Smith P, Bullock JM, Booker BM, Haas CE, Berenson CS, Jusko WJ (2004) The influence of St. John's Wort on the pharmacokinetics and protein binding of imatinib mesylate *Pharmacotherapy* 24:1508-1514 doi:10.1592/phco.24.16.1508.50958
- Sontakke S, Thawani V, Naik S (2003) Ginger as an antiemetic in nausea and vomiting induced by chemotherapy: A randomized, cross-over, double blind study. *Indian J Pharmacol* 35:32-36
- Sparreboom A, Cox MC, Acharya MR, Figg WD (2004a) Herbal Remedies in the United States: Potential Adverse Interactions With Anticancer Agents *J Clin Oncol* 22:2489-2503 doi:10.1200/jco.2004.08.182
- Sparreboom A, Cox MC, Acharya MR, Figg WD (2004b) Herbal remedies in the United States: Potential adverse interactions with anticancer agents *Journal of clinical oncology : official journal of the American Society of Clinical Oncology* 22:2489-2503 doi:10.1200/jco.2004.08.182
- Sridar C, Goosen TC, Kent UM, Williams JA, Hollenberg PF (2004) Silybin inactivates cytochromes P450 3A4 and 2C9 and inhibits major hepatic glucuronosyltransferases *Drug metabolism and disposition: the biological fate of chemicals* 32:587-594 doi:10.1124/dmd.32.6.587
- Stanton RA, Gernert KM, Nettles JH, Aneja R (2011) Drugs that target dynamic microtubules: a new molecular perspective *Medicinal research reviews* 31:443-481 doi:10.1002/med.20242
- Tobin PJ, Beale P, Noney L, Liddell S, Rivory LP, Clarke S (2006) A pilot study on the safety of combining chrysin, a non-absorbable inducer of UGT1A1, and irinotecan (CPT-11) to treat metastatic colorectal cancer *Cancer Chemother Pharmacol* 57:309-316 doi:10.1007/s00280-005-0053-0
- van der Stelt M, Di Marzo V (2003) The endocannabinoid system in the basal ganglia and in the mesolimbic reward system: implications for neurological and psychiatric disorders *Eur J Pharmacol* 480:133-150 doi:https://doi.org/10.1016/j.ejphar.2003.08.101
- van Erp NPH et al. (2005) Effect of milk thistle (*Silybum marianum*) on the pharmacokinetics of irinotecan *Clinical cancer research : an official journal of the American Association for Cancer Research* 11:7800-7806 doi:10.1158/1078-0432.ccr-05-1288
- Venkataramanan R, Ramachandran V, Komoroski BJ, Zhang S, Schiff PL, Strom SC (2000) Milk thistle, a herbal supplement, decreases the activity of CYP3A4 and uridine diphosphoglucuronosyl transferase in human hepatocyte cultures *Drug metabolism and disposition: the biological fate of chemicals* 28:1270-1273
- Walsh D, Nelson KA, Mahmoud FA (2003) Established and potential therapeutic applications of cannabinoids in oncology *Supportive care in cancer : official journal of the Multinational Association of Supportive Care in Cancer* 11:137-143
- Wang JC (2002) Cellular roles of DNA topoisomerases: a molecular perspective *Nature reviews Molecular cell biology* 3:430-440 doi:10.1038/nrm831
- Wang ZQ, Gorski C, Hamman MA, Huang SM, Lesko LJ, Hall SD (2001) The effects of St John's wort (*Hypericum perforatum*) on human cytochrome P450 activity *Clin Pharm Ther* 70:317-326 doi:10.1016/s0009-9236(01)17221-8
- Whitten DL, Myers SP, Hawrelak JA, Wohlmuth H (2006) The effect of St John's wort extracts on CYP3A: a systematic review of prospective clinical trials *Br J Clin Pharmacol* 62:512-526 doi:doi:10.1111/j.1365-2125.2006.02755.x
- Xu H, Lv M, Tian X (2009) A review on hemisynthesis, biosynthesis, biological activities, mode of action, and structure-activity relationship of podophyllotoxins: 2003-2007 *Curr Med Chem* 16:327-349

- Yu DH, Bao YM, Wei CL, An LJ (2005) Studies of chemical constituents and their antioxidant activities from *Astragalus mongholicus* Bunge *Biomedical and environmental sciences* : BES 18:297-301
- Zhang Q-Y, Wang F-X, Jia K-K, Kong L-D (2018) Natural Product Interventions for Chemotherapy and Radiotherapy-Induced Side Effects *Front Pharmacol* 9:1253-1253 doi:10.3389/fphar.2018.01253
- Zhu H-J, Wang J-S, Markowitz JS, Donovan JL, Gibson BB, Gefroh HA, DeVane CL (2006) Characterization of P-glycoprotein Inhibition by Major Cannabinoids from Marijuana *J Pharmacol Exp Ther* 317:850-857
- Zuber R, Modriansky M, Dvorak Z, Rohovsky P, Ulrichova J, Simanek V, Anzenbacher P (2002) Effect of silybin and its congeners on human liver microsomal cytochrome P450 activities *Phytotherapy research* : PTR 16:632-638 doi:10.1002/ptr.1000

Appendix III: Clofarabine sensitises paediatric ETP-ALL to PR-104

Manuscript in preparation

Toscan C., Manesh M.D, Geisen S.M, Danielli S., Sturla S.J. and Lock R.

Toscan C. conceived the research, performed PDX, gene expression and comet assay. Manesh M.D. conceived the research, performed the preliminary PDX studies and the drug screen. Danielli S. performed PDX studies and comet assay. Geisen S.M. performed mass spectrometry analysis, interpreted results and was the master's thesis supervisor of Danielli S. while she conducted experiments at the Children's Cancer Institute, Sydney, Australia. Sturla S.J. and Lock R. conceived the research and evaluated and interpreted data. All collaborators are participating in writing a manuscript from this study. The focus of this thesis chapter mainly is on results of experiments involving mass spectrometry analysis, i.e. performed between Danielli S. and Geisen S. M. These are presented and discussed here and will be integrated into a pending manuscript.

Clofarabine sensitises paediatric ETP-ALL to PR-104

Manuscript in preparation

Toscan C.,¹ Manesh M.D.,¹ Geisen S.M.², Danielli S.², Sturla S.J.² and Lock R.^{1*}

¹ Children's cancer Institute Australia, Lowy Cancer Research Centre, Sydney, Australia

² Laboratory of Toxicology, ETH Zürich, 8092 Zürich, Switzerland

*Correspondence to Prof. Richard Lock, Email: RLock@ccia.org.au

Introduction

Arising from immature, quickly growing lymphocytes, acute lymphoblastic leukemia (ALL) is the most common leukemia affecting children, but almost half of the cases are in adults as well. Cure rates especially amongst children and adolescents are high, due to marked improvements including risk-based stratification in ALL-therapy (Cooper and Brown 2015). Certain patients respond poorly to therapy and experience relapses, which have a very low cure rate and relapsing patients tend to be more resistant to many drugs commonly used for ALL therapy (Bassan and Hoelzer 2011; Klumper et al. 1995; Wheeler et al. 1998). The capacity to identify ALL cases that may be prone to resistance and responsive to alternative therapeutic strategies is expected to reduce the incidence of relapses in ALL patients and improve long-term survival (Tasian and Hunger 2016). A current gap concerns the identification of molecular characteristics predictive of relapse risks and the development of companion diagnostics/therapeutics that are more potent for resistant cases of ALL.

PR-104 is a dinitrobenzamide mustard pre-pro-drug designed to target hypoxic cells in tumors (Patterson et al. 2007). It undergoes systemic hydrolysis to form the pro-drug PR104A, which is further activated by reduction to DNA-alkylating metabolites PR-104H and PR-104M (Patterson et al. 2007). Under hypoxic conditions, PR-104A metabolism involves the formation of an oxygen-sensitive nitro-radical in a reduction catalyzed by the one-electron oxidoreductase NADPH: cytochrome P450 (POR) and related flavoproteins (Guise et al. 2007). In addition, PR-104A is also activated by the two-electron reductase aldo-keto reductase 1C3 (AKR1C3) (Guise et al. 2010). Aldo-keto reductases (AKRs) are a superfamily of NAD(P)H-linked oxidoreductases responsible for reducing aldehydes and ketones, including drugs and chemical carcinogens, to their primary and secondary alcohols (Barski et al. 2008). In *in vitro* and in cell studies 19 PR-104-derived mono- and crosslinked DNA adducts could be detect and relatively quantified (Stornetta et al. 2015) (Stornetta et al. 2017a) and further, relative adduct levels were found to be correlating with cytotoxicity indicating the potential use of drug-derived DNA adducts as biomarkers for PR014A-susceptibility (Stornetta et al. 2017a). Although there have been limited examples of the use of DNA adducts as clinical biomarkers, their levels were found to positively correlate with biological responses in a number of primarily pre-clinical examples (Stornetta et al. 2017b). Seminal examples include *in vitro* and in vivo studies with nitrogen mustard drugs in leukemia relevant biological samples demonstrating the negative correlation between drug-derived DNA crosslinks and survival rate affirmed by a significant reduced percentage of induced interstrand-crosslinks (ICLs) in lymphocytes of resistant patients.

Studies in acute myeloid leukemia (AML) and ALL xenografts and clinical trials in both relapsed and refractory AML/ALL, as well as in solid tumors showed that PR-104 exhibited notable activity but the high administered dose caused adverse side effects suggesting the need for personalized pre-treatment assessments (Houghton et al. 2011; Jameson et al. 2010; Konopleva et al. 2011; Konopleva et al. 2015; McKeage et al. 2011). A motivation for addressing leukemias with AKR1C3-activated drugs is motivated by data suggesting its high expression in AML cells (Birtwistle et al. 2009; Jamieson et al. 2014; Mahadevan et al. 2006). A causal relationship between PR-104 sensitivity and AKR1C3 expression has been

demonstrated in patient-derived xenografts (PDX) suggesting AKR1C3 as a biomarker for PR-104 efficacy (Moradi Manesh et al. 2015). Expression of AKR1C3 was significantly higher in T-lineage ALL (T-ALL) compared with B-cell precursor ALL (BCP-ALL), and correlated with PR-104 sensitivity *in vivo* and *in vitro*.

Despite the high activity of PR-104 for T-ALL, early T-cell precursor ALL (ETP-ALL) xenografts have intrinsic resistance to PR-104, despite AKR1C3 function. To attempt to reverse this resistance, a combinatorial screen of NCI Oncology Drugs was performed with PR-104 and amongst the 96 FDA-approved anticancer drugs tested, clofarabine, an antimetabolite, was found to completely reverse PR-104A resistance (Toscan C. unpublished results). In follow-up studies, a synergistic effect was demonstrated for clofarabine and PR-104A in ETP-ALL xenografts *in vitro* and *in vivo* (Toscan C. unpublished results). Finally, gene expression profile data for ETP-ALL PDXs suggest that overexpression of DNA cross-link repair 1A (DCLRE1A) is involved in the repair of DNA ICLs (Toscan C. unpublished results). The working hypothesis is that clofarabine inhibits the repair of PR-104A-derived ICLs and the increased persistence of ICLs results in improved PR-104A activity. The goal of this study was to test whether clofarabine downregulates DNA repair activity, allowing PR-104A-derived-adducts to persist. Thus, we assessed PR-104-derived DNA adduct levels in sensitive and resistant PDXs with and without co-treatment of clofarabine. Cell viability changes were compared with changes in DNA adduct levels (MS). These data indicate a potential basis for how co-treatment with clofarabine may help overcome drug resistance.

Results

PR-104A-DNA adduct levels in drug-responsive PDX

Based on the observation that certain PDXs are intrinsically sensitive to PR-104A, we hypothesized the formation of significant DNA adduct levels in this model. DNA adducts are informative mechanistic and diagnostic biomarkers of cellular responsiveness to DNA alkylating drugs (Stornetta et al. 2017b), and PR-104A DNA adducts have been quantified in various cell lines (Stornetta et al. 2018; Stornetta et al. 2017a), but, to our knowledge, there are no reports of PR-104A or any other DNA-drug adduct quantification in PDX models *in vitro*. Further, PR-104A gives rise to a mixture of adducts resulting from different degrees of bioreduction, mono- and crosslinking of DNA, reactions with different nucleobases, and base- and nucleoside adduct structures. Thus, a previously established LC-MS/MS method for relative quantitation of up to 19 PR-104A-derived DNA adducts (Stornetta et al. 2017a) was used to quantify relative levels of drug-DNA-adducts in three PR-104A sensitive PDXs, i.e. ALL-8, ALL-27 and ALL-31 (Moradi Manesh et al. 2015). By this strategy, the relative abundance of a particular DNA adduct or crosslink can be compared between different biological models, but accurate comparisons cannot be made across structurally different adducts within the same model, and no distinction between intrastrand and interstrand crosslinks (ICLs) can be made, since both give rise to the same m/z transition. After retrieving PDXs from cryostorage, cells were washed and directly exposed to 150 μ M PR-104A for 4 or 24 h. Cultured REH cells, in which PR-104A adduct levels were measured previously (Stornetta et al. 2018), were subject to the same exposure as a positive control. Adducts could be detected if $S/N > 3$ (limit of detection, LOD) and relatively quantified if $S/N > 10$ (limit of quantitation, LOQ). After 4 h drug exposure, 10 of the 19 detectable adducts were observed in both REH cells and ALL-8, while 15 and 13 adducts were detectable in ALL-27 and in ALL-31, respectively (Figure 1). Increasing the drug exposure to 24 h, additional adducts were observed (Figure 1) and in most cases, adduct abundance was increased. This study demonstrated the feasibility of measuring PR-104A-derived DNA adducts in PDXs with the LC-MS/MS approach.

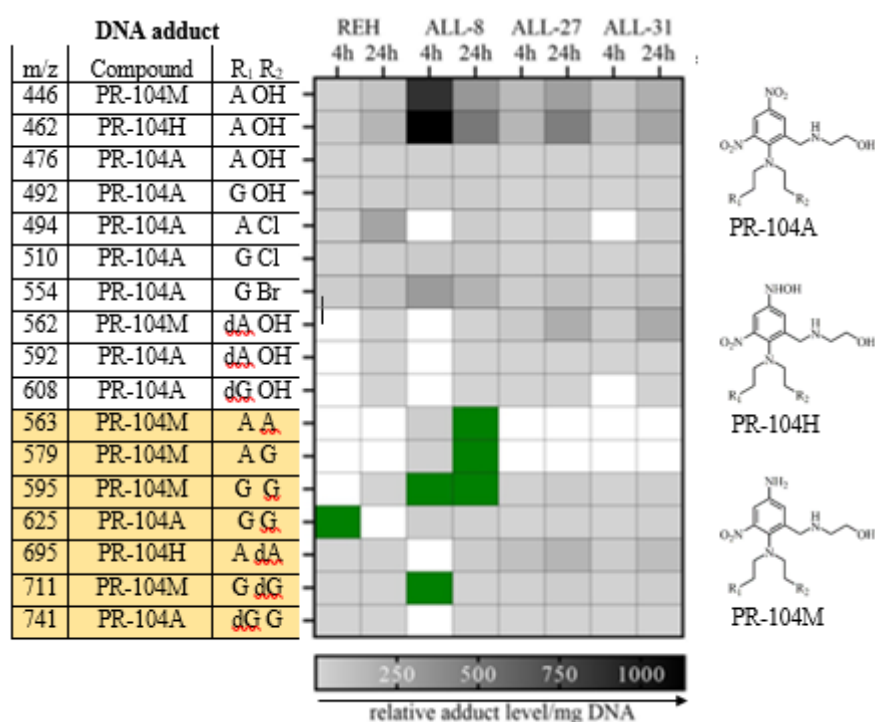


Figure 1. PR-104A-derived DNA adducts in REH, ALL-8, ALL-27 and ALL-31. DNA adducts were detected ($S/N > 3$) in three PR-104A-sensitive PDXs and the REH cell line after treatment with $150 \mu\text{M}$ PR-104A for 4 and 24 h. Relative adduct abundance for each m/z is presented from light grey to dark grey. White: not detected, green: below limit of quantitation (LOQ, $S/N < 10$). Crosslinks are highlighted in yellow. Except for ALL-8, adduct abundance increases from 4 to 24 h.

PR-104A-DNA adduct levels increase with increasing drug responses in PDXs

Having established for the first time that DNA adduct formation could be quantified in PDXs, we tested the dose-response relationship between drug exposure levels and adduct levels as a function of drug sensitivity. The models evaluated were the PR-104A-sensitive ALL-8 and the PR-104A-resistant ETP-2. PDXs were treated for 4 h with increasing PR-104A concentrations ranging from 10 to $150 \mu\text{M}$, and adducts were measured using the same LC-MS/MS approach described above. The same adducts could be relatively quantified in ALL-8 and ETP-2, including PR-104A- and metabolite-derived monoadducts, and crosslinks as well (Figure 2B). Relative adduct levels positively correlated with drug concentration (Figure 2A). While monoadducts could be quantified after exposure to $75 \mu\text{M}$ PR-104A, crosslinks were only quantifiable for drug concentrations higher than $100 \mu\text{M}$ (Figure 2B). To ensure the quantification of the biological relevant crosslinks also in the resistant PDX, a PR-104A dose of $150 \mu\text{M}$ was chosen for further studies.

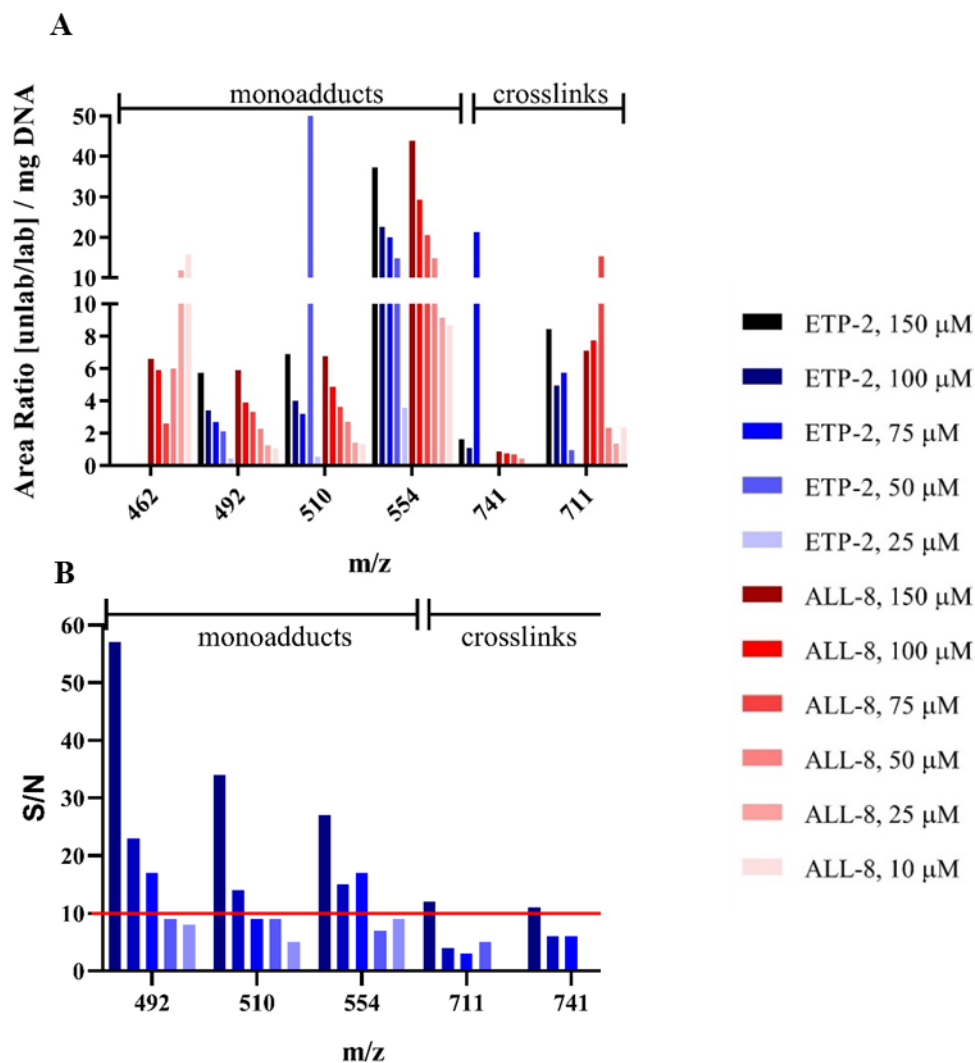


Figure 2. PR-104A dose response in ETP-2 and ALL-8. PDX were treated for 4 h with PR-104A concentration from 10 to 150 μ M and adduct levels relatively quantifies by LC-MS/MS ($n=1$). Limit of detection (LOD) is determined as $S/N > 3$, while limit of quantification (LOQ) is $S/N > 10$. A. relative adduct levels correlate with drug-dose. B. S/N ratio for PR-104A-derived DNA adducts in ETP-2. 150 μ M PR-104A is required for quantification of drug-derived DNA crosslinks in ETP-2.

Persistence of PR-104A adducts as a potential basis for drug synergy

Having established that clofarabine sensitizes PR-104A-resistant PDXs, and that DNA adduct levels increased with PDX responses, we hypothesized that a potential basis of synergy between the two drugs is clofarabine inhibiting the repair of cytotoxic DNA adducts induced by PR-104A. We therefore aimed to test the influence of clofarabine on PR-104A adduct levels in the PR-104-sensitive ALL-8 and in the PR-104A-resistant ETP-2 by mass spectrometry. To identify appropriate treatment conditions, PDXs were exposed to 150 μ M PR-104 for 4 h (conditions we established to be suitable for detecting all types of DNA adducts), and after exchanging the media, cells were exposed to clofarabine (1.25 μ M) or media as a control. Cell viability was determined by flow cytometry at selected time points up to 20 h exposure to clofarabine (Figure 3). ALL-8 was highly responsive to PR-104A both alone and in combination with clofarabine (< 5 % live cells at 20 h), whereas ETP-2 cells

were sensitive only when both drugs were applied (20% live cells in combination at 20 h vs. 40% live cells after PR-104A alone). Analysis of these data with the Bliss model (Geary 2013) confirmed a similar PR-104A-clofarabine synergy in ETP-2 as with a direct co-exposure to a fixed ratio of the two drugs for 48 h. (Figure 4). Importantly, no synergy was detectable in ALL-8, indicating that the experimental protocol is appropriate to understand the role of DNA adduct dynamics in the synergistic response of ETP-2 to PR-104A and clofarabine.

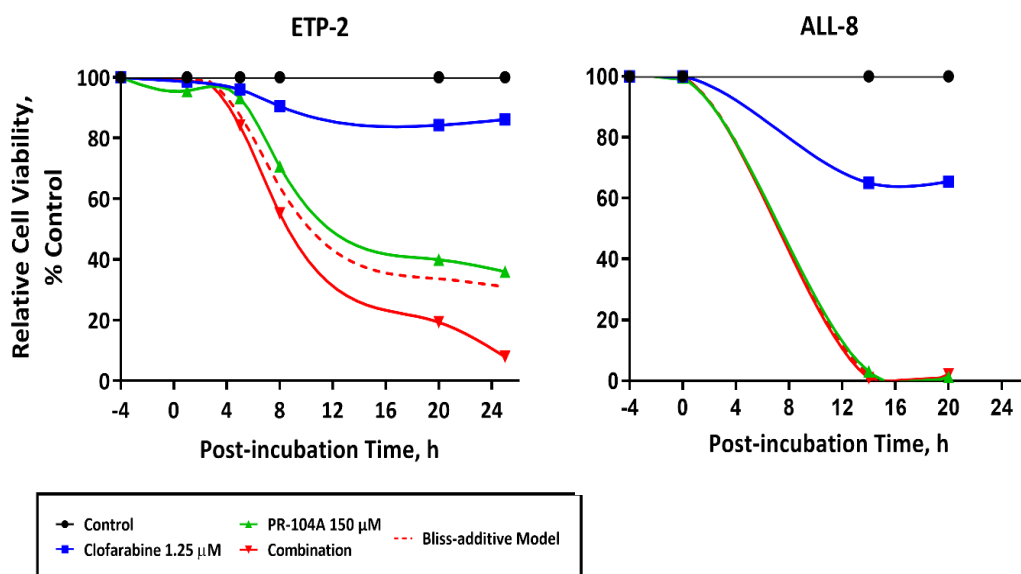


Figure 3. Annexin V/7AAD time course analysis of cell viability. ETP-2 and ALL-8 xenograft cells were pre-treated with 150 μ M PR-104A for 4 h, and then incubated in the presence or absence of 1.25 μ M clofarabine (n=1). Cell viability was assessed by flow cytometry at the selected time points and is expressed as a % of viable cells relative to the untreated control. The combination of PR-104A with clofarabine was synergistic in ETP-2 but not in ALL-8, as calculated with the Bliss-additive model (combination line below the Bliss-additive line).

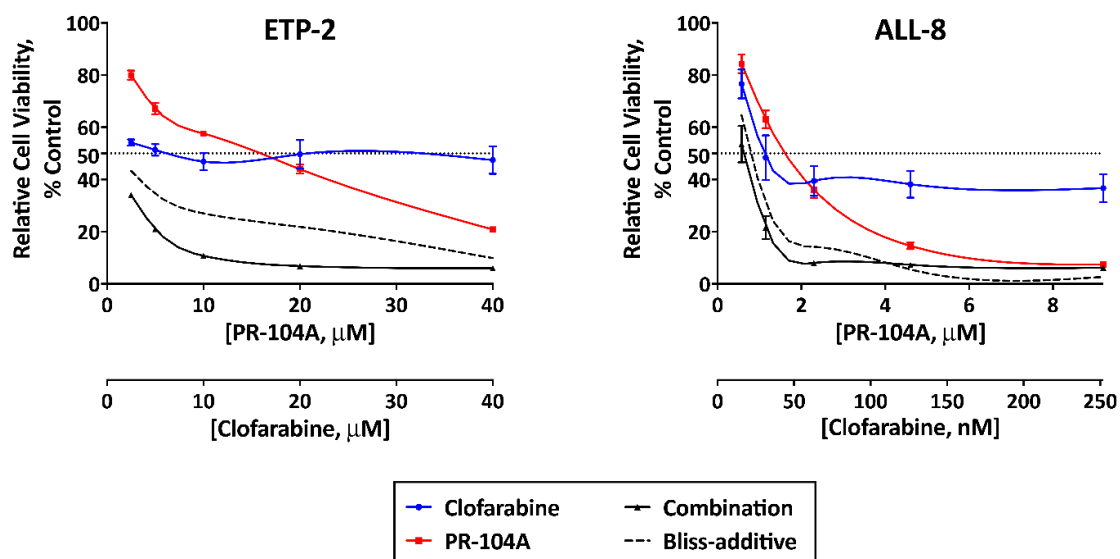


Figure 4. Resazurin cell viability assay for fixed-ratio concentrations for PR-104A and clofarabine. ALL-8 and ETP-2 were treated for 48 h with PR-104A and clofarabine at a fixed concentration-ratio. Drug concentrations were specific for each xenograft, considering their respective sensitivity towards the drugs (n=3). The combination of PR-104A with clofarabine was synergistic in ETP-2 but not in ALL-8, as calculated with the Bliss-additive model (combination line below the Bliss-additive line).

To test the influence of clofarabine on PR-104A adduct levels, PDXs were subject to the sequential PR-104A-clofarabine exposure described above. A total of 13 adducts were detected, including eight monoadducts and five cross-links derived from PR-104A and from the reduced metabolites, PR-104H and PR-104M (Figure 5). Differential analysis of adduct levels using fixed-effect linear regression was applied to test whether PR-104A resistance in ETP-2 is related to reduced adduct levels compared to responsive ALL-8. Further, adduct levels between ETP-2 single to combination treatment were compared to test if synergy is based on higher adduct levels, as a result of putative DNA repair inhibition. Statistical analysis revealed two PR-104M-monoadducts as candidate adducts that may be more effectively repaired in ETP-2 compared to ALL-8: the adenosine- and guanosine-derived PR-104M monoadducts with m/z 446 and 462, respectively. There was no evidence, however, for an adduct whose persistence was promoted in the resistant PDX ETP-2 when exposed to the combination with clofarabine. While these results were inconclusive regarding the role of any particular adducts responsible for the synergy between the two drugs, given the high experimental variance in individual adduct levels amongst experiments, resolving this question would likely require developing a new absolute quantitation targeted mass spectrometry analysis approach, outside the scope of the present study, or integrated evaluation of general adduct types known to be highly cytotoxic such as ICLs.

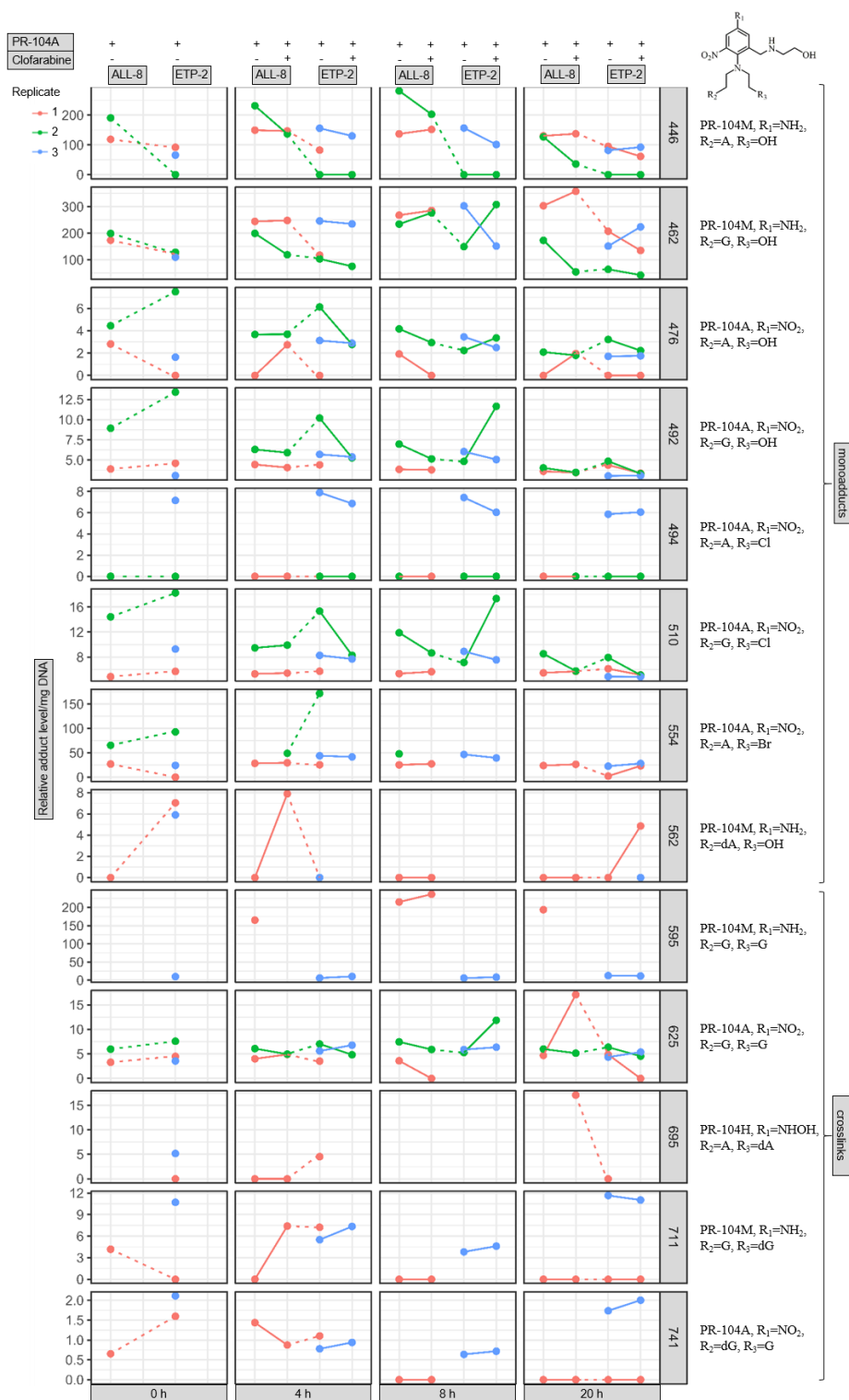


Figure 5. Overview of PR-104A adduct levels over time in ALL-8 and ETP-2. PR-104A-derived adduct levels were measured in PDXs after treatment with 150 μ M PR-104A for 4 h ($t = -4$) followed by post-incubation for 0, 4, 8 and 20 with (+) or without (-) clofarabine (ALL-8 $n=2$, ETP-2 $n=3$). Each panel corresponds to a unique adduct-time point with respective relative adduct abundance normalized per amount of DNA on the y-axis. Treatment conditions, PR-104A single and PR-104A + clofarabine, are distributed along the x-axis. PR-104A-adducts are characterized on the right in the order of respective m/z from monoadduct to crosslinks. Statistical analysis was performed by slope comparison, represented in here by continuous or dashed lines within or comparing biological samples respectively.

Decreased DNA ICL repair in resistant PDXs after combined PR-104A and clofarabine treatment

To investigate the formation and repair of ICLs induced by PR-104A as a basis of the synergistic effect of PR-104A and clofarabine in ETP-ALL PDXs, a modified version of the alkaline Comet assay was used applying irradiation to detect ICLs (Patterson et al. 2007). We first tested the dose-response relationship between drug concentration and ICL formation as a function of drug sensitivity. Again, cells from ALL-8 (sensitive) and ETP-2 (resistant) PDXs were exposed to increasing PR-104A concentrations for 4 h and DNA damage compared between irradiated and un-irradiated cells. As expected, un-irradiated control cells showed no DNA damage (Figure 6B) and after 10 Gy exposure, tail moments strongly increased due to random DNA strand breaks introduced by X-ray irradiation (Figure 6B). In the un-irradiated PR-104A treated cells, a linear increase in tail moment resulted with increasing drug concentrations. At the same time, in both irradiated xenograft types a linear decrease in tail moment was observed with increasing PR-104A concentrations (Figure 6 A1) thus providing a basis to quantify DNA ICL that could be detected at PR-104A doses in the range of the IC₅₀ values of each ALL type (9.4 μ M in ALL-8, 28.0 μ M in ETP-2, Figure 6 A3). Exposing both ALLs to equal PR-104A concentrations resulted in more than 2-fold higher ICL formation in sensitive ALL-8 cells, compared to resistant ETP-2 cells. These results indicate that ICL formation correlates with the chemosensitivity of ALL PDXs to PR-104A.

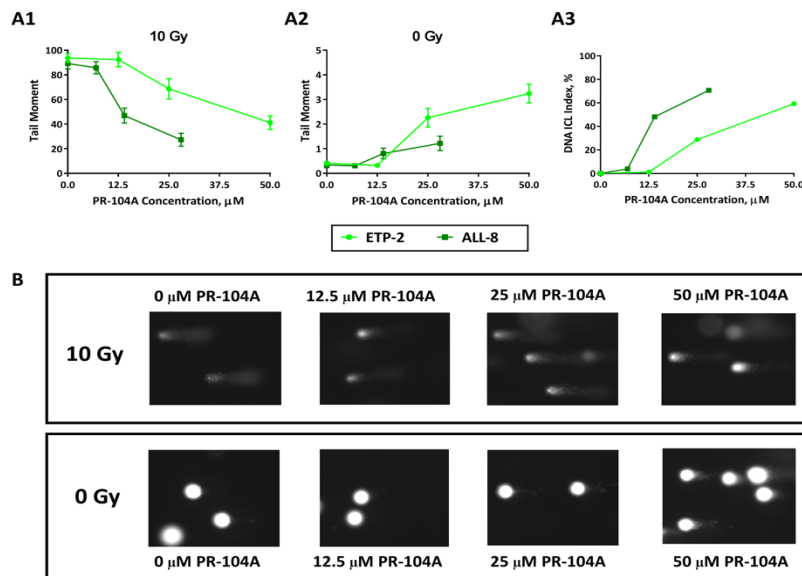


Figure 6: PR-104A concentration-dependent effect on the tail moment and ICL formation of ALL-8 and ETP-2 xenografts. (A) Cells were treated *in vitro* for 4 h with increasing drug concentrations and exposed to either 10 Gy (A1) or 0 Gy (A2). Points represent the mean tail moment \pm SEM of at least 30 visualized comets. The mean values of tail moment were used to calculate the DNA ICL index curve (A3). (B) Characteristic comet images are also shown for ETP-2 at 10x magnification. The experiment was performed in n = 1.

We next sought to determine the effect of clofarabine on the persistence of PR-104A-induced ICLs in ETP-2. Cells were exposed for 4 h to a PR-104A concentration that caused significant ICL formation based on the results above (100 μ M). After removal of PR-104A ($t = 0$ h), the cells were exposed to clofarabine (1.2 μ M) for 6 h or 20 h and DNA ICL levels were compared. After irradiation, similar tail moment was obtained in untreated and clofarabine-treated cells at both $t=0$ h and $t=20$ h, but was strongly decreased in cells exposed to PR-104A ($t = 0$ h, Figure 7A and B), indicating substantial ICL formation (80% cross-linking index, Figure 7D). After 20 h drug-free exposure, tail moment was increased compared to cells analyzed immediately after 4 h PR-104A exposure ($t=0$ h, Figure 7B) thus indicating the removal of ICLs (Figure 7D). However, when cells were exposed to clofarabine after PR-104A, tail moment was further decreased suggesting diminished capacity of the cells to remove the damage (Figure 7D). These results suggest clofarabine leads to an inhibition in the repair of ICLs induced by PR-104A as a basis for the synergistic effect of PR-104A and clofarabine in ETP-2.

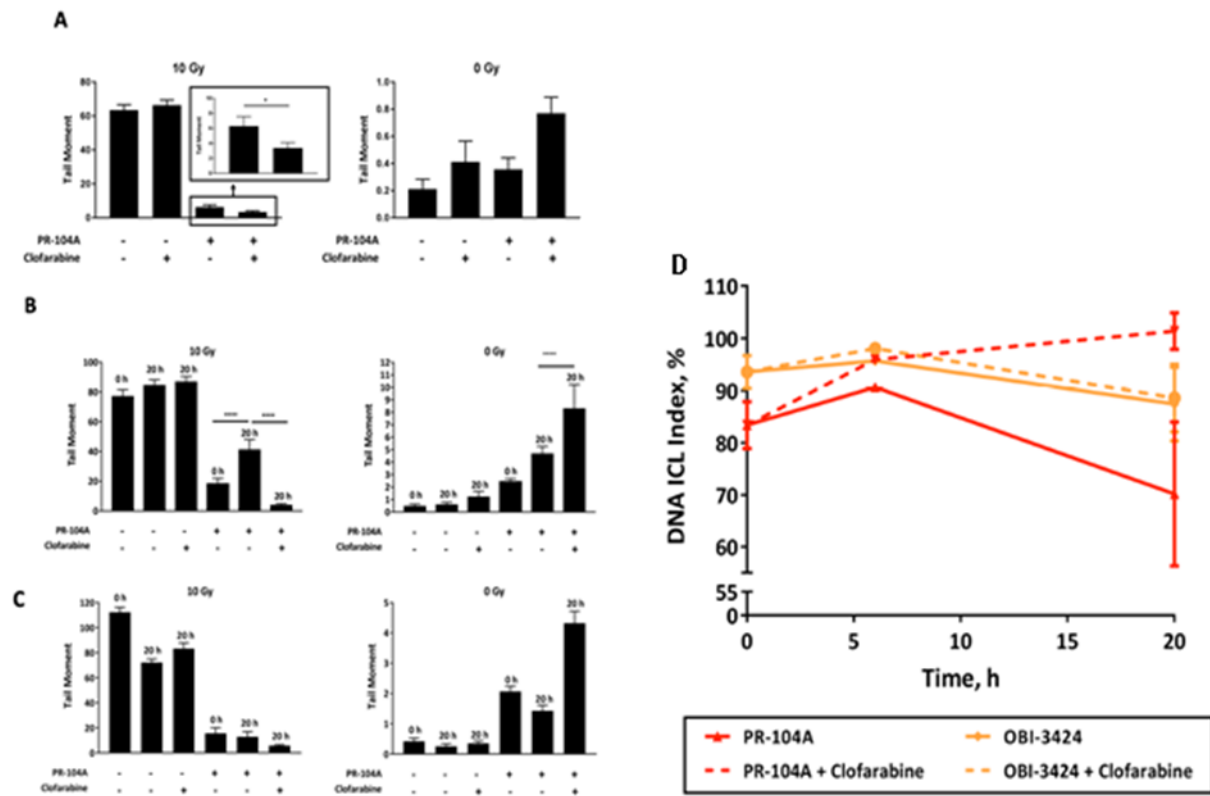


Figure 7. Combination of PR-104A and clofarabine leads to increased overall tail moment in un-irradiated cells and decreased tail moment in cells exposed to 10 Gy. ETP-2 were treated with 100 μ M PR-104A for 4 h followed by drug removal and 6 h (A) or 20 h (B and C) post-incubation with 1.25 μ M clofarabine. Based on the results, DNA ICL index (%) was calculated over time for PR-104A only and in combination with clofarabine (D). The experiment was performed in $n=2$.

Discussion

To investigate the chemical basis of ALL sensitization to PR-104A, we first used a mass spectrometry approach that allowed us to quantify for the first time drug-DNA adducts in *in vitro* PDXs as a function of responsiveness and drug dose. PR-104A derived DNA adducts in ALL PDXs detected by LC-MS/MS showed similar adduct profiles as observed in cell lines, including several direct PR-104A, as well as pro-drug bioactivation derived PR-104H and M monoadducts and crosslinks (Stornetta et al. 2018). Adducts were observed to form after 4 h and increase over the course of 24 h (Figure 1). In cell studies with short time treatment of clinically relevant concentrations of the nor-nitrogen mustard melphalan and cisplatin, maximum drug-monoadduct levels were reached 2 h after drug removal, while ICLs were demonstrated to be maximal after 8 h drug-free incubation time, followed by a decline to up to 10 or 20% of maximal levels after 48 h (Buschfort-Papewalis et al. 2002; Hansson et al. 1987; Souliotis et al. 2003). Therefore, the accumulation of PR-104A adducts over 24 h in PDXs as presented in this study differs from literature data for other alkylating agents demonstrating decline in adduct levels.

To understand the mechanism driving the PR-104A-clofarabine synergy uncovered in this study, we carried out studies in PDX models showing either additive or synergistic effects. By tracking the accumulation of several different DNA adduct forms, we addressed the hypothesis that the repair of particular toxicity-inducing adducts, or specifically of DNA ICLS, may be inhibited by clofarabine, thus contributing to more effective PR-104A response. For instance, clofarabine has been shown to interfere with the repair of DNA strand breaks in chronic lymphocytic leukaemia lymphocytes following treatment with 4-hydroperoxycyclophosphamide (Yamauchi et al. 2001). Similarly, clofarabine has been shown to act as powerful radiosensitizer by interfering with the DNA (Cariveau et al. 2008). Moreover, clofarabine was one of the ICL repair inhibitors recently identified during a screen (Fujii et al. 2015).

While 13 adducts were quantified in both PDXs under all exposure scenarios, these data could suggest candidate structures that persist under sensitive conditions, but the experimental variance associated with addressing individual adducts was high (Figure 5), particularly compared with data from cell lines (Stornetta et al. 2018; Stornetta et al. 2017a), allowing no significant conclusion. A potential limiting factor is the limited understanding of the temporal relationship between inducing DNA damage in PDXs and function of the DNA damage response. Also, the PR-104A concentration used in the MS approach was 10-90 times higher than the respective IC₅₀ values for ETP-2 and ALL-8, thus adduct levels may be overall saturated and not realistically reflecting changes at therapeutic doses. A potential strategy to overcome this limitation would be to focus on quantifying relatively more abundant monoadducts, which is possible at lower PR-104-doses (Figure 1) and have been shown to correlate with crosslink levels in cells (Stornetta et al. 2018). Although ICLs represent a small fraction of the cytotoxic lesions induced after PR-104A treatment, these lesions are extremely toxic and are believed to be the critical cytotoxic mechanism for most alkylating agents including PR-104A (Gu et al. 2009; Singleton et al. 2009). As alterations in the kinetics of DNA ICL formation and repair have been associated with resistance to nitrogen mustards

(McHugh et al. 2001) we therefore looked in more detail for the potential of clofarabine to preserve PR-104A-induced DNA ICLs.

The alkaline comet assay and its modifications have been used to measure the repair of drug-induced DNA damage in cells, xenografts, or patient tissues (Azqueta et al. 2014). In this study, we show that DNA ICLs induced by PR-104A can be detected in PDX ALLs after short drug treatment (4 h) and at low drug doses (in the range of IC_{50} , Figure 6A). Moreover, formation of ICL is consistent with the chemosensitivity of PDXs to PR-104A, as the drug doses required to induce the same level of ICLs were more than 2-fold higher in the resistant ETP-2 than in the sensitive ALL-8 cell. This is in line with previous studies, which observed a significant correlation between ICL formation and cytotoxicity in multiple human tumour cell lines after 2 h PR-104A exposure (Singleton et al. 2009). These findings suggest that the levels of immediate DNA ICLs could predict and determine the xenograft sensitivity to PR-104A. We then carried out a timecourse study for the repair of ICLs. ALL-PDXs showed increasing levels of ICLs during the first 6 h after removal of the drug, and then a decrease by 20% in the following 14 h (Figure 7D). A similar kinetic for the removal of PR-104A-ICL was also found in cells (Singleton et al. 2009). In this study, combinatorial treatment resulted in overall increased DNA damage and delayed ICL repair kinetics in resistant PDXs further highlighting the potential of clofarabine to preserve PR-104A-induced DNA ICLs as basis for drug synergy. Even though a mechanistic explanation was out of the scope of this work, previous studies suggested that clofarabine inhibits the repair of DNA ICLs either through inhibition of ribonucleotide reductase (RNR) (Fujii et al. 2015) or through inhibition of DNA polymerases (Xie and Plunkett 1995). To test if the synergy is mediated by RNR inhibition, stronger RNR inhibitors than clofarabine, such as gemcitabine (Fujii et al. 2015) should be tested in combination with PR-104A. Once the mechanism of inhibition will be characterized at the DNA level, these results could elucidate new compounds to increase responsiveness of resistant subtypes ALL to PR-104A.

Material and Methods

General consideration

PR-104A (W.A. Denny 2005) and d4-PR-104A (Atwell and Denny 2007) were synthesized as previously described. Clofarabine was purchased from Sigma-Aldrich (St. Louis, USA). Drug dilutions were prepared in complete Quality Biologicals Serum Free-60 (QBSF) media supplemented with 20 ng/mL fms-like tyrosine kinase 3 (FIT-3, complete QBSF).

In vitro culture of xenografts

PDX cells were retrieved from cryostorage, thawed in a water bath at 37 °C and washed twice with pre-warmed complete RPMI media supplemented with 10 % (v/v) fetal calf serum (FCS). Cells were then resuspended in complete QBSF-60 media and allowed to equilibrate overnight at 37 °C, 5 %. After Ficoll density gradient purification to purify live cells, cells were counted by trypan blue exclusion and resuspended in complete QBSF at the specified cell density.

Analysis of cell viability in drug-exposed PDXs

PDX cells were retrieved from cryostorage as described above and resuspended in complete QBSF at cell density of 10×10^6 cells/ml. A solution of PR-104A (150 μ M) in complete QBSF-60, or complete QBSF-60 alone as untreated control, was added to the cells for 4 h. Cells then were washed twice with PBS and further treated with 1.25 μ M clofarabine in QBSF, or complete QBSF alone as untreated control for additional time up to 20 h. At the selected time points, samples were stained with 7-amino-actinomycin D (7-AAD) and Annexin V APC according to the manufacturer's instructions (BD Biosciences, Franklin Lakes, USA, (Casciola-Rosen et al. 1996). Data were acquired on a BD FACSCanto™ II fluorescence-activated cell sorting system (Franklin Lakes, USA). Viable cells (cells double negative for Annexin V and 7-AAD), are expressed as percentage of the corresponding untreated control.

Modified version of the comet assay

To study the concentration-dependent formation of DNA ICLs, PDX cells were retrieved from cryostorage as described above and resuspended in 96-well clear, U-bottom tissue culture treated plates at a cell density of 4×10^6 cells/ml. Cells were then exposed to different PR-104A concentrations in the range of the IC_{50} (0-50 μ M) or to complete QBSF as an untreated control. To study the DNA ICL repair kinetics, ETP-2 cells were cultured in 6-well plates at a cell density of 10×10^6 cells/ml, and exposed to 100 μ M PR-104A for 4 h ($t = -4$ h). Straight after removal of the drugs ($t = 0$ h), 0.3×10^5 cells were processed for the modified version of the Comet assay as explained below. Remaining cells were washed twice with warm PBS to remove traces of PR-104A and seeded in 96-well clear, U-bottom tissue culture treated plates at a cell density of 4×10^6 cells/ml. Xenografts were then treated in triplicate wells with either 1.25 μ M clofarabine or complete QBSF as a drug-free control for further 6 h or 20 h, to allow DNA repair. At the selected time points, 0.3×10^5 cells were washed with cold PBS, and processed for the single cell gel electrophoresis assay (also known as modified version of the comet assay). The details of the procedure are described in Spanswick et al. (1999) (Spanswick et al. 1999) All procedures were carried out on ice and samples were kept in the dark. After washing with cold PBS, cells were irradiated with 10 Gy under a X-Rad 320 biological irradiator (Precision X-Ray, Inc., USA) to deliver a fixed number of random DNA strand break. An unirradiated control was processed similarly but without irradiation. The alkaline comet assay was performed based on the protocol from CometAssay® Kit (25 x 2 well slides) (Trevigen, Bio Scientific, Australia). Samples were then stained with 100 μ l of diluted SYBR™ Safe DNA Gel Stain for 30 min. Slides were visualised using a Zeiss Axiovert 200 M inverted microscope at 20x magnification and fluorescence emission was detected using Zeiss filter FITC channel, Filter Set 38 HE, excitation BP 470/40, beamsplitter FT 495, emission BP 525/50. Images were captured using an AxioCam HRm camera and analysed with ImageJ open source software using the OpenComet plugin. DNA ICL index was calculated as described in Singleton et al. (2009) (Singleton et al. 2009).

Exposure of PDX and isolation of DNA for DNA adduct analysis

To study the formation and repair of PR-104A-induced DNA adducts, 1000 M xenograft cells were thawed as described above, resuspended in 35 mL of complete QBSF, and let equilibrate overnight at 37 °C, 5% CO₂. After Ficoll purification, viable cells were counted and resuspended in complete QBSF, at a density of 5-10 x 10⁶ cells/ml. ALL-8, ALL-27, ALL-31 or ETP-2 were treated with PR-104A in complete QBSF, or QBSF alone as untreated control for 4 or 24 h, at 37 °C, 5% CO₂. PR-104A concentrations were 10, 25, 50, 75, 100, 150 µM final concentration. Cells were processed as described below for DNA extraction and adduct analysis. For the synergy study, cells either received a 4 h pre-treatment with 150 µM PR-104A, or complete QBSF as untreated control (t = - 4 h). At t = 0 h, cells were washed twice in warm PBS to remove PR-104A and incubated in the presence or absence of 1.25 µM clofarabine for further 4, 8, or 20 h. At the selected time points, cells were washed with cold PBS by centrifugation at 1400 rpm for 5 min, and DNA was extracted as previously described (Stornetta et al. 2018). The dried DNA pellets were stored at -20 °C and shipped from Sydney to Zurich at room temperature over 3 days.

LC-MS/MS relative quantification of PR-104A-adducts

DNA was isolated from PDX cell pellets and enzymatically digested and further processed by solid-phase-extraction as previously described (Stornetta et al. 2017a). Dried samples were reconstituted in 10 µl of 20% MeOH in H₂O for MS analysis. Samples of 1 µl (0.6-55 µg genomic DNA) were analyzed by an ACQUITY UPLC M-Class System (Waters Co., Milford, MA) equipped with a 1 µl injection loop and coupled to a TSQ Quantiva mass spectrometer (Thermo Scientific, Waltham, MA). SRM scanning in positive ionization mode was performed using nano-electrospray as detailed previously (Stornetta et al. 2017a). A handpacked Luna C18 capillary column (75 µm ID, 10 cm length, 15 µm orifice) was applied for separation with a gradient from 2 to 50% acetonitrile in 5 mM ammonium acetate (pH = 5.5) at a flow rate of 300 nl/min. For MS-SRM scanning, mass resolutions were set at 0.7 u full width at half maximum (FWHM, unit mass resolution) for both quadrupoles and scan time was 0.05 s. Other parameters were: spray voltage 1.9 kV; capillary temperature 270 °C; collision gas pressure 1.0 mTorr; collision energy 20 V (base adducts) or 15 V (nucleoside adducts). Following transitions were monitored: PR-104A monoadducts *m/z* 476.2 to 341.1, *m/z* 492.2 to 341.1, *m/z* 494.1 to 359.1, *m/z* 510.1 to 359.1, *m/z* 554.1 to 403.0, *m/z* 592.2 to 476.2 and *m/z* 608.2 to 492.2, PR-104A crosslinks *m/z* 625.2 to 474.2 and *m/z* 741.3 to 625.2, PR-104AH/M monoadducts *m/z* 446.2 to 311.1, *m/z* 462.2 to 311.1 and *m/z* 562.2 to 446.2, PR-104H/M crosslinks *m/z* 563.2 to 428.2, *m/z* 579.2 to 444.2, *m/z* 579.2 to 428.2, *m/z* 595.2 to 444.2, *m/z* 611.3 to 460.2, *m/z* 695.3 to 579.2 and *m/z* 711.3 to 595.2 and the 19 isotope labeled corresponding standards (+ 4 amu). MS instrument control and data acquisition were performed using Xcalibur (version 4.0, ThermoFisher Scientific). A solution containing buffer and enzymes served as negative control for PR-104A adducts in the sample preparation blank. Further, control samples (PR-104A⁻, clofarabine^{+/-}) were evaluated for background noise and exclusion of false positive PR-104A adduct signals. Only DNA adducts with S/N > 3 were considered above LOD, and only adducts with S/N > 10 were above LOQ.

Statistical analysis of LC-MS/MS analysis

Differential adduct formation analysis was performed using fixed-effect linear regression with the donor as a covariate. Modeling was performed with R version 3.2.1 with Bioconductor 1, and was performed as a service of NEXUS Personalized Health Technologies, ETH Zurich, Switzerland.

Acknowledgement

The authors wish to thank Dr. Alessia Stornetta, Masonic Cancer Center, University of Minnesota, for advice on sample preparation for PR-104A-derived adduct detection by LS-MS/MS. Further, the authors thank Dr. Michael Prummer of NEXUS Personalized Health Technologies, ETH Zurich, Switzerland for assistance with the statistical analysis of the MS data, and the Functional Genomics Center Zurich (FGCZ) for providing LC-MS/MS instrumentation. Also, thanks to the Biological Resources Imaging Laboratory (BRIL), UNSW for access to the irradiator. This research was supported by the Krebsliga Schweiz (grant KFS-4443-02-2018-R), and the Hochstrasser Foundation.

References

- Atwell GJ, Denny WA (2007) Synthesis of H-3- and H-2(4)-labelled versions of the hypoxia-activated prodrug 2-((2-bromoethyl)-2,4-dinitro-6-(((2-(phosphonoxy)ethyl)amino)carbonyl)anilino)ethyl methanesulfonate (PR-104) *J Labelled Compd Rad* 50:7-12 doi:10.1002/jlcr.1147
- Azqueta A, Slyskova J, Langie SAS, O'Neill Gaivão I, Collins A (2014) Comet assay to measure DNA repair: approach and applications *Front Genet* 5:288-288 doi:10.3389/fgene.2014.00288
- Barski OA, Tipparaju SM, Bhatnagar A (2008) The Aldo-Keto Reductase Superfamily and its Role in Drug Metabolism and Detoxification *Drug metabolism reviews* 40:553-624 doi:10.1080/03602530802431439
- Bassan R, Hoelzer D (2011) Modern Therapy of Acute Lymphoblastic Leukemia *J Clin Oncol* 29:532-543 doi:doi:10.1200/JCO.2010.30.1382
- Birtwistle J et al. (2009) The aldo-keto reductase AKR1C3 contributes to 7,12-dimethylbenz(a)anthracene-3,4-dihydrodiol mediated oxidative DNA damage in myeloid cells: Implications for leukemogenesis *Mutation Research/Fundamental and Molecular Mechanisms of Mutagenesis* 662:67-74 doi:https://doi.org/10.1016/j.mrfmmm.2008.12.010
- Buschfort-Papewalis C, Moritz T, Liedert B, Thomale J (2002) Down-regulation of DNA repair in human CD34⁺ progenitor cells corresponds to increased drug sensitivity and apoptotic response *Blood* 100:845-853 doi:10.1182/blood-2002-01-0022
- Cariveau MJ, Stackhouse M, Cui XL, Tiwari K, Waud W, Secrist JA, 3rd, Xu B (2008) Clofarabine acts as radiosensitizer in vitro and in vivo by interfering with DNA damage response *International journal of radiation oncology, biology, physics* 70:213-220 doi:10.1016/j.ijrobp.2007.09.012
- Casciola-Rosen L, Rosen A, Petri M, Schlissel M (1996) Surface blebs on apoptotic cells are sites of enhanced procoagulant activity: implications for coagulation events and antigenic spread in systemic lupus erythematosus *Proceedings of the National Academy of Sciences* 93:1624-1629 doi:10.1073/pnas.93.4.1624
- Cooper SL, Brown PA (2015) Treatment of Pediatric Acute Lymphoblastic Leukemia *Pediatr Clin North Am* 62:61-73 doi:10.1016/j.pcl.2014.09.006
- Fujii N, Evison BJ, Actis ML, Inoue A (2015) A novel assay revealed that ribonucleotide reductase is functionally important for interstrand DNA crosslink repair *Bioorganic & medicinal chemistry* 23:6912-6921 doi:10.1016/j.bmc.2015.09.045
- Geary N (2013) Understanding synergy *American Journal of Physiology-Endocrinology and Metabolism* 304:E237-E253 doi:10.1152/ajpendo.00308.2012
- Gu Y, Patterson AV, Atwell GJ, Chernikova SB, Brown JM, Thompson LH, Wilson WR (2009) Roles of DNA repair and reductase activity in the cytotoxicity of the hypoxia-activated dinitrobenzamide mustard PR-104A *Molecular cancer therapeutics* 8:1714-1723 doi:10.1158/1535-7163.MCT-08-1209
- Guise CP et al. (2010) The bioreductive prodrug PR-104A is activated under aerobic conditions by human aldo-keto reductase 1C3 *Cancer research* 70:1573-1584 doi:10.1158/0008-5472.CAN-09-3237
- Guise CP, Wang AT, Theil A, Bridewell DJ, Wilson WR, Patterson AV (2007) Identification of human reductases that activate the dinitrobenzamide mustard prodrug PR-104A: a role for NADPH:cytochrome P450 oxidoreductase under hypoxia *Biochem Pharmacol* 74:810-820 doi:10.1016/j.bcp.2007.06.014
- Hansson J, Lewensohn R, Ringborg U, Nilsson B (1987) Formation and Removal of DNA Cross-Links Induced by Melphalan and Nitrogen Mustard in Relation to Drug-induced Cytotoxicity in Human Melanoma Cells *Cancer research* 47:2631-2637
- Houghton PJ et al. (2011) Initial Testing of the Hypoxia-Activated Prodrug PR-104 by the Pediatric Preclinical Testing Program *Pediatric Blood & Cancer* 57:443-453 doi:10.1002/pbc.22921
- Jameson MB, Rischin D, Pegram M, Gutheil J, Patterson AV, Denny WA, Wilson WR (2010) A phase I trial of PR-104, a nitrogen mustard prodrug activated by both hypoxia and aldo-keto reductase 1C3, in patients with solid tumors *Cancer Chemotherapy and Pharmacology* 65:791-801 doi:10.1007/s00280-009-1188-1
- Jamieson SM et al. (2014) A novel fluorometric assay for aldo-keto reductase 1C3 predicts metabolic activation of the nitrogen mustard prodrug PR-104A in human leukaemia cells *Biochem Pharmacol* 88:36-45 doi:10.1016/j.bcp.2013.12.019
- Klumper E et al. (1995) In-Vitro Cellular-Drug Resistance in Children with Relapsed/Refractory Acute Lymphoblastic-Leukemia *Blood* 86:3861-3868
- Konopleva M et al. (2011) Phase I/II Study of PR104, a Bioreductive Prodrug, in Patients with Relapsed/Refractory Acute Myeloid Leukemia (AML) Using Patient-Specific Adaptive Dose Selection *Blood* 118:1523-1523

- Konopleva M et al. (2015) Phase I/II study of the hypoxia-activated prodrug PR104 in refractory/relapsed acute myeloid leukemia and acute lymphoblastic leukemia *Haematologica* 100:927-934 doi:10.3324/haematol.2014.118455
- Mahadevan D et al. (2006) Transcriptome and serum cytokine profiling of an atypical case of myelodysplastic syndrome with progression to acute myelogenous leukemia *American Journal of Hematology* 81:779-786 doi:10.1002/ajh.20690
- McHugh PJ, Spanswick VJ, Hartley JA (2001) Repair of DNA interstrand crosslinks: molecular mechanisms and clinical relevance *The Lancet Oncology* 2:483-490 doi:https://doi.org/10.1016/S1470-2045(01)00454-5
- McKeage MJ, Gu YC, Wilson WR, Hill A, Amies K, Melink TJ, Jameson MB (2011) A phase I trial of PR-104, a pre-prodrug of the bioreductive prodrug PR-104A, given weekly to solid tumour patients *BMC Cancer* 11 doi:Artn 432 10.1186/1471-2407-11-432
- Moradi Manesh D et al. (2015) AKR1C3 is a biomarker of sensitivity to PR-104 in preclinical models of T-cell acute lymphoblastic leukemia *Blood* doi:10.1182/blood-2014-12-618900
- Patterson AV et al. (2007) Mechanism of action and preclinical antitumor activity of the novel hypoxia-activated DNA cross-linking agent PR-104 *Clinical cancer research : an official journal of the American Association for Cancer Research* 13:3922-3932 doi:10.1158/1078-0432.CCR-07-0478
- Singleton RS et al. (2009) DNA Cross-Links in Human Tumor Cells Exposed to the Prodrug PR-104A: Relationships to Hypoxia, Bioreductive Metabolism, and Cytotoxicity *Cancer research* 69:3884-3891 doi:10.1158/0008-5472.can-08-4023
- Souliotis VL, Dimopoulos MA, Sfrikakis PP (2003) Gene-specific Formation and Repair of DNA Monoadducts and Interstrand Cross-links after Therapeutic Exposure to Nitrogen Mustards *Clinical Cancer Research* 9:4465-4474
- Spanswick VJ, Hartley JM, Ward TH, Hartley JA (1999) Measurement of Drug-Induced DNA Interstrand Crosslinking Using the Single-Cell Gel Electrophoresis (Comet) Assay. In: Brown R, Böger-Brown U (eds) *Cytotoxic Drug Resistance Mechanisms*. Humana Press, Totowa, NJ, pp 143-154. doi:10.1385/1-59259-687-8:143
- Stornetta A, Deng KK, Danielli S, Liyanage HDS, Sturla SJ, Wilson WR, Gu Y (2018) Drug-DNA adducts as biomarkers for metabolic activation of the nitro-aromatic nitrogen mustard prodrug PR-104A *Biochem Pharmacol* 154:64-74 doi:10.1016/j.bcp.2018.04.004
- Stornetta A, Villalta PW, Gossner F, Wilson WR, Balbo S, Sturla SJ (2017a) DNA Adduct Profiles Predict in Vitro Cell Viability after Treatment with the Experimental Anticancer Prodrug PR104A *Chem ResTox* 30:830-839 doi:10.1021/acs.chemrestox.6b00412
- Stornetta A, Villalta PW, Hecht SS, Sturla SJ, Balbo S (2015) Screening for DNA Alkylation Mono and Cross-Linked Adducts with a Comprehensive LC-MS3 Adductomic Approach *Analytical Chemistry* 87:11706-11713
- Stornetta A, Zimmermann M, Cimino GD, Henderson PT, Sturla SJ (2017b) DNA Adducts from Anticancer Drugs as Candidate Predictive Markers for Precision Medicine *Chem Res Toxicol* 30:388-409 doi:10.1021/acs.chemrestox.6b00380
- Tasian SK, Hunger SP (2016) Genomic characterization of paediatric acute lymphoblastic leukaemia: an opportunity for precision medicine therapeutics *bjh* 176:867-882 doi:10.1111/bjh.14474
- Toscan C. MDM, Lock R. (unpublished results)
- W.A. Denny GJA, S. Yang, W.R. Wilson, A.V. Patterson, N.A. Helsby (2005) Novel Nitrophenyl Mustard and Nitrophenylaziridine Alcohols and Their Corresponding Phosphates and Their Use as Targeted Cytotoxic Agents. New Zealand Patent,
- Wheeler K, Richards S, Bailey C, Chessells J (1998) Comparison of bone marrow transplant and chemotherapy for relapsed childhood acute lymphoblastic leukaemia: the MRC UKALL X experience. Medical Research Council Working Party on Childhood Leukaemia *British journal of haematology* 101:94-103
- Xie C, Plunkett W (1995) Metabolism and Actions of 2-Chloro-9-(2-deoxy-2-fluoro- β -arabinofuranosyl)-adenine in Human Lymphoblastoid Cells *Cancer research* 55:2847-2852
- Yamauchi T, Nowak BJ, Keating MJ, Plunkett W (2001) DNA Repair Initiated in Chronic Lymphocytic Leukemia Lymphocytes by 4-Hydroperoxycyclophosphamide Is Inhibited by Fludarabine and Clofarabine *Clinical Cancer Research* 7:3580-3589

